UNIVERSITY OF NEWCASTLE UPON TYNE
SCHOOL OF CIVIL ENGINEERING AND GEOSCIENCES

Hydraulic and Thermal Conductivities of Soils

By

Ali Faisal Agab

A thesis submitted in partial fulfilment of the requirements for the degree of Doctor of Philosophy

Supervisor: Prof. B. G. Clarke

July 2005

Abstract

The aim of this research is to investigate the hydraulic and thermal conductivities of different types of soils. These two parameters are the main ones controlling the heat flow in the ground beneath a building. Therefore in this thesis, a system, including a testing and analysis methodology has been designed that will allow the construction of new laboratory apparatus in order to determine the required thermal parameters and thus reduce the uncertainty in the design of energy piles.

This thesis presents and discusses the effects of physical properties on determining both the hydraulic and thermal conductivity of soils. Two flexible wall permeameters using the constant rate of flow technique were used to determine the hydraulic conductivity of two types of clayey soil. This technique proved to be accurate and produced results in a relatively short time. One of the aims of this research was to develop a better technique for testing coarse soils; therefore these permeameters were developed to work using falling head technique. The falling head technique proved to be accurate and produced results in relatively shorter time than the constant flow technique. Tests at low and high hydraulic gradient and over a range of effective stress show the hydraulic conductivity varies with these two parameters.

A part of the thesis describes the methods of interpreting the results from both the constant flow and falling head techniques, also it describes how the falling head tests can be interpreted as a constant head test for clayey soils. A comparison between the results showed the advantages of using the new systems. It is also demonstrated how the new system can determine the hydraulic conductivity of a soil in a relatively short time of one hour.

The second aim of the research was to design a simple device to determine the thermal conductivity of soils. Two thermal conductivity cell devices were designed. A test procedure and its method of interpretation are discussed and presented. The thermal conductivity results were compared with the published results and proved to be within the same range (0.15 to 4 W/m.^{o}C). These experimental results were also compared and discussed with the predicted results produced by different thermal conduction models.

The thermal results for deferent types of soils can be used to model the heat transfer between the ground and the energy piles, in which the ground can be used as a heat sink or source. It is believed that the water content of the soils together with their mineralogical constituents can be particularly valuable, not only as a basis for understanding the behaviour of the soils but also to enable a reasonably good estimate of the thermal conductivity using the thermal conduction models.

Acknowledgements

I wish to sincerely thank Allah subhanaho wa taala who has given me this opportunity to complete my PhD degree.

I would like to express my gratitude and appreciation to Prof. Barry G. Clarke who initiated and supervised this research. His helpfulness, generosity and encouragement, made the years of research with him enjoyable and memorable.

I am indebted to my country, Libya, for its continuous financial support without which this project would not have been possible.

In particular, thanks are due to the workshop group especially Mr. Keith Tweddle, Mr. David Dick, Mr. Rob Hunter, Mr. Bill Cragie and Mr Fred Beadle for their cooperation during the modification and construction of the apparatuses.

I would like also to thank Dr Mohamed Rouainia and Professor David Manning who were welling to spend their time for help.

Thanks also to those who helped directly and indirectly during the research period.

Finally, I would like to send my deep thanks to my family especially my father and mother for their support and encouragement until the end of this research period. Also my great thanks to my wife Maisa and daughters; Rahaf, Arwa and the little one Fatima Elzhra who were with me step by step towards the end of this great work providing the warm environment and reducing the felling of homesick.

List of Contents

Chapter 3
Determination of Hydraulic Conductivity

Chapter 4
Design of the Thermal Apparatus and its Experimental Procedure

Chapter 5
Hydraulic Conductivity Results and Discussions

Chapter 6
Thermal Conductivity Results and Discussions

Chapter 7
Conclusion and Recommendations

List of Figures

Chapter 1

Chapter 2

Chapter 3

Chapter 4

Chapter 5

Chapter 6

List of Tables

List of Symbols

v	Discharge velocity
i	Hydraulic gradient
k_h	Hydraulic conductivity
q	Rate of flow
Δh	Head difference
A	Cross sectional area
K	Intrinsic permeability
μ	Viscosity of permeant
γ	Unit weight of permeant
T	Double layer thickness
D	Dielectric constant
n_o	Electrolyte concentration
D_s	Particle diameter
e	Void ratio
C	Shape factor
D_{10}	Effective particle diameter
S_o	Specific grain surface
C_k	Hydraulic conductivity change index
Q	Heat transfer rate
k_t	Thermal conductivity
ΔT	Temperature difference
ΔL	Length of specimen
T_∞	Surrounding temperature
σ	Stefan-Boltzmann constant
ρ	Density
c_p	Specific heat
C	Volumetric heat capacity
α	Thermal diffusivity
γ_d	Dry density
w_c	Water content
K_e	Kersten number
k_a	Air thermal conductivity
k_s	Solid thermal conductivity
k_w	Water thermal conductivity
h_1	Hydraulic head at time t_1
h_2	Hydraulic head at time t_2
t	Elapsed time
a_{in}	Cross sectional area of influent pipe
a_{out}	Cross sectional area of effluent1 pipe
Δx	Sample thickness
n	Porosity
k_f	Fluid thermal conductivity
r	Distance between electrodes
t_o	Heat pulse duration
x_a	Volumetric fraction of air
x_s	Volumetric fraction of solids
x_w	Volumetric fraction of water
S	Saturation degree
m_{water}	Mass of water

m_{soil}	Mass of solids
G_s	Particle density
V_o	Initial volume of specimen
V_s	Volume of specimen after saturation
V_c	Volume of specimen after consolidation
m_s	Mass of sample before placing in the oven
m_d	Mass of sample after 24 hours in the oven
c_v	Coefficient of consolidation
m_v	Coefficient of volume compressibility
e_s	Void ratio after saturation
e_c	Void ratio after consolidation
B	Skemton's1 parameter
$\delta\sigma`$	Effective stress
$t_{50\%}$	Time representing 50% consolidation
$Q_{conv.}$	Amount of heat loss by convection
$T_{conv.}$	Temperature at the convection surface
h	Convection heat transfer coefficient
T_{base}	Temperature at base of specimen
T_{top}	Temperature at top of specimen
E_{stored}	Stored energy
E_{out}	Lost energy

Chapter 1

Introduction

1.1 Introduction

There is a widespread interest among civil engineers, soil scientists, hydro-geologists, and geologists in the hydraulic, thermal and electrical conductivities of soils. Of all the principal soil properties, soil conductivities are the most variable, the easiest to misjudge, and the hardest to measure accurately. Civil engineers have shown that hydraulic conductivity is one of the most important physical properties since most of the major problems of soil and foundation engineering have to do with the recognition, evaluation and proper handling of water encountered in the construction and performance of structures. More recently interest in hydraulic conductivity has increased substantially because of concerns over ground-water contamination.

An accurate measurement of the hydraulic conductivity of soils leads to an accurate assessment of the potential for continued or future contamination at a site. The extensive use of engineered cohesive fills as a barrier to prevent such contamination has required a better understanding of the behaviour of materials used in these barriers.

Electrical conductivity is a measure of how well a material accommodates the transport of electric charge. Electrical conductivity of soils is also of a great importance due to its application in various engineering fields. Electrical conductivity can be used to estimate the amount of total dissolved salts or the total amount of dissolved ions in the water. It is also used to assess the soil salinity (Rhoades et al, 1989), therefore commercial devices are available to rapidly and economically measure and map bulk soil electrical conductivity across agricultural fields.

The electrical conductivity is the inverse of the electrical resistivity which has a wide range of use in site investigations. There are two basic field procedures which are commonly used in electrical resistivity exploration. Electrical traversing which is practically suited for prospecting for sand, gravel, and ore deposits and for locating fault zones. And the electrical sounding which is designed to provide information on the variation in subsurface conditions with depth. Sounding is typically used to help

determine the depth to water table, the thickness of sand, gravel and rock layers, and the actual value of electrical resistivity versus depth (Mitchell 1993).

Research carried out in the University of Newcastle upon Tyne into the use of the electro-osmosis phenomenon to remove the heavy metals from contaminated sites and to dewatering by using the electro kinetics technology. Electrical conductivity of soils is out of the scope of this research since the work focuses on the parameters needed to assess the ground as a source of energy.

Studies have also demonstrated that soil thermal properties are of great importance in many engineering projects and other situations where heat transfer takes place in the soil. This has been mainly because of applications such as preventing frost heave in roads, buildings in cool regions, analysis of heat dissipation from buried electrical cables, prediction of depth of frost penetration in soils, insulation and heat transfer analyses related to tanks, pipelines, and underground storage chambers, and moisture migration under thermal gradients.

There are three distinct areas of interest in thermal conductivity. The first area was developed by soil scientists who were interested in the effects of soil temperature on vegetation. In situ and laboratory tests were developed and theoretical and empirical models produced to explain the behaviour of soil subject to temperature changes.

The second area of interest was developed by geotechnical engineers who were interested in ground freezing and the effect that this has upon near surface soils. This has been extended to include the effects of ground freezing as a construction process.

The most recent area of interest has been in the use of energy piles (Figure 1.1) in which the ground is used as either a heat source or a heat sink. This work has taken place in Austria, Germany, Sweden, Switzerland, France and America, and for the first time in the UK the energy piles were used in the year 2001 (Suckling and Smith 2001).

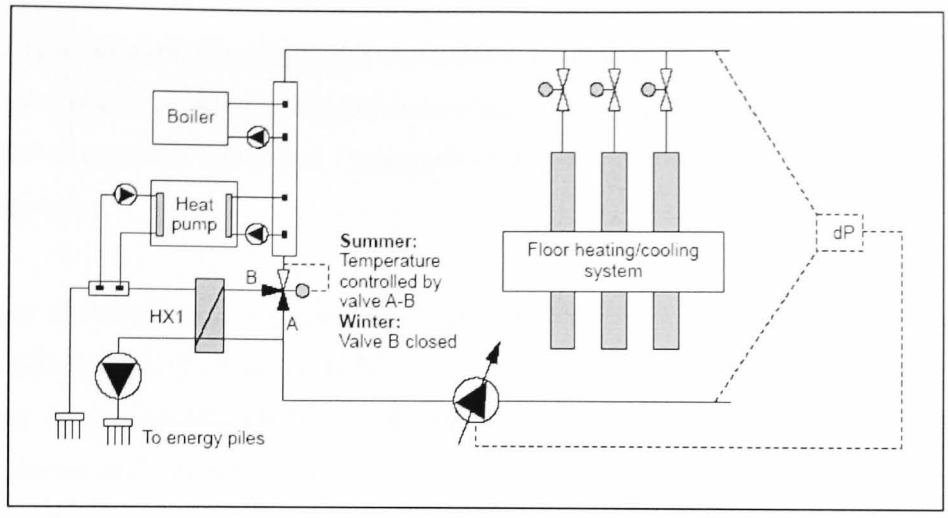

Figure 1.1 A typical layout of an energy pile configuration (Koene, 2000)

Different investigative and design methodologies have been developed for the three areas which is a reflection of the different disciplines of soil scientists and geotechnical engineers. As a result there are different methods to measure the same parameters, different symbols used and different methods of interpretation of tests. In all cases the parameters that describe the ability for heat to flow through soil and the capacity of soil to absorb heat are thermal conductivity, specific heat, volumetric heat capacity, thermal resistance and thermal diffusivity with the most important being thermal conductivity.

There are three components used to model ground storage of building energy. The first is the model of the building, the second is the model of the ground and the third is the climatic model. Part of this research covers the input data needed to model the ground to make use of energy piles in the ground sourced heat pump systems.

The ground sourced heat pump systems (GSHP) work by utilising the constant temperature of the ground or groundwater beneath a building (typically 10 to 14 degrees Celsius in the UK) to provide cooling in the summer and/or heating in the winter to the building.

The hydraulic and thermal conductivities and the volumetric specific heat capacity of soils are the properties that most affect the design of a ground source heat pump system (Austin, et al. 2000). The hydraulic and thermal conductivities will control the rate at which heat will be transferred to and from the heat exchange tubing installed into the energy piles. This will affect the number of energy piles required (the higher the thermal conductivity of soil the lower the number of piles), while the volumetric specific heat

capacity is important in calculating the amount of energy that can be extracted or stored in a unit volume of ground. Finding these parameters is more problematic, and as such a number of methods have been suggested or are currently used. These are described in chapter two.

Ground sourced heat pump systems can greatly reduce the energy demand for heating and cooling requirements of buildings by exchanging heat with the ground. Since there is little reliance on other fuels, geothermal energy is less sensitive to the conditions of the international energy markets. This will reduce risk of over reliance on imported energy from regions that are not necessarily stable as the Middle East which is the world's largest producer of oil. Therefore, there is a requirement to reduce energy consumption for environmental, economic and strategic reasons.

The ground will act as either a heat source or a heat sink. When there is a difference in thermal potential between the building and the ground, heat will be transferred from the building to the ground and vice versa. There are two techniques used to transfer the heat; namely an open system or a closed system. An open system (Figure 1.2) is one in which water is pumped from the ground into the building. This system operates only in granular soils in which the hydraulic conductivity is great enough to allow groundwater to flow at sufficient rate to conduct heat away from the boreholes. In this case convection becomes significant and the hydraulic conductivity will be the key parameter of the soil. This can be measured using existing laboratory and in situ testing techniques.

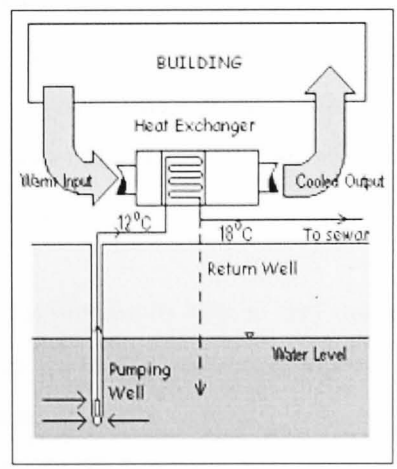

Figure 1.2 An open system to exchange heat between the building and the ground (http://www.arup.com)

A closed system (Figure 1.3) operates in any soil. Heat will be transmitted into the soil by either conduction or convection. In this case thermal conductivity of the soil mass is the key factor to an economic design of the system. Again convection could become significant in granular soils in which the hydraulic conductivity is high enough to allow water to flow through the soil. The rate of heat transfer partly depends on the thermal capacity of the ground to store heat. Thus the thermal characteristics of the soil will include the hydraulic conductivity, thermal conductivity and thermal capacity of the ground.

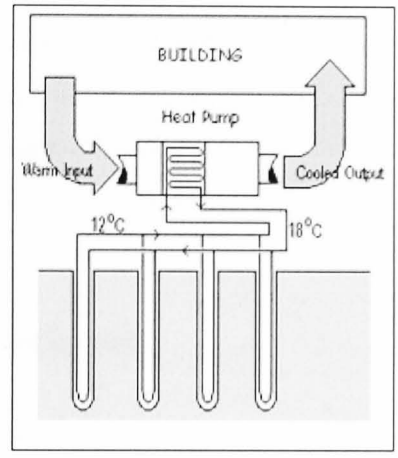

Figure 1.3 A closed system to exchange heat between the building and the ground (http://www.arup.com)

In order to design such systems knowledge of the hydraulic and thermal properties of the ground such as hydraulic conductivity, thermal conductivity and volumetric specific heat are required. Ideally these parameters need to be measured in situ at full scale to take into account any effects of fabric and background hydrological aspects of ground water movement, because movement of ground water will increase the rate of heat transfer in the ground. The characteristics of an element of soil can be measured in a laboratory test on a representative soil sample. This will enable more tests to be carried out during the investigative stage.

The problem of water and heat transfer in soils is very complicated, because, the term of soil, as used by engineers, refers to a complicated material consisting of solid particles of various compositions (mineral and/or organic) and various shapes and sizes that are randomly arranged with pore spaces between them. These pores contain air and usually water in its various phases as vapor, liquid or ice. The water may also contain mineral salts and ions.

The soil characteristics affecting hydraulic and thermal conductivities are interrelated in a very complex manner. The various properties, which affect these two parameters, include particle size, soil composition, fabric, void ratio and degree of saturation as well as the pore fluid characteristics. These factors are discussed further in the following sections.

The hydraulic and thermal properties of the soils can be estimated, for many applications, to sufficient accuracy using published relationships by linking the physical characteristics with the hydraulic or thermal characteristics based on laboratory tests on a range of soils. In other applications, however, more precise values may be required. Therefore laboratory or in-situ tests have to be carried out to determine the exact values of these applications.

1.2 Flow of water through soils

There are differences between flow through a pipe or open channel and flow through soils. When water flows though a conduit, the velocities near the edges are somewhat smaller than those in the centre because of friction or viscosity effects (Bowles, 1984). When water flows through a soil mass under a uniform hydraulic gradient there is no difference of velocity between the centre of the mass and its edges. There is, however a variation within individual pores and discontinuities, such as: cracks and fissures through which the water is flowing.

Figure 1.4 shows the variation of velocity with the hydraulic gradient. This figure can be divided into three zones; zone I is the laminar flow zone, zone II is the transition zone and zone III is the turbulent flow zone.

When the hydraulic gradient is gradually increased the flow remain laminar in zones I and II, and the velocity, v, bears a linear relationship to the hydraulic gradient. At a higher hydraulic gradient the flow becomes turbulent (zone III). In most soils, the flow of water through the void spaces can be considered laminar (Lambe and Whitman 1979, Das 1998) thus:

$$v \propto i \qquad 1.1$$

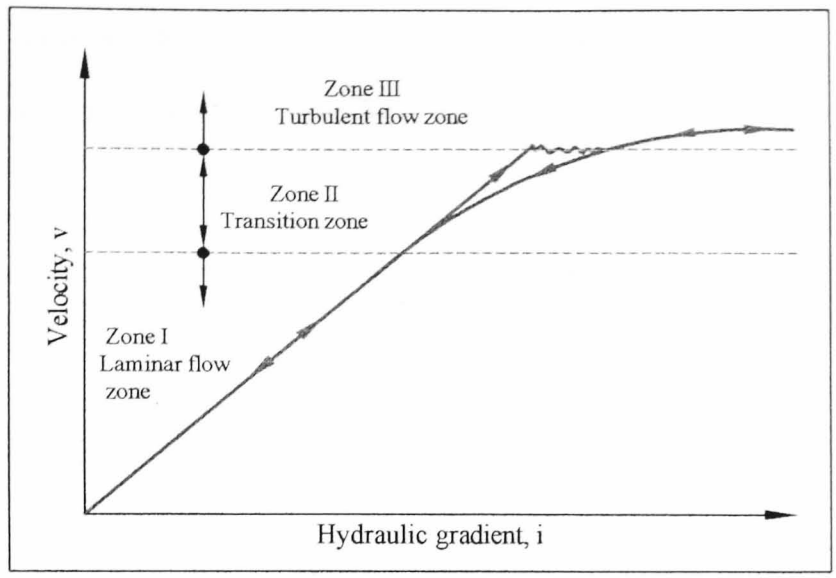

Figure 1.4 Variation of velocity with hydraulic gradient (Das, 1998).

Henri Darcy (1856) quantified the flow of water through soil when he published a simple equation for the discharge velocity of water through clean saturated sand, which may be expressed as:

$$v = k_h \cdot i \qquad 1.2$$

where v is the discharge velocity, which is the quantity of water flowing in unit time through a unit gross cross-sectional area of soil at right angles to the direction of the flow. k_h is the coefficient of hydraulic conductivity, and i is the hydraulic gradient.

Equation (1.2) was based on Darcy's observations about the flow of water through clean sand. Where Darcy's law states that the flow of a liquid through a porous medium is in the direction of force, and at a rate proportional to the driving force acting on the liquid (i.e. hydraulic gradient) and the proportional factor is the property of the conducting medium to transmit the liquid known as the coefficient of hydraulic conductivity (permeability). This law can be written as follows:

$$q = -k_h \cdot i \cdot A = -k_h \cdot \frac{\Delta h}{L} \cdot A \qquad 1.3$$

where q is the rate of flow (m^3/s), i is the hydraulic gradient ($i = -\frac{\Delta h}{L}$), Δh is the head loss across specimen (m), L is the length of a specimen (m), and A is the cross-sectional area of a specimen perpendicular to the flow direction. Figure 1.5 is a schematic diagram used to show the principal of Darcy's law.

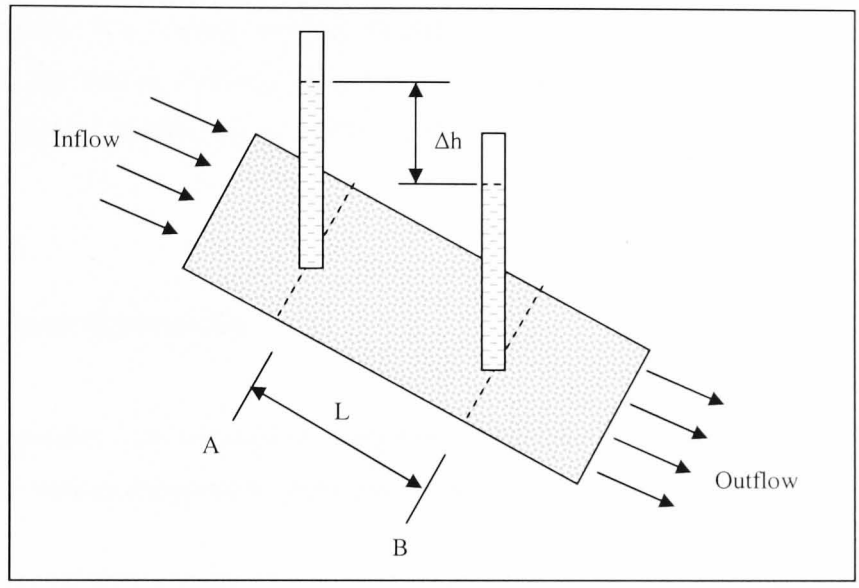

Figure 1.5 Darcy's test diagram

The constant of proportionality, k_h, expressed in equation (1.3) is also termed the coefficient of permeability and is used to define the ability of a fluid to flow through a porous material. This terminology is used by civil engineers, but scientists and hydrogeologists have called it hydraulic conductivity (Daniel, 1994). Daniel argued that the hydraulic conductivity term is consistent with other fields of engineering and science, since constants of proportionality involved in other flow processes are termed conductivity (e.g. electrical and thermal conductivity). Also the use of term hydraulic conductivity helps to eliminate any confusion with intrinsic permeability, K (equation 1.5). Therefore, in this research hydraulic conductivity will be denote by the coefficient k_h in equation (1.3). This coefficient has units of velocity (length per time), m/s in the SI system.

1.3 Factors influencing Hydraulic Conductivity of soils

The hydraulic conductivity of soil is not constant; it depends on the soil characteristics and on the permeant characteristics. The various characteristics which affect the hydraulic conductivity of a soil include particle size, void ratio, soil composition, fabric, degree of saturation, and effective stress. These characteristics are interrelated in a very complex manner (e.g. fabric usually depends on particle size, void ratio and composition). The testing method and procedure can also affect hydraulic conductivity. Some of the factors influencing hydraulic conductivity are discussed in the following paragraphs.

1.3.1 Influence of permeant

Different permeants can be used to perform a hydraulic conductivity tests. These permeants can vary in composition from pure water.

The governing permeant properties are viscosity and specific weight. Taking these properties of the permeant into account, an alternative form of Darcy's law can be expressed as:

$$q = K \cdot \frac{\gamma}{\mu} \cdot i \cdot A \qquad 1.4$$

Where γ is the unit weight of the permeant and μ is the viscosity of the permeant. K is specific or absolute permeability (Lambe and Whitman, 1979), it is in units of length^2 but it is sometimes termed intrinsic permeability (Olson and Daniel, 1981).

$$K = \frac{k_h \cdot \mu}{\gamma} \qquad 1.5$$

Other important characteristics of the permeant water are the amount of dissolved air in the water, the type and concentration of electrolytes, turbidity, nutrient content and population of micro organisms (Daniel, 1994). Air contained in the water tends to form bubbles as it flows through the narrow voids between soil particles. These bubbles of air

in the voids can obstruct the flow of water, there by giving an inaccurately low measurement of hydraulic conductivity (Head, 1994). Therefore deaired water was used to perform the hydraulic conductivity tests in this research.

Hydraulic conductivity of clayey soils can be influenced by electrolytes. Most clay minerals are negatively charged, plate shaped particles. The soil water and cations (positively charged ions) in the soil water are attracted to the surface of the clay particles. The forces of attraction are so strong that the water and cations immediately adjacent to the clay particles are said to be "adsorbed" to the particle and to form what is known as a "diffuse double layer" or "electrical double layer" around soil particle. The adsorption is of sufficient strength that both the soil particles and the double layer serve to block flow paths (Daniel, 1994). Figure 1.6 indicates that the thicker the double layer, the more narrow the flow paths through the soil and, hence the lower the hydraulic conductivity.

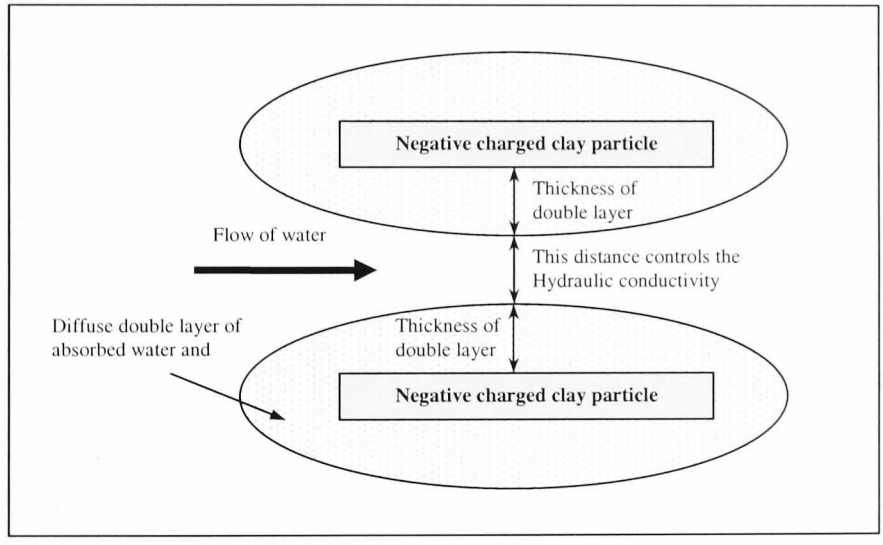

Figure 1.6 Diffuse double layer and its effect on Hydraulic conductivity (from Daniel, 1994).

This influence of permeant on hydraulic conductivity may be predicted by the Gouy-Chapman theory (Mitchell, 1993). The theory states that the thickness of the double layer surrounding the soil particle, T, is proportional to the dielectric constant, D, of the pore liquid and the electrolyte concentration, n_o, and the cat ion valence, i.e.

$$T\alpha\sqrt{\frac{D}{n_o \cdot v^2}} \qquad 1.6$$

According to the Gouy-Chapman theory, an increase in electrolyte concentration or an increase in cation valence will tend to decrease the hydraulic conductivity. Permeation with distilled water tends to produce a very low hydraulic conductivity because its electrolyte concentration is equal to zero, i.e. $n_o = 0$. Therefore, distilled water should never be used with clayey soils, except for special research applications, because it leaches electrolytes from the soil water, which expands double layers and reduces hydraulic conductivity (Daniel 1994).

Olson and Daniel (1981) presented data on the effects of micro organisms on the hydraulic conductivity. Nutrient content can also affect hydraulic conductivity, where Nutrients can promote growth of micro organisms, which tends to reduce hydraulic conductivity (Daniel, 1994).

1.3.2 Influence of particle size

Taylor (1948) developed an equation (1.7) that reflects the influence of the permeant and the soil characteristics on hydraulic conductivity. This equation is based on considering the flow through a porous media similar to flow through a bundle of capillary tubes.

$$k_h = D_s^{\,2} \frac{\gamma}{\mu} \frac{e^3}{(1+e)} C \qquad 1.7$$

where

D_s = some effective particle diameter

γ = unit weight of permeant

μ = viscosity of permeant

e = void ratio

C = shape factor

This equation suggests that hydraulic conductivity varies with the square of some particle diameter. It is logical that the smaller the soil particle the smaller the voids, which are the flow channels, and thus the lower the hydraulic conductivity. A relationship between hydraulic conductivity and particle size is much more reasonable in silts and sands than in clays, since in silts and sands the particles are more

equidimensional and the extremes in fabric dimensions are less (Lambe and Whitman, 1979).

From experimental work in water treatment plants on rapid sand filters, with D_{10} ranging from 0.1 and 3 mm and a uniformity coefficient less than 5, Hazen proposed the following expression (Head, 1994):

$$k_h = C \cdot D_{10}^{\ 2} \qquad 1.8$$

Where k_h is the hydraulic conductivity in cm/s and D_{10} is the effective particle size obtained from the particle size distribution curve in cm. C is a coefficient that varies with particle size and particle size distribution (Table 1.1).

Table 1.1 Value for Hazen's coefficient C (Bowles, 1984)

C	Sand (any or all of the following applies)
40-80	Very fine, well graded or with appreciable fines
80-120	Medium coarse, poorly graded; clean, coarse but well graded
120-150	Very coarse, very poorly graded, gravely, clean

In coarse materials, the finer particles have the most influence on hydraulic conductivity. Therefore, Hazen chose the 10% size, D_{10}, as the effective particle size. It is believed that in coarse grained materials where inter particle bonding (hydrodynamic stability) is relatively weak compared to fine grained materials, the smallest particles can move under the seepage force imposed by a hydraulic gradient. As a result, the hydraulic conductivity of some materials can be altered. In uniform coarse soils containing fines, the fines can be removed by the flow increasing hydraulic conductivity. Also in well graded coarse soils, flow could displace fines clogging some pores, thus reducing the hydraulic conductivity.

1.3.3 Influence of Void Ratio

A decrease in void ratio for any given soil will lead to a decrease in hydraulic conductivity since the void passages will decrease in size. Several empirical equations for estimating the coefficient of hydraulic conductivity have been developed.

For sandy soils, there is an equation proposed by Kozeny in 1927 and modified by Carman in 1939. This equation is now known as the Kozeny-Carman equation and is written as:

$$k_h = \frac{1}{C_o \cdot S_o^{\,2}} \cdot \frac{\gamma}{\mu} \cdot \frac{e^3}{(1+e)} \qquad 1.9$$

where

C_o = shape factor, equal to 5 for spherical particles

S_o = specific surface of the grains of the soil

γ = density of the permeating fluid

μ = viscosity of the permeating fluid

Equation (1.9) relates hydraulic conductivity to particle size (D_{10}), void ratio (e), angularity of particles (C_o), specific surface (S_o), and viscosity of fluid (μ). They also indicate that the coefficient of hydraulic conductivity is a linear function of $e^3/(1+e)$. Other theoretical equations have suggested that k_h is a linear function of $e^2/(1+e)$ or e^2. In general, e versus log k_h is close to a straight line for nearly all soils (Lambe and Whitman, 1979). According to Taylor (1948), theoretical equations including the Kozeny-Carman equation, work adequately for sands but could not be applied to clays. For clayey soils, he suggested that a plot of void ratio against logarithm of the coefficient of hydraulic conductivity approximates a straight line, i.e,

$$\log k_h = \log k_o - \frac{e_o - e}{C_k} \qquad 1.10$$

where

k_h = coefficient of hydraulic conductivity at a void ratio e

k_o = in situ coefficient of hydraulic conductivity at a void ratio e_o

C_k = hydraulic conductivity change index

Tavenas *et al.* (1983) suggested that a linear relationship such as equation (1.10) is more representative of the hydraulic conductivity of natural clays in the range of void ratio values usually encountered in practice, i.e. $0.8 \le e \le 3$. The constant of proportionality

C_k in equation (1.10), the hydraulic conductivity change index, was defined as the slope of the Δe versus $\Delta \log k_h$ curve. He observed that C_k could be related to the initial void ratio of natural normally consolidated clays by

$$C_k = 0.5 e_o \qquad 1.11$$

A similar value was obtained by other researchers (Leroueil *et al.*, 1990, 1992, Sivakumar Babu *et al.*, 1993 and Mesri *et al.*, 1994). More recently, there has been a tendency of normalising the void ratio-hydraulic conductivity relationship with respect to the void ratio at liquid limit state, e_L i.e.

$$\frac{e}{e_L} = a + b \log k_h \qquad 1.12$$

Where a and b are constants as presented by Nagaraj *et al.* (1993 and 1994). According to these authors, the water content at the liquid limit state can be considered as a reference state, since at this state the consolidation-suction pressures are usually of the order of 5 to 6 kPa for all fine-grained soils and the shear strength at the liquid limit is usually of the order of 1.7 to 2.2 kPa for all clays. However, experimental results do not always support such relationships (Achari and Joshi, 1994; Stepkowska *et al.*, 1995; Harwood *et al.*, 1996). Achari and Joshi (1994) and Harwood *et al.* (1996) suggested that equation (1.12) cannot generalize the hydraulic conductivity characteristics of all soils and only has limited accuracy. Stepkowska *et al.* (1995) studied the consolidation and hydraulic conductivity of specimens of dredged sludge in odometer tests and triaxial tests. They observed that the liquid limit value could be influenced by pore fluid viscosity and therefore might not be a reliable parameter to use in such relationships.

1.3.4 Influence of soil composition

The hydraulic conductivity of a soil depends on the type of minerals, on the amount of each mineral, on the type of absorbed cation, on the size distribution and shape of particles, and on the pore water composition. The influence of soil composition on hydraulic conductivity is more accentuated in clays. Increasing the amount of clay minerals lowers the hydraulic conductivity. Such a factor is of little importance when

considering the hydraulic conductivity of silts, sands and gravels, unless organic matter is present (Lambe and Whitman, 1979).

The surface of soil particles, i.e. the interface between the solid phase and liquid phase, is the seat of many physico-chemical phenomena, which play a major role in the nature and behaviour of a given soil. The intensity of physico-chemical phenomena varies with different soils and depends on the mineralogical composition of the soil particles, on the chemical composition of the pore water and on the surface of the particles.

Soil particles, as a result of the unbalanced nature of the ions located within the surface, are capable of attracting and holding water layer and ionic double layer around the particle. The type of cation and the thickness of the double layer, as mentioned previously, have a considerable effect on hydraulic conductivity. The thicker the double layer surrounding the surface of the soil particle, the smaller is its hydraulic conductivity, because a greater proportion of the volume of pores is occupied by the very strongly held adsorbed water.

1.3.5 Influence of soil structure (Fabric)

According to Mitchell (1993), the term fabric is associated with the arrangement of particles, particle groups and pore spaces in soils. Lambe and Whitman, 1979 state that the term soil structure, some times called fabric, refers to the orientation and distribution of particles in a soil mass. They also believe that fabric is one of the most important soil characteristics influencing hydraulic conductivity, especially for fine-grained soils. The fabric of a particular soil depends on the conditions during deposition, and on the subsequent history of chemical, physical and stress changes which have occurred. Laboratory measured hydraulic conductivity on small specimens of clay cannot be representative of the in situ condition because of the effects of fabric. Therefore in situ tests can provide more valuable data than laboratory methods since larger masses of soil and effects of fabric are tested.

Two extremes of soil structure (Figure 1.7), namely "dispersed" and "flocculated", exhibit a great difference in hydraulic conductivity. It has been found, Lambe and Whitman (1979), that by comparing soil specimens at the same void ratio, the specimen which is in the most flocculated state has the highest hydraulic conductivity, and the one

in the most dispersed state has the minimum hydraulic conductivity. The main factor is that in a flocculated soil there are some large channels available for flow. Since flow through one large channel is much greater than flow through a number of small channels having the same size of total channel areas as the one large channel (Lambe and Whitman, 1979). The implication of this conceptual model is that there can not be a simple relationship between void ratio and hydraulic conductivity.

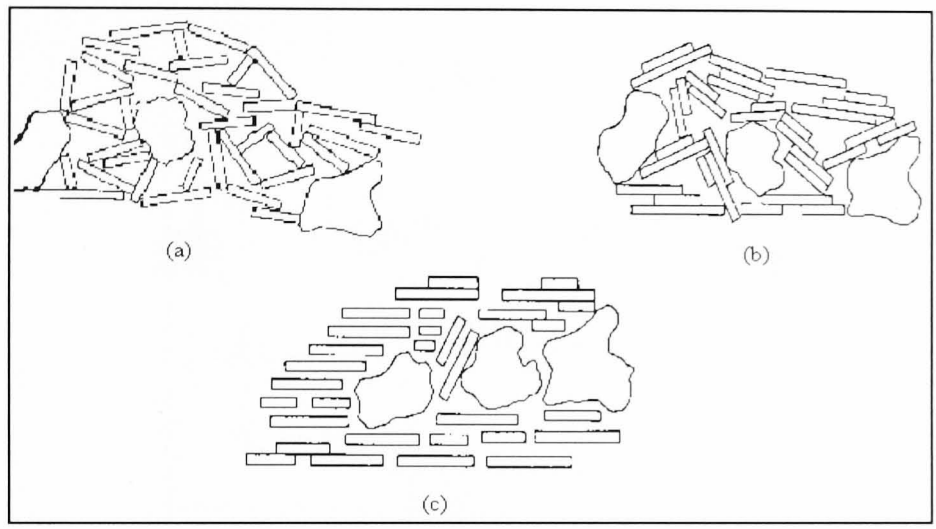

Figure 1.7 Structure of soil a) Flocculated b) Moderately flocculated c) Dispersed (After Lambe and Whitman 1979).

1.3.6 Influence of Saturation

The degree of saturation of a soil has an important influence on its hydraulic conductivity. During flow, depending on the magnitude of the gradient and the size of the soil particles, bubbles of air can flow through the specimen or stop in a channel constriction and clog it (Araruna, 1995), consequently reducing the hydraulic conductivity. The higher the degree of saturation the higher the hydraulic conductivity. Figure 1.8 presents test data on four sands. Although it suggests a unique relationship between degree of saturation and hydraulic conductivity, the development of a relationship between the two is not feasible because of the great influence of fabric (Lambe and Whitman, 1979).

Various methods have been used for specimen saturation. In a flexible wall cell the use of back pressure is used to ensure a satisfactory degree of saturation and yield the best results (Head, 1986).

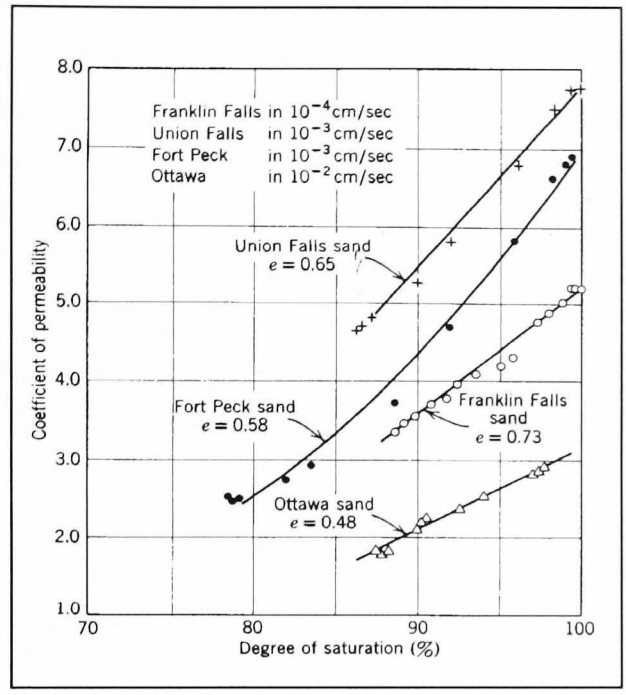

Figure 1.8 Hydraulic conductivity versus degree of saturation
(after Lambe and Whitman, 1979)

1.3.7 Influence of temperature

It can be seen from equation 1.5 that the hydraulic conductivity is not constant for a given soil but it is related to the viscosity of the fluid, μ. Viscosity varies with temperature. Hydraulic conductivity of a soil using water as permeant changes about 3% for every 1 °C change in temperature (Head 1994 and Daniel 1994). Therefore the hydraulic conductivity at any temperature (k_{hT}) can be related to a standard temperature of 20°C by the following relation using the ratio of the fluid viscosity at any temperature (μ_T) to that at 20 °C (μ_{20}).

$$k_{h20} = k_{hT} \cdot \left(\frac{\mu_T}{\mu_{20}} \right) \qquad 1.13$$

1.3.8 Influence of Effective Stress

Effective stress controls changes in volume of soil. Therefore it is reasonable to assume that hydraulic conductivity is influenced by effective stress since it is related to the volume of pores. Therefore, to determine the relevant coefficient of hydraulic conductivity, tests should be carried out at the correct stress level, that is at the in situ stresses and at the final stress level after loading or unloading (Chen, 1997). The effective stress at the effluent end of the test specimen is always higher than that at the influent end (Figure 1.9), and the higher the hydraulic gradient, the larger this difference. Since the application of increasing effective stress tends to reduce void ratio and hydraulic conductivity, there is a tendency for the test specimen to have lower hydraulic conductivity at the effluent end compared to the influent end (Daniel, 1994).

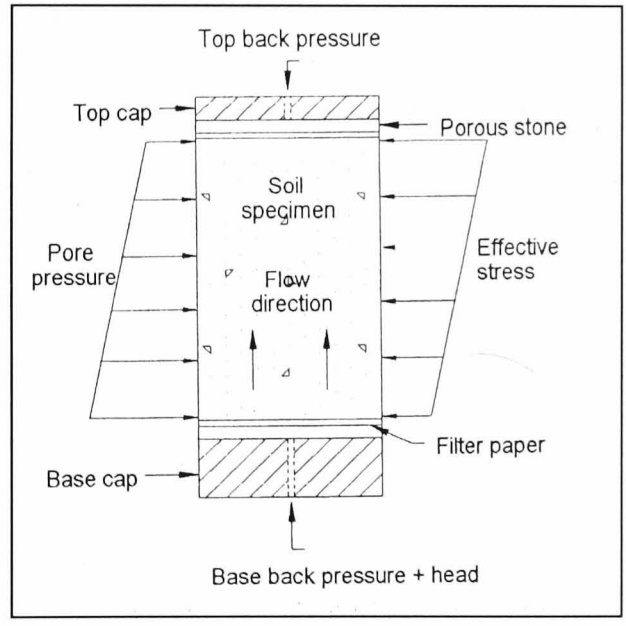

Figure 1.9 Effective Stress Distribution on test specimen
(After Carpenter and Stephenson, 1986)

1.4 Flow of heat through soils

Heat flow through soils is almost entirely by conduction, with radiation unimportant and convection important only if there is a high flow rate of water or air, as might possibly occur through a coarse sand or rockfill. Therefore the thermal conductivity is the essential property that controls heat flow (Mitchell 1993). Heat always conducts in soils

from warmer regions to cooler regions. The composition of any soil affects its conduction rate.

1.4.1 Mechanisms of heat transfer in soils

The thermal conductivity is a physical property of the material. It is a measure of the materials ability to transfer heat. The thermal conductivity of a soil is the rate at which heat energy flows across a unit area of the soil due to a unit temperature gradient. To achieve economical and efficient design of energy piles systems, it is important that we understand the physical mechanisms of heat transfer and that we be able to use the right equations that quantify the amount of energy being transferred per unit time between the building and the ground. Heat transfer in soils occurs due to a number of mechanisms. There are three major mechanisms, include conduction, convection and the transfer of heat due to water phase change, also known as latent heat of vaporisation. It should be noted that the transfer of heat by radiation can occur in certain specialised cases. Although, heat is transferred mainly by conduction in normal circumstances which justifies the use of the term conductivity, other mechanisms may contribute in some measure to the heat transfer (Farouki, 1986).

1.4.1.1 Conduction heat transfer

Heat conduction occurs in all soil constituents, i.e. in the soil solids, the water (liquid, vapor or ice) and the pore air. When a temperature gradient exists in soil, energy is transferred from the high-temperature region to the low temperature region by conduction and the heat transfer rate per unit area is proportional to the normal temperature gradient (Holman, 1997). This is known as Fourier's law.

Fourier made very significant contributions to the analytical treatment of conduction heat transfer and summarized them in Fourier's law of heat conduction. It is an empirical law based on observation. It states that the rate of heat flow, $\Delta Q/\Delta t$, through solid or porous materials is directly proportional to the area, A, of the section at right angles to the direction of heat flow (Figure 1.10), and to the temperature gradient in the direction of the heat flow, $\Delta T/\Delta L$ i.e.

$$Q = B \cdot A \cdot \Delta T \qquad 1.13$$

Defining the proportionality constant B as the thermal conductivity (k_t) (W/m.°C) of the material, Fourier's Law can be expressed as:

$$Q = -k_t \cdot A \cdot \frac{\Delta T}{\Delta L} \qquad 1.14$$

Where:

Q = the heat transfer rate, Watts,

k_t = the thermal conductivity, W/m °C,

A = the surface area, m^2,

ΔT = the temperature difference across the material, °C and

ΔL = the length of the material, °C.

The minus sign indicates that heat flows in the direction of decreasing temperature. Therefore Fourier's Law is a vector relationship. The rate of heat transfer has magnitude and direction.

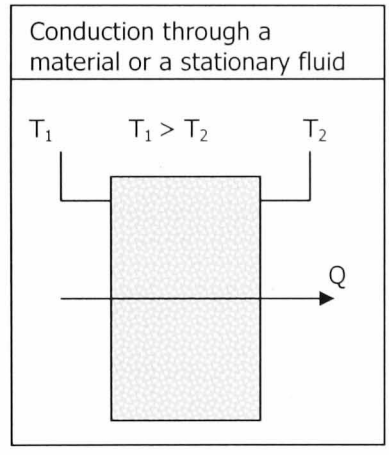

Figure 1.10 Conduction heat transfer.

1.4.1.2 Convection heat transfer

It is well known that a hot plate of a metal will cool faster when placed in front of fan than when exposed to still air. It is said that the heat is convected away, and this process is called convection heat transfer. Convection heat transfer may be classified according to the nature of the flow. It is forced convection when the flow is caused by external means, such as by a fan (Figure 1.11*a*), a pump (hydraulic gradient), or atmospheric winds. In contrast, for free or natural convection the flow is induced by buoyancy forces, which arise from density differences caused by temperature variations especially

in coarse dry soils. Figure 1.11*b* show an example of natural convection (free convection) occurs from hot components on a vertical array of circuit boards in still air. Air that makes contact with the soil surface experiences an increase in temperature and hence a reduction in density. Since it is now lighter than the surrounding air, buoyancy forces induce a vertical motion causing warm air to rise from the soil surface and be replaced by an inflow of cooler ambient air. However there are convection processes for which there is latent heat exchange. This latent heat exchange is generally associated with phase change between liquid and vapor states of the fluid. Two special cases are boiling and condensation (Figure 1.11 *c* & *d*) convection occurs in granular soils in which the hydraulic conductivity is great enough to allow groundwater to flow at sufficient rate. In this case convection becomes significant and the hydraulic conductivity will be the key parameter of the soil, because this will cause a substantial increase in the thermal conductivity of soil mass (Sanner et al. 2000, Enercret, 2004). The heat flux generated by liquid or gas convection is governed by Newton's law of cooling:

$$Q = h \cdot A \cdot (T - T_{\infty}) \qquad 1.15$$

Where:

Q = the heat transfer rate, Watts,

h = the convection heat transfer coefficient, $W/m^2\,^{\circ}C$,

A = the surface area, m^2,

T = the surface temperature, $^{\circ}C$ and

T_{∞} = the surrounding temperature, $^{\circ}C$.

Convection, which occurs in fluids, becomes increasingly important as the pore size increases and can become significant in granular soils. Convection can be due to a change in density created by temperature changes or by differences in potential (hydraulic gradient) causing ground water to flow. Therefore it becomes significant only in granular soils in which the hydraulic conductivity is high enough to allow water to flow through the soil at sufficient rate, because this will cause a substantial increase in the thermal conductivity of the soil mass.

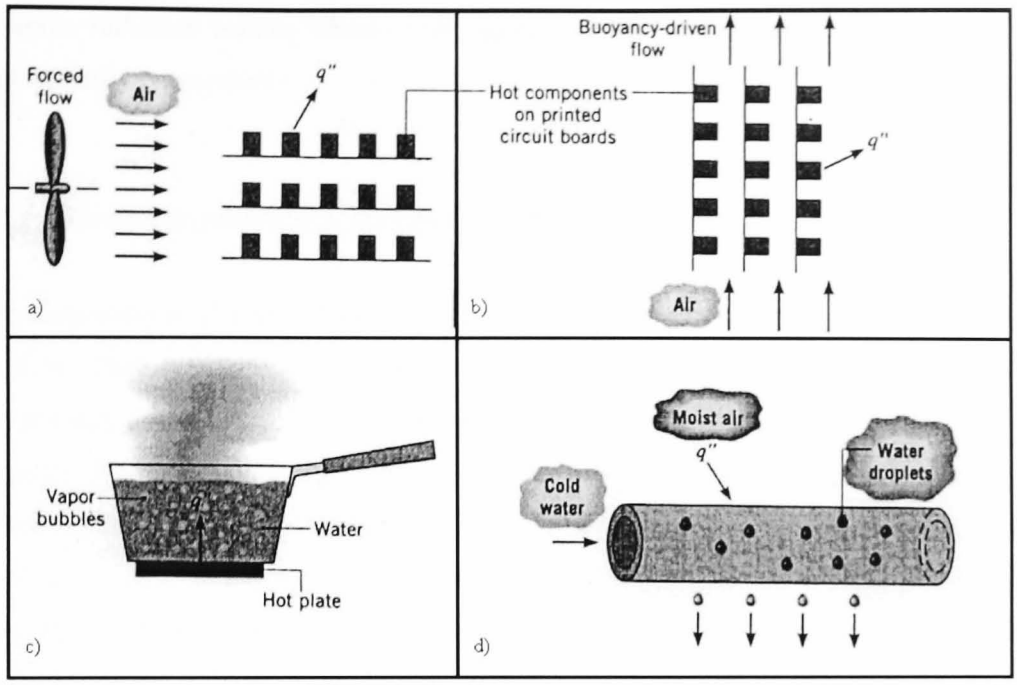

Figure 1.11 Convection heat transfer processes. (a) Forced convection. (b) Natural convection. (c) Boiling. (d) Condensation. (after Incropera and DeWitt, 1996)

1.4.1.3 Radiation heat transfer

In contrast to the mechanisms of conduction and convection, where energy transfers through a material medium is involved, heat may also be transferred through regions where a perfect vacuum exists. The mechanism in this case is electromagnetic radiation which is propagated as a result of a temperature difference; this is called thermal radiation. Thermodynamic considerations show that an ideal radiator will emit energy at a rate proportional to the fourth power of the absolute temperature of the body and directly proportional to its surface area (Holman, 1997). Thus

$$q_{emitted} = \sigma \cdot A \cdot T^4 \qquad 1.16$$

Where

q = the heat transfer rate, Watts,

σ = Stefan-Boltzmann constant, 5.669×10^{-8} W/m^2. K^4,

A = the surface area, m^2, and

T = the surface temperature, ^{o}C.

In soils, radiation usually makes a negligible contribution to heat transfer at normal atmospheric temperatures.

1.5 Factors influencing thermal conductivity of soils

The transmission of heat within soil is dependent on the physical properties of the soil particles, their degree of compaction, and the moisture content of the soil. Because of the porosity and the variability of the amounts of air and water contained in the soil, the analysis of heat flow through soil is much more complicated than for a homogeneous solid, for which thermal conductivity and heat capacity are stable, well-defined parameters. Soil is a composite of mineral particles, organic matter, and pores which may contain either water or air. All these differ widely in their thermal characteristics. Physical characteristics of soils are interrelated, for example any changes in soil structure, leads to change in density or porosity. Drying of cohesive soil leads to shrinkage and consequent fissuring, while water intake leads to swelling. The processes of freezing and thawing similarly lead to excessive compositional and structural changes, with consequent changes in the soil's thermal conductivity.

1.5.1 Influence of pore and particle size

The importance of heat transfer at the contacts or interfaces between soil particles has been recognized and stressed (Smith 1942, Baver et al. 1972, Farouki 1986, Tarnawski et al. 2002). No matter how high the intrinsic solid thermal conductivity, the contact conduction will be the major factor limiting the effective overall conduction (Farouki 1966). While this applies particularly to dry soils and soils with low water contents, general interfacial effects (i.e. solid/liquid, solid/air and liquid/ air as well as solid/solid) maintain their importance to heat transfer in all types and conditions of soils. At low water content the water molecules form films on the soil particles which are only a few molecules thick. The films are uniform thickness and do not improve the thermal contact between the soil particles, so that heat flow is not appreciably enhanced. The amount of water required to produce films of a given thickness depends on the specific surface area of particles which is a function of particle size and shape (Sepaskhah and Boersma 1979).

Nusier and Abu-Hamdeh (2003) found that sandy soils had higher thermal conductivity values than loam soils at all bulk densities. They explained that based on Tavman's (1996) conclusion. Tavman (1996) concluded that the decrease of effective thermal conductivity with decrease in grain size due to the fact that as the grain size decrease, more particles are necessary for the same porosity, which means more thermal resistance between particles. It is also due to the fact that fine grained soils have a higher thermal resistivity than coarse grained soils, and that thermal diffusivity is greater in coarse grained soils.

1.5.2 Influence of soil composition

Typically it has been observed that fine grained soils have a higher thermal resistivity than coarse grained soils, and that thermal diffusivity is greater in coarse grained soils. The thermal conductivities of some of the important soil components are given in Table 1.2. They vary greatly. Quartz has the greatest thermal conductivity and air the least. The differing mineralogy and composition of sand and clay soils are likely to be the primary reason that sandy soils display higher thermal conductivity and diffusivity than clay soils, as the sandy soils contain a greater proportion of quartz. Therefore, the volumetric proportions of the various soil components will influence the effective thermal conductivity of the soil.

Abu-Hamdeh and Reeder (2000) investigated the effects of density, moisture, salt concentration and organic matter on soil thermal conductivity of four types of soils. These soils were classified as sand, sandy loam, loam, and clay loam. Their results showed that the thermal conductivity, for the four soils at similar density and water content, changed as the soil texture changed. It was also found that the sand had higher values of thermal conductivity than clay loam.

Table 1.2 Thermal Properties of soil constituents (Modified after Farouki, 1986)

Material	Density ρ (Mg/m^3)	Specific heat c_p (J/kg °C)	Volumetric heat capacity C (kJ/m^3 °C)	Thermal conductivity k_t (W/m °C)	Thermal diffusivity α (10^{-3} m^2/s)
Quartz	2.65	732.69	1941.6	8.4	4.3
Many soil minerals	2.65	732.69	1941.6	2.9	1.5
Soil organic matter	1.3	1925.92	2503.7	0.25	0.1
Water	1.0	4186.8	4186.8	0.6	0.143
Air	0.0012	1004.8	1.2	0.026	21.56

1.5.3 Influence of Soil Structure or Fabric

The soil structure or packing is important because it describes the arrangement of the solid primary or secondary particles, with respect to each other, and a certain orientation with respect to the direction of the heat flow or the imposed temperature gradient. The finer colloidal grains in natural soils are usually aggregated into larger secondary units of different shapes and sizes. Micro pores exist between the primary particles and macro pores between the larger secondary aggregates (Farouki, 1986).

Other important structural factors influencing the effective thermal conductivity of a soil are the number and nature of the contacts between the soil particles themselves and the effect on these contacts of the other soil components, particularly water. This is because most of the heat transfer occurs across these contact points or areas, especially in the case of dry or nearly dry soils (Farouki, 1986). Present knowledge regarding the bonds between individual soil particles is that in clays, the particles are flat plate shaped and they carry negative charges on the flat surface and positive charges around the edges and at the corners. Therefore interparticle forces of attraction are developed whenever edges or corners chance to come into contact with flat surfaces. The contacts may be end to face or edge to face types as shown in Figure 1.12, A and B. While type C bond when two particles come into contact in a face to face arrangement (Figure 1.12-C), where forces of repulsion between like charges become dominant, but this may

overcome by the combined effect of external loads, cation bonds and hydrogen bonds of the adsorbed water molecules. However in sands, the bonds between the solid grains can be cemented together, e.g. by a clay or other binder, the thermal contact is much improved. Small amounts of clay colloidal particles added to a cohesionless granular material act as a binder and improve the thermal conductivity. With kaolinite, about 8% was found to be the optimum, giving the highest value of thermal conductivity (Farouki 1966). The effective thermal conductivity improved considerably in spite of the much lower thermal conductivity of kaolinite as compared with the quartz grains. Figure 1.13 shows the effect of the percentage of kaolinite on thermal conductivity in a quartz soil. The kaolinite was thought to improve the interfacial conduction characteristics, especially in the nearly dry state. Together with its associated adsorbed water films, the kaolinite provided thermal bridges between the granular skeleton. The overall thermal conductivity of the soil increases as the total contact area increases.

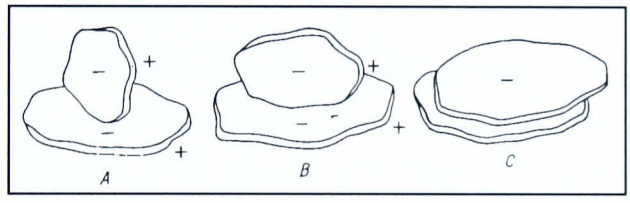

Figure 1.12 Types of bond between plate-like clay particles:
A-Bond on a tip; B-Bond along an edge; C-contact along a plane (Kezdi, 1974)

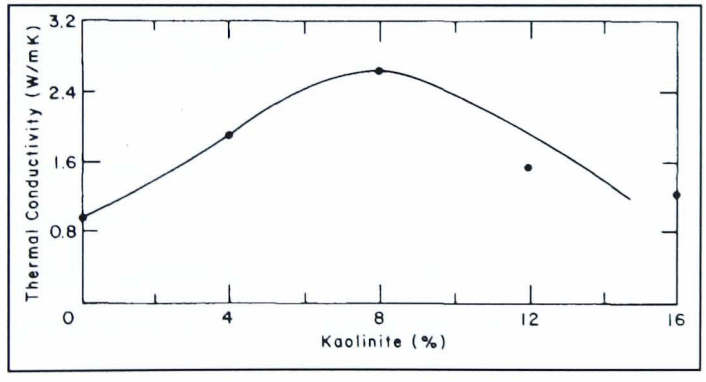

Figure 1.13 Thermal conductivity of quartzite granular material
with kaolinite binder in the nearly dry state (after Farouki 1986).

Thermal conductivity of clayey soil may increases if it contains coarser grains of sand or silt as a result of particle-contact enhancement. The skeleton structure of the soil is made up of sand and silt grains with large voids between them. These large voids are filled with a clay matrix (Figure 1.14) which is more conductive than water or air.

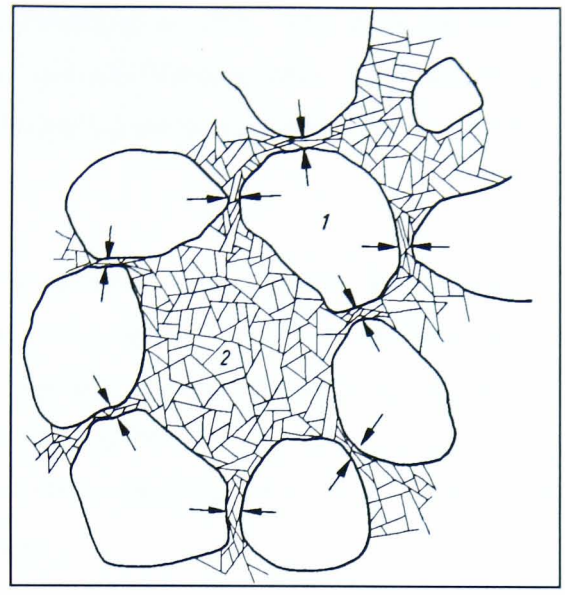

Figure 1.14 Structure of clay when coarse particles are present:
1- Sand particles; 2- Clay particles (Kezdi, 1974)

Data on dry soil materials show that the thermal conductivity of crushed rocks is appreciably greater than that of natural soils having a similar mineralogical composition (Kersten 1949). Van Rooyen and Winterkorn (1959) attributed this to better particle-to-particle contact, possibly due to the different physicochemical properties of the fresh (crushed) material.

1.5.4 Influence of water content

At very low water contents, water is held with extreme tenacity on the surface of the soil particles and within the lattice of crystalline clay minerals (Farouki 1986). More water begins to collect around the points of contact between the particles. This water bridge improves the heat transfer from one grain to another.

An increase in the water content of the soil is directly related to an increase in the soils capacity to transfer heat. This is due to the replacement of air or vapour in pore spaces, by water. As air has a significantly lower thermal conductivity than water (0.024 W/m.°C for air vs. 0.6 W/m.°C for water) the bulk thermal resistivity of the soil is reduced, therefore increasing the effective thermal conductivity of the soil.

In experiments (e.g. Penner et al. 1975, Speaskhah and Boersma 1979, Cary 1979, Farouki 1986, Nusier and Abu-Hamdeh 2003, Abu-Hamdeh and Reeder 2000) it has been found that the thermal conductivity of a soil can vary widely between dry soils and wet soils.

The relationship between thermal conductivity and amount of water in a soil was explored in some details by Kersten (1949) on the basis of numerous tests (Farouki 1986). He proposed empirical equations based on the fact that the thermal conductivity is linearly related to the logarithm of the water content at constant dry density. For unfrozen silt and clay soils containing 50% or more silt and clay, the equation using metric units as following:

$$k_t = 0.1442 \cdot (0.9 \log w_c - 0.2) \cdot 10^{0.6243\gamma_d} \qquad \text{For } w \geq 7\% \qquad 1.24$$

While for unfrozen sandy soils (clean sand) it is

$$k_t = 0.1442 \cdot (0.7 \log w_c - 0.4) \cdot 10^{0.6243\gamma_d} \qquad \text{For } w \geq 1\% \qquad 1.25$$

where γ_d is the dry density in g/cm^3.

Johansen (1975) introduced the following concept of the Kersten number, K_e, to calculate the thermal conductivity of a soil at partial saturation from known values of the thermal conductivity in the saturated state, $k_{t\,sat}$, and that in the dry state, $k_{t\,dry}$.

$$k_t = (k_{t\,sat} - k_{t\,dry}) \cdot K_e + k_{t\,dry} \qquad 1.26$$

This equation of Johansen is basically a simple interpolation between the conductivities in the saturated and the dry conditions that is based on K_e which depends on the degree of saturation. Figure 1.15 shows a plot of the measured and predicted thermal conductivities of sandy and silty soils against the degree of saturation. It indicates that the thermal conductivity increases as the degree of saturation increases (Bachmann et al., 2001).

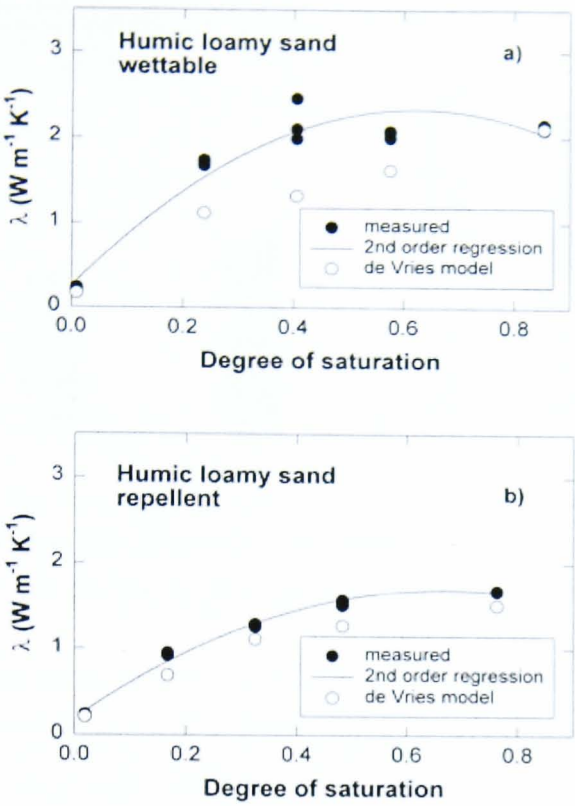

Figure 1.15 Measured and de Vries model-predicted thermal conductivity values for (a) wettable and (b) water-repellent humic sandy loam soil (after Bachmann et al., 2001).

1.5.5 Influence of Soil Density and Porosity

The density and porosity of a soil have an effect on heat transfer. It has been shown that an increase in the dry density of a soil with its associated decrease in porosity leads to an increase in a soil's thermal conductivity characteristics due to the fact that there is more solid matter per unit soil volume, less pore air or pore fluid per unit soil volume and better heat transfer across the inter-granular within the soil. Nusier and Abu-Hamdeh (2003) investigated the thermal conductivity of two soils as a function of the bulk density using single and dual probe methods. The soils used were classified as sand and loam. Figure 1.16 and Figure 1.17 show the thermal conductivity increased with increasing bulk density for the two soils. They concluded that the thermal conductivity increased with increasing bulk density for the two soils as a result of particle contact enhancement as porosity is decreased.

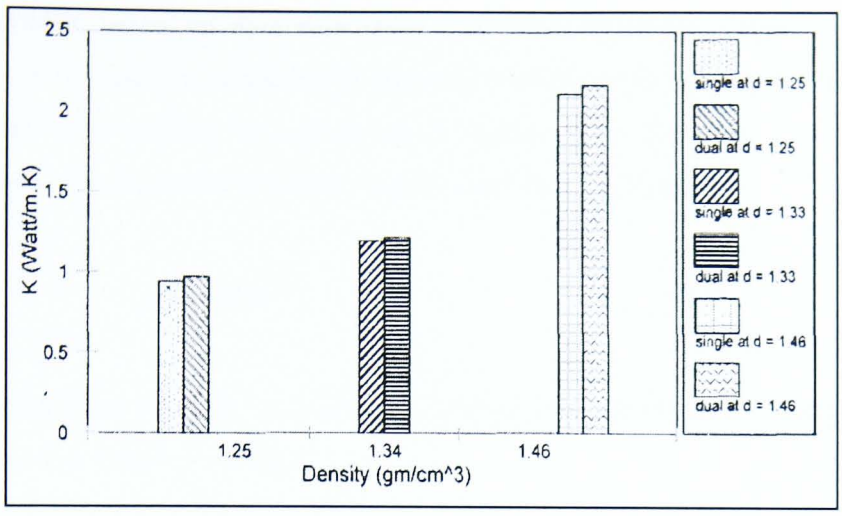

Figure 1.16 Thermal conductivity for sandy soil at three soil densities using single and dual probe methods (Nusier and Abu-Hamdeh, 2003).

An increase in the density of a soil with constant water content effectively leads to an increase in saturation of the soil, again decreasing the air volume in pore spaces and so leading to decreased thermal resistivity in the soil.

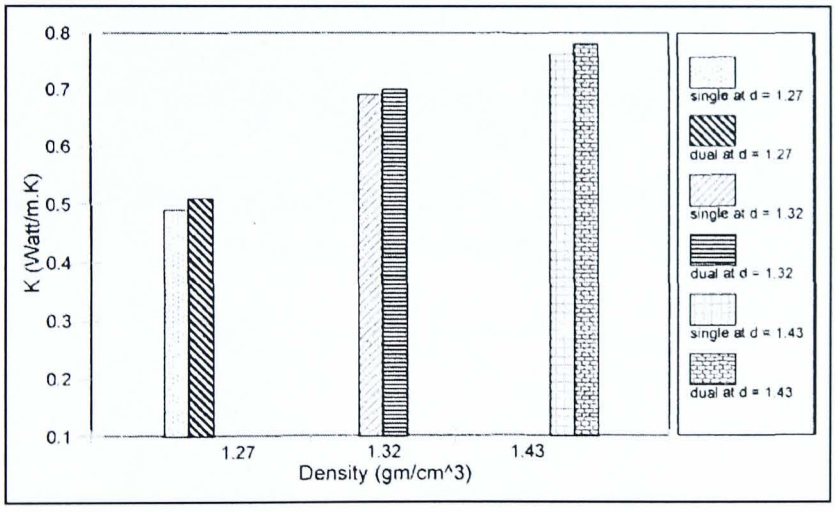

Figure 1.17 Thermal conductivity for loamy soil at three soil densities using single and dual probe methods(Nusier and Abu-Hamdeh, 2003).

In general, researchers (e.g. Smith and Byers 1938, Kersten 1949, Woodside and De Bruyn 1959, Penner 1962) have found a linear trend between the thermal conductivity of a soil or its logarithmic value and the dry density or porosity of that soil (Figure 1.18 to Figure 1.20).

Kersten (1949), based on numerous tests, found that at constant water content the logarithm of the thermal conductivity increased linearly with the dry density and the slope of the linear relation for a given soil is approximately the same for the different water content. He expressed this behaviour by the following equation:

$$k_t = A \cdot (10)^{B \cdot \gamma_d} \qquad 1.27$$

Where A and B are empirical parameters depend on whether the soil is sandy or clayey and whether it is frozen or unfrozen.

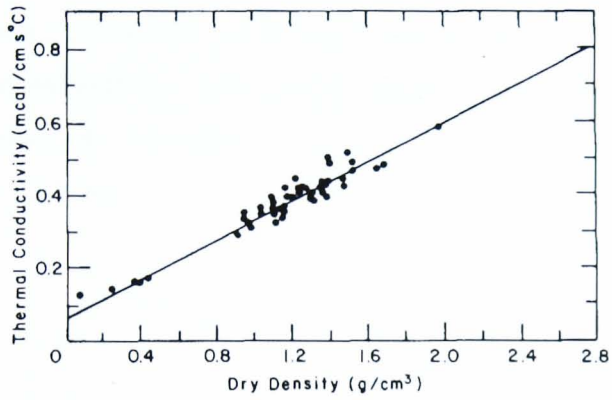

Figure 1.18 Thermal conductivity of dry soils as a function of dry density (after Smith and Byers 1938)

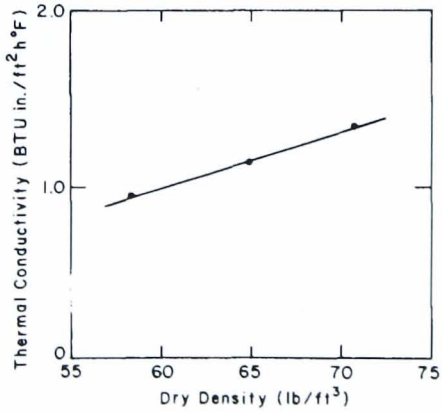

Figure 1.19 Thermal conductivity of dry Leda clay as a function of dry density (after Woodside and De Bruyn 1959)

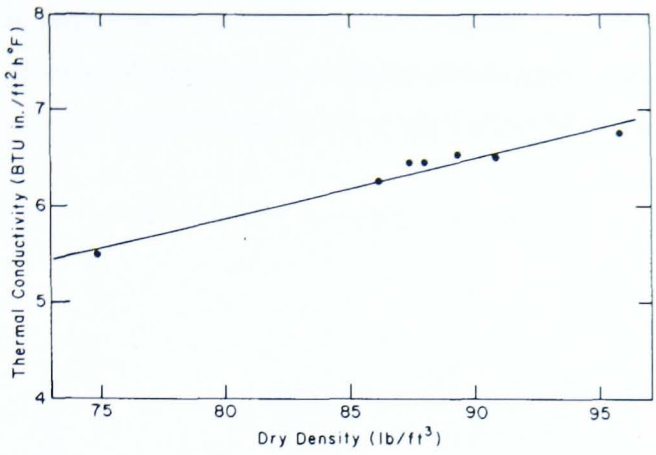

Figure 1.20 Thermal conductivity of saturated Leda clay vs. dry density (after Penner 1962)

The thermal conductivities of sandy and clayey soils at different water content and dry density which were tabulated by the U.S.S.R. Building code (1960) were plotted by Farouki 1986. Figure 1.21 and Figure 1.22 show the lines at various water contents being parallel for a given soil.

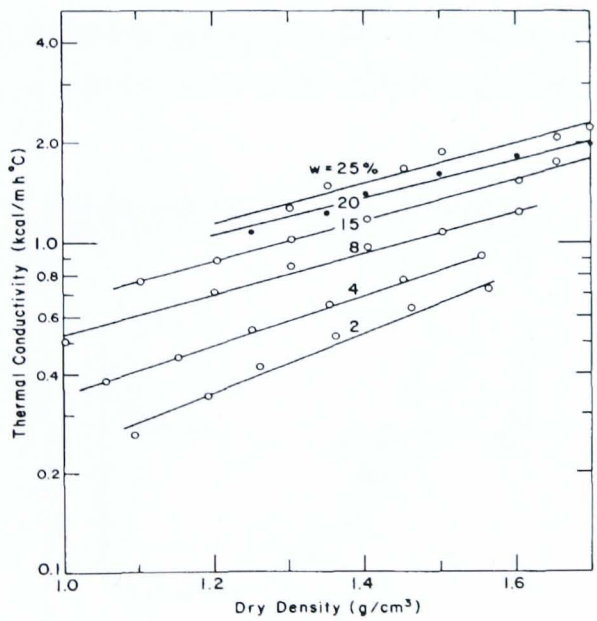

Figure 1.21 Thermal conductivity of sandy soils vs. dry density at constant water content (after Farouki 1986).

Data from Kersten (1949) and Terzaghi (1952) (Farouki, 1986), shown in Figure 1.23, illustrates the variation with porosity of the thermal conductivity of sands and clays,

frozen or unfrozen. Frozen soils are out of the scope of this research, but it can be seen from the Figure that thermal conductivity of frozen soils is appreciably greater than that of unfrozen soils because thermal conductivity of ice is about four times that of water.

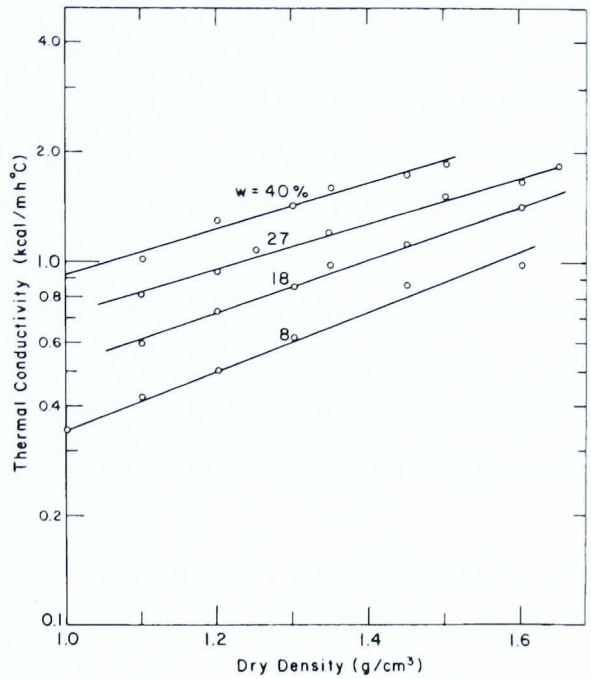

Figure 1.22 Thermal conductivity of clayey soils vs. dry density at constant water content (after Farouki 1986).

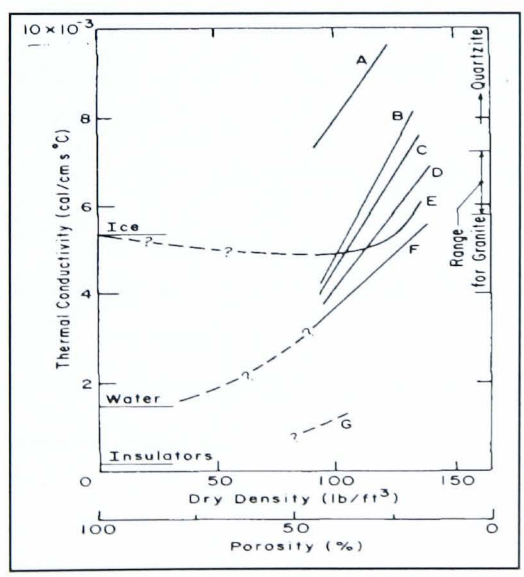

Figure 1.23 Thermal conductivity of Sand and Clay as a function of dry density (after Farouki 1986).

1.6 Aim and Objectives

This thesis is concerned with an experimental investigation for determining the hydraulic and thermal conductivities of different types of soils. The experimental investigation performed for this purpose was carried out using different techniques. Particular emphasis is placed on developing and designing new techniques to determine both the hydraulic and thermal conductivity of soils. The effect of the physical properties of soils on these two parameters was also investigated.

The main aims of this research were to develop a technique for rapidly determining the hydraulic conductivity and to design a simple device to measure the thermal conductivity of soils. This will lead to a better understanding of the effect of the measuring techniques and the effect of the physical properties on these two parameters.

The experimental investigation presented herein consisted of a variety of objectives to achieve the aim of the research.

- A review of the factors affecting the hydraulic and thermal conductivities of soils.
- A review of the different techniques used to determine the hydraulic and thermal conductivities of soils.
- Develop the constant flow flexible wall permeameter for a rapid determination of the hydraulic conductivity of fine soils.
- Design a simple device and produce a testing procedure to determine the thermal conductivity of different types of soils.
- Develop an understanding of the effect of the physical properties on a soil's hydraulic and thermal conductivities.
- Evaluate results of the thermal device by comparing them with published data and thermal conduction models.

1.7 Thesis Outline

Few details are given in other published works regarding specific techniques and equipment used in determining the hydraulic and thermal conductivities of soils.

Therefore it is often difficult to compare results from different authors. This chapter gave a brief review of the theories behind the flow of water and heat in soils and a discussion of the factors affecting the determination of the hydraulic and thermal conductivities of soils. Chapter two presents a review of the existing methods for determining the hydraulic and thermal conductivities of soils in the laboratory.

In Chapter three, the description of the flexible wall permeameters using the constant flow technique and its development to work using the falling head technique are given. In addition a detailed calibration of the instrumentation and the experimental procedure are described.

Chapter four provides information regarding the design criteria and principles are given, as well as theory behind the design and the description of the new device for determining the thermal conductivity of soils. In addition the experimental procedure used is described.

The results of the hydraulic conductivity of soils determined by the flexible wall permeameter using both the constant flow and the falling head techniques are discussed in Chapter five. It is also presents the effect of the void ratio, density and effective stress on the determination of the hydraulic conductivity of soils. A comparison between the results obtained by the constant flow, falling head and constant head techniques to evaluate the modified testing systems are also given in this chapter.

Chapter six presents a discussion of the thermal conductivity results obtained by the new testing system. It gives also a comparison between the experimental results and published thermal conductivity data. The experimental thermal conductivity results are compared with the thermal conductivity results predicted by number of thermal conduction models. Conclusion and recommendations are given in chapter seven.

Chapter 2

Measurement of Hydraulic and Thermal Conductivity of Soils in the Laboratory

2.1 Introduction

There are number of standard and non standard methods to measure the hydraulic and thermal conductivity of soil. There are those that create a constant hydraulic or thermal gradient and the resulting hydraulic or thermal flow is measured. Others allow the hydraulic or thermal gradient to fall as the change in flow is monitored. There are also indirect methods, for example those in which volume changes of the specimen are measured and the hydraulic conductivity is theoretically inferred from those measurements. And finally there are empirical or semi-empirical methods which are used to predict the thermal conductivities.

The following sections give an over view of both the laboratory methods of measuring hydraulic and thermal conductivities and the empirical methods.

2.2 Measurement of Hydraulic Conductivity in the Laboratory

Hydraulic conductivity is one of the most variable engineering properties of soils, and slight change in measurement technique or test equipment can cause a change in the value determined. The coefficient of hydraulic conductivity of a soil is best obtained from a direct measurement which can be performed either in the laboratory or in situ. Laboratory tests are preferred since they are cheaper than in situ tests, and the boundary conditions can be controlled, however in situ tests provide more valuable data since larger masses of soil and effects of fabric are tested. Laboratory tests are more advanced since that the degree of saturation, the hydraulic gradient and the direction of flow can be controlled and monitored using very accurate transducers.

Various laboratory techniques can be used for measuring the coefficient of hydraulic conductivity of soils, namely, constant head, falling head and constant flow. All methods rely on the validity of Darcy's law (Head 1986) which states that the

coefficient of hydraulic conductivity is the ratio of the flow rate to the hydraulic gradient. A summary of their advantages and disadvantages is presented in Table 2.1, and a brief literature review on these various measurement techniques is presented in this section.

Table 2.1 Comparison of hydraulic conductivity measurement techniques in Laboratory

Method	Falling Head	Constant Head	Constant Flow
Principle	Continuous change of hydraulic gradient during test.	Constant gradient is imposed corresponding flow quantity is measured.	Constant quantity of permeant is forced through the specimen corresponding hydraulic gradient is evaluated.
Soil Type	Fine-grained soils such as: fine sand, silt and clay.	Coarse and fine-grained soils such as: sand, silt and clay.	Coarse and fine-grained soils such as: sand, silt and clay.
Advantages	• Simplicity.	• Simple to use. • Simplicity in calculations. • Steady state conditions can be achieved.	• The hydraulic gradient can be minimised. • Seepage induce consolidation can be minimised. • Precise control of flow rate. • Much shorter duration of test, minimises interference due to bacterial growth. • Steady state condition. • Technique suitable for automatic data acquisition.
Disadvantages	• High hydraulic gradient, also seepage induced consolidation. • Longer duration of test required. • No steady state condition achieved. • Complicated equations.	• High hydraulic gradient, also seepage induced consolidation. • Longer duration of test required.	• Complex equipment needed and slightly higher initial cost for the equipment. • Development of extremely large hydraulic gradient when large flow rate is used.

(Modified After Chen, 1997)

2.2.1 Falling Head Technique

The falling head technique is used for testing soils with relatively low hydraulic conductivity such as silts and clays (Olson and Daniel, 1981; Tavenas, et al. 1983; Carpenter and Stephenson, 1986; Head, 1986). It is the one in which the water level in the stand-pipe changes during permeation. There are two possible types of falling head tests, one is falling head with a constant tail-water pressure test and the other is falling head with a rising tail-water pressure test. The test with constant tail-water pressure tends to be more convenient for testing soils with hydraulic conductivity greater than about 1×10^{-5} m/s while the rising tail-water pressure test tends to be more convenient for hydraulic conductivity less than about 1×10^{-9} m/s (Daniel, 1989; Das, 1997).

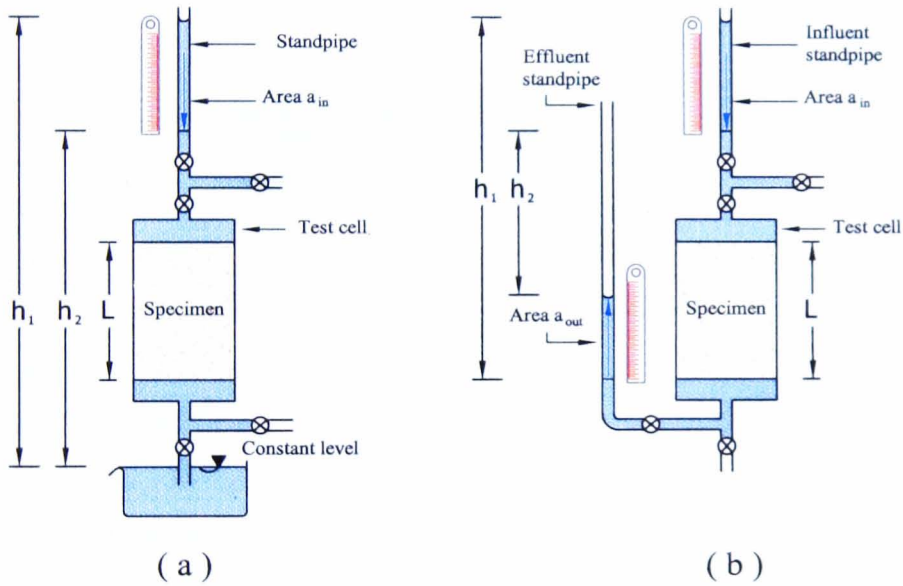

Figure 2.1 Typical arrangement of Falling head Tests:
(a) with constant tail-water pressure, (b) with rising tail-water pressure.

A typical arrangement of the falling head techniques are shown in Figure 2.1a and Figure 2.1b. Figure 2.1a shows the head or height of water in the stand pipe falls from h_1 to h_2, over an elapsed time t_1 and t_2. The vertical coefficient of hydraulic conductivity, k_h can be calculated from the following equations:

1. For constant tail-water pressure:

$$k_h = \frac{a \cdot L}{A \cdot t} \cdot \ln\left(\frac{h_1}{h_2}\right) \qquad 2.1$$

where

a = area of cross-section of the influent standpipe

A = area of cross-section of the soil specimen

L = length of soil specimen

t = elapsed time between determination of h_1 and h_2

h_1 = hydraulic head at time t_1

h_2 = hydraulic head at time t_2

2. For raising tail-water pressure:

$$k_h = \frac{a_{in} \cdot a_{out} \cdot L}{A \cdot t \cdot (a_{in} + a_{out})} \ln\left(\frac{h_1}{h_2}\right) \qquad 2.2$$

where

a_{in} = area of cross-section of the influent standpipe

a_{out} = area of cross-section of the effluent standpipe

A = area of cross-section of the soil specimen

L = length of soil specimen

t = elapsed time between determination of h_1 and h_2

h_1 = hydraulic head deference at time t_1

h_2 = hydraulic head deference at time t_2

The primary advantage of a falling head test is that equipment is simpler than for a constant head test. A slight disadvantage of the falling head test is that the equations for computing hydraulic conductivity are more complicated. However, there are significant limitations of the falling head test that have been discussed by some researchers (Pane, *et al.*, 1983; Tavenas, *et al.*, 1983a; Daniel, 1994). The main concern arises from the variation of the head difference imposed on the test specimen during the test. Daniel stated that as the head falls, the pressure drops and any gas bubbles in the test specimen expand.

The amount of dissolved gas that can be held by the liquid decreases, which could release dissolved gas from the permeant liquid and formation of air bubbles if the permeant liquid is saturated with dissolved gas at the initial pressure; and in flexible wall cells for which a constant total stress is maintained, a decline in pore water pressure causes an increase in effective stress- an increase in effective stress causes consolidation and a reduction in void ratio and hence in hydraulic conductivity. Pane et al. (1983) and Tavenas et al. (1983a) suggested that as a result of the variation of the head difference, a steady state flow condition required by Darcy's law is never achieved because the hydraulic gradient is continuously being modified by the falling head. Test durations can be lengthy and if high hydraulic gradients are used to speed up the test, seepage induced consolidation and change of effective stress can affect the specimen.

2.2.2 Constant Head Technique

The constant head technique is described in standards, including BS 1377: 1990, ASTM D2434-68 and D5084-90. It has been used to measure the hydraulic conductivity of coarse soils and fine-grained soils such as sand, silt (Silva, et al. 1981; Tavenas, et al. 1983; Yang and Barbour 1992; Araruna 1995; Chen 1997). A typical set up of the technique is shown in Figure 2.2.

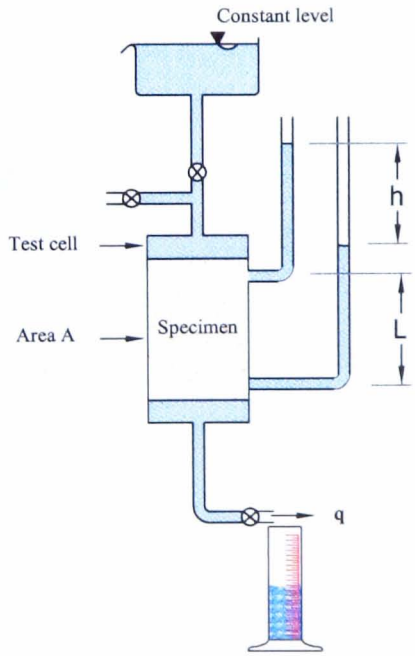

Figure 2.2 Typical arrangement of Constant head test.

The principle in this set up is that the hydraulic head causing flow is maintained; the quantity of water flowing through the specimen of known cross-sectional area and length is measured. Then from Darcy' law:

$$k_h = \frac{q \cdot L}{A \cdot h} \qquad 2.3$$

where

q = flow rate,

L = length of the soil specimen,

A = cross-sectional area of the soil specimen,

h = hydraulic head causing flow.

The constant head technique is widely used owing to its simplicity in principle. Its main advantages are its simplicity, low capital costs and steady state conditions.

The main limitation of this technique is the fact that it is difficult to measure small flow rates and this difficulty is overcome by extending test durations or to use very high hydraulic gradients that can affect the specimen by seepage induced consolidation and change in effective stress hence a variation in void ratio. In an effort to reduce these effects, ASTM D5084 recommends maximum hydraulic gradients in flexible-wall hydraulic conductivity tests as given in Table 2.2.

Table 2.2 Recommended maximum hydraulic gradients in flexible-wall Hydraulic conductivity tests (D5084-90).

Hydraulic conductivity of Soil (m/s)	**Recommended Maximum Hydraulic Gradient**
1×10^{-6} *to* 1×10^{-7}	2
1×10^{-7} *to* 1×10^{-8}	5
1×10^{-8} *to* 1×10^{-9}	10
1×10^{-9} *to* 1×10^{-10}	20
Less than 1×10^{-10}	30

This technique can also be used in conjunction with a modified oedometer or a Rowe cell that both have the advantage that the stress state of the soil can be controlled and changed as well. The Rowe cell has the added advantages of being able to apply back

pressure to the specimen to achieve satisfactory saturation, specimens of larger diameter can be tested so some in situ fabric can be retained and the direction of permeant flow can be orientated to be either vertical or horizontal.

2.2.3 Constant Flow Technique

The constant flow technique has been used to measure the hydraulic conductivity of fine-grained soils such as fine sands, silts and clays (Daniel, 1994; Araruna, 1995; Chen, 1997). It has been suggested as a standard method in the Unites States (ASTM D5084-90 Standard Test Method for Measuring of Hydraulic Conductivity of Saturated Porous Materials Using a Flexible Wall permeameter).

This technique is performed by pumping permeant liquid through a soil specimen at a controlled rate using a multispeed syringe pump and measuring the pressure difference induced across the specimen with a differential pressure transducer (DPT). This procedure avoids the errors in conventional techniques that arise from atmospheric contamination and from the long time intervals needed to obtain measurable flow rates.

Once a steady state condition is achieved which is indicated by steady differential pressures across the specimen and balanced inflow and outflow, the test is complete. A schematic diagram of the technique is shown in Figure 2.3.

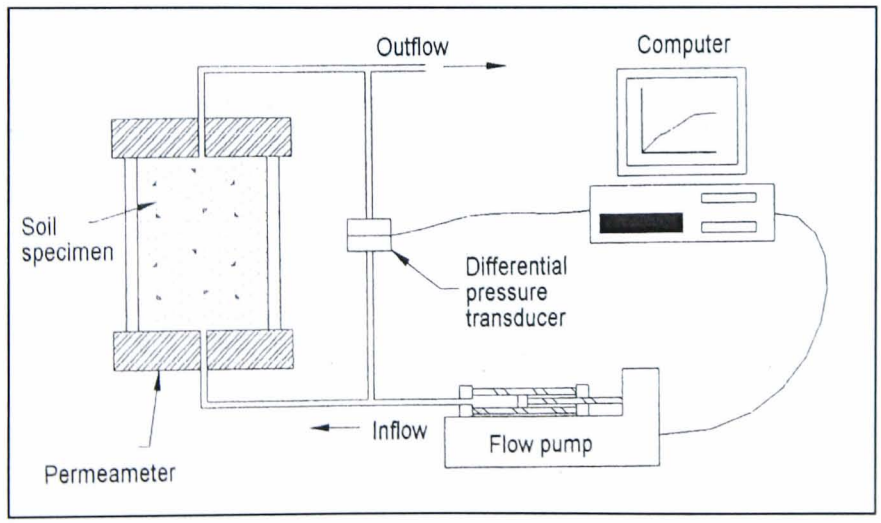

Figure 2.3 Schematic diagram of the constant flow rate technique (Chen, 1997).

The advantages of this technique in comparison to the other two techniques are:

1. Measurements of hydraulic conductivity can be determined in very much shorter time periods and at smaller hydraulic gradients. Therefore, the seepage induced consolidation effect and changes in effective stress in the specimen can be minimised, but they can not be avoided entirely. Pane et al. (1983) concluded that if the clay is very soft and normally consolidated, even small gradients can cause significant seepage induced consolidation.
2. The test can be fully automated with computer control of all pressures and flow rates.
3. When the permeant liquid is a chemical or waste liquid, one can set the flow pump to deliver a known amount of liquid in a given amount of time which can be helpful in making sure that sufficient throughput of liquid occurs within the time restrictions of a project (Daniel, 1994).

The disadvantages of the technique are:

1. The high capital costs involved.
2. The operation of the equipment is somewhat more complicated.
3. Possibility of developing extremely large hydraulic gradient if too large a flow rate is used.

2.3 Types of Permeameters

Numerous variations of laboratory hydraulic conductivity permeameters are available for testing soils. The permeameters cells may be divided into two categories: rigid–wall and flexible-wall cells. The major difference is, in the former, consolidation is one-dimensional; in the later it is three dimensional. A summary of these two permeameter types is presented below.

2.3.1 Rigid Wall Permeameters

Rigid-wall permeameters consist of a rigid tube that contains the specimen to be tested. The tube is almost always circular and constructed of metal, plastic or glass. Two types of rigid-wall permeameters are commonly used namely a compaction-mold permeameter and a consolidation-cell permeameter (Rowe cell) (Figure 2.4).

The compaction-mold permeameter (Figure 2.4a) is the most commonly used type. Two main advantages of this type of permeameter are its simplicity and cost. The specimen in this type of permeameter is confined in a rigid ring. To prevent side leakage, compaction stresses should be applied to ensure a good contact between the soil and the rigid ring. The disadvantages associated with this permeameter are the lack of control over the state of stress and the means of saturating the specimen. Most of the rigid wall permeameters have no provisions for back-pressure saturation. Although a vacuum may be applied to the outflow end of the cell, it is still unlikely that the specimen will be saturated completely. Therefore the hydraulic conductivity measured using these devices will normally be lower than the corresponding value for fully saturated soil, because bubbles of air reduce the hydraulic conductivity.

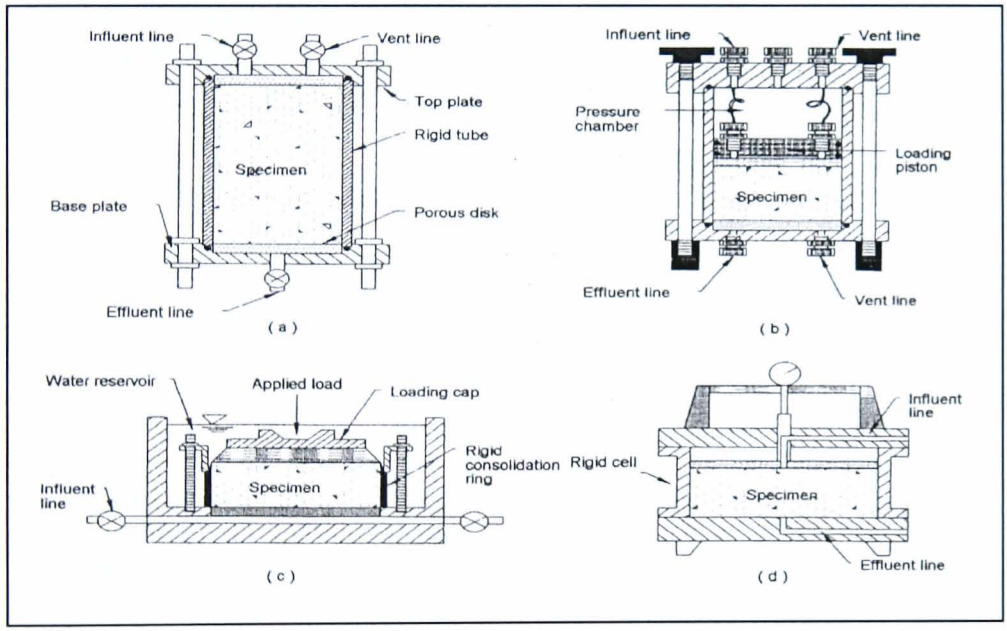

Figure 2.4 Schematic diagram of varies types of rigid-wall permeameters
a) Compaction-Mold b) Consolidometer cell c) Oedometer cell
d) Rowe cell (Chen, 1997)

Compaction-mold permeameters are best suited for testing engineered fills that will be subjected to low overburden stresses in the field and coarse material when the side wall leakage is less of a problem because of the higher hydraulic conductivity of the specimen.

The consolidation-cell permeameter is a modified consolidation cell, such as that shown in Figure 2.4b and Figure 2.4d. One advantage the consolidation-cell permeameter has over the compaction-mold permeameter is that the vertical loads may be applied to the

specimen. This helps prevent side wall leakage, since the soil is forced laterally against the ring during consolidation (Shackelford, 1994). Some of the consolidation cells like the Rowe cell (Figure 2.4d), have back-pressure capability which can be used to present dissolved air being released.

The consolidation-cell permeameter is best suited to testing undisturbed samples of relatively compressible soil such as soft to moderately stiff clay that will be subjected to significant overburden pressure.

2.3.2 Flexible Wall Permeameter

The flexible-wall permeameter (Figure 2.5) is used for hydraulic conductivity testing and standard procedure has been developed for its use (Zimmie, 1981; Daniel, et al., 19984; ASTM D5084-97).

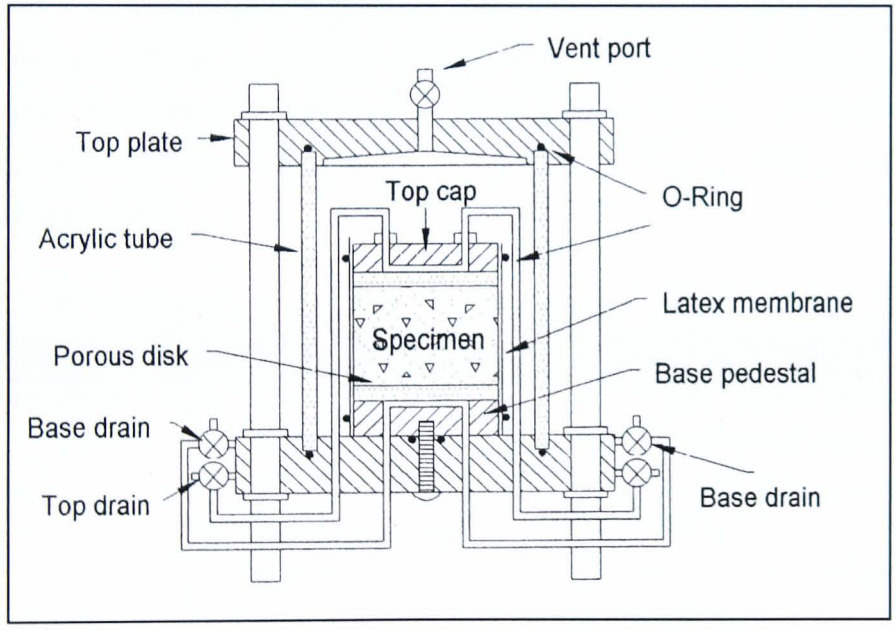

Figure 2.5 Flexible-wall permeameter (after Daniel, 1994)

The specimen is confined in a flexible membrane inside a conventional or modified triaxial cell. The membrane is held tightly in place against the soil by pressure applied by the cell fluid. Because the membrane is flexible, it conforms to surface irregularities along the side of the specimen and adjusts itself to changes in specimen dimensions, thus minimising or preventing side wall leakage. The ability to saturate the specimen under back pressure and the ability to control the state of stress are two other important

advantages of the flexible-wall permeameter. It may also be desirable when testing permeants other than water. The main disadvantage of the flexible-wall permeameters may well be their cost.

In general, the flexible-wall permeameters are best suited to soil specimens with irregular surface (e.g. undisturbed natural specimen). It is also ideal for soils that will be subjected to substantial overburden pressure, such as natural sample obtained at depth. More details of its components, calibration and testing procedures are provided in chapter three.

2.3.3 Comparison between Flexible and Rigid Wall Permeameters

The major differences between rigid and flexible wall permeameters are the method of confining and saturating the specimen. Several studies have shown that large differences in measured hydraulic conductivity values can occur depending on the type of the permeameter used in a test (Daniel, et al. 1985; and Shackelford 1994). Other studies suggest that the method does not influence the result (Tavenas et al 1983a). Table 2.3 summarises the relative advantages and disadvantages of rigid and flexible wall permeameters that were discussed by Daniel et al. (1985); Daniel (1994) and Shackelford (1994).

Table 2.3 Advantages and disadvantages of different permeameters

Permeameter Type	Advantages	Disadvantages
Compaction-Mold	• Low cost • Simplicity • Useful for compacted soil • No confining pressures required	• Difficult to saturate the specimen • Volume and/or deformation change cannot be measured or controlled • Stresses on specimen are unknown and uncontrollable • Side wall leakage is possible • Large hydraulic gradient may result in hydraulic fracturing of specimen or piping
Consolidation-Cell	• Vertical pressure in field can be simulated • Vertical deformation can be measured • A range of vertical stresses can	• Thin specimen may not be representative • Potential for side-wall leakage • Some samples may be difficult to trim into consolidation ring

	be tested on one specimen • Useful for undisturbed or compacted specimens • Short testing time with thin specimens • Cost effective for measuring Hydraulic conductivity over a range of specimen states	resulting in specimen disturbance • Higher cost than compaction-mold permeameter • Horizontal stresses on specimen are unknown • Back pressure saturation not recommended
Flexible-Wall	• Specimen can be saturated by back pressure and degree of saturation confirmed via B coefficient measurement • Irregular specimen surfaces can be accommodated easily • Side-wall leakage minimized • Principal stresses on specimen can be controlled • Volume changes and/or deformation can be measured	• More complicated operation of equipment than fixed-wall cell • Membrane may be incompatible with chemical permeant • Large hydraulic gradient may result in unreasonable effective stresses in specimen • Inappropriate for testing soft specimens such as slurry mixture • Higher cost than fixed-wall permeameter

(Modified after Shackelford, 1994)

2.4 Measurement and prediction of Thermal Conductivity in the Laboratory

Thermal conductivity can be either measured or predicted. There are two methods to measure thermal conductivity; the steady state method and the transient method. The measured properties are the thermal conductivity and the thermal diffusivity, these being interrelated by means of the volumetric heat capacity. The thermal conductivity governs the steady state condition of the soil, while the thermal diffusivity applies to the case where the temperature varies with time (Farouki 1986).

The general concept of measuring the thermal properties is that it is necessary to set up a temperature gradient across the soil sample being tested and then either from the transient state or the steady state condition these properties can be determined.

There are also numbers of conduction models that can predict the thermal conductivity of a soil to some extent. Some of these models are presented in the following section.

2.4.1 Steady state methods

After applying the initial temperature difference, it may take some time to achieve steady state conditions when the measurements are made. The laboratory steady state methods include the guarded hot plate (GHP) and the radial heat flow. These methods which employ steady state measurement of the thermal conductivity apply Fourier's law of heat conduction.

2.4.1.1 The guarded hot plate (GHP)

The guarded hot plate test is considered the most accurate and most widely used method for the measurement of thermal conductivity of poor conductors of heat. It has been standardised by the American Society for Testing and Materials as ASTM C 177 (Standard Test Method for Steady-State Heat Flux Measurements and Thermal Transmission Properties by Means of the Guarded-Hot-Plate Apparatus). This test method gives only the general design requirements necessary to construct and operate a satisfactory guarded hot plate apparatus. It does not give detailed design. Therefore the success of the technique depends on a proper design of the apparatus.

The apparatus shown in Figure 2.6 which conforms to the ASTM specifications was used at CRREL (US Army Cold Regions Research and Engineering Laboratory). It is a 20 inches guarded hot plate apparatus (GHP) capable of measurements in the range -50 ^{o}F to +250 ^{o}F. Two identical test specimens (G in Figure 2.6) are placed above and below a flat-plate main heater unit which is surrounded by an outer guard heater (Figure 2.6). The guard eliminates horizontal heat losses and causes heat from the main heater to flow vertically up or down through the test specimens. Liquid-cooled heat sinks are placed adjacent to the outer surfaces of the specimens. The heat input, Q, is monitored. After steady state has developed, as shown by stable temperatures of the heating and cooling plate, the thermal conductivity can be calculated from the heat input, the temperature differential, ΔT, across the sample, the sample dimensions thickness, Δx, and heat transfer area, A. The apparent thermal conductivity of the specimen is calculated from the equation (Fourier's law):

$$k_t = \frac{Q}{A} \cdot \frac{\Delta x}{\Delta T} \qquad 2.4$$

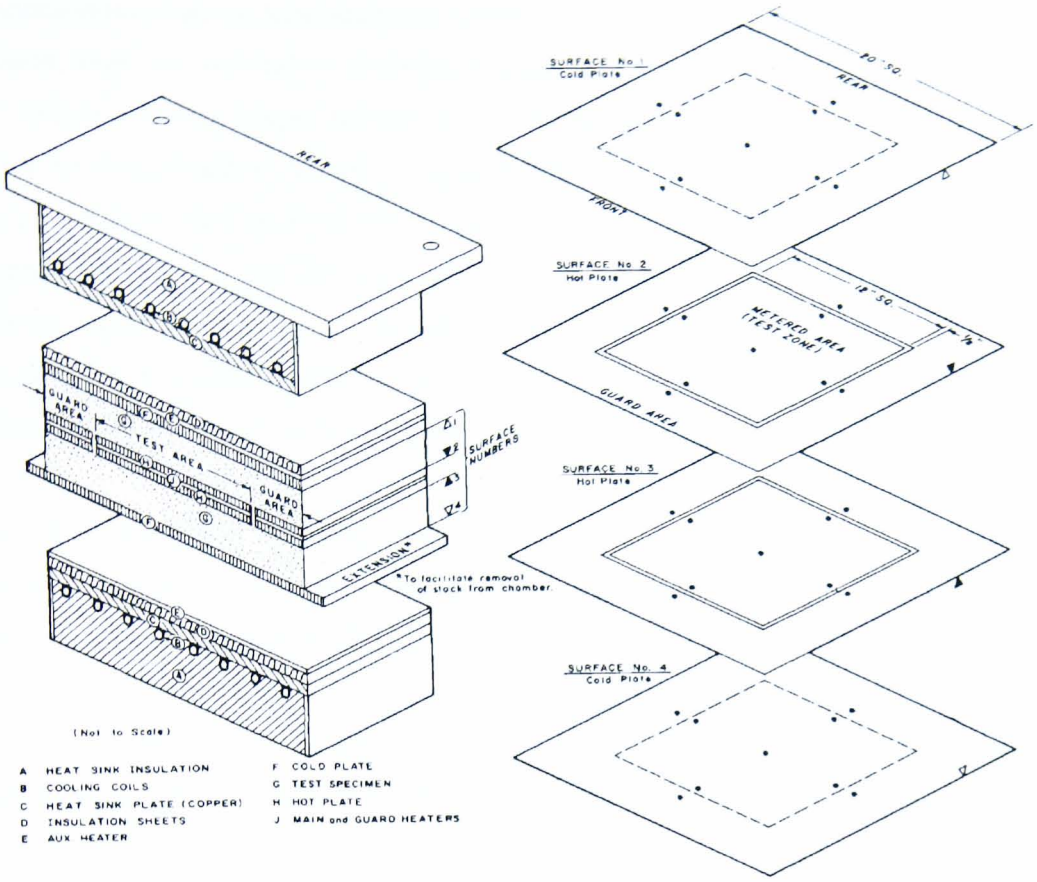

a. Stack assembly cross section. *b. Thermocouple locations in plate surfaces.*

Figure 2.6 CRREL guarded hot plate apparatus (From Farouki 1986).

Although GHP test results obtained by different experimenters on the same material can vary by as much as 20%, the GHP method is generally regarded as accurate (Farouki 1986). However, it is usually quite time consuming (Mitchell et al. 1978). Due to the considerable time required to achieve steady state condition and the relatively high temperature differential that needs to be applied, appreciable moisture migration may take place in unsaturated soils (Hutcheon and Paxton 1952, Mitchell et al. 1978). This process is known as thermo-osmosis. De Vries (1963) has pointed out that the resulting measured value of the thermal conductivity would be lower than the value corresponding to the average water content.

2.4.1.2 Radial Heat Flow

Whereas the guarded hot plate is generally used for measuring the thermal conductivity of samples that can be formed into a slab, radial heat flow steady state methods are more commonly used with powdered or granular material (Farouki 1986).

Various experimenters have used cylindrical arrangements for the steady state test (e.g. Kersten 1949 and Mitchell et al. 1978). A cylindrical test device employs a central line (or cylindrical) heat source (Figure 2.6). End effects are assumed negligible due to either the large length to diameter ratio of the test apparatus or the use of guard heaters. To achieve the steady state the device has to be allowed to run for about 10 hours before taking measurements (Mitchell et al. 1978). After steady state has been established, the thermal conductivity can be calculated from the heating power, the length of the cylinder, the temperature differential between two internally (to the medium) located sensors and their radial position (Farouki 1986).

Kersten (1949) tested soil samples in a cylindrical arrangement shown in Figure 2.7. The main heater is in the center and is guarded by upper and lower heaters. The soil specimen is placed in the surrounding annular space. The heat flows radially outward across the soil and towards the cooling chamber through which alcohol is circulated at the required temperature. Wolfe and Thieme (1964) used a similar setup for measuring thermal conductivity of frozen soils and ice. Another cylindrical arrangement was used by Flynn and Watson (1969) for testing soils at high temperatures (up to 1700°C) (Farouki 1986).

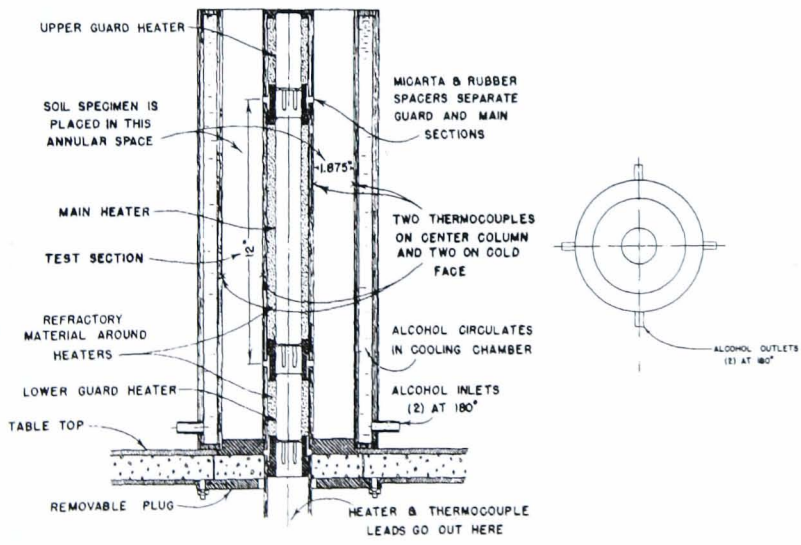

Figure 2.7 Cylindrical arrangements for thermal conductivity tests (Farouki, 1986).

2.4.2 Transient state methods

A disadvantage of steady state methods are the long measurement times involved. Therefore, transient methods are preferred for measuring the thermal conductivity of moist soils. They are rapid as data are obtained in minutes or even less compared to hours for a steady state measurement.

Steady state methods are only capable of measuring thermal conductivity. When the measured properties are to be used in the study of transient heat transfer, density and specific heat have to be found independently. They are combined with thermal conductivity to find the thermal diffusivity. Methods based on transient heat transfer have the potential of directly determining thermal diffusivity, but they are not as accurate as steady state methods with dry materials (Mohsenin, 1980).

The line heat source theory is widely used for determining of thermal properties of soils. Three transient methods based on this theory, including the hot wire, the thermal needle probe (Single Probe), and dual probe will be presented.

2.4.2.1 Transient Hot Wire Method

The hot wire method is one of the most commonly used transient state methods. It has been standardised by the American Society for Testing and Materials as ASTM C 1113 (Standard Test Method for Thermal Conductivity of Refractories by Hot Wire). The theory is based on a line heat source of infinite length and infinitesimal diameter. Abu-Hamdeh et al (2001) used this method to investigate the effect of the bulk density and the water content on the thermal conductivity of some Jordanian soils (Figure 2.8). It is simply used in soils by embedding a thin straight wire (heat source) in the centre of a specimen contained in a steel box. When the specimen and the wire are at a constant temperature, constant power is supplied to the wire to heat the specimen. The radial temperature difference across the specimen is measured by a thermocouple. In that case the external temperature can simply be the room temperature. The temperature response of the specimen is a function of its thermal properties. The thermal conductivity can be calculated from the temperature rise measured at a known distance from the heat source and the power input as:

$$k_t = \frac{Q}{4\pi(T_2 - T_1)} \ln\left(\frac{t_2}{t_1}\right) \qquad 2.5$$

where

Q = the input power per unit length.

T_1 = temperature at time t_1.

T_2 = temperature at times t_2.

The values d(ΔT)/d(Δln t) can be read from the straight line portion of a plot of ΔT versus $ln\ t$ obtained from the test record (Tavman, 1996). In the simplest form this method can only be applied to cohesive soils. Once a test becomes more sophisticated with controlled boundaries then this test becomes easier to operate and interpret.

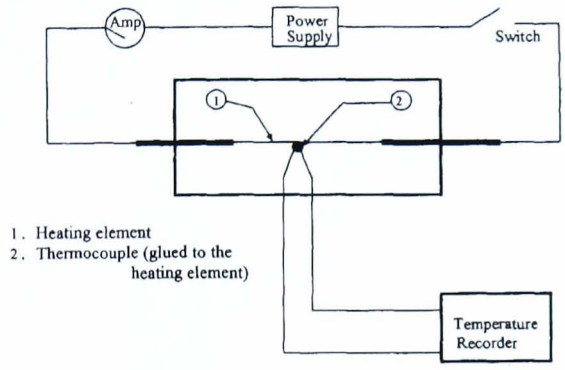

(a) Top view

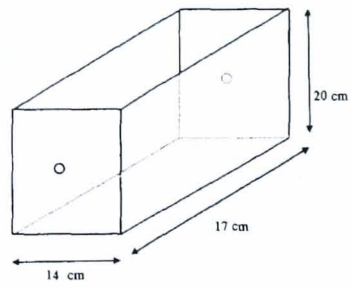

(b) Rectangular steel box shown without wiring

Figure 2.8 Schematic diagram of hot wire method
(Abu-Hamdeh et al 2001)

2.4.2.2 Thermal Needle Probe Method (Single Probe)

The thermal needle probe method (single probe) is based also on the theory of the line heat source method. Probes are constructed around a rigid straight rod like, e.g. a metal tube. A heating element and a thermocouple are placed inside, or on the outside of, the

tube or rod. The first applications of the probe were by Van der Held and Van Drunen in 1949 to measure the thermal conductivity of liquids, and by Hooper and Lepper in 1950 to measure that of soils using large probe of about 47 cm length and 0.47 cm in diameter (Farouki 1986). The American Society for Testing and Materials (ASTM) published a testing method for determining the thermal conductivity of soils and soft rocks by thermal needle probe (D5334-92) that was suggested by Chaney et al. (1983). They stated that this test method is suitable only for isotropic materials and applicable over the temperature range from 20 to 100 °C. Their probe consisted of a stainless steel hypodermic tubing containing a heater and thermocouple as shown in Figure 2.9. The probe is 100 mm long and has an outside diameter of 1.8 mm. An insulated heater element was inserted along the full length of the tube. An insulated thermocouple is located inside the tube at the halfway point. The tube is bonded to a miniature thermocouple connector.

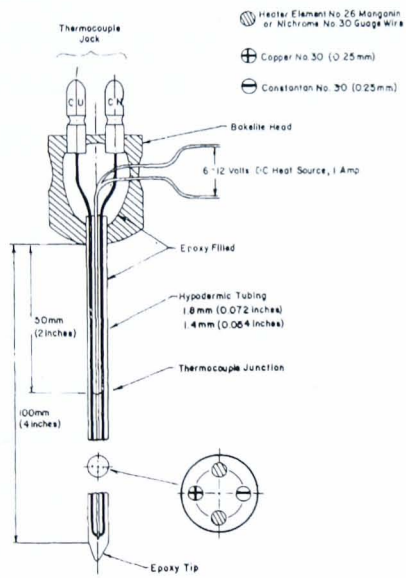

Figure 2.9 Thermal Needle Probe Components
(Chaney et al 1983)

To make a measurement, the probe is embedded into the soil specimen. The specimen is allowed to come to equilibrium with room temperature. The heater wire is connected to a constant current source. The thermocouple is connected to the readout unit. The probe heater is energized and heats the soil with constant power. The variation in temperature at the heat source is monitored with time. Following a brief transient period, a plot of the temperature versus the natural logarithm of time became linear. The thermal conductivity can be calculated from the relation:

$$k_t = \frac{Q}{4\pi(T_2 - T_1)} \ln\left(\frac{t_2}{t_1}\right) \qquad 2.6$$

This probe can be used in laboratory specimens of soil from the base of boreholes and in near surface soils. It has the advantage of being a simple apparatus. It is also a rapid method (Mitchell et al. 1978, Chaney et al. 1983, Nusier and Abu-Hamdeh 2003). Besides the advantage of being rapid, the probe requires only a small sample size. It has also the advantage that the thermal resistivity can be computed directly from the test data without knowledge of the heat capacity of the soil (Mitchell et al. 1978).

Although this method has been often reported as an absolute method, it is still suffers from some disadvantages including the assumption of specific heat that can induce an error, and a small (1%) variations in current supply during the test can result in significant errors (Mitchell et al. 1978). This highlights the need to calibrate the probe. Calibration takes care of inaccuracies in measured resistance of heater wire and of temperature effects on resistance of wire. Agar-gelled water and glycerine are commonly used as thermal references. Thus it is a comparative method. The method is not precise according to ASTM.

2.4.2.3 Dual Probe Method

An additional temperature sensor with known distance (r) from the single probe can be used to measure thermal properties of soils (Nusier and Abu-Hamdeh 2003). This method is known as dual probe method. Campbell et al (1991) developed an instrument that allows measurements several millimetres away from the line heat source, but their theoretical approach only gave the volumetric heat capacity. The other thermal properties (e.g. thermal diffusivity and conductivity) can be extracted by using the short-duration heat-pulse theory presented by Bristow et al (1994). This theory is based on a solution of the radial heat conduction equation for an infinite-line heat source and isotropic medium at uniform initial temperature. The thermal properties can be calculated from the following equations:

$$\rho c = \left(\frac{q}{4\pi\alpha \cdot \Delta T_m}\right)\left[Ei\left(\frac{-r^2}{4\alpha \cdot (t_m - t_o)}\right) - Ei\left(\frac{-r^2}{4\alpha \cdot t_m}\right)\right] \qquad 2.7$$

$$\alpha = \left(\frac{r^2}{4}\right) \cdot \frac{\left[\frac{1}{(t_m - t_o)} - \frac{1}{t_m}\right]}{\ln\left(\frac{t_m}{(t_m - t_o)}\right)} \qquad 2.8$$

$$k_t = \alpha \cdot \rho \cdot c_p \qquad 2.9$$

$$k_t = \left(\frac{q}{4\pi \cdot \Delta T_m}\right) \cdot \left[Ei\left(\frac{-\ln\left(\frac{t_m}{(t_m - t_o)}\right)}{\left(\frac{t_o}{t_m}\right)}\right) - Ei\left(\frac{-\ln\left(\frac{t_m}{(t_m - t_o)}\right)}{\left(\frac{t_o}{(t_m - t_o)}\right)}\right)\right] \qquad 2.10$$

where q is the amount of heat input per unit time and unit of length of a probe, α is the thermal diffusivity, k_t is the thermal conductivity, ρc_p is the volumetric heat capacity, r is the distance between electrodes, ΔT_m is the maximum temperature change at a distance r from the heater, t_m is the time at which ΔT_m is recorded, t_o is a heat pulse duration, and –Ei (-x) is the exponential integral.

2.4.3 Prediction methods

Numbers of thermal conduction models for predicting the thermal conductivity of soils have been found in the literature. Some of these models that can be applied to soils are presented and discussed in the following sections. All the models depend on the thermal conductivity of each individual constituent of the soil composition (solid, water and/or air).

2.4.3.1 Maxwell Model

Maxwell (1954) came up with a model that can give a solution for the effective thermal conductivity using the potential theory for electrical conduction via heterogeneous media of both randomly distributed and non-interacting homogenous solid spheres (k_s) in a homogenous continuous medium (k_f) (Tavman, 1996), as shown below.

$$k_t = k_f \cdot \frac{2n \cdot k_f + (3 - 2n) \cdot k_s}{(3 - n) \cdot k_f + n \cdot k_s} \qquad 2.11$$

Where:

k_t = effective thermal conductivity

k_s = solid's thermal conductivity

k_f = fluid's thermal conductivity

n = porosity.

This can only be applied if the porosity (n) is large, as the derivation of this equation was based on the assumption that there is no mutual interaction between the solid spheres as the distance between them is far enough apart. According to Tavman (1996) the Maxwell equation is unable to estimate the thermal conductivity of granular porous media which has a low porosity in the range of 0.3 to 0.5, because it was derived from the assumption that the solid spheres are far enough apart so that they do not mutually interact.

2.4.3.2 De Vries Model

One of the methods discussed by Farouki (1986) to determine the thermal conductivity of the soils is the De Vries method, and this is based on Maxwell equation. This method is used to determine the thermal conductivity of ellipsoidal soil particles in a continuous medium consisting of air or water which results in the following equation:

$$k_t = \frac{x_f \cdot k_f + F \cdot x_s \cdot k_s}{x_f + F \cdot x_s} \qquad 2.12$$

The subscripts f and s in the equation refer to the fluid and solid respectively, where as x is the volume fraction of the soil components in a unit soil volume. The factor F can be determined using the following equation:

$$F = \frac{1}{3} \cdot \sum_{a,b,c} \left[1 + \left(\frac{k_s}{k_f} - 1 \right) \cdot g_a \right]^{-1} \qquad 2.13$$

The sum of g_a, g_b and g_c are equal to *one*, and in 1952 De Vries (Farouki 1986) suggested to assume that $g_a = g_b = 0.125$.

The results obtained by De Vries equation are accurate to within 10% of those produced by experimental work, for soils with a low solid/liquid thermal conductivity ratio. However, if the solid /liquid thermal conductivity ratio is approximately equal to a hundred, then De Vries equation gives a lower value than those obtained from experiment by approximately 25%. Therefore, De Vries suggested multiplying the thermal conductivity by a factor of 1.25, and this equation is applicable to just dry soils. However, for saturated soils the results obtained by De Vries method are considered acceptable.

The derivation of De Vries's equation is based on these assumptions:- there is no contact between the soil's solid particles, and the values for g assume that the shapes of the particles are needle-like.

These assumptions are not representative of most soil particles, as they are formed by different shapes. g_a, g_b and g_c are originally meant to be shape factors, however De Vries uses them instead as parameters that can be adjusted to fit the empirical data.

In the case of partially saturated soils where the solid particles and the air voids are considered to be two components dispersed in the continuous water medium, the following equation is used:

$$k_t = \frac{x_w \cdot k_w + F_a x_a \cdot k_a + F_s \cdot x_s \cdot k_s}{x_w + F_a \cdot x_a + F_s \cdot x_s} \qquad 2.14$$

Where:

$$F_s = \frac{1}{3} \cdot \left[\frac{2}{1 + \left[(k_s / k_w) - 1 \right] \cdot 0.125} + \frac{1}{1 + \left[(k_s / k_w) - 1 \right] \cdot 0.75} \right] \qquad 2.15$$

$$F_a = \frac{1}{3} \cdot \left[\frac{2}{1 + \left[(k_a / k_w) - 1 \right] \cdot g_a} + \frac{1}{1 + \left[(k_a / k_w) - 1 \right] \cdot g_c} \right] \qquad 2.16$$

De Vries assumed as g_a or g_b approaches a maximum value of 0.333 where the soil is nearly saturated, it then decreases linearly to a minimum of 0.035 where the soil is nearly dry. These assumptions are only applicable to spherical shaped particles, and the following condition $0.09 < x_w < n$ must be met, where x_w is the volume fraction of water and n is the porosity of the soil. At which point the parameters can be determined using the equation shown below.

$$g_a = 0.333 - (x_a / n) \cdot (0.333 - 0.035) \qquad 2.17$$

2.4.3.3 Parallel or Series and Geometric mean Equations

The thermal conductivity of a soil lies between an upper and lower limit, close to the upper limit the thermal conductivity is determined by the parallel flow model, and close to the lower limit the thermal conductivity is determined by the series flow model. For these types of models two considerations are made, the particles are clustered together and the fluid is continuous (Farouki, 1986).

The following equations represent thermal conductivity for the parallel and series models respectively.

$$k_t = n \cdot k_f + (1 - n) \cdot k_s \qquad 2.18$$

$$k_t = \frac{k_s \cdot k_f}{n \cdot k_s + (1 - n) \cdot k_f} \qquad 2.19$$

Where k_f and k_s are the fluid and solid thermal conductivities respectively, and n is the porosity of the soil.

Tavman (1996) states that the average of both the parallel and the series models is considered to be important and is determined by the geometric mean model, and it assumes random distribution of the different phases in the soil using the following equation:

$$k_t = {k_f}^n \cdot {k_s}^{(1-n)} \qquad 2.20$$

2.4.3.4 Kersten's empirical equations

The empirical equations developed by Kersten in 1949 to determine thermal conductivity are based on data obtained from four or five different soils. Although Kersten developed equations that can determine the thermal conductivity of both frozen and unfrozen soil conditions. However, for this study only unfrozen soil conditions are considered. These equations are based on the water content (w_c) and its dry density (γ_d) (Farouki, 1986).

The thermal conductivity based on the Kersten empirical equations for unfrozen silt-clay soils containing 50% or more silt and clay, metric units is given by:

$$k_t = 0.1442 \cdot (0.9 \log w_c - 0.2) \cdot 10^{0.6243\gamma_d} \qquad \text{For } w \geq 7\% \qquad 2.21$$

For unfrozen sandy soils it is as follows:

$$k_t = 0.1442 \cdot (0.7 \log w_c - 0.4) \cdot 10^{0.6243\gamma_d} \qquad \text{For } w \geq 1\% \qquad 2.22$$

The thermal conductivities obtained by the Kersten's empirical equation for unfrozen silt-clay soils and unfrozen sandy soils were 25% less than the measured thermal conductivities for the five different soils used earlier in determining the above equations. It has also been noted by Kersten that for unfrozen silt-clay soils the above equation is only applied if the water content is greater than 7% (Farouki 1986).

2.4.3.5 Johansen's Model

In 1975 Johansen (Farouki 1986) developed equations for determining the thermal conductivity under both dry and saturated conditions at the same dry density. These equations are then used to determine the thermal conductivity identified as Kersten's number, K_e, and this is given by:

$$K_e = \frac{(k_t - k_{t\,dry})}{(k_{t\,sat} - k_{t\,dry})} \qquad 2.23$$

This equation is applicable to both unfrozen and frozen soils, where k_t is the thermal conductivity at an intermediate degree of saturation, and the dry density was kept constant, as it has been noted from earlier investigations carried out by Smith and Byers (1938), Smith (1942) and Johansen that the dry density or porosity was an important contributing factor in determining the thermal conductivity in the dry state.

In the case of dry natural soils the thermal conductivity equation in terms of dry density developed by Johansen based on the Maxwell-Fricke's equation where the solid/liquid thermal conductivity ratio equals 120 is shown below.

$$k_{t\,dry} = \frac{0.135 \cdot \gamma_{dry} + 64.7}{2700 - 0.94 \cdot \gamma_{dry}} \pm 20\% W/m.^{\circ}C \qquad 2.24$$

In the case of saturated soils Johansen concluded that the variations in the microstructure effected the thermal conductivity was negligible. Therefore, Johansen suggested using the geometrical mean equation which is based on the thermal conductivities of the soil components and the respective soil volume fractions as shown below:

$$k_t = k_f^{\,n} \cdot k_s^{(1-n)} \qquad 2.25$$

In order to determine the thermal conductivity of an unsaturated soil, first the Kersten number has to be estimated based on the degree of saturation, S, using the following relationships:

For coarse unfrozen soil where S>0.05:

$$K_e \cong 0.7 \cdot \log S + 1.0 \qquad 2.26$$

For fine unfrozen soil where S>0.1:

$$K_e \cong \log S + 1.0 \qquad 2.27$$

The thermal conductivity of partially saturated soils can then be determined from k_{tdry}, k_{tsat} and K_e using the following equation developed by Johansen:

$$k_t = \left(k_{t\,sat} - k_{t\,dry}\right) \cdot K_e + k_{t\,dry} \qquad 2.28$$

2.4.3.6 Zehner and Schlünder Model

In 1970 Zehner and Schlünder (Tavman, 1996) carried out an experiment to determine thermal conductivity that is based on one dimensional heat flow model through a packed bed of spherical particles and it is assumed that the point of contact between the particles is in the same direction of the heat flow, and this is given as follows:

$$k_t = k_f \cdot \left(1-(1-n)^{0.5} + \frac{2(1-n)^{0.5}}{1-K\cdot B}\cdot\left(\frac{(1-K)\cdot B}{(1-K\cdot B)^2}\cdot\ln\left(\frac{1}{K\cdot B}\right) - \frac{B+1}{2} - \frac{B-1}{1-K\cdot B}\right)\right) \quad 2.29$$

Where

$$K = \frac{k_f}{k_s} \quad and \quad B = 1.25\cdot\left(\frac{1-n}{n}\right)^{10/9} \quad 2.30$$

This equation is based upon the fluid/solid thermal conductivity ratio, the thermal conductivity of the fluid and the porosity of the soil.

2.4.3.7 Krupiczka Model

Another numerical model for determining the effective thermal conductivity was derived by Krupiczka in 1967 (Tavman, 1996) using granular materials. Two models were developed one with long cylinders having a porosity of 0.215 and the other model using spheres in a cubic lattice having a porosity of 0.476. Due to the complexity of the formula obtained for both models, Krupiczka made approximations to these equation using correlations that take into account the effect of porosity, which is given below, this equation is only valid for when porosity is greater than or equal to 0.215 and less than or equal to 0.476. However, outside this range there is not too much error in determining the thermal conductivity for porosities that are considered in that region.

$$k_t = k_f \cdot \left(\frac{k_s}{k_f}\right)^{A+B\cdot\log\left(k_s/k_f\right)} \quad 2.31$$

Where;

$$A = 0.28 - 0.7571\cdot\log(n) \quad and \quad B = -0.057 \quad 2.32$$

2.4.3.8 Woodside and Messmer Model

In 1961 Woodside and Messmer (Tavman, 1996) recommended a model that combined the parallel and series flow equations (Farouki, 1986), and used the similarity for electrical conductivity of an aggregate of conductive particles that were saturated with a conductive electrolyte, to produce a resistive model equation to predict the effective thermal conductivity of porous media:

$$k_t = \frac{a \cdot k_s \cdot k_f}{k_s \cdot (1-d) + d \cdot k_f} + c \cdot k_f \qquad 2.33$$

Where;

$$a = 1 - c \quad , \quad c = n - 0.03 \quad and \quad d = \frac{1-n}{a}$$

Where c is determined from experimental data that was developed by Stephenson and Woodside in 1958 based on a model of spheres having a porosity of 47.6% packed in a cubic lattice (Tavman, 1996).

2.4.3.9 Numerical Simulation Model

Cosenza et al. (2003) concluded that a simple relationship between the thermal conductivity of the soil and its volumetric water content could not be found, as this is heavily influence by the thermal conductivity of the solid fraction and its porosity which play a key role in the determination of the effective conductivity. Due to the lack of experimental data a numerical model was used, and it was found that the microscopic arrangement of the water has an influence on the thermal conductivity of the soil and its volumetric water content. The equation developed by Cosenza et al. shown below takes into account the porosity, the thermal conductivity of the solid and the volumetric water content. These are based on a range of values, for porosity (n) the range is 0.4 to 0.6, thermal conductivity of the solid fraction (k_s) the range is 2 to 5 (W/m.K), and the volumetric water content (θ) the range is 0.1 to 0.4.

$$k_t = (0.8908 - 1.0959n) \cdot k_s + (1.2236 - 0.3485n) \cdot \theta \qquad 2.34$$

The results from the above equation can be used to investigate the effects of water content and porosity on the thermal conductivity of the soil. Additional information about the development of this model can be obtained from the research published elsewhere (Cosenza, et al., 2003).

2.4.3.10 Campbell Model

Another equation that can be used to determine the soil thermal conductivity was developed by Campbell in 1985 (Abu-Hamdeh, 2000). By varying the water content, the density of the soil and the soil texture, the following equation was derived:

$$k_t = A + B\theta_v - (A - D)\cdot \exp\left[-(C\theta_v)^E\right] \qquad 2.35$$

The parameters shown above are soil coefficients that were developed by Campbell, and these are related to the soil properties, in the following way:

$$A = 0.65 - 0.78\rho_b + 0.6\rho_b^{\,2} \qquad 2.36$$

$$B = 1.06\rho_b \qquad 2.37$$

$$C = 1 + \frac{2.6}{\sqrt{m_c}} \qquad 2.38$$

$$D = 0.03 + 0.1\rho_b^{\,2} \qquad 2.39$$

$$E = 4 \qquad 2.40$$

Where m_c is the clay fraction.

2.5 Summary

The different laboratory techniques are reviewed, for the measurement of the soil's hydraulic and thermal conductivity. It can be concluded there are several methods available in determining these parameters. Even when following careful instructions, there is still an inherent variation in the results obtained by these different techniques.

However, for determining hydraulic conductivity of soils, it appears that the constant flow method using the flexible wall permeameter is a better tool in obtaining a true representative value of the hydraulic conductivity for a given fine soil. It can also be developed to determine the hydraulic conductivity for fine soils more rapidly. This technique and its development are described in Chapter three.

For the determination of the soil's thermal conductivity, the steady state methods are simpler to use than the transient methods. However, the necessary equipment required to carryout this experiment for the steady state is far more complex than in the transient state. Therefore, a new simple device is designed to make it easier to use for the determination of the soil's thermal conductivity.

Chapter 3

Determination of Hydraulic Conductivity

3.1 Introduction

This chapter provides information about the equipment used to determine hydraulic conductivity, the apparatus, its modification, its calibration and the experimental procedure used through out the study. The original permeameters were designed by Araruna in 1995 as a part of a research programme at the University of Newcastle upon Tyne investigating laboratory measurement of the hydraulic conductivity of fine grained soils. The author modified these two permeameters to suit the present research work which is explained in section 3.3.

3.2 Description of the flexible wall permeameters

Two flexible wall permeameters designed by Araruna in 1995 were used in this research (Figure 3.1), they have the same components. Each permeameter, Figure 3.2, has three main components. These components are the permeameter cell (1), two volume change gauges (2 and 3) and the flow pump (4). The permeameter was also instrumented with different types of electronic transducers to measure pressure, displacement and volume changes. They were as follows: three pressure transducers (PT) (5) (back pressures and cell pressure), three differential pressure transducers (DPT) (6) (cell volume change gauge, specimen volume change gauge and differential pressure to measure the pressure difference between the pressures at the top and the bottom of the specimen), and a linear variable differential transformer (LVDT) (7).

A data logger unit (ADU) was used to distribute voltage to the transducers and return the transducers output signals to the recording system within the unit. A computer was used to run software that receives voltage readings of each transducer from the data logger and convert these readings to displacement or pressure using calibration constants stored in the computer's memory.

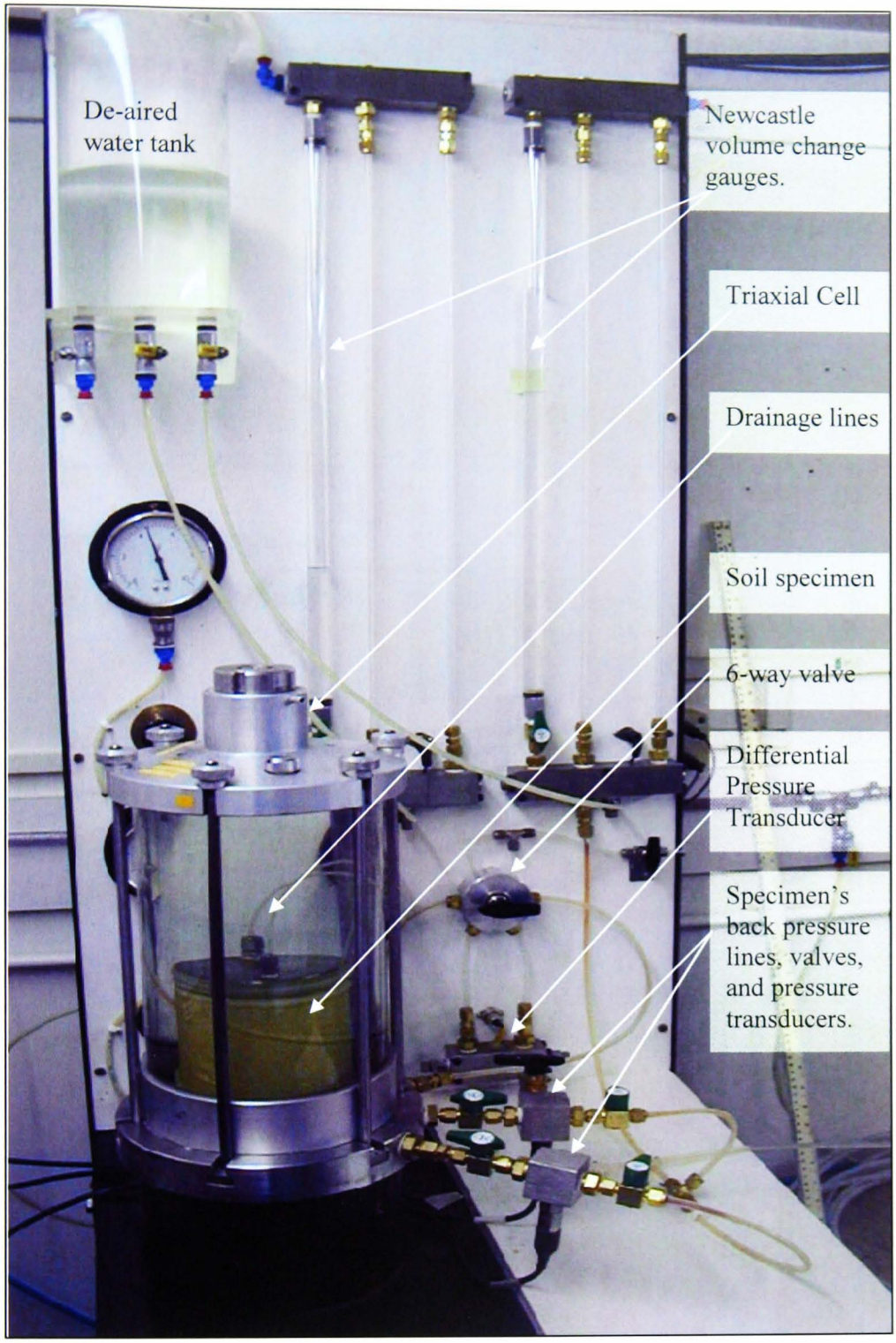

Figure 3.1 The flexible wall permeameter.

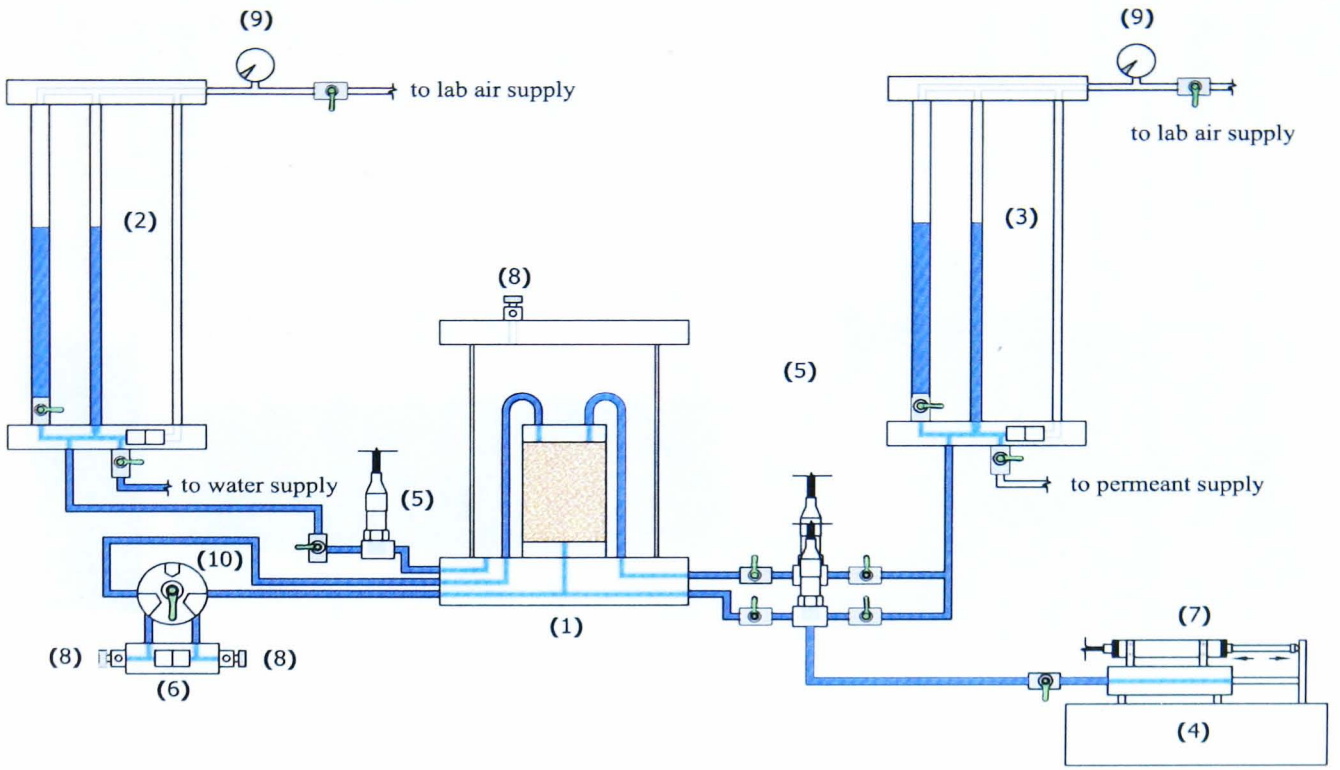

(1) triaxial cell
(2) cell volume change system
(3) in/outflow volume change system
(4) flow pump
(5) pressure transducer
(6) DPT
(7) LVDT
(8) de-airing valve
(9) pressure regulator
(10) 6-way valve

Figure 3.2 Schematic of the flexible wall permeameter for constant flow test.

At any time during a test, the operator could request a display or printout of the previous data, stop the test or proceed to the next stage. At the end of each testing stage (saturation, consolidation and permeation), files containing the raw data and the calibrated data were stored on a floppy disk. These data were then analysed, graphically displayed and printed by the computer using a spreadsheet.

The various types of transducers shown in Figure 3.3 were used to measure pressure, displacement and volume changes, where the pore water and cell pressures were measured by pressure transducers (PT) (Figure 3.3a), linear displacement was measured by linear variable differential transformer (LVDT) (Figure 3.3b), and volume changes and pressure difference were measured by differential pressure transducers (DPT) (Figure 3.3c).

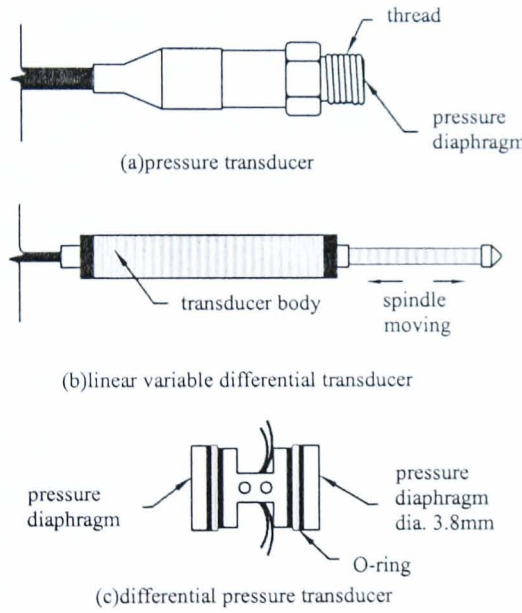

Figure 3.3 Types of the used transducers.

During hydraulic conductivity testing the data logger was used to continuously monitor the differential pore pressure between the top and the bottom of the specimen. Testing was continued until a steady-state condition is achieved.

3.2.1 Permeameter cell

The permeameter cell (1in Figure 3.2) is a conventional triaxial cell excluding the loading piston. Its wall is made from clear acrylic to allow observation of the specimen

and drainage lines during a test. The cell consists of interchangeable impermeable top caps and base pedestals of different sizes as well as four drainage lines leading to the specimen to provide flexibility in controlling drainage and in measuring hydraulic pressures during a test. Normally, one drainage line at the base of the specimen is used for inflow of permeant while one line at the top is used for outflow. The other drainage lines are connected to a differential pressure transducer (DPT) to read the pressure difference across the specimen or to flush bubbles of air from the system.

3.2.2 Newcastle volume change gauge

To obtain a direct measurement of the flow rate in fine-grained soils under a relatively low hydraulic gradient, it is essential that the flow measurement system be sensitive enough to take accurate readings at very low flow rates yet flexible enough to handle a large range of test conditions. The Newcastle volume change gauge was designed by J. T. Araruna in 1995 as a part of a research programme at the University of Newcastle upon Tyne investigating laboratory measurement of the hydraulic conductivity of fine grained soils. It was designed based on the burette principles proposed by Bishop and Donald (1961) (Araruna 1995).

There are three tubes which are pressurised internally to the same pressure. As shown in Figure 3.4. The water levels in tube (1) and (2) are compared to that in the reference tube (3), by a differential pressure transducer. In fact, the sensor determines the pressure due to the weight of fluid in the flow tubes relative to the pressure in the reference tube, and hence the volume of fluid can be calculated from the known density of the fluid. Alternatively and more accurately especially when using different permeants or pore fluid from water, the volume change gauge can be calibrated directly by comparing the DPT output with the flow into a burette.

The two tubes shown in Figure 3.4 have different diameters, to allow a coarse setting with relatively large capacity for specimen volume change during saturation, consolidation, permeation stages for a coarse specimen, however a fine setting with a small capacity for permeation stage for a fine specimen when the selection valve (5 in Figure 3.4), a two-way valve is closed to give higher degree of sensitivity by isolating the large tube. The large tube is of acrylic plastic, resistant to solution of most salts and

acids, but incompatible with toluene, benzenes, phenols and some other organic compounds (Araruna, 1995).

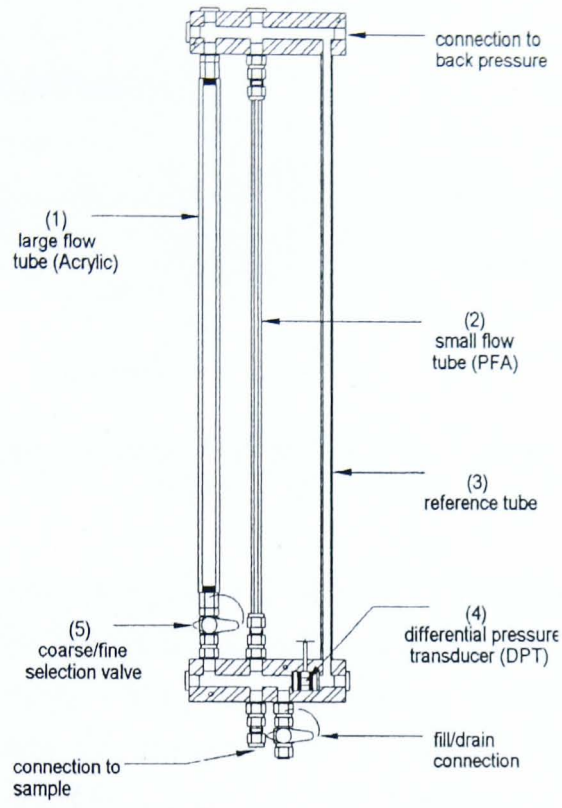

Figure 3.4 Newcastle volume change gauge (After Araruna, 1995).

The large tube has a capacity of approximately 120 cm^3 with a safe working pressure of 2000 kPa. The smaller tube is of PFA (perfluoroalkoxy), a copolymer version of Teflon with excellent corrosion resistance capabilities; its capacity is 5.3 cm^3 and has a safe working pressure of 1900kPa (Araruna, 1995). Connections were made with stainless steel Swagelock® fittings, guaranteed leak-tight to 27,000 kPa.

3.2.3 Flow pump system

The flow pump used in this system is a combination of a stainless steel syringe mounted on a standard variable-speed driver and a linear variable differential transformer (LVDT) (Figure 3.5). The stainless steel syringe consists of a 10mm diameter stainless steel piston within a cylinder. It has the features of low compliance, no leakage and easy deairing. The driver is a Harvard apparatus model 2274 micro litter pump commonly used in the medical profession.

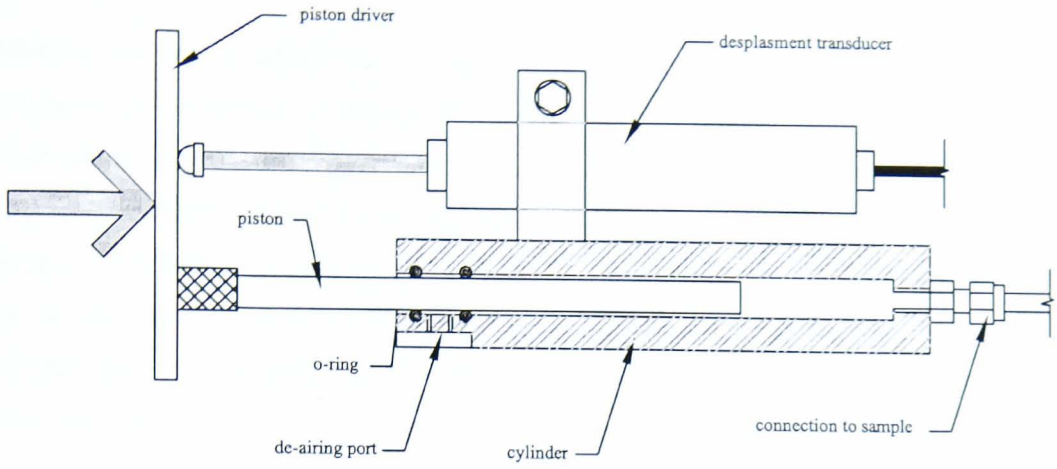

Figure 3.5 Schematic diagram of the flow pump system
(After Araruna, 1995).

The syringe piston is driven by a variable-speed direct-current motor through a transmission box with 30 combinations of gears between the worm gear and the motor. The controls on the pump, a switch and a gear selector, enable the syringe piston to be driven at 30 different speeds ranging from about $1.26*10^{-5}$ to $7.28*10^{-10}$ m/sec up to a distance of 115mm. The flow rate (q) is controlled by setting a constant speed for the displacement of the piston. The displacement which is measured by the LVDT is directly related to the flow rate because the piston is of known diameter. The correlation between the speed setting and the inflow rate is presented in Table 3.1.

Table 3.1 Speed setting against the inflow rate

Setting	Inflow Rates (ml/sec)
1	9.89E-04
2	7.07E-04
3	5.05E-04
4	3.61E-04
5	2.58E-04
6	1.84E-04
8	9.38E-05
10	4.79E-05
12	2.44E-05

3.3 *Systems modification*

Making use of the advantages of the flexible wall permeameter system such as its accuracy in measuring pressures and volume changes and also the full ability of continuous data logging, the flexible wall permeameters were modified to work not just as a constant flow system but also as a falling head system. A Newcastle volume change gauge was added by fixing a two way valve at the flow pump connection with the base of the specimen as can be seen in Figure 3.6. The purpose of the modification is to shorten the test duration and to compare the falling head technique with the constant flow technique.

3.4 *Calibration of equipment*

An understanding of the characteristics of transducers is essential to determine the accuracy and confidence of the measurements. A transducer is designed to give a changing output signal as the parameter being measured changes. The original signal from a transducer is usually an electrical current or voltage. Therefore it has to be processed before the signal is suitable for displaying, recording or controlling purposes.

Calibration of a transducer provides the relationship between the physical measurement and the transducer output signal and this relationship is called the transducer constant. Linear regression analyses were carried out on the linear portion of the output in order to calibrate each transducer. The calibration procedures that were carried out to calibrate the transducers used in the testing systems are presented in Appendix A. Calibration constants for the transducers used in this research are summarised in the following Table 3.2.

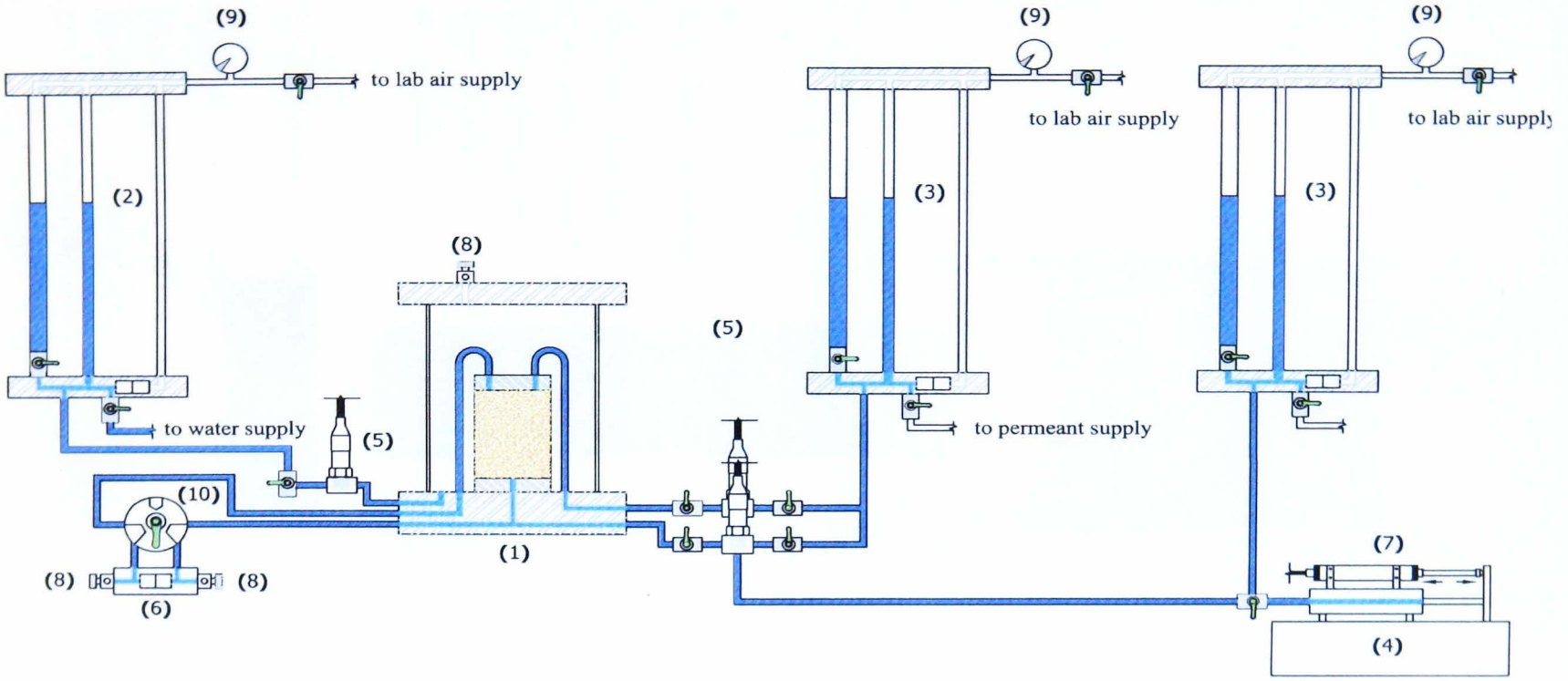

(1) triaxial cell
(2) cell volume change system
(3) in/outflow volume change system
(4) flow pump
(5) pressure transducer
(6) DPT
(7) LVDT
(8) de-airing valve
(9) pressure regulator
(10) 6-way valve

Figure 3.6 Schematic of the new modified flexible wall permeameter for constant flow and falling head tests.

Table 3.2 Summary of calibration results

Type of Transducer	Apparatus	Transducer Serial Number	Channel Number	Measurement	Transducer Constant	Unit
PTs	No. 1	215627	39	Top back Pressure	-0.5682	kPa
		409995	38	Bottom back Pressure	0.5807	kPa
		393106	37	Cell Pressure	0.5759	kPa
	No. 2	408343	32	Cell Pressure	0.5736	kPa
		393111	27	Top back Pressure	0.5719	kPa
		395385	26	Bottom back Pressure	0.5700	kPa
DPTs	No. 1	N/A	33	Cell vol. change Coarse setting	-0.1221	ml
				Cell vol. change Fine setting	-4.132	microl
		N/A	34	Back press. vol. change Coarse setting	-0.0624	ml
				Back press. vol. change Fine setting	-2.205	microl
		N/A	36	Head difference	-23.59	Pa
	No. 2	N/A	29	Cell vol. change Coarse setting	-0.1168	ml
				Cell vol. change Fine setting	-6.473	microl
		N/A	30	Back press. vol. change Coarse setting	0.0885	ml
				Back press. vol. change Fine setting	4.85	microl
		N/A	28	Head difference	-20.014	Pa
LVDT	Flow pump	3843-50	31	Inflow	2.11	microl
DPT	Inflow gauge	N/A	25	Inflow, coarse setting	-0.1147	ml
				Inflow, fine setting	-3.8	microl

3.5 Test Procedure

The test procedure for determining hydraulic conductivity in a flexible-wall permeameter includes specimen preparation and set-up, saturation stage, consolidation stage and permeation stage. A typical procedure is described here as shown in the flow chart in Figure 3.8, which was based on ASTM D5084 (1990), BS 1377 (1990), Daniel, et al. (1984), reported by Araruna (1995) and Chen (1997).

3.5.1 Specimen Preparation

Since the hydraulic conductivity can be influenced by many variables, great care was taken in preparing the test specimens to allow a comparison of results. The sandy specimen was prepared and set-up at the same time as explained in the following section (3.5.2.2). However the clayey specimen was prepared by mixing it with de-aired water

in a blender (Figure 3.7) to the desired water content which was 1.25 times the liquid limit, this was to obtain a homogenise and saturated specimen.

Figure 3.7 Sample mixing.

This slurry-like mixture was poured into a stainless steel consolidation cell (150mm diameter, 290mm length) so that uniformity could be expected and stress history controlled. Before putting the mixture under consolidation, the consolidometer applied axial stresses was checked. The axial pressure on the consolidometer was determined in SI units by filling the cell with water and increasing the axial pressure while a pressure transducer reading was taken (5 in Figure 3.10). Figure 3.9 shows a plot of the gauge reading in kg/cm^2 versus the pressure transducer reading in SI units (kPa).

The mixture was then loaded to the desired stress in the consolidometer, as shown in Figure 3.10, and allowed to drain. The stress was applied gradually to prevent a surge of slurry around the piston. When excess pore pressures were dissipated the sample was considered to be fully consolidated, the load was then released and the sample extruded. After removing the prepared sample from the consolidation cell, the sample was placed on a soil lathe and trimmed with a wire saw to the required diameter, i.e. 100mm.

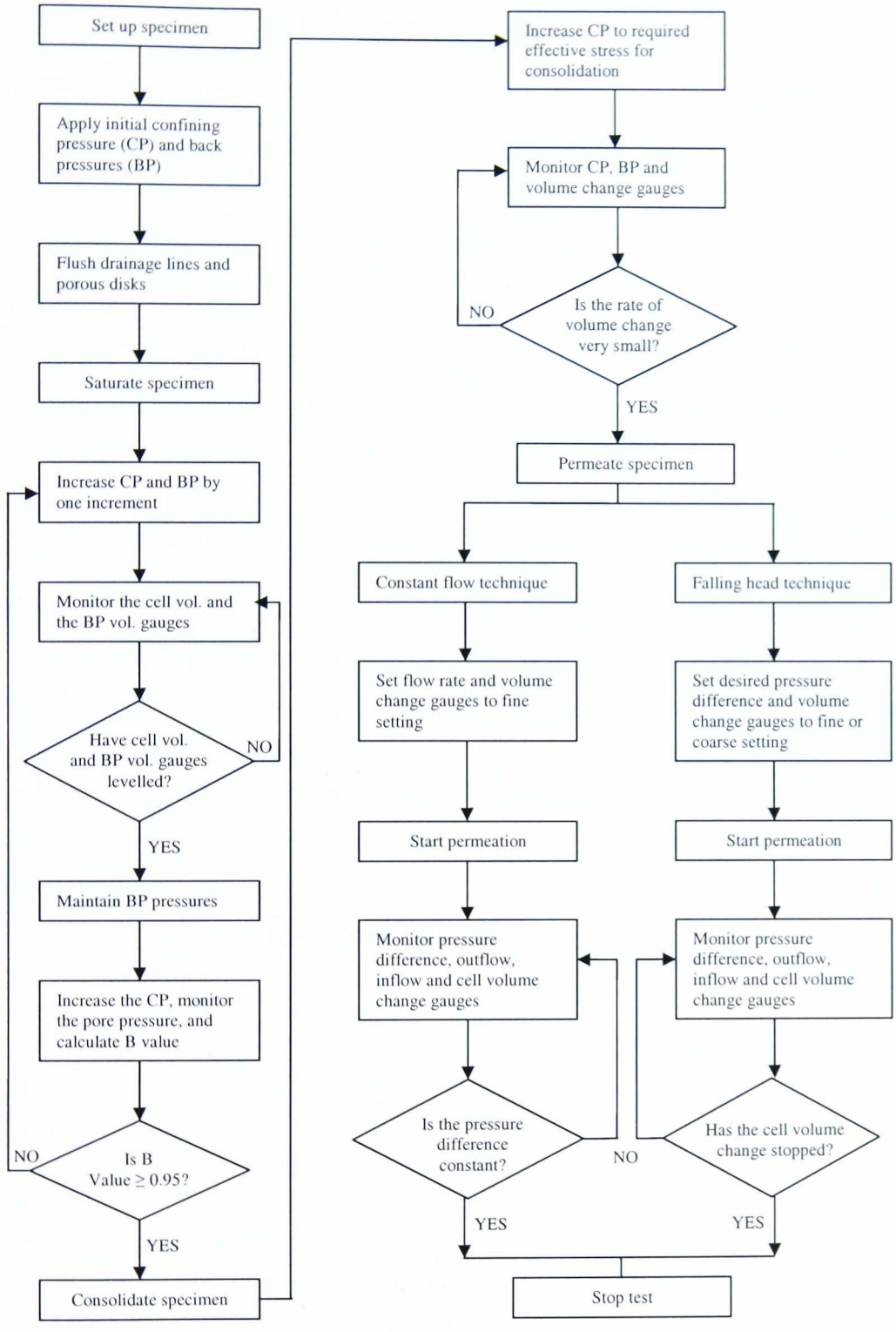

Figure 3.8 Flow chart of test procedure.

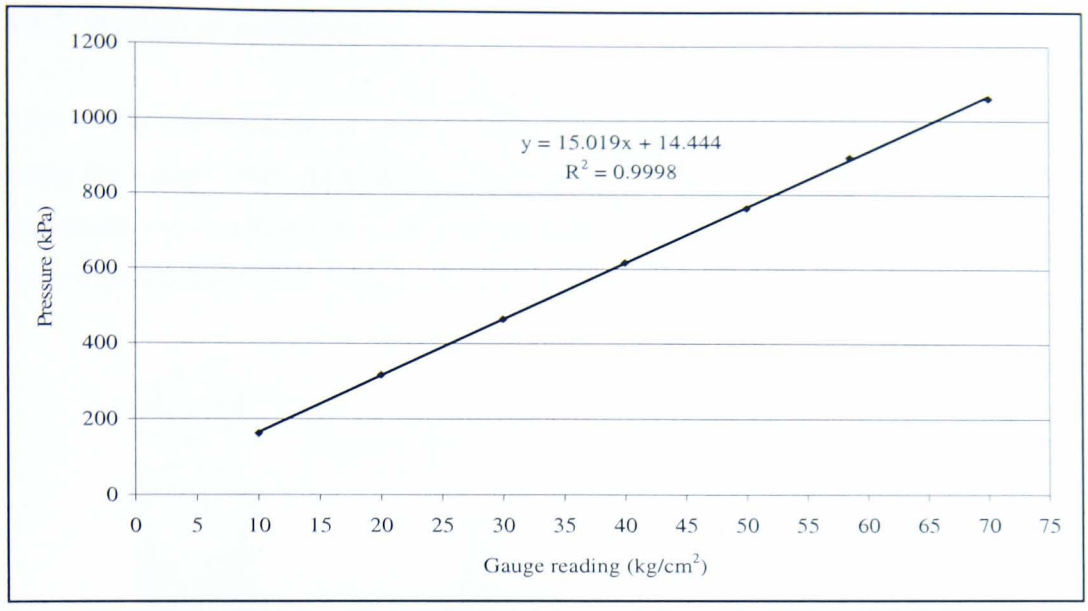

Figure 3.9 Determination of the axial pressure on consolidometer.

The 100mm sub-sample was placed in cradle mould where it was further trimmed in order to have a final specimen 100mm in high and 100mm diameter with flat parallel ends. The specimen was weighed and its diameter and length were measured using a calliper. The remaining parts of the sample were used to evaluate the physical indices of the specimen, i.e. dry density, void ratio and water content.

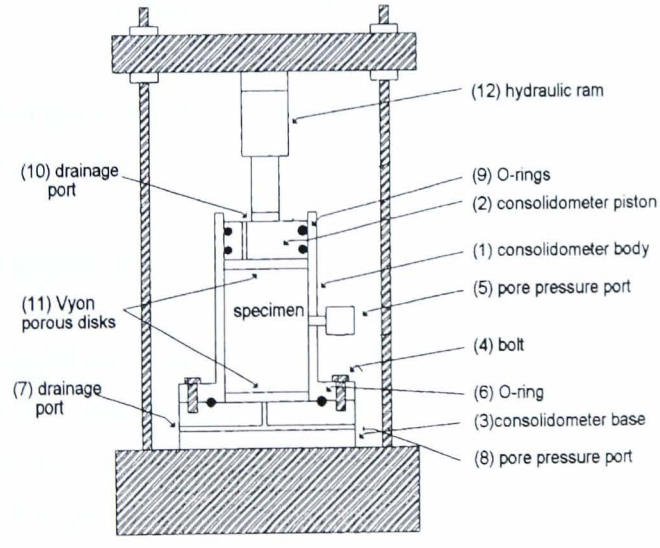

Figure 3.10 Consolidometer (Araruna, 1995)

3.5.2 Set-up of Specimen

Prior to the specimen set-up, volume change unit and pipes were flushed, deaired and tested for leakage. The permeameter reservoirs were filled with de-aired water. A rubber membrane was tested in a water tank; making sure no punctures existed, by a membrane tester that was designed for this purpose (Figure 3.11).

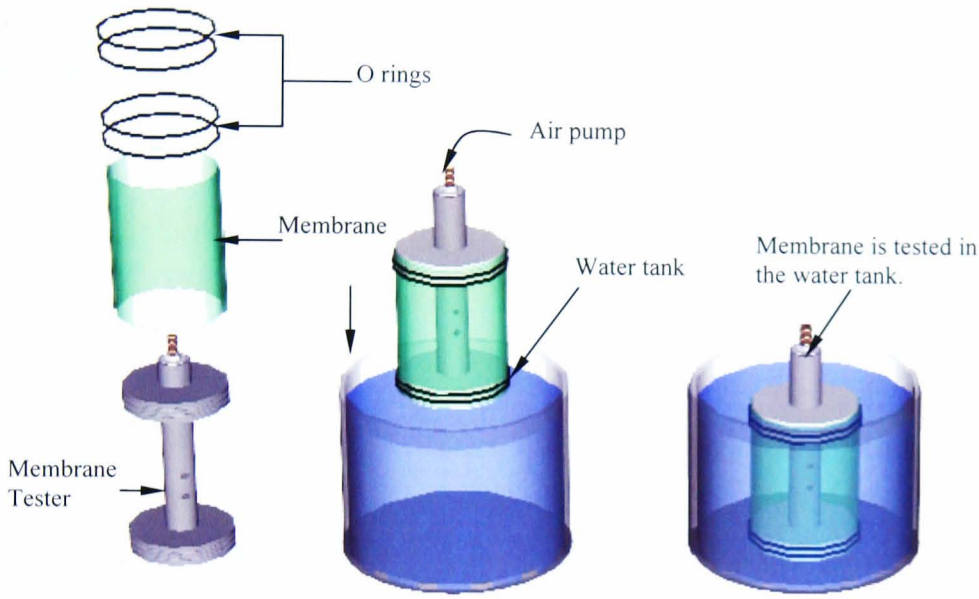

Figure 3.11 Membrane testing.

Based on the type of the tested soil specimen (clay or sand), two different methods were used to set-up the specimen.

3.5.2.1 For clay specimens

Two filter papers were cut to approximately the same diameter as the cross section of the test specimen. Two porous discs were soaked in a container of permeant water. One of the saturated porous discs was placed on the base pedestal, after that one of the filter papers was placed followed by the test specimen. Then, the second filter paper was placed on top of the specimen and subsequently the second saturated porous disc was placed followed by the top cap, with the drainage lines disconnected (Figure 3.12c). To eliminate the leakage between the membrane and the top cap and the base pedestal a very thin layer of silicon grease was applied on both of them.

Two O rings were placed around the membrane expander. Then the tested membrane was placed on the membrane expander and subsequently was placed around the test specimen (Figure 3.12 d, e and f). The O-rings were then placed to seal the membrane to the base pedestal. Using the membrane expander, two further O-rings were placed to seal the membrane to the top cap. The drainage tubes were then attached to the top cap (Figure 3.12).

The permeameter cell was assembled and carefully filled with deaired water from the de-aerator making sure no air was trapped inside it. A small confining pressure (50 kPa) was applied to the cell and a pressure less than the confining pressure (30 kPa) was applied to the influent and effluent system, and permeant water was flushed through the flow system to ensure that all visible air was removed from the flow lines the control valves were closed. At this stage the specimen was ready to be saturated.

3.5.2.2 For sand specimens

The preparation and set-up procedure for sandy specimens (e.g. fine, medium and coarse sands) involved in sealing a rubber membrane (100mm dia.) with two O rings around the base pedestal. A PVC split former (102mm dia.) was placed around the base pedestal. The membrane was stretched around the top rim of the former (Figure 3.13b). A batch of dry coarse grained soil was weighed (m_1) in a plastic container. To obtain a fully saturated specimen, the amount of water required to saturate the dry specimen was determined. Knowing the dry density, the void ratio (e) and the specific gravity of the sand particles (G_s), the water content (w_{sat}) for a fully saturated specimen was determined from the equation:

$$w_{sat} = \frac{e}{G_s} \qquad 3.1$$

then the amount of de-aired water to be added (m_{water})was calculated as following:

$$m_{water} = \left(\frac{w_{sat}}{100}\right) \times m_{soil} \ (grams\ or\ ml) \qquad 3.2$$

One third of this amount of de-aired water was poured into the split former. Then the sand was poured into the former maintaining a steady rate of pouring. The pouring was in a spiral motion from the periphery towards the centre. It was poured in three layers.

To reach the desired density, every layer was compacted using a steel rod (Figure 3.13d). Then the top surface was levelled carefully with the minimum disturbance. The top cap was placed on the top surface of the specimen and the membrane was sealed around it with the O rings. After that the sand left over, together with any other quantity which was spilled (m_2) was weighed. The difference (m_1-m_2) gives the actual mass of sand in the specimen (m).

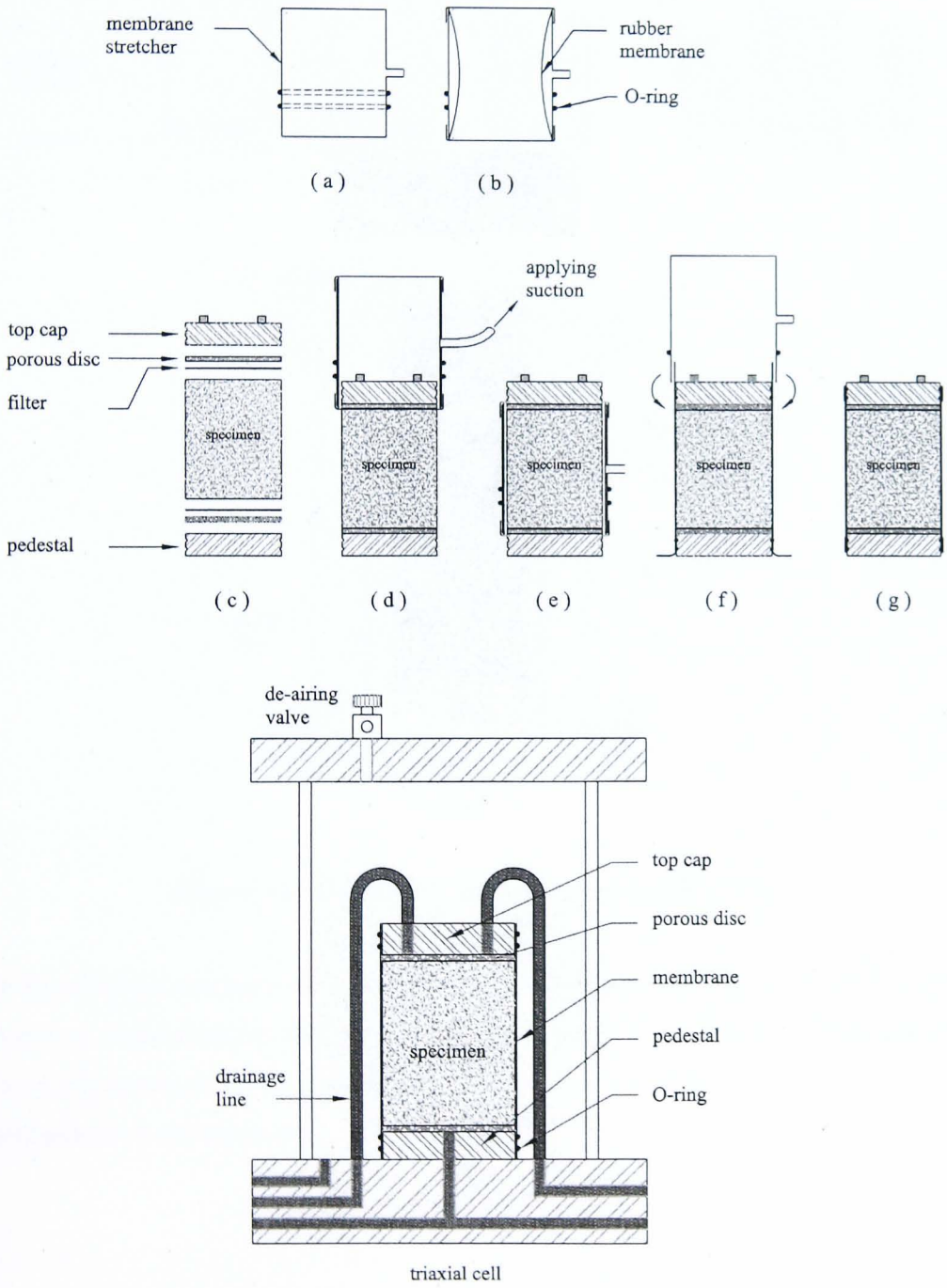

Figure 3.12 Clay specimen set-up.

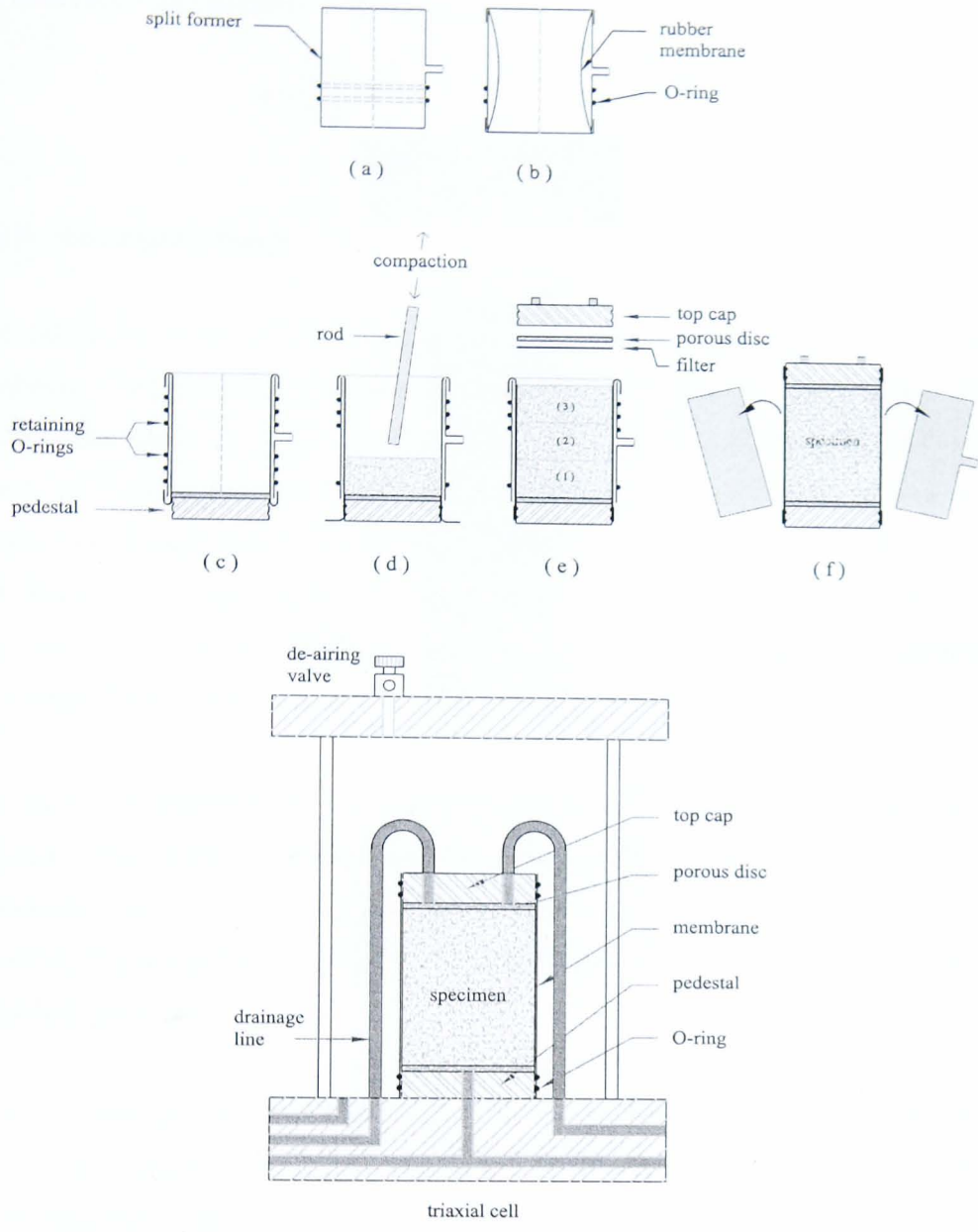

Figure 3.13 Coarse specimen preparation and set-up.

The mean height and diameter of the specimen were calculated by taking the average of number of measurements that were measured across the specimen at three positions around the perimeter to the nearest 1mm. This enabled the placement dry density to be calculated from the equation

$$\rho_d = \frac{m}{AL} \qquad 3.3$$

the void ratio was calculated from the equation:

$$e = \frac{G_s}{\rho_d} - 1 \qquad 3.4$$

3.5.3 Saturation Stage

The saturation of both clay and sand specimens was accomplished by backpressure saturation. The applied confining pressure and the back pressures were maintained from the previous stage. The back pressure using de-aired water was applied to the top and bottom of the specimen. This application of back pressure increments to achieve full saturation is widely used as a procedure for routine effective stress tests (Head, 1986). The objective is to apply sufficient back pressure to pore fluid in the specimen to cause any pore air to dissolve completely into the surrounding pore water thus obtaining a fully saturated specimen.

The procedure described below is typically good practice. The cell pressure and back pressure were raised in 50kPa increments, and a differential pressure of 20kPa was maintained between them. The pressure for each increment was applied to allow the pressures reach equilibrium. Figure 3.14 and Figure 3.15 were used to illustrate the following procedure:

1. A new file was set in the computer to monitor the cell pressure, back pressures, cell volume change, and specimen volume change for the first saturation increment. Both the cell volume change gauge and the back pressure volume change gauge were set to the course setting and the transducer constants were input in the computer.
2. The pressure around the specimen was raised to 50kPa, valve a in Figure 3.15 was opened to allow the confining pressure represented by c_1 in Figure 3.14 into the cell. The increase in confining pressure caused an increase in pore water pressure (u_1) within the specimen.
3. The t2 and b2 valves were opened and the back pressure in the pipes connecting the top and bottom of the specimen was raised to 30kPa.
4. The t1 and b1 valves were opened and the flow of water into the specimen through the back pressure volume change gauge was monitored and recorded by the computer at intervals.

5. When the pressures reached equilibrium, the cell volume changes and the back pressure volume changes became steady, at this stage the t2 and b2 valves were closed before applying a second increment of confining pressure (c_2). At this time, if the t2 and b2 valves were not closed the specimen started to consolidate under the effective stress of 20kPa.
6. The confining pressure was increased by 50 kPa. The saturation degree was checked by calculating the ratio between the increments and confining pressure (Skemton's parameter B) with the drainage pipes closed. In practice, the specimen was considered to be adequately saturated if the B value was equal to or greater than 95%.
7. If the B value was not adequate, the procedure from 4 to 6 was repeated, after increasing the confining and back pressures by 50 kPa maintaining the difference as 20kPa, as many times as necessary until the B value reached 95% or greater.

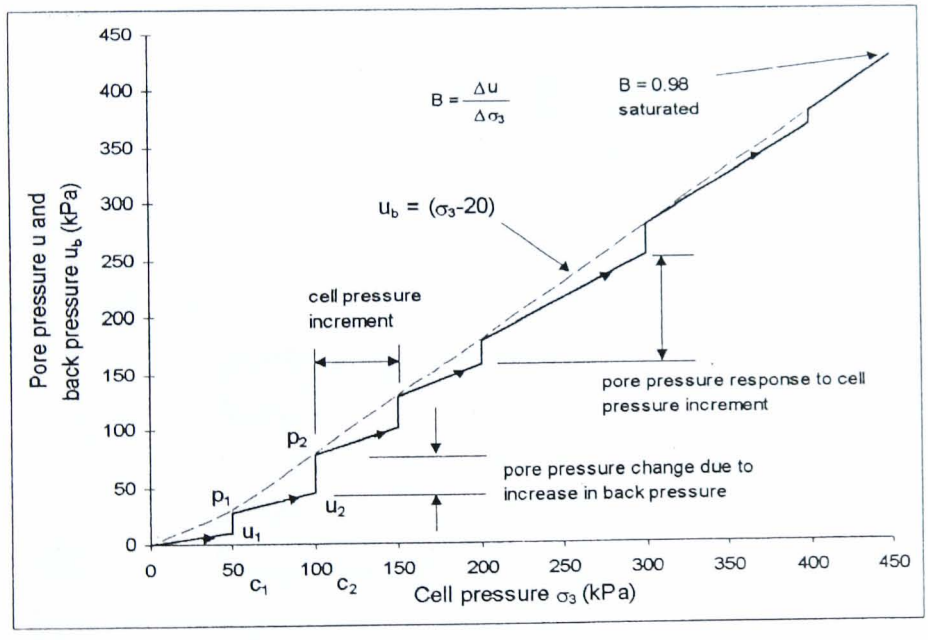

Figure 3.14 Plot of pore pressure, back pressure and cell pressure changes during saturation stage (Head, 1986).

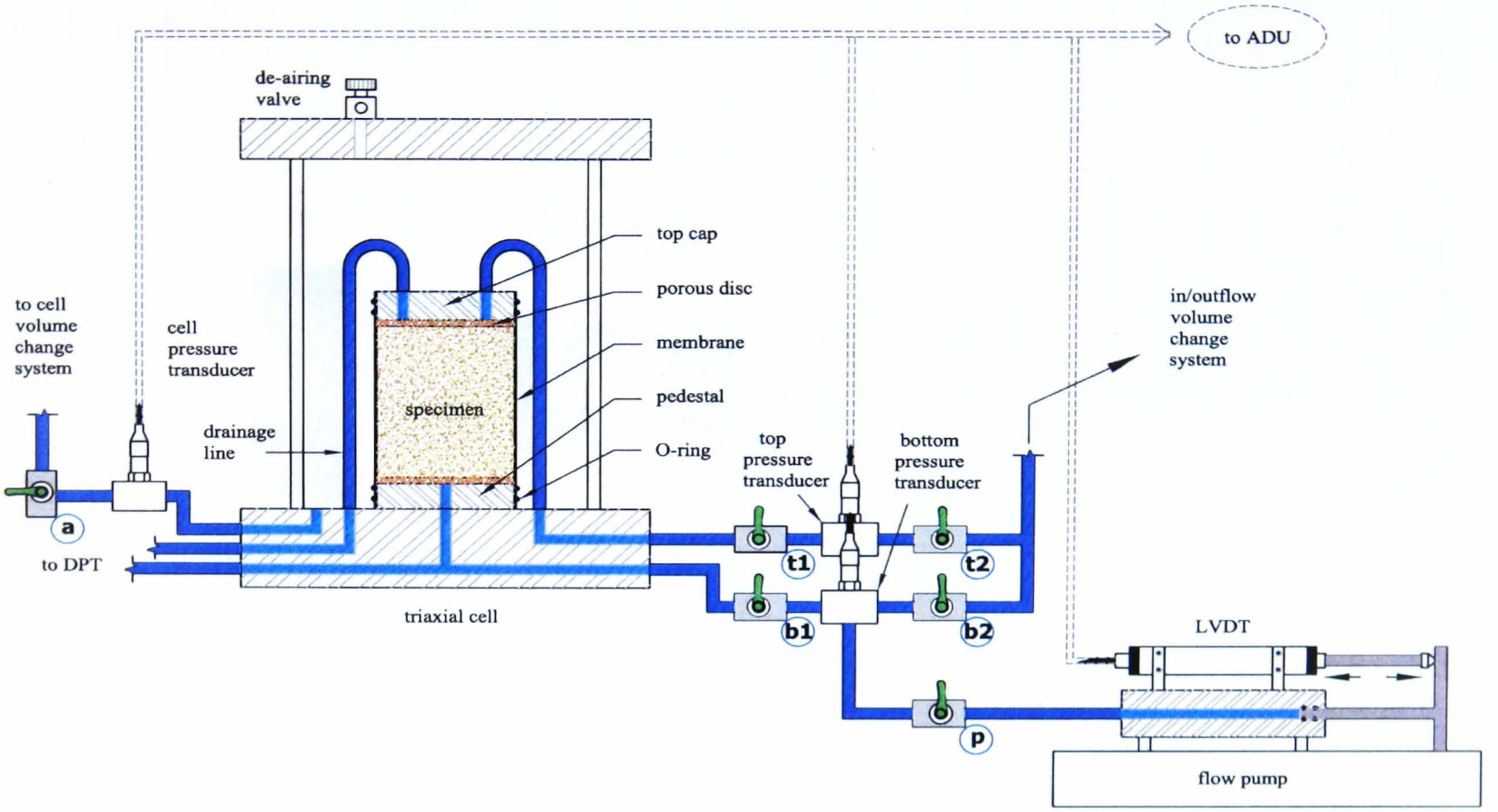

Figure 3.15 Details of a specimen in the flexible wall permeameter.

3.5.4 Consolidation Stage

Following the back pressure saturation, the specimen was consolidated at a desired effective stress. The volume change gauges at the course setting were used to consolidate a specimen. The cell volume gauge was filled with the de-aired water while the back pressure volume gauge was flushed to remove any air bubbles in the drainage lines and its water level kept low. The t1 and b1 valves in Figure 3.15 were closed to prevent drainage, while the t2 and b2 valves were opened to set the required back pressure. The desired effective consolidation stress was applied by increasing the cell pressure and keeping the back pressure constant in order to prevent releasing air bubbles. Consolidation was started by opening the t1 and b1 valves. Double drainage was allowed. The cell volume change and the back pressure volume change were monitored and recorded. The consolidation was terminated when the rate of the volume changes measured by the volume change gauges were very small. For a fully saturated specimen the cell volume change should be equal to the back pressure volume change. Figure 3.16 shows typical results from a consolidation stage.

After a specimen was consolidated, the volume change was determined and the results were used to calculate the changes in physical properties of void ratio and density and the consolidation parameters.

3.5.5 Permeation Stage using constant flow technique

The valve P in Figure 3.15 was set to the pump position for constant flow tests. Different inflow rates were used to produce a hydraulic gradient in order to determine the effect on hydraulic conductivity of soils. The desired gear position of the flow pump was selected. The flow pump was turned on 30 minutes before permeation started to give time for the gears to catch up to produce a steady inflow rate. During this time a new file was set in the computer and the differential pressure transducer was set and calibration constants for the fine setting of the volume change gauges were input in the computer. Just before the permeation started valve 5 in Figure 3.4 was closed setting the volume change gauges to their fine setting.

Permeation was started by closing valve b2 in Figure 3.15 that connected the base of the specimen with the volume change gauge and opening valve b1. At this time the pressure

at the base of the specimen started to gradually increase producing a pressure difference between top and bottom of the specimen which simultaneously created flow through the specimen. Data were recorded from the start of permeation until the pressure difference reached a steady state condition at which the test was terminated. If the chosen infusion rate did not result in a measurable pressure difference, the test was stopped and the specimen allowed to reach equilibrium. Then, a higher infusion rate was selected and the procedure repeated until an appropriate pressure difference was obtained. Otherwise the test was complete and the data were analysed to determine the coefficient of hydraulic conductivity.

3.5.6 Permeation Stage using falling head technique

The valve P in Figure 3.15 was set to the added Newcastle volume change gauge for the falling head technique. Different hydraulic gradients were used in order to determine the effect on hydraulic conductivity of soils. A new file was set in the computer and the differential pressure transducer was set and calibration constants for the fine or coarse setting of the volume change gauges were input in the computer according to the type of the soil. The calibration constants for fine setting were used when the specimen was made of fine soil, otherwise the calibration constant for the coarse setting were used and valve 5 in Figure 3.4 left open.

The desired pressure difference between the base and the top of the specimen was selected. Permeation was started by closing valve b2 in Figure 3.15 that connected the base of the specimen with the volume change gauge and opening valve b1. At this time the pressure at the base of the specimen rapidly increased producing a maximum pressure difference between top and bottom of the specimen which simultaneously created flow through the specimen. Data were recorded from the start of permeation until the test was terminated. Then, a higher pressure difference was selected and the procedure repeated and further test results obtained. When each test was complete, the data were analysed to determine the coefficient of permeability.

3.6 Data Analysis

During preparation of the specimen as described previously, the initial height, diameter and weight of the specimen were measured and used to analyse test data. This section

contains formulas that were used and describes the interpretation of a test. A typical test is used to demonstrate the process.

3.6.1 Initial condition

Using the measured height and diameter of the specimen L_o and D_o respectively, the initial cross-section area A_o, in cm^2, was calculated from the following equation:

$$A_o = \frac{\pi \cdot D_o^{\,2}}{4} \qquad 3.5$$

The initial volume V_o in cm^3 was calculated as following:

$$V_o = A_o \cdot L_o \qquad 3.6$$

The initial water content was determined by an oven drying method using the remaining part of the sub-sample before and after placing it in an oven for 24 hours. The initial water content, w_o, was calculated by the following equation:

$$w_o = \frac{m_s - m_d}{m_d} \times 100\% \qquad 3.7$$

where

m_s = initial mass of the sub-sample in grams before placing it in the oven.

m_d = dry mass of the sub-sample in grams after 24 hours in the oven.

The bulk density, ρ_o (Mg/m^3), was calculated from the mass of the specimen M_o (g), and its initial volume V_o (cm^3), using the following equation

$$\rho_o = \frac{M_o}{V_o} \qquad 3.8$$

The initial dry density ρ_d (Mg/m^3), was calculated using the bulk density ρ_o (Mg/m^3) and the initial water content w_o (%), using the following equation

$$\rho_d = \frac{100}{100 + w_o} \rho_o \qquad 3.9$$

the initial void ratio (e_o) was calculated the value of the measured particle density (G_s) and calculated dry density (ρ_d), according to

$$e_o = \frac{G_s}{\rho_d} - 1 \qquad 3.10$$

the initial degree of saturation (S_o)(%), was calculated using the initial water content (w_o)(%), the initial void ratio (e_o) and the particle density (G_s), according to

$$S_o = \frac{\omega_o \cdot G_s}{e_o} \quad (\%) \qquad 3.11$$

3.6.2 After Saturation

The specimen volume changes (ΔV_s) (cm^3), during saturation stage, were determined from the sum of the cell volume change gauge readings after each increment. So that the volume of the specimen after saturation (V_s) was calculated from the following equation:

$$V_s = V_o - \sum \Delta V_s \qquad 3.12$$

The length of the specimen (L_s) (cm) and its void ratio (e_s) after saturation were calculated, assuming the changes in dimension were equal in all direction, as following:

$$L_s = L_o\left(1 - \frac{1}{3}\frac{\Delta V_s}{V_o}\right) \qquad 3.13$$

$$e_s = e_o - (1 + e_o)\frac{\Delta V_s}{V_o} \qquad 3.14$$

The cross-section area of the specimen after saturation (A_s) (cm^2) was calculated using the following relation:

$$A_s = \frac{V_s}{L_s} \qquad 3.15$$

3.6.3 After Consolidation

Each specimen was consolidated under three effective stresses, 50, 100 and 200 kPa. At each effective stress, the specimen was consolidated in which a volume change (ΔV_c) was determined from the volume change reading on the back pressure volume change gauge or the cell volume change gauge since the specimen was assumed to be fully saturated.

The volume of the specimen after consolidation (V_c) (cm^3) was then determined by the following equation:

$$V_c = V_s - \Delta V_c \qquad 3.16$$

The length of the specimen after consolidation (L_c) (cm) was calculated using the following formula:

$$L_c = L_s\left(1 - \frac{1}{3}\frac{\Delta V_c}{V_s}\right) \qquad 3.17$$

The mean length during consolidation (L_{mean}) (mm) was taken as the average length before and after consolidation, as following:

$$L_{mean} = \frac{L_s + L_c}{2} \qquad 3.18$$

The cross-section area after consolidation (A_c) (cm^2) was calculated using the following equation:

$$A_c = \frac{V_c}{L_c} \qquad 3.19$$

The void ratio after consolidation (e_c) was calculated as following:

$$e_c = e_s - (1 + e_s)\frac{\Delta V_c}{V_s} \qquad 3.20$$

The coefficient of consolidation (c_v) (m^2/year) was calculated using Taylor's method from time representing 50% consolidation (t_{50}) obtained from the curve of specimen volume change versus square root time (min) (Figure 3.16).

$$c_v = \frac{0.026 L^2_{mean}}{t_{50}} \qquad 3.21$$

The coefficient of volume compressibility (m_v) (m^2/MN) was calculated from the following equation:

$$m_v = \frac{(e_1 - e_2)}{\delta\sigma'} \frac{1000}{1+e_1} \qquad 3.22$$

where

e_1 = void ratio before consolidation stage

3 e_2 = void ratio after consolidation stage

$\delta\sigma'$=effective stress during the consolidation stage

Based on Terzaghi's theory (Head, 1994), the calculated value of hydraulic conductivity (k_{cal}) was determined from the following formula:

$$k_{cal} = c_v \times m_v \times \rho_w \times g \qquad 3.23$$

For practical purpose the above formula was simplified as following:

$$k_{cal} = \left(\frac{c_v}{365.25 \times 24 \times 3600}\right)\left(\frac{m_v}{10^6}\right)\left(1 \times 10^3\right) \times 9.81$$

$$k_{cal} = c_v \times m_v \times 0.31 \times 10^{-9} \quad \text{(m/s)} \quad 3.23$$

Where:

c_v = Coefficient of consolidation, m^2/year

m_v = Coefficient of volume compressibility, m^2/MN

The calculated value of hydraulic conductivity was then used to estimate the desired infusion rate (q) (cm^3/s) by the following equation assuming value of hydraulic gradient equals to one in order to induce a small head difference across the specimen during permeation.

$$q = k_{cal} \times A_c \times 10^{-9} \qquad 3.24$$

3.6.4 After Permeation

The applied pressure difference (Δp) across the specimen was measured by the DPT as the permeant flowed from the bottom to the top of the specimen. When the constant flow technique was used, the inflow was generated by the flow pump while the outflow was measured by the volume change gauge, in its fine setting, connected to the top of the specimen.

The hydraulic gradient (i) at the steady state condition was calculated as following:

$$i = \frac{1000 \times \Delta p}{9.81 \times L} \qquad 3.25$$

The hydraulic conductivity (k_h) (m/sec) using the constant flow technique was calculated from the following equation using the inflow and outflow average value:

$$k_h = \frac{q}{i \times A} \qquad 3.26$$

When the falling head technique was used, the inflow was generated by applying a pressure difference between the top and bottom back pressures. This pressure difference was measured by the DPT as the permeant flowing from the bottom to the top of the specimen. The inflow and outflow rates were measured by the volume change gauges connected to the bottom and top of the specimen respectively. The hydraulic conductivity (k_h) (m/sec) using the falling head technique was calculated from the following equation using the pressure differences at the start (Δp_1) and the end of the test (Δp_2):

$$k_h = \frac{a_{in} \cdot a_{out} \cdot L}{A \cdot \Delta t \cdot (a_{in} + a_{out})} \ln\left(\frac{\Delta p_1}{\Delta p_2}\right) \qquad 3.27$$

3.6.5 Presentation of Data

Hydraulic conductivity data are presented and reported in tabular and graphical form. There are two relevant graphical plots: one for consolidation stage and one for the permeation stage. An example of the presentation of data is given in Table 3.3; Figure

3.16 for consolidation results; Figure 3.17 for constant flow permeation results; and Figure 3.18 for falling head permeation results. The other related data will be appeared and discussed in chapter 5 and in Appendix B.

3.7 Summary

This chapter presents a detailed description of the flexible wall permeameter using the constant flow technique and its modification for using the falling head technique. The constant flow technique is carried out by generating a constant flow using a flow pump; the pressure difference is then monitored by DPT from which the induced hydraulic gradient is determined. While the falling head technique is carried out by setting a pressure difference across the specimen using the Newcastle Volume Change Gauges connected to the top and bottom of the specimen. The flexible wall testing system allows control of the stresses acting on the soil specimen; it also reduces the risk of the side-wall leakage. A full test procedure for both techniques is also presented.

The use of the different types of electronic transducers to allow of for the flow and pressure measurements makes it necessarily to assess and calibrate all transducers. Therefore, detailed calibration procedures are carried out for every transducer and are found in this chapter in order to gain confidence in the results obtained. The results from using both techniques are presented and discussed in Chapter five. Finally they are then to evaluate the accuracy due to the new modification carried out on the flexible wall permeameter.

Table 3.3 Example of Data Presentation

Stage	Data	SAMPLE NO.12
Initial	Meight (g)	1411.6
	Length, L_o (mm)	100.5
	Diameter, D_o (mm)	102.5
	Area, A_o (mm^2)	8251.6
	Volume, V_o (cm^3)	829.28
	Bulk density, ρ_o (Mg/m^3)	1.70
	Water content, w_o (%)	47.9
	Initial dry density, ρ_d (Mg/m^3)	1.15
	Particle density, G_s	2.63
	Initial void ratio, e_o	1.28
	Initial degree of saturation, S_o (%)	98.1

Saturation	Effective saturation stress, (kPa)	20
	B value	0.95
	Total volume change, δV_s (cm^3)	-3
	Volume, V_s (cm^3)	832.28
	Length, L_s (mm)	100.6
	Area, A_s (mm^2)	8271.5
	Void ratio, e_s	1.29
Consolidation	Effective consolidation stress, kPa	50
	Volume change, δV_c (cm^3)	7.75
	Volume, V_c (cm^3)	824.53
	Length, L_c (mm)	100.5
	Area, A_c (mm^2)	8204.3
	L_{mean} (mm)	100.6
	Void ratio, e_c	1.27
	$t_{50\%}$, (min)	30.25
	c_v (m^2/year)	4.57
	m_v (m^2/MN)	0.19
	k_{cal} (m/s)	2.6E-10
Consolidation	Effective consolidation stress, kPa	100
	Volume change, δV_c (cm^3)	11.39
	Volume, V_c (cm^3)	813.14
	Length, L_c (mm)	100.2
	Area, A_c (mm^2)	8116.4
	L_{mean} (mm)	100.3
	Void ratio, e_c	1.24
	$t_{50\%}$, (min)	25
	c_v (m^2/year)	5.50
	m_v (m^2/MN)	0.14
	k_{cal} (m/s)	2.4E-10
Consolidation	Effective consolidation stress, kPa	200
	Volume change, ΔV_c (cm^3)	17.75
	Volume, V_c (cm^3)	795.39
	Length, L_c (mm)	99.7
	Area, A_c (mm^2)	7976.5
	L_{mean} (mm)	100.0
	Void ratio, e_c	1.19
	$t_{50\%}$, (min)	26.5
	c_v (m^2/year)	5.15
	m_v (m^2/MN)	0.11
	k_{cal} (m/s)	1.7E-10

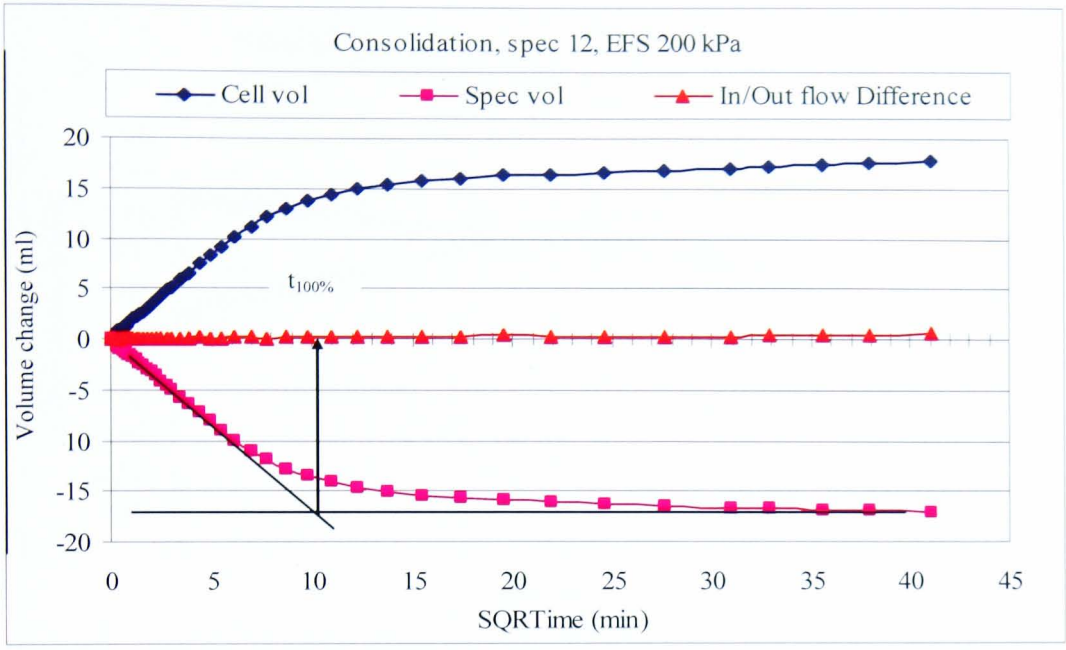

Figure 3.16 Typical consolidation stage results.

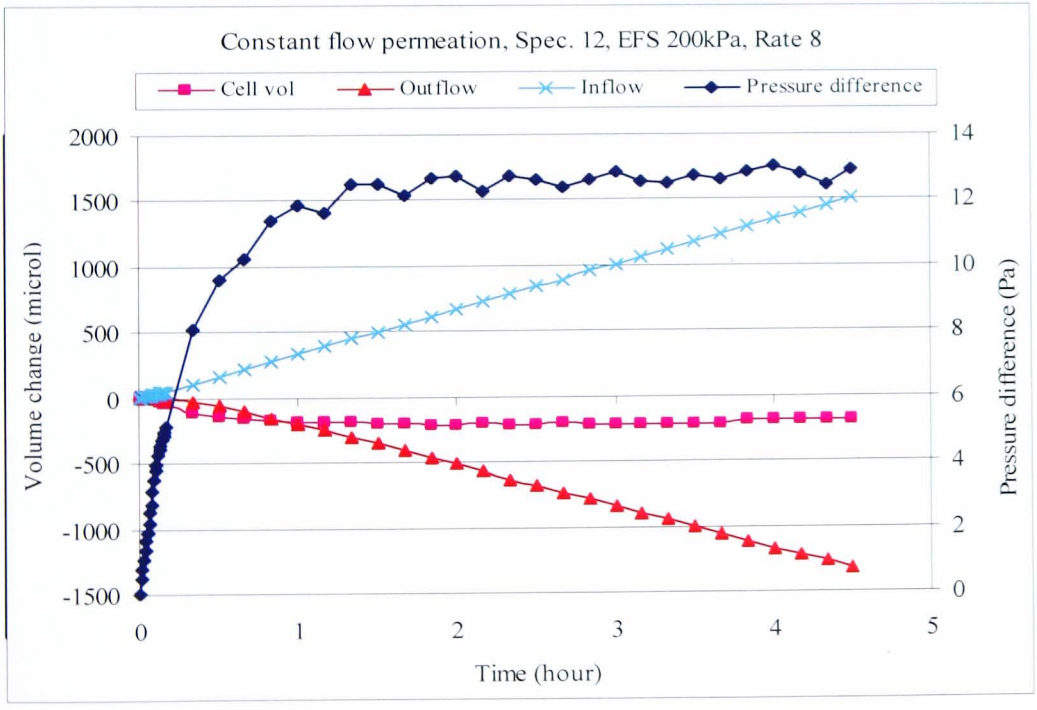

Figure 3.17 Typical constant flow permeation results.

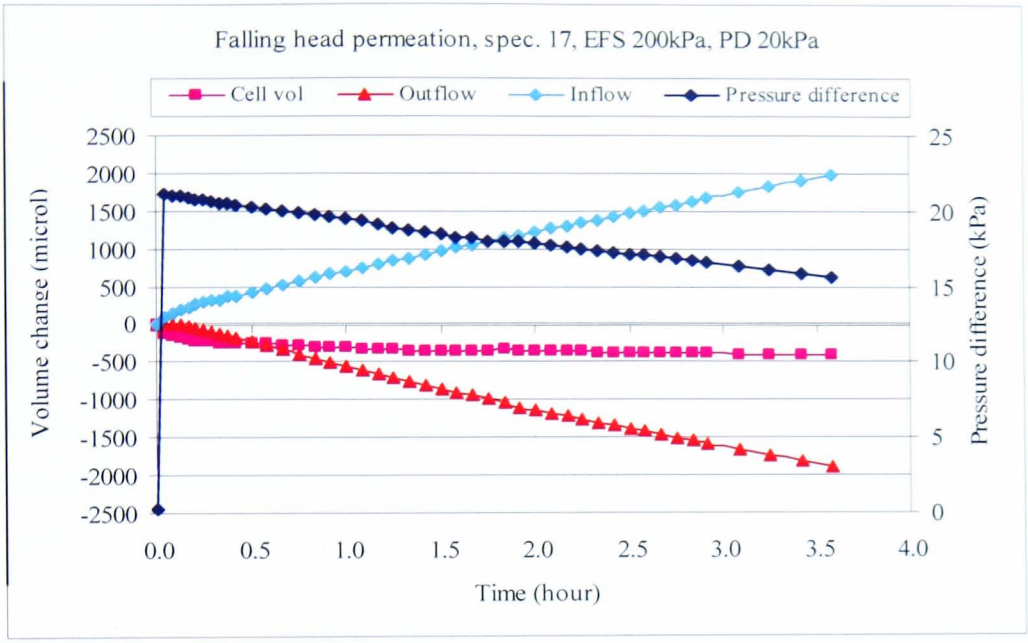

Figure 3.18 Typical falling head permeation results.

Chapter 4

Design of the Thermal Apparatus and its Experimental Procedure

4.1 Introduction

This chapter provides information about the design criteria, the principles behind the design and the test theory for the new thermal conductivity testing systems. It also presents the experimental procedure and the method of interpretation that were used to determine the thermal conductivity of disturbed and undisturbed soil specimens in this research.

In the review of the methods for determining the thermal conductivity of soils presented in chapter two, the steady state methods are quite complicated and required a large sample. Therefore, it was decided to design a new device to determine the thermal conductivity of soils.

4.2 Design criteria

The design of the thermal cell device is carried out to establish the criteria for the laboratory measurement of the steady state heat conduction through a cylindrical soil specimen, when its base is in contact with an aluminium heater held at constant temperature. This criterion is based on the one dimensional heat flow theory. One-dimensional steady state heat conduction experiments require a constant temperature gradient from the bottom of the specimen to the top of the specimen continuing until the temperature at the convection surface of the specimen reaches its maximum steady state condition.

This test method is comparable, but not identical, to the steady state heat flux measurement and thermal transmission properties by means of the guarded hot plate apparatus (ASTM C177).

4.3 *Design principles*

The principle of the design is to provide a simple thermal conductivity testing system to determine the thermal conductivity of a soil. It should accommodate a representative soil sample, such as the size of the specimen that is obtained from the U-100 type of sample which represents the most common type of sample that can be obtained from a geotechnical site investigation.

The engineering design principles behind the operation of the thermal conductivity testing system are fairly simple. To create a heat flow in a soil specimen, a thermal gradient should be generated across it. This can be carried out by placing a cylindrical soil specimen on a heater with the same cross sectional area and keeping its top exposed to room temperature. The specimen's side should be insulated to ensure one dimensional heat flow. The heater should be held at a desired constant temperature. To insure the one dimensional heat flow, the specimen should be insulated by surrounding it with a very low thermal conductivity insulator such as glass wool, an acrylic tube to stop air circulation around the specimen (Figure 4.1). The heat will flow from the bottom of the specimen towards its top and then convected to the surrounding medium. The temperature gradient was measured at the top and bottom of a specimen and a two points within the specimen.

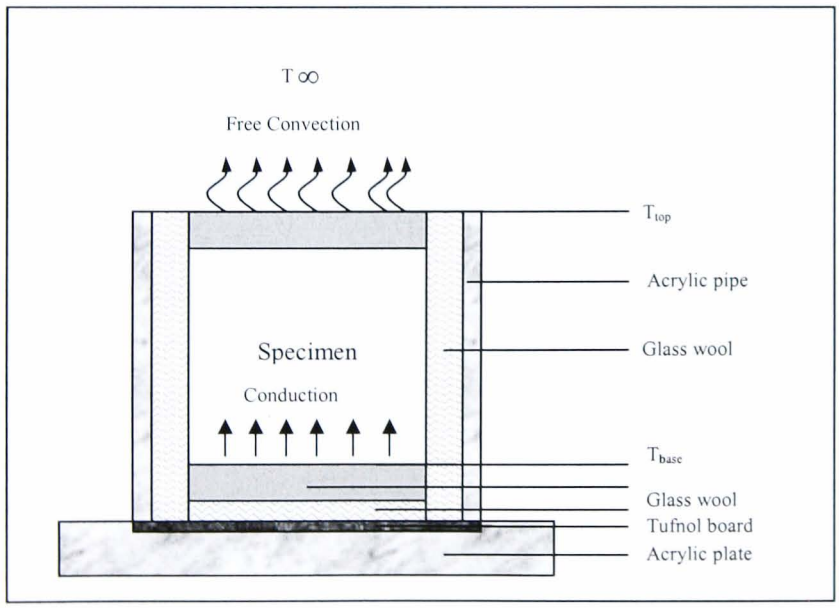

Figure 4.1 Schematic diagram of the heat transfer in the cell.

4.4 *Test theory*

The equation describing one-dimensional steady state conduction is given below. It is known as Fourier's law (Holman 1997), where the thermal conductivity, k_t, is defined as the quantity of heat flow in a unit time through a unit area of a substance caused by a unit thermal gradient.

$$k_t = \frac{Q}{A \cdot (\Delta T / \Delta L)} \qquad 4.1$$

Where

Q = the amount of heat passing through the specimen, Watt

A = specimen's cross section area, m^2

ΔT = temperature difference across the specimen. °C

ΔL = specimen's height, m

Q / A is known as the heat flux (q) which is causing the thermal gradient, $\Delta T / \Delta L$. In this test the specimen height is normally 100mm; A is the cross sectional area of the specimen which is nominally 7854 (mm^2).

The amount of heat passing through the specimen (Q) (input power per unit time) can be determined in two ways. The first is to determine the rate of the input electrical power provided to the heater and the second is to determine the dissipation of stored energy during cooling after reaching the steady state condition.

Several attempts were made to determine the input electrical power at the steady state condition by measuring it directly. The first attempt was with using a power meter; however the power meter used was for monitoring a high rate of energy comparing to that used in the system. The second attempt was to measure the power consumption of the heater; the electronics circuit shown in Figure 4.2 was designed. It is basically an operational amplifier circuit that is used to amplify the current that passes through the heater so that it can be monitored with a PC to draw an ON/OFF diagram of the power. The final power consumption will be computed as the averaged power over the steady state period. A voltage divider rule idea is applied by connecting a small value resistor, 1.5 ohm, in series with the heater, 150 ohm, hence the voltage across the resistor is ≈ 2.37 V AC. This voltage is used to supply the operational amplifier circuit. The

operational amplifier circuit consists of the widely used 741 amplifier and some resistors. As can be seen from Figure 4.2, the 741 amplifiers are connected in series where the first amplifier works as a buffer that buffers the current flowing through the heater before it passes to the non-inverting input of the second amplifier which is differentiated by the inverting input, which is supplied from +15 V supply. Finally the amplified output is fed to the PC logger port. The PC logger calculates the power that is consumed by the heater and produces ON/OFF pulses of the power. By averaging these pulses over the steady state period the dissipated power can be estimated. The input voltage to the amplifier is an AC voltage, which means that the input voltage at the amplifier will be positive for half cycle and negative for the other half. This fluctuation caused the amplifiers to malfunction. Therefore, it was thought that the amplifiers should be supplied with a DC voltage. Hence a diode was installed, which has a voltage drop equal 0.6 volt, before the first amplifier. Although the amplifier supply was ≈ 1.8 volt, it worked, however as the supply of the circuit was only the positive half cycles the performance was not convincing. Therefore, a full wave rectifier should be installed instead of one diode. However, as the rectifier consists of four diodes and with the voltage drop of each diode 0.6, a 2.4 volt drop will be needed which is almost the supply voltage; hence the supply has to be increased which requires, in turn, a new design.

A more sensitive meter could have been developed but the rapid switching rate meant that this would have been a complex device and beyond the scope of this research. Further the equipment had to be simple to operate and available for used in routine investigations. Appendix C shows a plate of the designed circuit box.

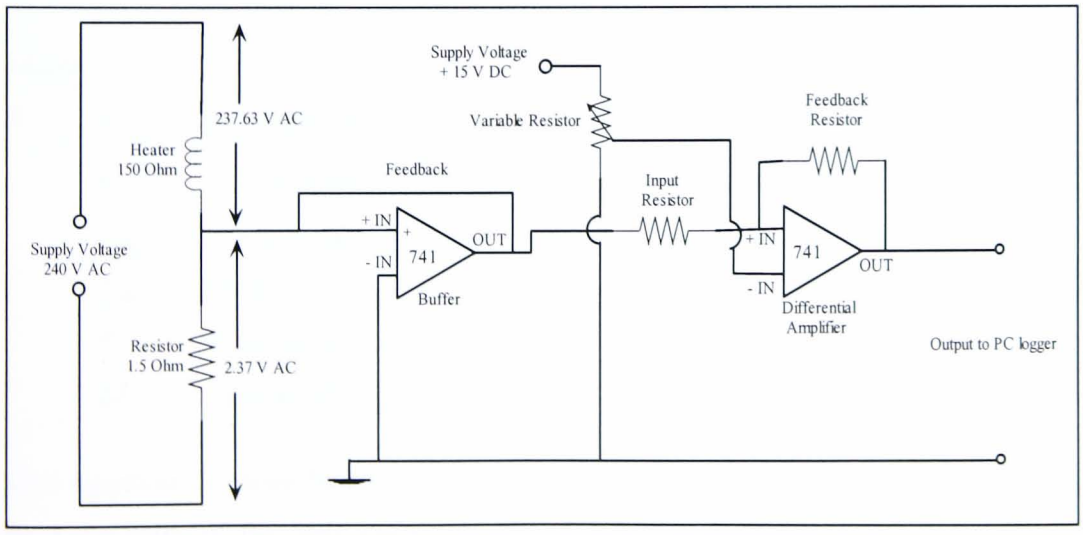

Figure 4.2 Proposed electrical circuit to monitor the input power for the heater.

The second method of analysis was based on the law of conservation of energy, by assuming that the energy put into the specimen from the heating element (Q_{cond}) during the steady state stage must be equal to the energy lost from the specimen by convection (Q_{conv}), whereby $Q_{conduction} = Q_{convection}$ (Figure 4.1). The convective heat loss from the top of the specimen is governed by Newton's law of cooling (Incropera and De Witt 1996, Holman 1997):

$$Q_{conv} = h \cdot A \cdot (T_{conv} - T_{\infty}) \qquad 4.2$$

where:

Q_{conv} = the amount of heat loss by convection, Watt

h = the convection heat transfer coefficient, W/m^2 °C

A = the cross-sectional area of the specimen, m^2

T_{conv} = the temperature at the convection surface, °C and

T_{∞} = the room Temperature °C.

Hence, the thermal conductivity is given by

$$Q_{conduction} = Q_{convection} \qquad 4.3$$

$$k_{t\,soil} \cdot A \cdot \frac{T_{base} - T_{top}}{\Delta L} = h \cdot A \cdot (T_{top} - T_{\infty}) \qquad 4.4$$

$$k_{t\,soil} = h \cdot \Delta L \cdot \frac{T_{top} - T_{\infty}}{T_{base} - T_{top}} \qquad 4.5$$

where:

$k_{t\,soil}$ = the thermal conductivity of the soil (W/m. °C),

h = the convection heat transfer coefficient (W/m^2 °C),

T_{top} = temperature at the specimen's top at the steady state condition, °C

T_{base} = temperature at the specimen's base at the steady state condition, °C

T_{∞} = room temperature, °C.

ΔL = specimen's height, m.

This equation can then be used to find the thermal conductivity of the soil specimen once the value of the convection heat transfer coefficient (h) is determined. The best

way of determining h is by comparing a theoretical convection cooling curve for a given h value to the measured cooling curve based on the temperature measurements taken at intervals from the specimen. This procedure is called the best fit method and is comparable with that in the interpretation of consolidation tests.

To generate the theoretical cooling curve it is necessary to assume that the convective heat loss from the top of the specimen after the power is switched off is equal to the decrease in the internal stored energy of the soil specimen (Holman 1997). Hence at any time, t, after the start of the cooling curve, the theoretical temperature can be calculated from the energy balance principle that the stored energy, E_{stored} must equal the lost energy, E_{out} as following:

$$E_{stored} = -E_{out} \qquad 4.6$$

$$m \cdot c_p \cdot \frac{dT}{dt} = -h \cdot A \cdot (T_o - T_\infty) \qquad 4.7$$

The initial condition $T = T_o \quad at \quad t = 0$, therefore the solution to equation 4.7 is as follow:

$$T = T_\infty + (T_o - T_\infty) \cdot e^{\frac{-h \cdot A}{m \cdot c_p} \cdot t} \qquad 4.8$$

The theoretical cooling curve can be generated by equation 4.8 but it is applicable only in the case of a dry specimen. T is the theoretical temperature of the base of the specimen during cooling as a function of time, t, T_∞ is the room temperature, T_o is the temperature at the top of the specimen at the start of the cooling curve, A is the cross sectional area of the specimen, m is the mass of the dry soil, h is the convection heat transfer coefficient and c_p is the soil specific heat capacity. However, in the case of partially saturated or saturated soils, the amount of water should be taken into account by adding its effect based on its mass and its specific heat to those for the dry soil particles using the following equation:

$$\Sigma m_i \cdot c_{pi} = (m \cdot c_p)_{soil} + (m \cdot c_p)_{water} \qquad 4.9$$

Hence, equation 4.8 can be rewritten in a general form as following:

$$T = T_\infty + (T_o - T_\infty) \cdot e^{\frac{-h \cdot A}{\Sigma m_i \cdot c_{p_i}} \cdot t} \qquad 4.10$$

The convection heat transfer coefficient, h, can be determined by placing the above equation in a spreadsheet and varying its value until a best fit curve is obtained between the measured cooling curve and the theoretical prediction of the curve (Figure 4.3). Once the value of h is established, k_t can be calculated using equation 4.5.

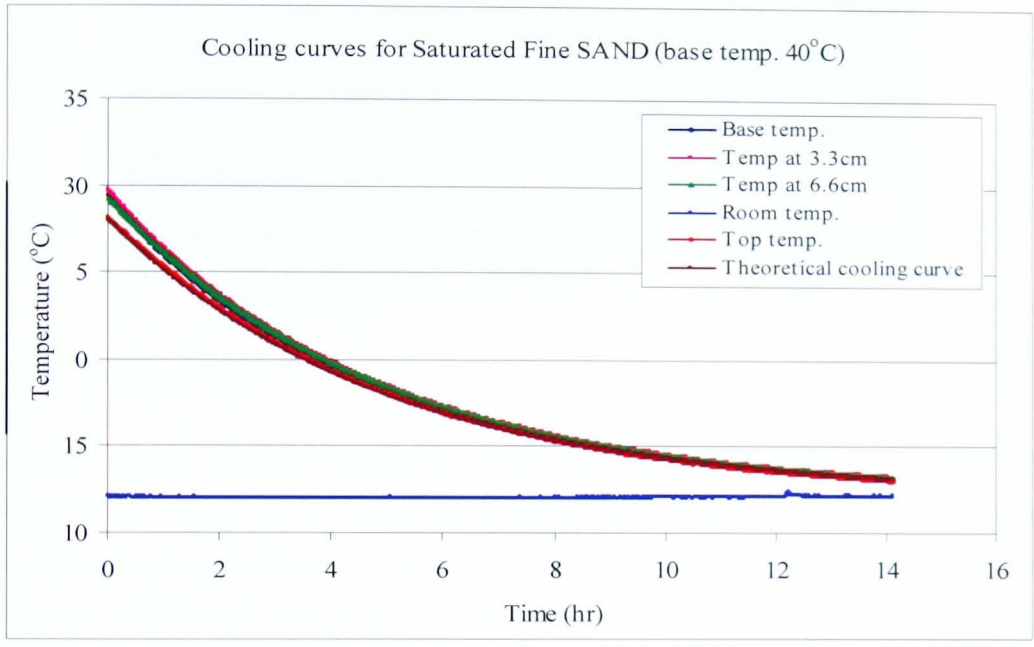

Figure 4.3 The best fit cooling curves to determine h.

4.5 *Description of the Thermal Conductivity Testing System*

Two thermal conductivity testing systems were designed and built. The thermal testing systems shown in Figure 4.4 consist of four components: the thermal cell, the temperature control unit, the Pico logger with PC, and the temperature sensors (Type K thermocouples). A brief explanation of each of these components is given below.

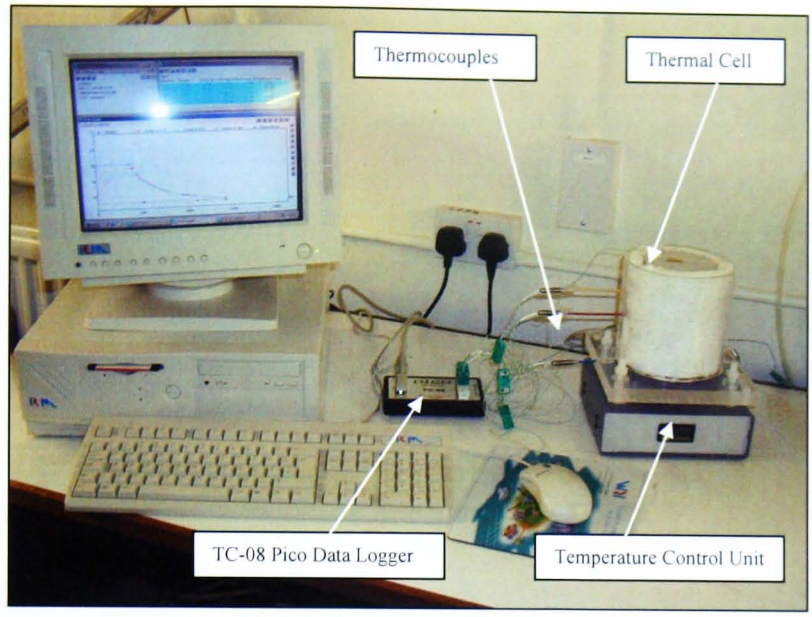

Figure 4.4 The thermal conductivity testing system.

4.5.1 Thermal Cell

The thermal cell, shown in Figure 4.5, consists of an acrylic base plate (12) (200mm by 200mmm) to support the base conducting aluminium cylinder (heater) (7) and to mount the cell onto the temperature control unit (14). Between the acrylic base plate (12) and the heater (7) there are two types of insulation, the glass wool insulation (8) (k_t = 0.038 W/m°C) and a Tefnol board (9) (130mm dia., 3mm thick). This insulates the base of the plate ensuring that the heat flows vertically towards the base of the specimen. Nylon screws with low thermal conductivity are used to clamp the heater with the glass wool and the Tefnol board together with the acrylic base plate to minimise any heat loss. The base conducting cylinder is made of a 100mm diameter, 20mm thick aluminium disc. A cartridge heater and two thermocouples (1.5 mm dia, 150 mm long) were inserted into the base conducting cylinder which acts as a uniform source of heat across the base of the specimen. One of these thermocouples is connected to the temperature control unit for a feedback to maintain a constant temperature and the other is connected to the Pico data logger to monitor and record the specimen base temperature.

The top conducting cylinder consists of an aluminium disc (5) that might contain an optional cartridge heater to control the temperature of the top of the specimen if the temperature is to be maintained above the room temperature. The aluminium has very high thermal conductivity (200 W/m.°C), for this reason it was chosen to dissipate the conducted heat from the top of the specimen to air through convection. To confirm that

it has no effect on the top temperature of a specimen, two thermocouples were used to determine the deference in temperature between the top and bottom surfaces of the aluminium top disc. The difference was found to be very small to the extent it had little impact on the interpretation.

The specimen's dimensions were 100mm in diameter and 100mm long (6) so that undisturbed specimens obtained from standard UK investigations can be used. It is also possible to test reconstituted representative soils. In order to maintain the water content of a specimen and to support coarse grained soils, the specimen is surrounded by a rubber membrane (3) which is sealed onto the bottom and top conducting cylinders (7 and 5 respectively) by O rings (4).

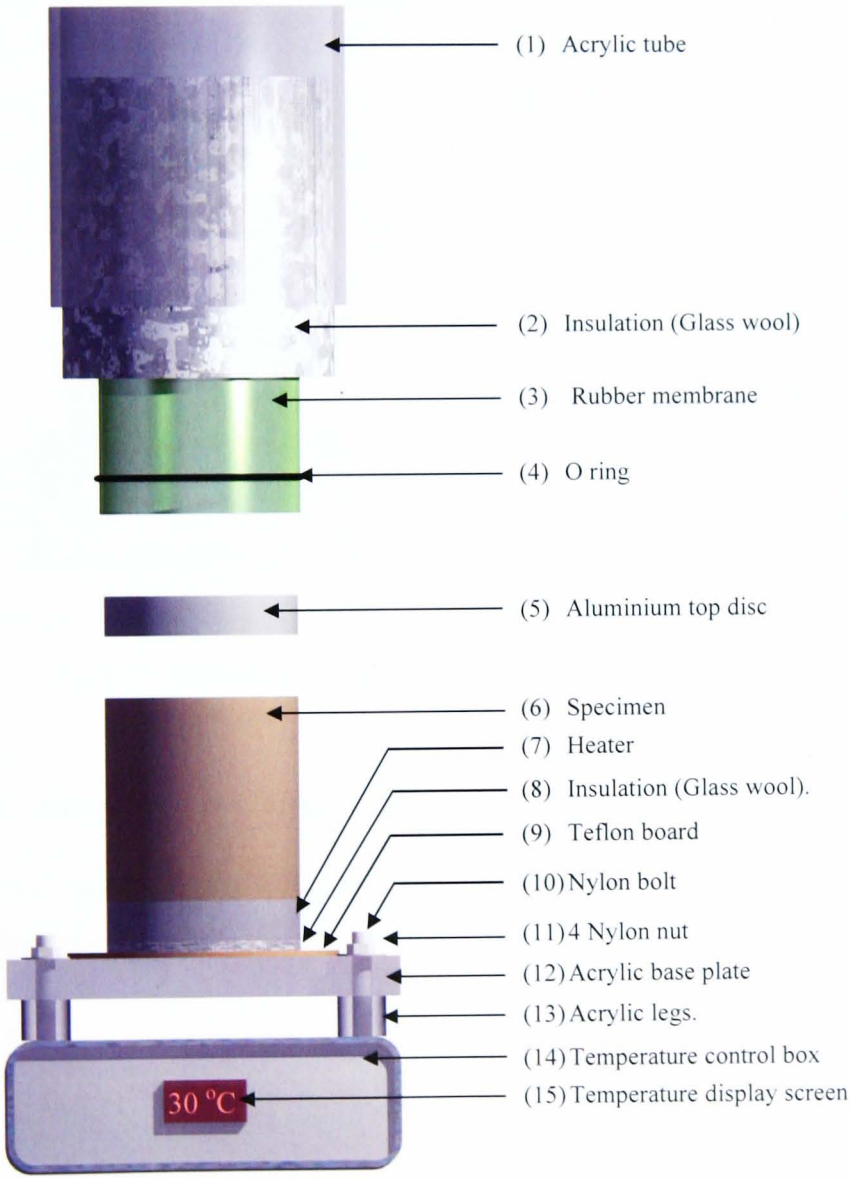

Figure 4.5 Schematic diagram of the thermal cell showing the key components.

The specimen is surrounded by insulation (2) to restrict the heat flow vertically and eliminate the side heat loss. This insulation is held in place by an acrylic tube (1). Both the insulation and the acrylic tube provided an extra support to the coarse grained soil specimens.

The temperature at the base of the specimen is controlled and monitored by a thermocouple (*a*) and (b) in Figure 4.6. Two further thermocouples (c) and (d) in Figure 4.6 are inserted into the specimen at 33mm and 66mm from the base of the specimen, so that the increase and decrease of the temperatures within the specimen can be monitored and recorded. These thermocouples (c) and (d) are mounted in hypodermic needles which are pushed through the membrane to the centre of the specimen. The temperature at the top surface of the specimen is monitored with a further thermocouple (e). Thermocouples (*a* and b) are built into the base heating cylinder.

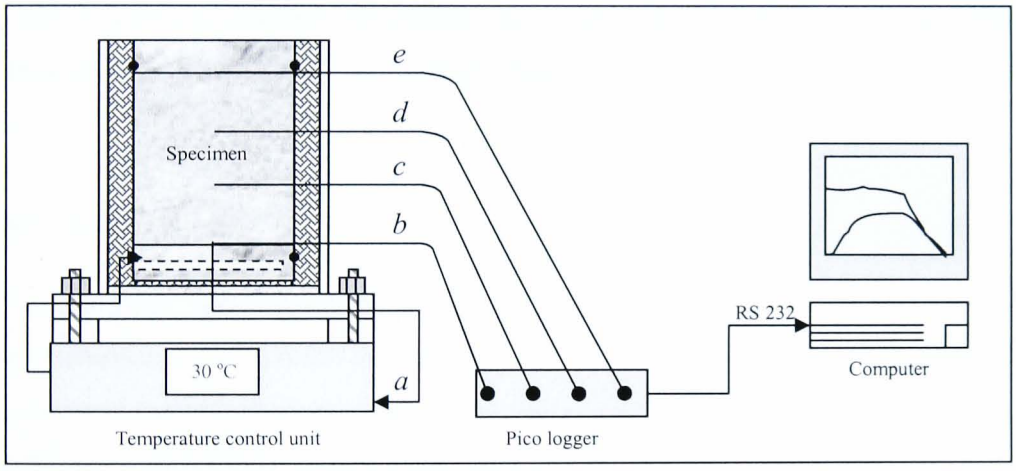

Figure 4.6 Complete experimental set up for thermal conductivity test.

4.5.2 Temperature Control Unit

The temperature was controlled by an Omron E5GN temperature control unit box (203mm W, 178 mm D, and 88mm H) (Figure 4.7).

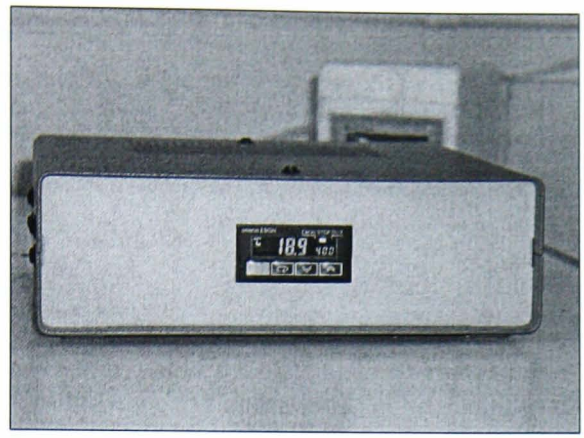

Figure 4.7 Temperature Control Unit.

The base temperature was controlled by the PID controller built into the temperature control unit. The aluminium base cylinder acts as a uniform heat source across the base of the specimen. The heat is generated by a cartridge heater (300W at 240V AC) with the aid of a thermocouple (*a* in Figure 4.6) to provide a feedback to the temperature control unit in order to maintain a constant temperature.

4.5.3 Data Logger

A TC-08 Pico data logger unit was used to read the output signals from the thermocouples. The TC-08 is an 8 channel thermocouple (Figure 4.8) to PC interface, it can measure the full range of temperatures from -270°C to +1800°C and works with all popular types of thermocouples (B,E,J,K,N,R,S,T).

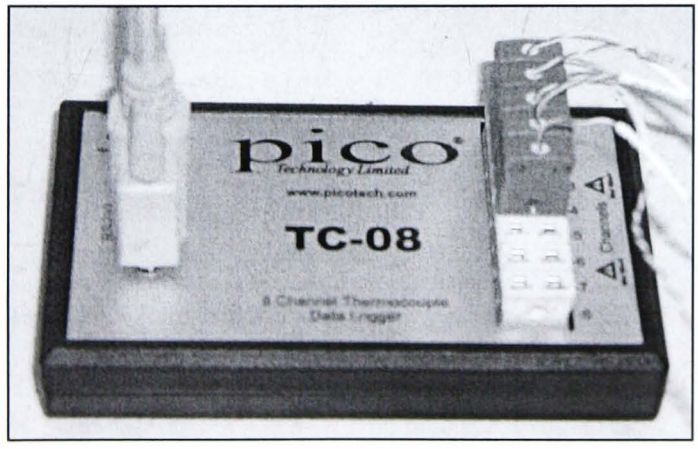

Figure 4.8 TC-08 Pico data Logger (Pico, 2004).

The data logger plugs into the serial port (RS 232) of the computer; the thermocouples are connected and then it is ready to measure temperatures. It has high resolution and accuracy. It is powered through the serial connection. It has a built-in cold junction compensation that is held at a relatively constant temperature. The built-in cold junction measures the ambient temperature at the connection of the thermocouple wire to the measuring device (Pico, 2004). This allows for accurate computation of the temperature at the measuring junction (hot junction) by the measuring device. A computer was used to run the supplied with Picolog data logging software (Figure 4.9) that receives voltage readings of each thermocouple from the TC-08 unit and convert these readings to temperature in degree Celsius.

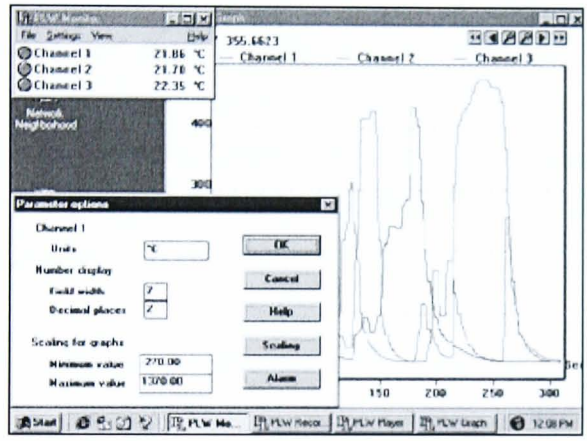

Figure 4.9 Picolog data logging software (Pico, 2004).

At any time during a test, the operator can request a display or printout of the previous data, stop the test or proceed to the end of the test. At the end of the test, a file containing the test was stored on the clipboard and pasted in a spreadsheet file. These data were then graphically and numerically analysed and printed by the computer using Excel software in order to determine the thermal conductivity of the soils.

4.5.4 Thermocouples

Thermocouples are temperature sensors suitable for use with any make of instrument designed or programmed for use with the same type of thermocouple. They are cheap, interchangeable, have standard connectors and can measure a wide range of temperatures. The diagram below (Figure 4.10) shows a K type thermocouple, which is the most popular and the one used in this study:

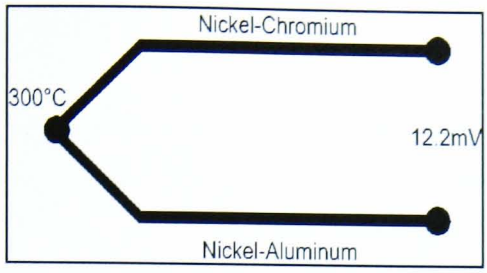

Figure 4.10 Diagram of K type thermocouple (Pico, 2004)

For example in the above diagram, the K type thermocouple at 300°C will produce 12.2mV. Unfortunately it is not possible to simply connect up a voltmeter to the thermocouple to measure this voltage, because the connection of the voltmeter leads will make a second, undesired thermocouple junction. To make accurate measurements, this must be compensated for by using a technique known as cold junction compensation (CJC) which is built into the Pico logger. This is governed by the law of intermediate metals that states that a third metal, inserted between the two dissimilar metals of a thermocouple junction will have no effect provided that the two junctions are at the same temperature.

Therefore, it was also required that thermocouple or thermocouple extension wire, of the proper type, to be used all the way from the sensing element to the measuring element. Large errors can develop if this practice was not followed, because different thermocouple types have very different voltage output. Most measurement problems and errors with thermocouples are due to a lack of understanding of how thermocouples work (Pico, 2004).

4.6 Test procedure

The test procedure for determining the thermal conductivity in the new thermal conductivity cell includes specimen preparation and set up. The essential steps in conducting the test are shown in the flow chart (Figure 4.11). The following is a description of the experimental setup of the equipment and materials used to prepare soil samples that were tested to establish the most appropriate testing regime and produce a test specification.

4.6.1 Specimen Preparation

Twenty two specimens were prepared and tested to determine their thermal conductivity coefficients. The specimens were 100mm long and 100mm in diameter. Most of the specimens were reconstituted; four of them were undisturbed specimens taken from U100 samples. The undisturbed specimens of fine grained soils were trimmed to size and transferred to the cell. The reconstituted specimens were made of both fine and coarse grained soils. They were either prepared in a consolidation cell and trimmed to the size and transferred to the cell or prepared in the thermal cell using PVC split former. Each of these preparation procedures are explained below.

4.6.1.1 Preparation of undisturbed specimen

The preparation of a specimen from the standard U-100 sampling tube was carried out by cutting a sub-sample of 150mm in length. The sub-sample was handled very carefully during extruding and transporting. It was placed on a soil lathe and trimmed with a wire saw to the required specimen diameter, i.e. 100mm. Then it was placed in cradle mould where it was further trimmed in order to produce a final specimen 100mm in high and 100mm diameter with flat parallel ends. The specimen was weighed and its diameter and length were measured using a calliper in order to calculate the bulk density. The trimmings were used to evaluate the physical indices of the specimen, i.e. dry density, void ratio and water content.

4.6.1.2 Preparation of reconstituted specimen

This procedure involved two methods depending on the type of the soil. For fine soils the same procedure that was explained in chapter three (section 3.5.1) was used to prepare the reconstituted clayey specimens. However for coarse grained soils, the preparation and set up procedure is similar to that explained in section 3.5.2.2. The only difference is that during the thermal conductivity tests filters and pores discs are not used in the thermal cell device.

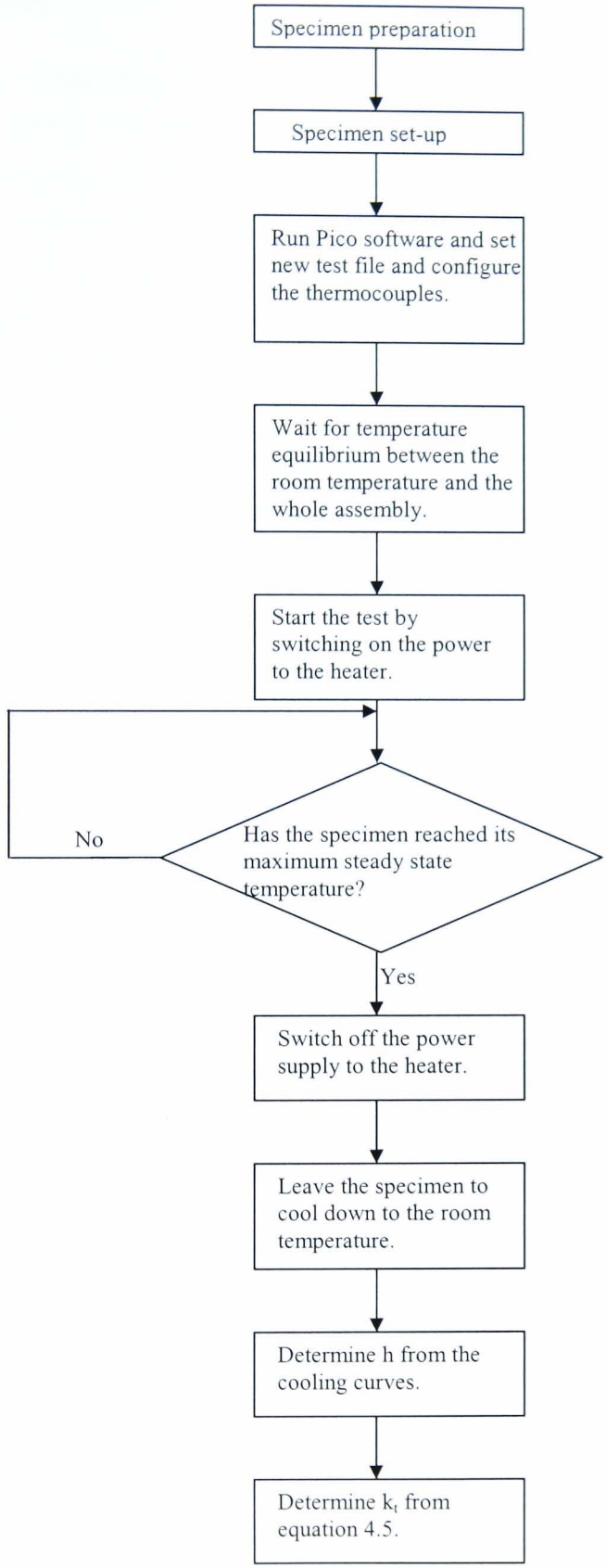

Figure 4.11 Flow chart of test procedure.

4.6.2 Test setup

Prior to the specimen setup, the conducting plates were cleaned with very fine sand paper (Figure 4.12a). The specimen was prepared by one of the methods mentioned above. If the specimen was fine grained, it was transferred to the cell after removing the cling film, the specimen was placed carefully on the base conducting plate, making sure that there was no air trapped underneath. A rubber membrane was placed on a membrane expander and subsequently placed around the specimen (Figure 4.12b). Using the membrane expander the first O ring was placed to seal the membrane to the base conducting plate (Figure 4.12b). The top conducting plate was then placed on the specimen followed by fixing the second O ring to seal the membrane to the top plate (Figure 4.12b). The cell was assembled with the specimen sealed onto the top and base conducting plates by O rings (Figure 4.12b).

Glass wool insulation (Figure 4.12c) that has a very low thermal conductivity (0.038 W/m.^{o}C) was placed around the specimen to eliminate side heat loss. It also provided a side support to the coarse grained soils. The acrylic tube was then assembled. Two stainless steel type k thermocouple probes (150mm long, 1.5mm dia.) were inserted into the specimen to the centre typically at one third and two thirds of the height above the base of the specimen (Figure 4.12d). Another type k thermocouple with a 7mm metal disc termination was attached to the clean surface of the top plate by an adhesive tape. All the thermocouples were plugged into the Pico data logger and subsequently the data logger was plugged into the computer via the RS 232 serial. A new file was opened and set into the logger's software. The thermocouple type was selected from a drop down window for each used channel so that an accurate reading of temperature can be taken from these sensors.

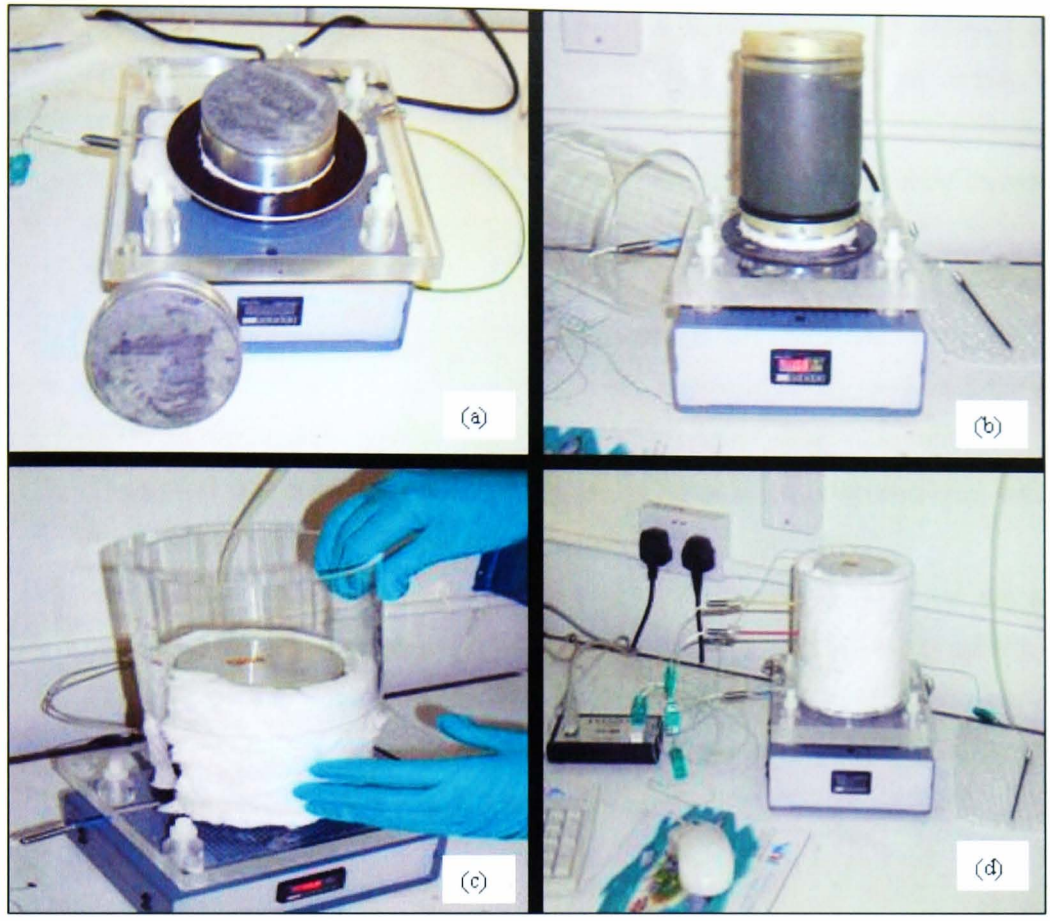

Figure 4.12 Test assembly.

4.6.3 Test stages

There are three stages for the test (Figure 4.13). The first was to bring the temperature gradient to a constant; the second was to maintain the temperature gradient until the steady state condition is reached; and the third was to switch off the power allowing the temperature gradient to decay to zero. To achieve that the following procedure shown in the flow chart (Figure 4.11) was applied:

1. The whole assembly was placed in a constant temperature room and allowed to reach the temperature equilibrium. After this stage the specimen was ready to be tested.
2. A test consists of applying constant heat to the base of a cylindrical specimen of soil and keeping its top at a lower constant temperature (room temperature).
3. A temperature gradient was chosen. Typically base temperatures of 30°C, 40°C, and 50°C were used.

4. The temperatures at the top and bottom of a specimen were monitored and recorded at one minute intervals until the temperature gradient across the specimen is constant. The outer surface of the specimen was insulated with glass wool (k_t = 0.03W/m.°C) and an acrylic tube (k_t = 0.13W/m.°C) in order to create a uniform temperature across the specimen (Figure 4.12c).
5. The temperature at the base of the specimen was controlled by temperature control unit using a cartridge heater and a thermocouple feedback.
6. The temperature at the thermocouples within the specimen and at the top the top of the specimen was checked regularly to establish the steady state condition.
7. The power was switched off when the temperatures at the thermocouples within the specimen and at the top reached the steady state condition.
8. The specimen was then allowed to cool with the temperatures at the top and bottom of the specimen and within the specimen being recorded every minute.
9. These data were used to determine the convection heat transfer coefficient (h) through an analysis of the temperature decay curve using the cooling phase.
10. The thermal conductivity was calculated using the following equation:

$$k_{t\,soil} = h \cdot \Delta L \cdot \frac{T_{top} - T_{\infty}}{T_{base} - T_{top}} \qquad 4.15$$

11. In a full cycle of tests three temperature gradients were used to ensure repeatability of results. Therefore the steps from 3 to 10 were repeated using higher base temperatures.

4.7 Data analysis

During preparation of a specimen as described previously, the initial height, diameter and weight of the specimen were measured and used to analyse the test data. This section refers to formulas that were used and describes the interpretation of a test. A typical test is used to demonstrate the process.

4.7.1 Initial condition

Using the measured height and diameter of the specimen (L) and (D) respectively, the cross-sectional area (A), volume (V), water content (w_c), void ratio (e), density (ρ) and degree of saturation (S) were calculated as presented in Chapter three section 3.6.1.

4.7.2 Heating stage

A thermal difference was created by setting the base temperature to a constant 30°C, 40°C or 50°C. Figure 4.13 shows a typical temperature profile from a thermal conductivity test on fine sand. The figure shows typical results of direct measurement of temperature over time at three points 3.3cm, 6.6cm and at the top surface of the specimen away from the base. The heat started to flow from the bottom of the specimen towards its top. The test temperature profile consists of three stages, the first is the transient stage, the second is the steady state stage and the final is the cooling stage. In the transient stage the soil specimen components start to store heat until they reach their maximum heat capacity, steady state is reached at the end of this stage when the temperature along the specimen profile reach their steady state maximum values, at this stage any extra heat passes through the specimen from its base to its top surface and then convects away to the surrounding medium. The maximum temperatures at the base (T_{base}) and top (T_{top}) of the specimen were determined from this stage.

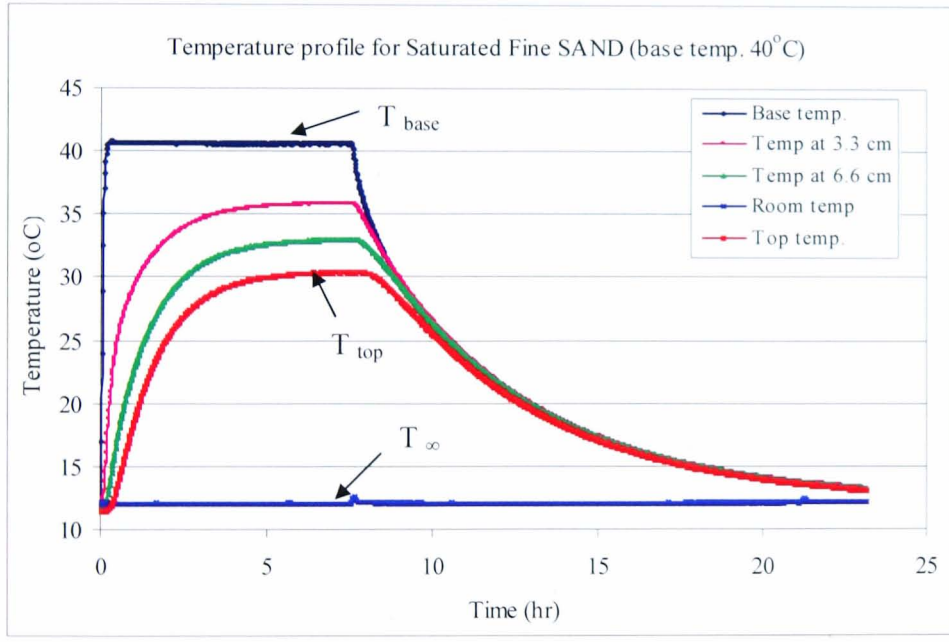

Figure 4.13 Typical temperature profile for a soil specimen.

4.7.3 Cooling stage

Once the steady state condition was achieved the power supply for the heater was switched off, then the cooling stage started and the specimen temperatures at the three points started to dissipate gradually over time to reach equilibrium within the specimen and with room temperature.

The cooling curves obtained during the cooling processes (Figure 4.13) were then used to determine the convection heat transfer coefficients (h) using equation 4.10. This was carried out by using the best fit method where the value of the convection heat transfer coefficient was altered until a best fit between the theoretical curve and the experimental curve were obtained (Figure 4.3).

After determining the convection heat transfer coefficient (h) and the top surface temperature at the steady state condition, the thermal conductivities (k_t) of the soil specimen were calculated using equation 4.5 for the various base temperatures. The average of these values was then taken as the thermal conductivity of the soil in question.

4.8 Summary

A detailed description of the new thermal conductivity testing device is found in this chapter, plus the testing procedure that has been developed and followed is also presented. The device used is a one dimensional heat flow system with accurate thermocouples to determine the temperature profile within the specimen under testing, in order to establish the steady state condition. The device will permit the operator to set the desired thermal gradient. Moreover it allows more thermal gradients to be used. It can also test the soils under various water contents.

The system is robust, simple, easy to use and can accommodate specimens of a representative size of 100mm in diameter and height. The results obtained by this new device are presented and discussed in Chapter six so as to evaluate its adequacy in determining the soil's thermal conductivities.

Chapter 5

Hydraulic Conductivity Results and Discussions

5.1 Introduction

Laboratory experiments were performed on different types of soils-clay, silty clay, fine sand, medium sand and coarse sand, using different techniques including constant flow, falling head and constant head techniques. The clayey soils were tested in both the flexible wall constant flow permeameter and the modified falling head permeameter as described in chapter three. The grading curves for these different soils are illustrated by the particle size distribution curves shown in Figure 5.1. It can be seen that the percentage of clay size for the clayey soils varies from about 40% for silty clay (kaolin grade E) to 90% for clay (kaolin). These clayey soils are known commercially as grade E clay and supreme clay. They were chosen because of the vast amount of research undertaken on kaolin. Four specimens of each clayey soil were tested to ensure the repeatability of the test results and in order to determine the effect of the physical properties on hydraulic conductivity under different stress conditions and under the different techniques mentioned in previous chapters. A fine sand specimen was tested using the modified flexible wall falling head permeameter. A conventional rigid wall constant head permeameter was used to determine the hydraulic conductivity of three types of coarse soils including fine sand, medium sand and coarse sand.

The classification properties of the clayey soils (supreme and silty clay) used in this research are given in Table 5.1. The penetrometer method recommended in BS 1377 (Part 2: 1990: 4.3) was used to determine the liquid limit (L.L). The plastic limit (P.L.) and the plasticity index were established according to the British Standards 1377 (Part 2: 1990: 5.3). All the hydraulic conductivity results on the soil specimens using the constant flow (CF), the falling head (FH) and the constant head (CH) techniques are presented in Appendix B. These results will be discussed in the following sections according to the technique that was used to determine them and according to the soil type.

Table 5.1 Engineering properties of clayey soils

Clay	Liquid limit (%)	Plastic limit (%)	Plasticity index (PI)	Group symbol
Supreme clay	72	16	56	CV
Silty clay	57	15	42	CH

The results presented here in this chapter are based on the results obtained from specimen No. 12 to specimen No. 21 as indicated in Table 5.2.

Table 5.2 List of the specimen's number and type

Specimen No.	Soil type	Remarks
1	Sandy silty Clay	Used to gain experience of the equipment and test procedure and develop the technique.
2	Sandy silty Clay	
3	Silty Clay, grade E	
4	Silty Clay, grade E	
5	Sandy silty Clay	
6	Silty Clay, grade E	
7	Silty Clay, grade E	
8	Silty Clay, grade E	
9	Silty Clay, grade E	Good results
10	Silty Clay, grade E	Good results
11	Silty Clay, grade E	Discarded
12	Supreme	Good results
13	Silty Clay, grade E	Good results
14	Silty Clay, grade E	Good results
15	Supreme	Good results
16	Silty Clay, grade E	Good results
17	Supreme	Good results
18	Fine sand	Good results
19	Medium sand	Good results
20	Silty Clay, grade E	Good results
21	Supreme clay	Good results

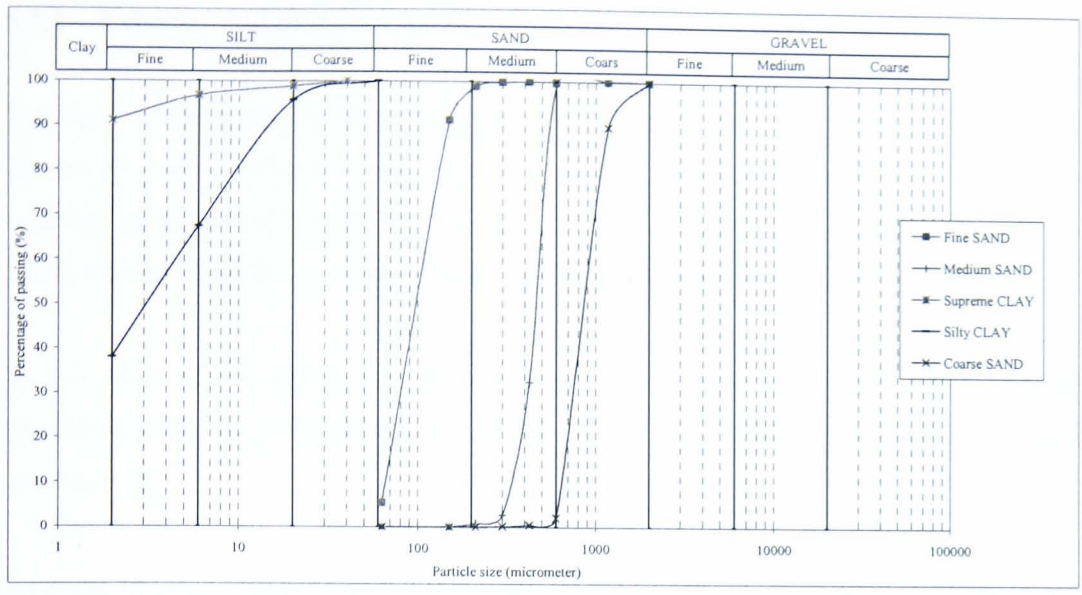

Figure 5.1 Particle size distribution for the soils used.

5.2 *Effect of testing system on the determination of hydraulic conductivity*

This section discusses some features of the testing system that affected the determination of hydraulic conductivity. These features include leakage, seepage induced consolidation, and pressure difference fluctuations due to either faulty air pressure regulators or flow pump. These problems were also reported by previous researchers who used the same testing equipment. As this is highly dependent on the reliability of the measuring instruments, all of these instruments were checked and calibrated at the start of the research. Table 5.3 shows the accuracy of the different instruments used.

Table 5.3 Accuracy of the testing system measuring instruments

Instrumentation	Accuracy	Units
Flow pump	±0.008	cm^3
Volume change gauge (fine)	±0.005	cm^3
Volume change gauge (coarse)	±0.125	cm^3
DPT	±0.03	kPa
PT	±1.5	kPa

5.2.1 External and internal leakages

Leakage is the greatest limiting factor in determining hydraulic conductivity in the laboratory. It can be divided into two categories; external and internal leakages. Leakage is particularly important when using low hydraulic gradient tests due to the small amount of inflow involved. These tests have little meaning if leakage occurs.

In this study about ten specimens were discarded due to the occurrence of leakage. Therefore it was necessary to set accepted criteria to detect leakage during an early stage of saturation.

External leakage occurs mainly at the valves and fittings. According to Araruna (1995) and Tavenas et al (1983a), these are important sources of error when measuring the hydraulic conductivity of fine soils. This type of leakage occurs when poor quality valves and fittings are used or when they are incorrectly assembled. It is easy to check by pressurising both the cell and pore pressure systems and observing if there are any volume and pressure changes. The valves connecting the permeameter were kept closed while increasing the pressure to about 600kPa. The cell and back pressures and volume change gauges were monitored while opening the valves one by one. An alternative method based on the B-test that was used to evaluate the degree of saturation of the specimen can be used to detect very small leaks in a relatively short time. This method was found to be sufficient for detecting external and internal leakages in this study. An example of an external leak was detected (Figure 5.2) during a B-test after one of the saturation increments from around the cell base. There were no changes in the top and bottom pore pressures and no changes in the specimen volume change gauge. The change was an increase only in the cell volume change gauge which indicated that water was going into the cell and out at the base.

Araruna (1995) stated that leaks inside the permeameter are the most important error associated with laboratory hydraulic conductivity determination, since they are very difficult to detect and, unlike the outside sources of leakage, once the test has started they cannot be eliminated. This type of leakage is commonly attributed to inadequate specimen set-up, and also due to faulty fittings or puncture of the membrane.

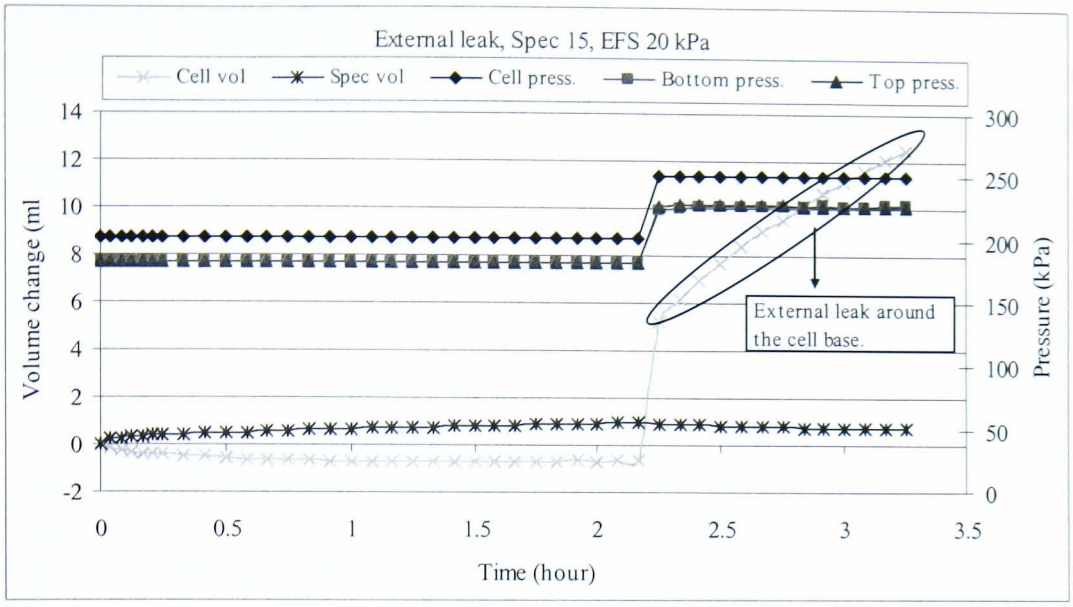

Figure 5.2 Example of a B-test after saturation stage with detected external leak.

Most of the discarded specimens were due to a leak caused by either inadequate set-up of the specimen or faulty valves. If the specimen was inadequately set-up and/or the rubber membrane was punctured, the difference between the confining pressure and the pore back pressure induces a hydraulic gradient and flow takes place. When the back pressure valves are open and drainage from the top and bottom of the specimen is allowed, the cell water penetrates the leakage spot, percolates the specimen mass and is collected in the outflow volume change gauge. It can be detected when there is a continuous increase in the cell volume change gauge and an equal decrease in the outflow volume change gauge. When the back pressure valves are closed and the drainage is prevented, the cell water penetrates through the leakage spot and starts increasing the pore pressure, until it eventually becomes equal to the confining pressure.

5.2.2 Seepage induced consolidation

During the experiment, erratic behaviour of the outflow was observed which appeared to be higher than the inflow into the specimen, indicating that the volume of the specimen decreased during the test (Figure 5.3). It was shown that there was a difference between the inflow and the outflow of 0.12 ml in 18 hours (effective stress 200 kPa and hydraulic gradient 3.7). This could be explained by two phenomena. The first is that the permeation started before the isotropic consolidation was complete, and the second phenomena could be the effect of seepage induced consolidation, as the inflow into the

specimen continued to cause rearrangement of the soil particles and consequently the pore fluid was expelled out of the voids. Other researchers have observed similar phenomena (such as Pane et al 1983; Aiban and Znidacic 1989; Araruna 1995; Chen 1997).

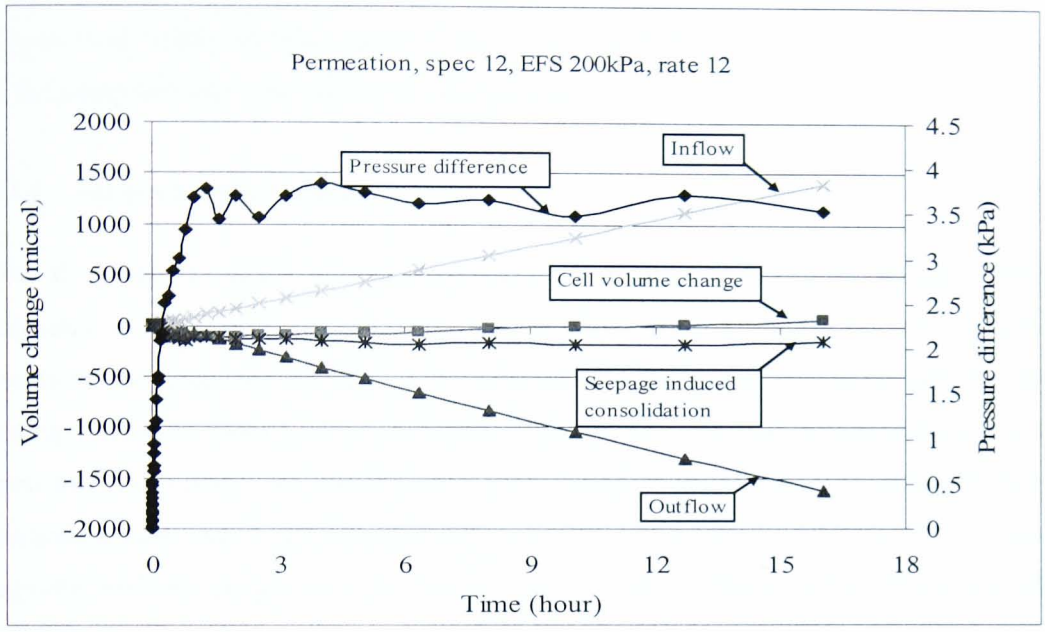

Figure 5.3 Seepage induced consolidation during a test.

Pane et al (1983) stated that seepage induced consolidation could produce a non-uniform distribution of void ratio, non-uniform distribution of flow rate and a non-uniform distribution of excess pore pressure during the transient flow condition. He further found that its magnitude was clearly dependent on the magnitude of the applied hydraulic gradient. Chen (1997), using the same equipment as in this research, found a difference between the inflow and the outflow of 0.5 ml in 12 hours (effective stress 300 kPa and hydraulic gradient 2.6). According to Chen's findings and the findings of this research, the phenomenon of seepage induced consolidation does not depend on the magnitude of the hydraulic gradient.

5.2.3 Fluctuation and variation of the pressure difference

The pressure difference between the top and bottom of the specimen should be constant during the steady state condition. Figure 5.3 shows that the pressure difference across the specimen does not level off with time, but fluctuates. This behaviour is generally assumed to be due to equipment error and not a property of the specimen. The

fluctuations may be due to various factors, including; accuracy of pressure regulators (Aiban and Znidarcic 1989; Araruna 1995; Chen 1997), mechanical imperfections of the flow pump (Olsen et al 1985; Redmond and Shackelford 1994; Araruna 1995; Chen 1997), temperature changes in the test environment (Morin and Olsen 1987; Redmond and Shackelford 1994) and the stability of the signal conditioning and recording system (Olsen et al. 1985). In this case they were most likely due to mechanical imperfections of the pump as they were unique to each gear speed.

5.2.4 Air pressure regulators

The air pressure supply system used in the hydraulic conductivity testing systems consisted of an electric compressor, an air receiver, a precision air filter pressure regulator installed downstream of the air tank and three precision regulators for each testing system installed on the cell pressure line and the pore back pressure lines. The air pressure in the main line supplier was maintained between 800 and 1000 kPa by the pressure switch that activates and shuts off the electric motor. The air filter/pressure regulator reduces the pressure in the main line to 700 kPa before supplying to the lines regulators.

A small increase or decrease of the air pressures in the cell and pore back pressure lines causes a volume decrease or increase respectively, especially when the fine setting was used during the permeation stages. A fluctuation in the volume change gauges was noticed due to a faulty air pressure regulator installed at the cell and back pressure lines. This problem was encountered only at the end of the experimental work during some of the last tests of specimens No.20 and 21 especially during the use of a small pressure difference between the top and bottom of specimen.

5.2.5 Flow pump delivery

The pump used in the hydraulic conductivity testing system used a synchronous motor and 30 position linear gear box to produce 30 delivery rates. Table 5.4 lists the inflow rates used in this research.

Table 5.4 Used inflow rates.

Setting	4	5	6	8	10	12
Inflow rate (ml/sec)	3.6E-4	2.6E-4	1.8E-4	9.4E-5	4.8E-5	2.4E-5

At the beginning of the research, the flow pump was checked and found to be working to an accuracy of about $\pm 0.008ml$. However, the flow pump has been used since 1994, and therefore some of its gears were worn. This mechanical imperfection in the flow pump became clear during the last tests in which it produced irregular inflow rates, and hence fluctuations in the measured pressure difference across the specimen (Figure 5.4). This could also be the reason for the fluctuations during the steady state condition (especially during tests using low inflow rates), because there was no fluctuation when the falling head technique was used (Figure 5.17). Figure 5.4 shows an example of the onset of this problem where there was a normal increase in the pressure difference across the specimen up to about one hour and a half, and then a sudden decrease in the pressure difference due to the malfunction of the flow pump. After a while, the pump started to work again as indicated by the increase in the pressure difference. This particular test was interpreted normally, since the steady state condition and the pressure difference were clear. In some other tests, such as the final tests on the silty and supreme clay specimens (N°.16 and 17), the flow pump was insufficient to produce a regular inflow (Figure 5.5). This was the reason that the falling head and the constant head techniques were introduced, since if successful, the number of errors could be reduced.

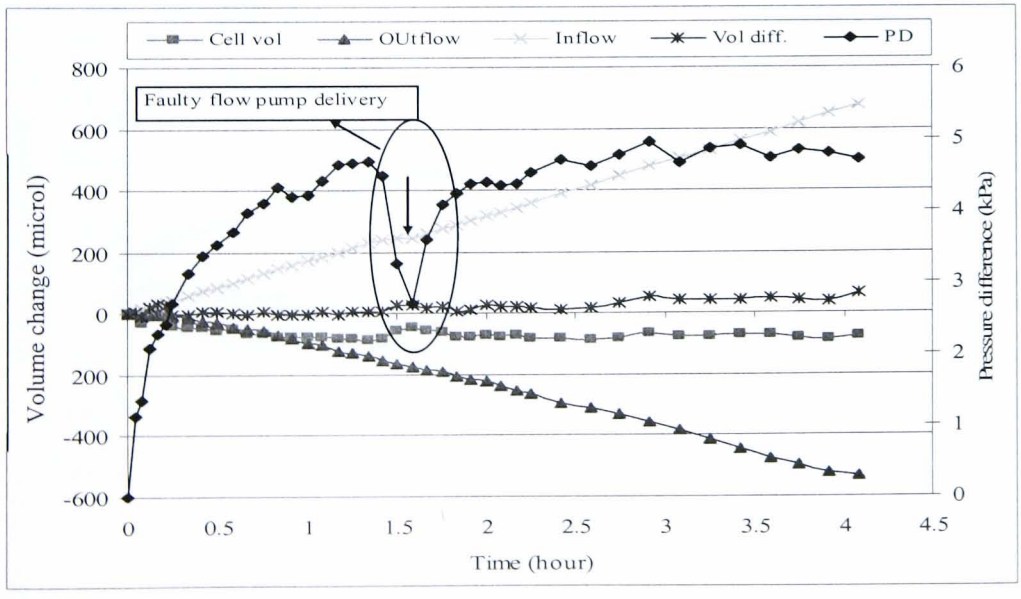

Figure 5.4 Pressure difference due to a flow pump delivery (test 151002).

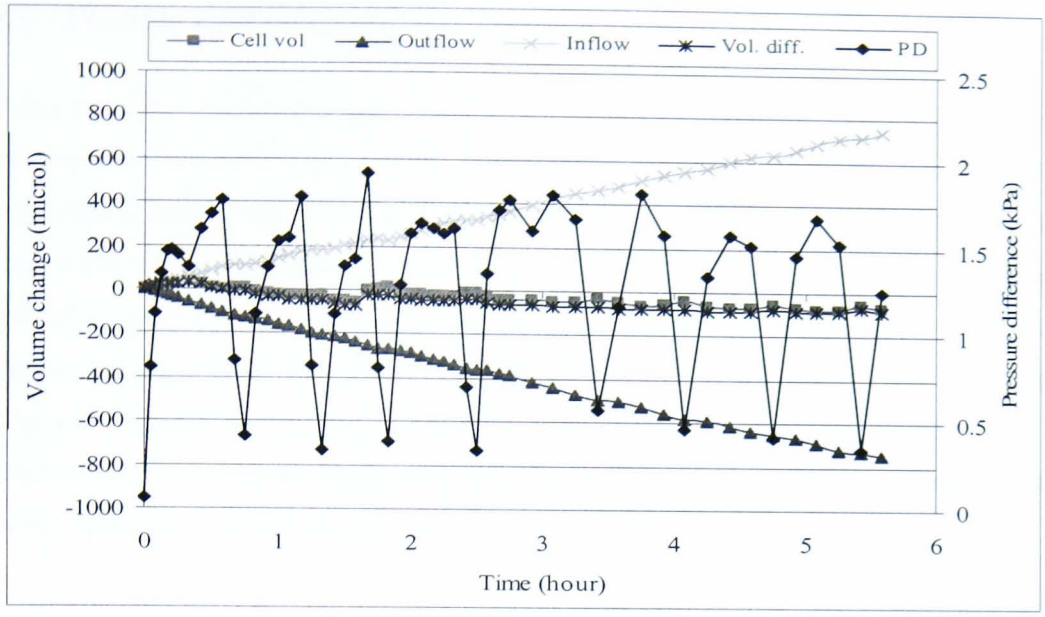

Figure 5.5 Faulty flow pump.

However in the falling head technique fluctuations were caused by an irregular inflow. This was because the air pressure regulator for the inflow volume change gauge was not able to maintain a constant air pressure in the line, especially during the test of a specimen using a small pressure difference such as 5kPa (Figure 5.6). Although this test could not be interpreted as a falling head test, it was possible to interpret it as a constant head test. This problem was less serious during tests using a higher pressure difference across the specimen (10, 20 and 30kPa).

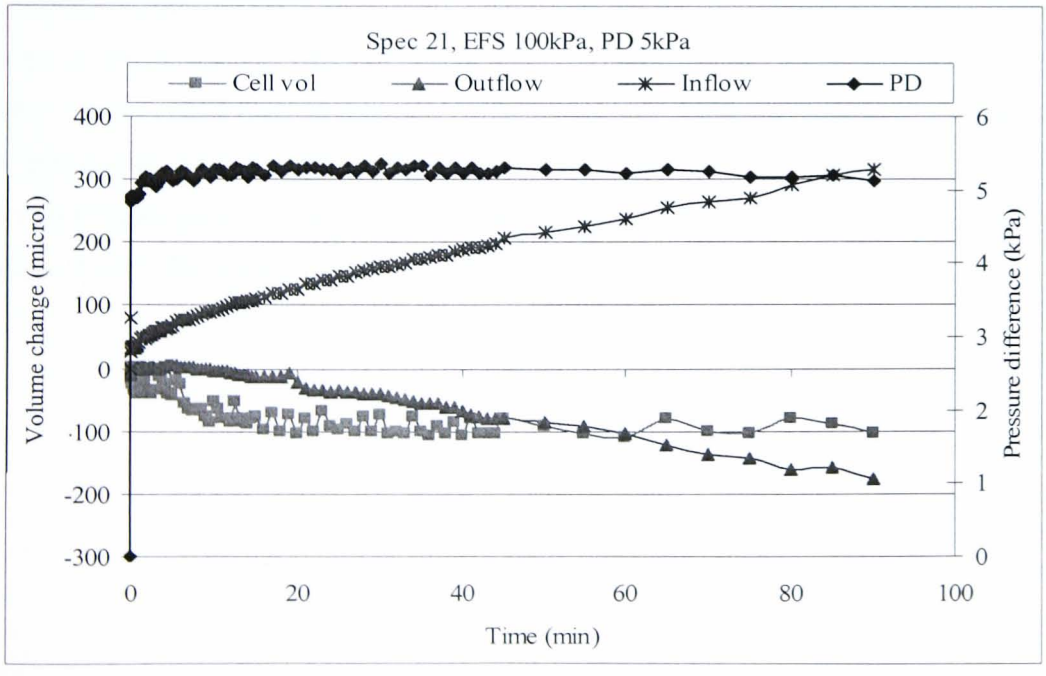

Figure 5.6 Effect of irregular air pressure supply on the falling head technique.

5.3 *Flexible wall constant flow technique*

Thirty six tests were carried out in the flexible wall permeameter using the constant flow technique to determine the hydraulic conductivity of six clayey specimens. These were reconstituted specimens, three of which were supreme clay and the other three were silty clay. Each of the specimens was prepared as explained in section 3.4.1, and tested according to the test procedure prescribed in chapter three, under three different effective stresses (50kPa, 100kPa and 200kPa). At each effective stress, different inflow rates were applied to generate a constant inflow at the base of the specimen in order to determine the effect of the induced hydraulic gradient and the change in effective stress on the hydraulic conductivity of soils using very accurate measurement devices.

Each specimen was prepared by mixing it at a water content of 1.25 times its liquid limit, and then the slurry-like mixture was consolidated under axial stress until excess pore pressure dissipated. The specimen was then trimmed to size and set up in the modified triaxial cell. The saturation procedure (section 3.4.3) was started at a low effective stress of about 20 kPa. A typical saturation result (Figure 5.7) shows that the water in the back pressure volume change gauge started to saturate the specimen (+ve values), and also there was an increase in the specimen size (swelling) due to stress relief. Consequently the volume of water in the cell was reduced as indicated by an increase in the cell volume change gauge (-ve values). The difference between the absolute readings of the cell volume change gauge and the specimen volume change gauge is due to the fact that some pore water was used to saturate the specimen. When there was not much water going into the specimen, the degree of saturation was checked by calculating the ratio between the increments of the pore pressure and the confining pressure (Skempton's parameter B) before moving to the next stage of consolidation, where the B value had to be 0.95 or more.

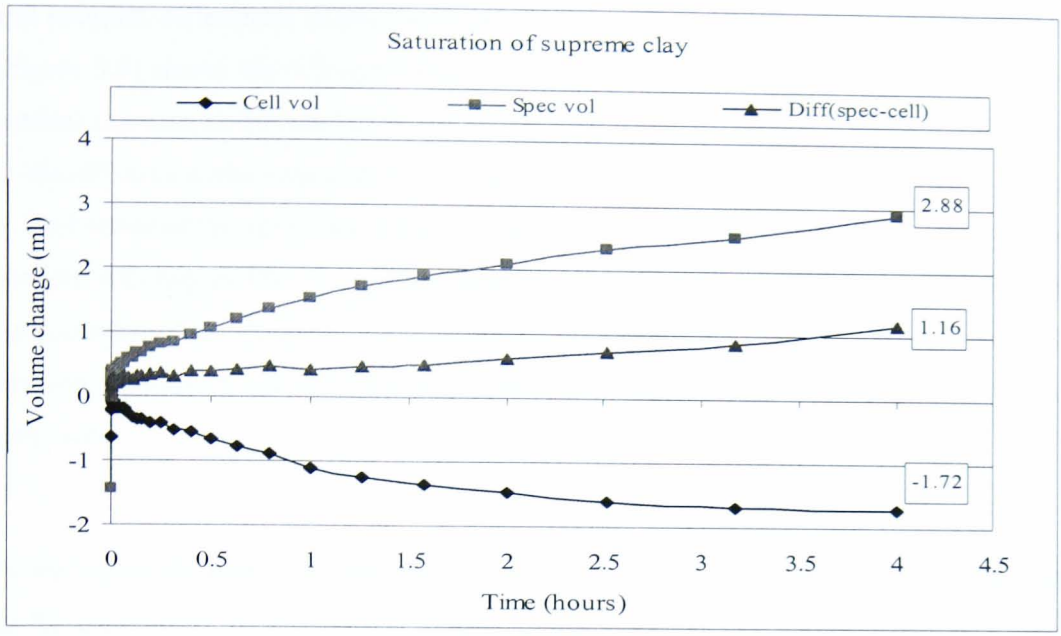

Figure 5.7 Typical result of saturation stage for a Supreme clay specimen.

The consolidation stage (Figure 5.8) was then started by increasing the confining pressure and leaving the back pressure as per the previous stage (in order to prevent separation of the dissolved air bubbles from the water). Each specimen was consolidated under three different effective stresses (50 kPa, 100 kPa and 200 kPa).

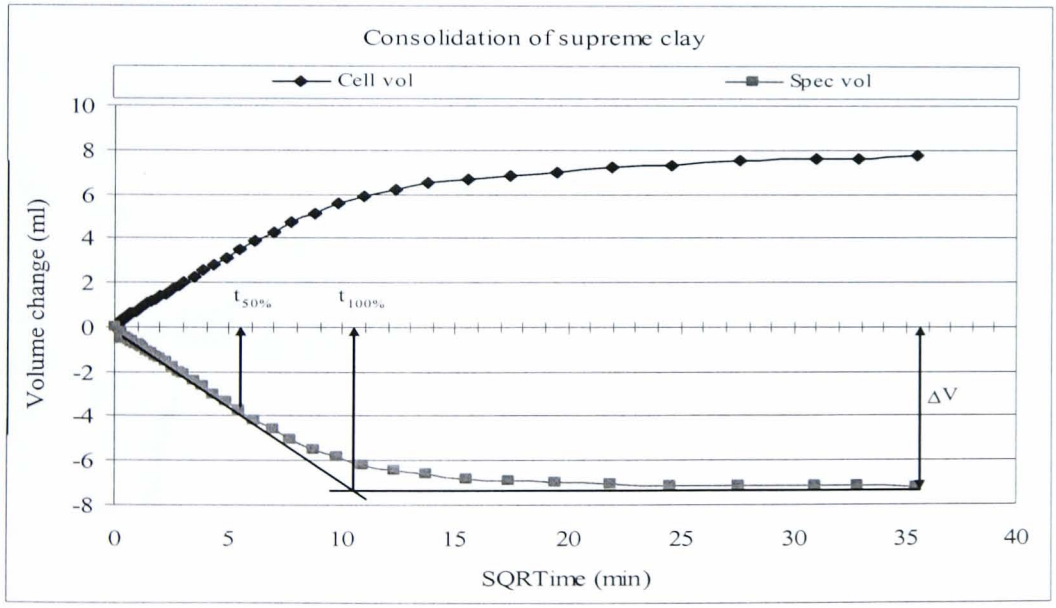

Figure 5.8 Typical result of consolidation for a Supreme clay specimen.

After the completion of the consolidation at each effective stress, the permeability tests were run using the constant flow and falling head techniques with different inflow rates

and pressure differences respectively. A typical permeation result using the flow pump (Figure 5.9) shows the infusion of water at the bottom of the specimen which caused a gradual increase in the pore pressure, and a corresponding swelling due to the decrease in the effective stress indicated by the cell volume change gauge. This volume increased at the bottom of the specimen caused a smaller outflow than inflow rate. However if the outflow was higher than the inflow, this indicates either a leakage or seepage induced consolidation. This phenomenon of seepage induced consolidation was noticed mostly at the first permeation test after the end of the consolidation stage when a low inflow rate was used.

At the top of the specimen there was an increase in the pore pressure due to the increase in the water level in the outflow volume change gauge. This increase was very small compared with that at the bottom (Figure 5.10), and hence the volume change at the top due to the corresponding decrease in the effective stress was negligible. When higher inflow rates were used in the next permeation stage, the volume changes at the bottom of the specimen were greater due to greater decreases of effective stress, and hence the difference between the inflow and the outflow became greater.

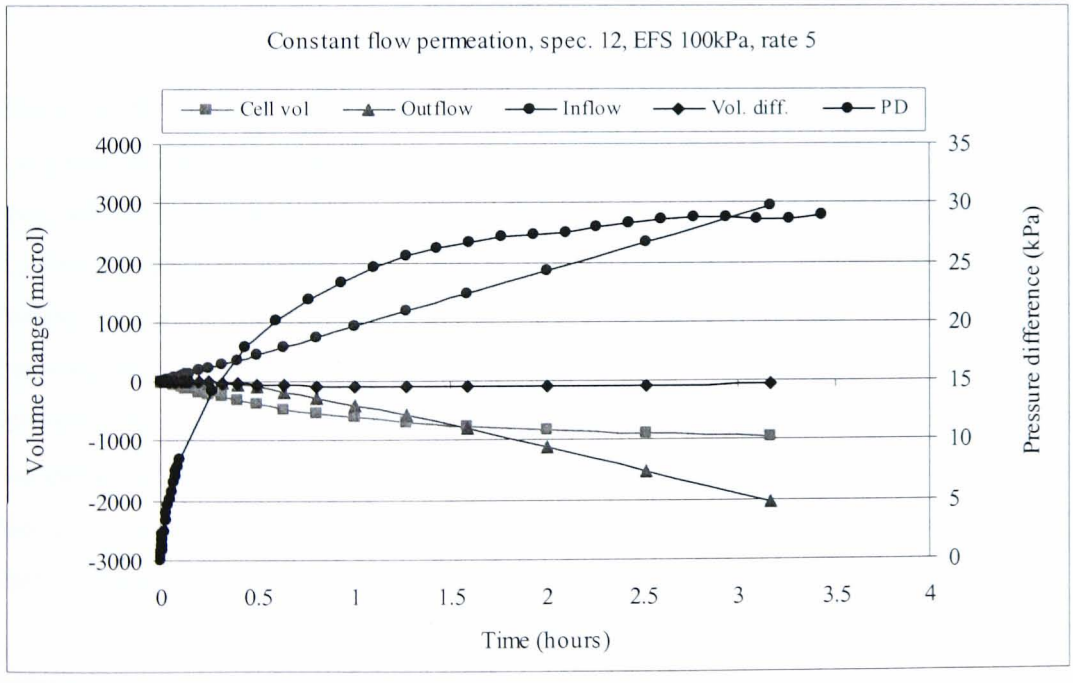

Figure 5.9 Typical result of constant flow permeation test for supreme clay.

The difference between the inflow and the outflow can be explained by the fact that as the specimen swelled, the inflow water was accommodated by the volume changes at the

bottom of the specimen, consequently decreasing the amount of outflow at the top of the specimen. Therefore the summation of the volume changes during the constant flow permeation should be equal to zero (Figure 5.9).

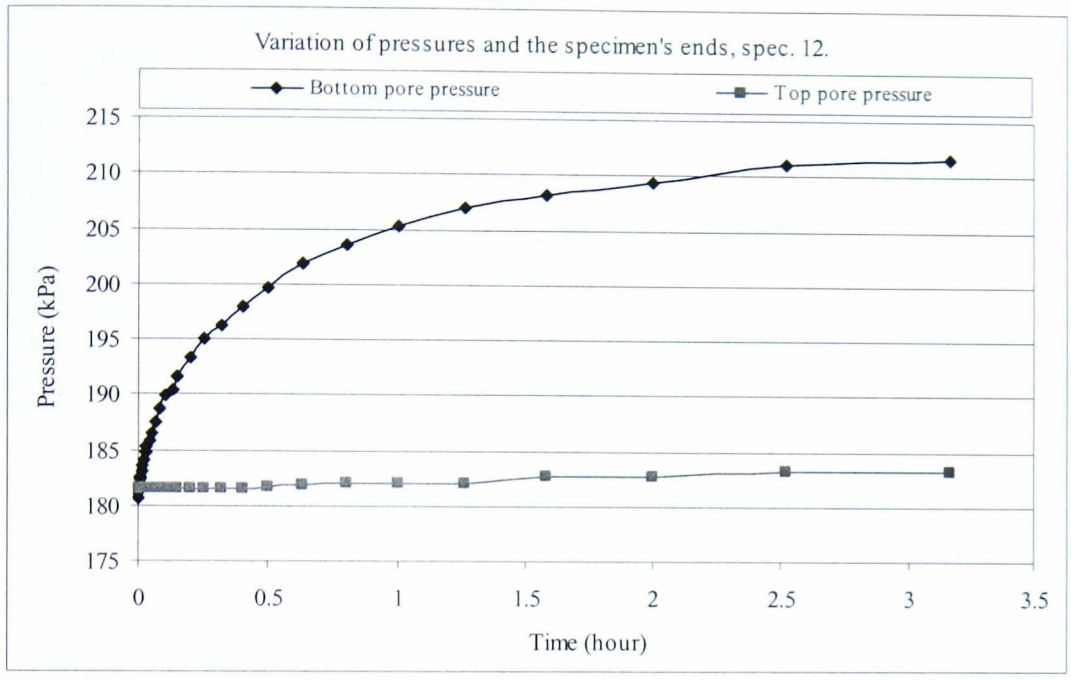

Figure 5.10 Pore pressure changes at the top and bottom of the specimen during a constant flow test.

The hydraulic conductivities of each clayey specimen were calculated at its bottom and top based on the inflow and the outflow rates respectively. The inflow was greater than the outflow due to the volume changes at the bottom of the specimens, and therefore the resulting hydraulic conductivity at the bottom of the specimen was greater than that at the top, as shown in Figure 5.11 and Figure 5.14. It can also be seen that the difference between the inflow and the outflow rates increased as the hydraulic gradient increased. However, this difference at similar hydraulic gradients decreased as the effective stress increased, because the ratio of the pressure difference between the bottom and the top of the specimen, and the effective stress, became smaller, leading to correspondingly smaller volume changes.

Figure 5.12 show the variation of hydraulic conductivity with the change of effective stress at the bottom of the specimen for different hydraulic gradients. It also shows that, at the top of the specimen, the hydraulic conductivity decreased as the hydraulic gradient

increased which is the same as the hydraulic conductivity tests in a rigid wall permeameter, where in a rigid wall cell there is no change in the specimen volume.

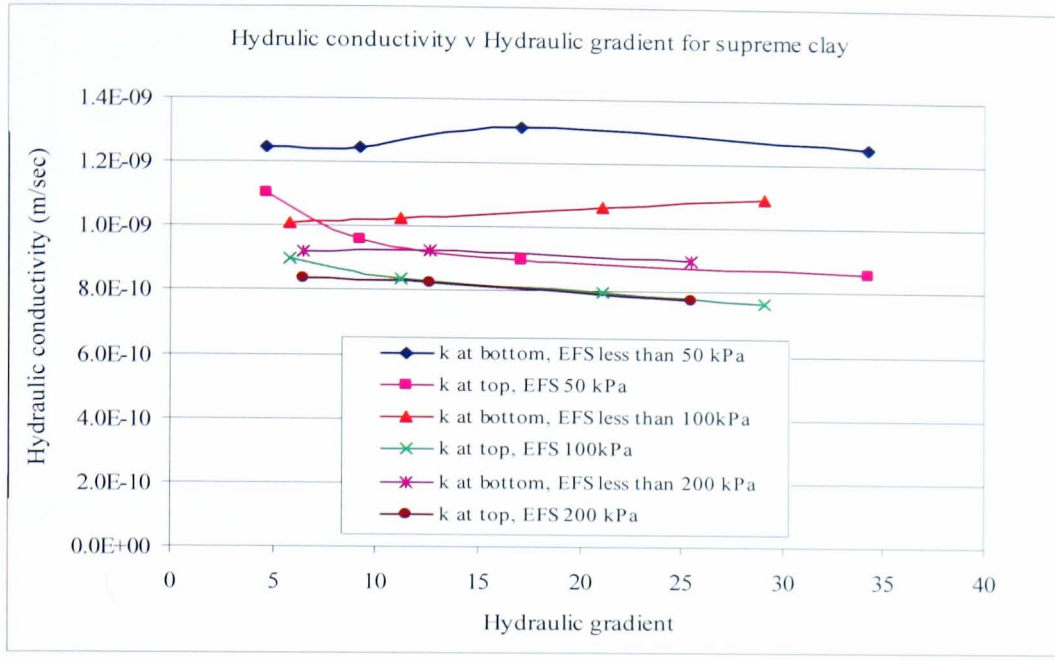

Figure 5.11 Variation of hydraulic conductivity at the top and bottom of the supreme clay specimen with change of hydraulic gradient.

When higher inflow rates were used in the next permeation stage, the volume changes at the bottom of the specimen were greater due to a greater decrease of effective stress, and hence the difference between the inflow and the outflow became greater. This resulted in a greater hydraulic conductivity at the bottom of the specimen than that at the top. Therefore, the hydraulic conductivity for every test was calculated based on the average value between the inflow and outflow rates (Figure 5.13).

The ASTM recommendation to use high hydraulic gradients when determining the hydraulic conductivity of such clayey soils was approved, because using high hydraulic gradients causes an increase in the volume change of a specimen during the test. Therefore, based on these research results, it is recommended that a low hydraulic gradient (15 or lower) should be used. The use of a low hydraulic gradient represents the in-situ condition and reduces the change in volume during a test which, results in small differences in hydraulic conductivities measured at the bottom and top of a specimen (Figure 5.12 and Figure 5.15).

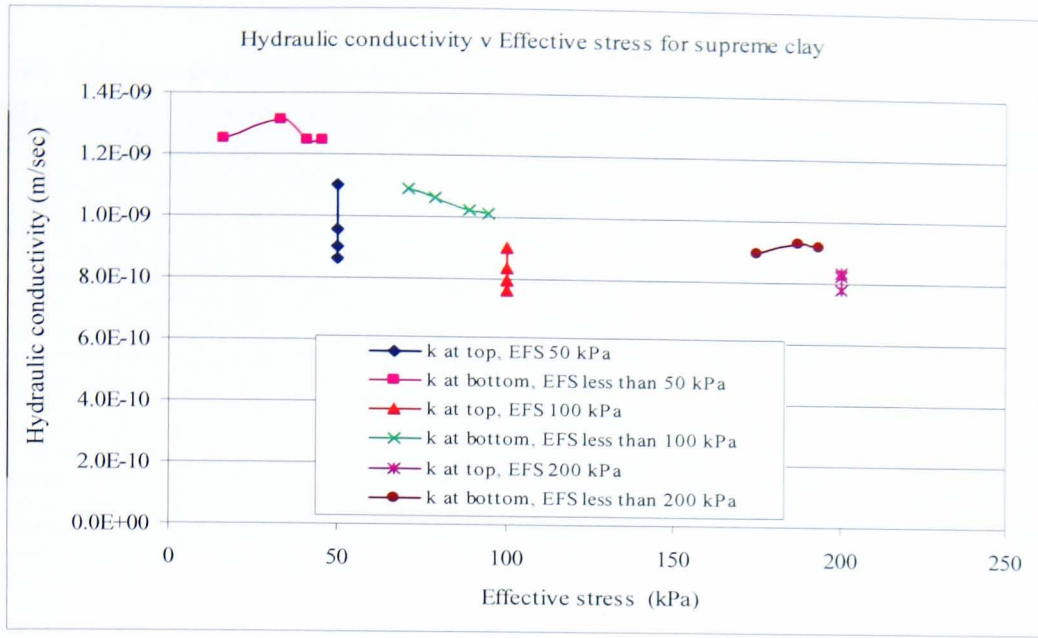

Figure 5.12 Variation of hydraulic conductivity at the top and bottom of specimen N°.12 of supreme clay with change of effective stress.

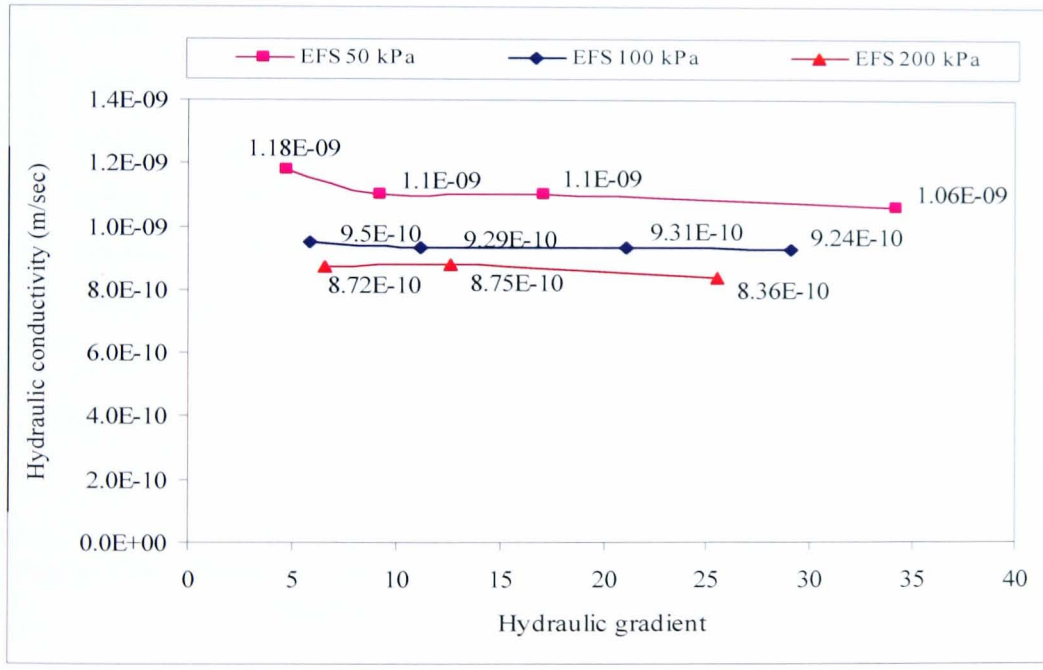

Figure 5.13 Average in/out hydraulic conductivities versus hydraulic gradient from specimen N°.12 of supreme clay.

Figure 5.13 and Figure 5.16 show that increasing the hydraulic gradient has an insignificant effect on the average calculated hydraulic conductivity. Therefore the hydraulic conductivity of the specimen at each effective stress was taken as the average of the values obtained with different hydraulic gradients (Table 5.5 and Table 5.6).

Table 5.5 Average hydraulic conductivities for supreme clays:

Specimen No.	EFS	l (mm)	D (mm)	A (cm^2)	V (cm^3)	W (g)	wc	e	n	bulk density	dry density	S (%)	Ave. k (CF)	Ave. k (FH)	Ave. k (CH)
Supreme CLAY Spec. 12	Intial	100.5	102.5	82.52	829.28	1411.6	0.48	1.26	0.56	1.70	1.16	98.1			
	50	100.6	102.2	82.04	824.53	1404.4		1.27	0.56	1.70	1.16		1.1E-09		
	100	100.3	101.7	81.16	813.14	1393.7		1.24	0.55	1.71	1.17		9.4E-10		
	200	100	100.8	79.77	795.39	1376.5		1.19	0.54	1.73	1.20		8.7E-10		
Supreme CLAY Spec. 15	Intial	100.5	102.3	82.19	826.05	1389.0	0.52	1.38	0.58	1.68	1.11	99.7			
	50	100.7	102.4	82.34	827.52	1380.0		1.39	0.58	1.67	1.10		1.2E-09		
	100	100.3	101.8	81.32	814.27	1366.7		1.35	0.57	1.68	1.12		1.1E-09		
	200	99.9	100.5	79.39	790.66	1343.1		1.28	0.56	1.70	1.15		9.5E-10	1.3E-09	1.2E-09
Supreme CLAY Spec. 17	Intial	100.0	102.5	82.52	825.16	1408.7	0.49	1.29	0.56	1.71	1.15	99.5			
	50	100.2	102.6	82.69	826.91	1400.8		1.30	0.57	1.69	1.14		1.1E-09		
	100	99.8	102.1	81.92	816.62	1390.5		1.27	0.56	1.70	1.16		9.8E-10	1.4E-09	1.4E-09
	200	99.5	100.9	79.93	793.40	1367.3		1.20	0.55	1.72	1.20			1.2E-09	1.2E-09
Supreme CLAY Spec. 21	Intial	100.0	103.0	83.32	833.23	1421.5	0.51	1.35	0.57	1.71	1.12	100			
	50	100.2	103.0	83.29	832.96	1413.3		1.33	0.57	1.70	1.13			1.4E-09	1.5E-09
	100	99.8	102.2	82.04	817.76	1398.1		1.28	0.56	1.71	1.15			1.0E-09	1.3E-09
	200	99.4	101.1	80.32	795.64	1376		1.22	0.55	1.73	1.18			9.5E-10	1.0E-09

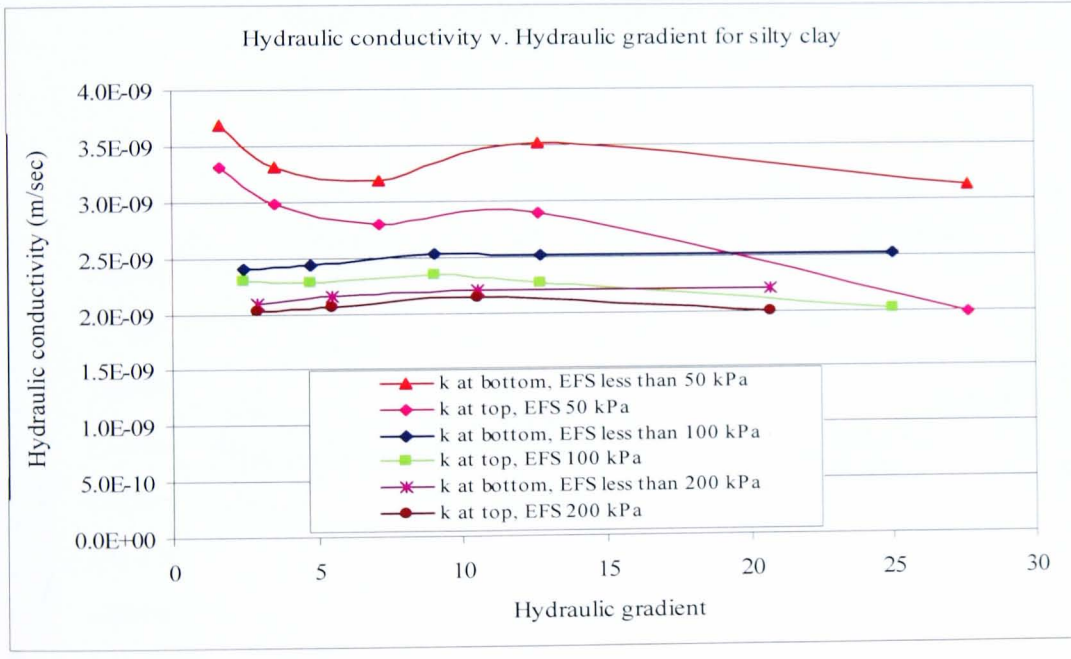

Figure 5.14 Variation of hydraulic conductivity at the top and bottom of the silty clay specimen with change of hydraulic gradient.

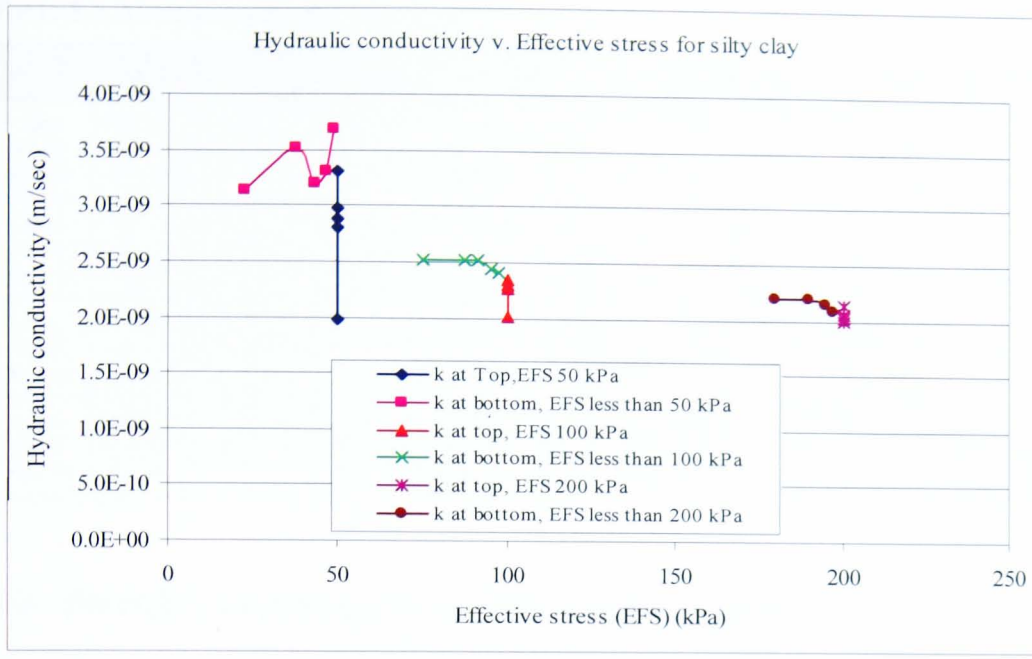

Figure 5.15 Variation of hydraulic conductivity at the top and bottom of the silty clay specimen with change of effective stress.

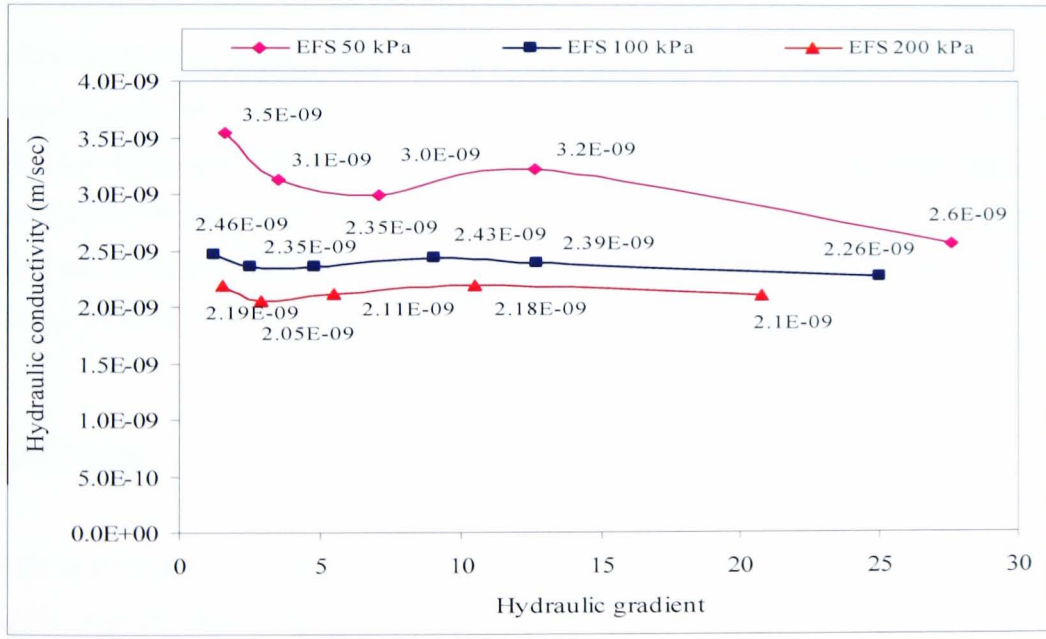

Figure 5.16 Average in/out hydraulic conductivities versus hydraulic gradient from specimen N°.13 of silty clay.

Table 5.6 Average hydraulic conductivities for silty clays:

Specimen No.	EFS	l (mm)	D (mm)	A (cm^2)	V (cm^3)	W (g)	wc	e	n	bulk density	dry density	S (%)	Ave. k (CF)	Ave. k (FH)	Ave. k (CH)
Silty CLAY Spec. 13	Intial	100.0	101.8	81.39	813.93	1440.7	0.41	1.11	0.53	1.77	1.25	99.9			
	50	100.0	101.7	81.22	812.23	1436.7		1.09	0.52	1.77			3.2E-09		
	100	99.8	101.2	80.38	801.81	1428.8		1.06	0.51	1.78			2.4E-09		
	200	99.5	100.4	79.22	786.81	1414.1		1.03	0.51	1.80			2.1E-09		
Silty CLAY Spec. 14	Intial	100.5	102.0	81.71	821.21	1459.4	0.41	1.10	0.52	1.78	1.25	99.2			
	50	100.5	102.2	82.00	824.11	1454.5		1.09	0.52	1.76			3.2E-09		
	100	100.3	101.7	81.16	814.05	1445.5		1.07	0.52	1.78			3.0E-09		
	200	100.1	100.8	79.81	797.17	1429.4		1.02	0.50	1.79			2.7E-09		
Silty CLAY Spec. 16	Intial	100.4	102.5	82.52	828.46	1470.3	0.42	1.11	0.53	1.77	1.25	99.9			
	50	100.5	102.4	82.42	827.47	1464.1		1.10	0.52	1.77			3.7E-09		
	100	100.3	102.0	81.68	818.00	1454.6		1.07	0.52	1.78			3.3E-09		
	200	100.0	101.2	80.38	801.85	1438.5		1.03	0.51	1.79			2.9E-09		
Silty CLAY Spec. 20	Intial	100.0	103.0	83.32	833.23	1481.0	0.42	1.12	0.53	1.78	1.24	101			
	50	100.1	103.1	83.42	834.22	1475.0		1.10	0.52	1.77				3.4E-09	3.9E-09
	100	99.9	102.5	82.49	822.89	1463.7		1.08	0.52	1.78				3.0E-09	3.0E-09
	200	99.5	101.4	80.83	802.66	1443.4		1.02	0.50	1.80				2.9E-09	2.6E-09

5.4 Flexible wall falling and constant head techniques

Twenty one tests were carried out in the flexible wall permeameter using the falling head technique to determine the hydraulic conductivity of five types of soil specimens. These were reconstituted specimens including supreme clay, silty clay, fine sand, medium sand, and coarse sand. Each of the specimens was prepared as explained in section 3.4.1, and tested according to the test procedure prescribed in chapter three, under three different effective stresses (50kPa, 100kPa and 200kPa). The sandy specimens were also tested under effective stresses of 300, 400 and 500kPa. At each effective stress, different pressure differences between the top and the bottom of the specimen were applied to generate an inflow at the base of the specimen in order to determine the effect of the induced hydraulic gradient and the change in effective stress on the hydraulic conductivity of soils.

5.4.1 Clays

Each specimen was saturated and consolidated by the same procedure that was followed in the constant flow technique. The permeability tests using the falling head technique were started by setting a maximum pressure difference (5, 10, 20 and 30 kPa) between the top and the bottom of the specimen. Figure 5.17 shows a typical permeation result for supreme clay using the falling head technique. The positive and negative flow quantities correspond to the inflow and outflow of the permeant. It can be seen that at the bottom of the specimen there was a swelling due to the rapid increase in pore

pressure and a corresponding decrease in effective stress indicated by the cell volume change gauge. This swelling did not increase after the first half an hour of the test's duration, unlike in the constant flow technique where this took about two hours. The pressure difference started to decrease as the water columns in both of the fine tubes of the inflow volume change gauge and outflow volume change gauge started to decrease and increase respectively (Figure 5.18). There was a small increase in pore pressure at the top of the specimen as the water column rose in the outflow volume change gauge. This volume change due to a very small decrease in effective stress (2.5 kPa), was negligible compared to that at the bottom of the specimen (30 kPa).

When a higher pressure difference was used in the next permeation stage, the volume changes at the bottom of the specimen were greater due to a greater decrease of effective stress, and hence the difference between the inflow and the outflow became greater.

During the testing of fine grained specimens (silty and supreme clays) using the modified system, the pressure difference across the specimen decreased by only a small amount compared to the back pressure, and therefore the tests were interpreted using both the falling head and constant head technique.

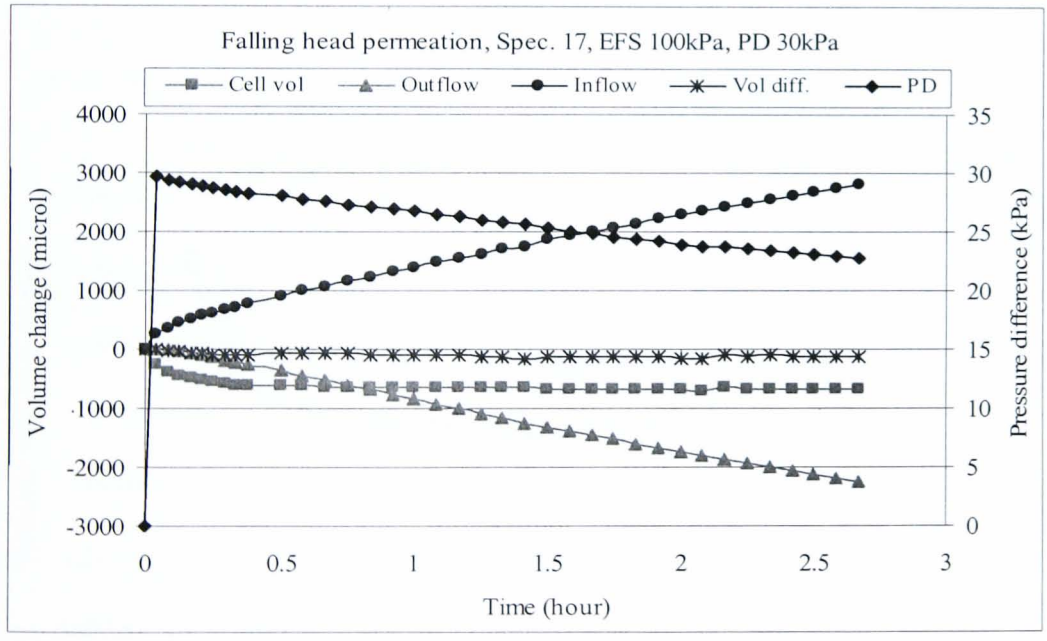

Figure 5.17 Typical result of falling head permeation test for supreme clay.

The hydraulic conductivities determined by the falling head and constant head formula are shown in Figure 5.19. It can be seen that the results were very close and levelled off

as soon as the specimen volume change due to reduction in the effective stress at the bottom was complete. At this stage the hydraulic conductivity of the specimen was taken as the average of the last portion of the plot of these results.

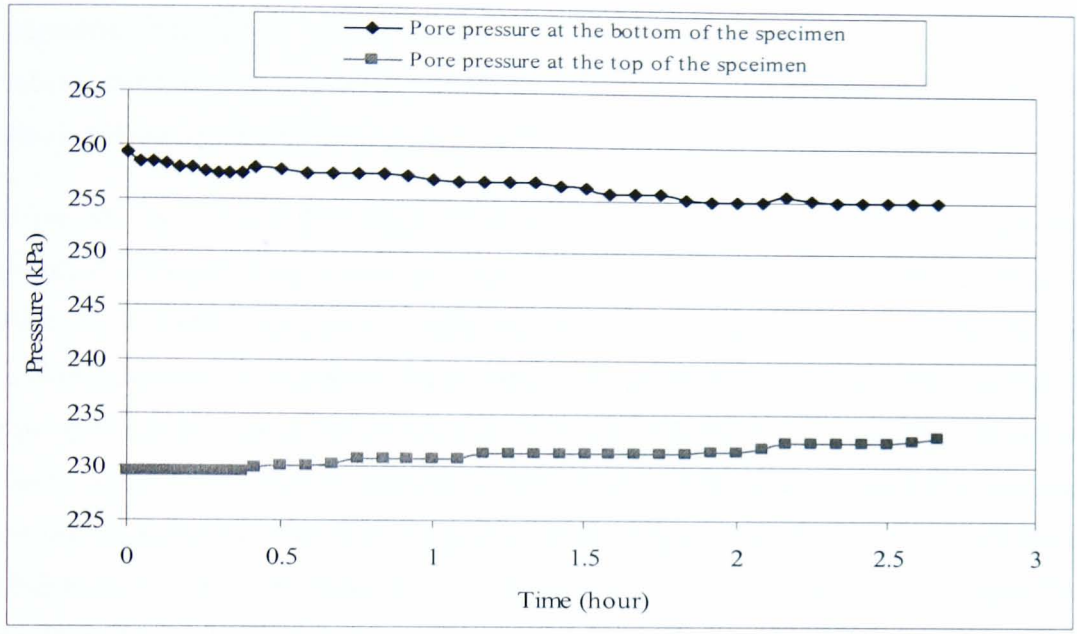

Figure 5.18 Pore pressure changes at the top and bottom of the specimen.

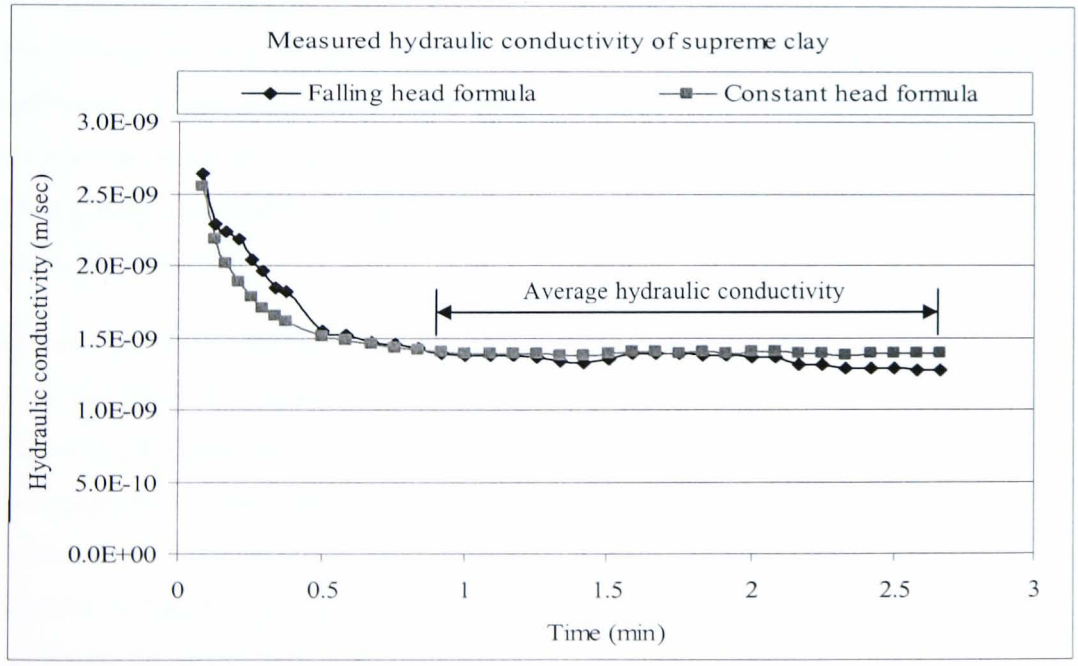

Figure 5.19 Calculated hydraulic conductivity during the test.

5.4.2 Sands

The sandy specimens were tested in the flexible wall permeameter using the falling head technique at different pressure differences across the specimen from 5 kPa up to 40 kPa. Figure 5.20 shows a typical test result for a fine sand specimen using the falling head technique. The inflow was equal to the outflow and there was no change in the cell volume, indicating that the volume of the specimen did not change due to the change in the effective stress at the bottom of the specimen.

It can also be seen that as soon as the inflow started permeating the specimen the pressure difference dropped unexpectedly from 20kPa to about 15kPa under an effective stress of 200 kPa. The pressure difference across the specimen was measured by the differential pressure transducer (DPT) and also by the difference between the readings of the top and bottom pressure transducers (PT) (Figure 5.20). The two readings should be equal; however there was a difference between these two pressure difference readings across the specimen. This difference was smaller when using a low pressure difference (Figure 5. 21) and was larger when using a higher pressure difference. Therefore this could be due to the velocity of the flow in the specimen causing a drop in the measured pressure at each transducer. However, during the testing of medium and coarse sand specimens, the differential pressure transducer was not able to read the pressure difference across the specimen, this could be because of the speed of flow, and therefore the calculated hydraulic conductivities of these types of soils were based on the pressure difference measured by the top and bottom pressure transducers, in a test duration of only a few seconds (30sec). The advantage of testing fine sand in the flexible wall falling head permeameter is that the effective stress and the hydraulic gradient were precisely controlled.

Figure 5.22 shows the effect of hydraulic gradient on the hydraulic conductivity of fine sand specimen. The hydraulic conductivity decreased with increasing hydraulic gradient. Figure 5.23 shows that increasing the effective stress (EFS) decreased the hydraulic conductivity of fine sand specimens, which proves that hydraulic conductivity is a function of effective stress for fine soils. This effect is very small for coarse soils because as the effective stress increased, there was a small decrease in void ratio of the specimen therefore there was a small increase in density, hence hydraulic conductivity decreased slightly. This effect was very small compared to that observed with clayey soils (Figure 5.29).

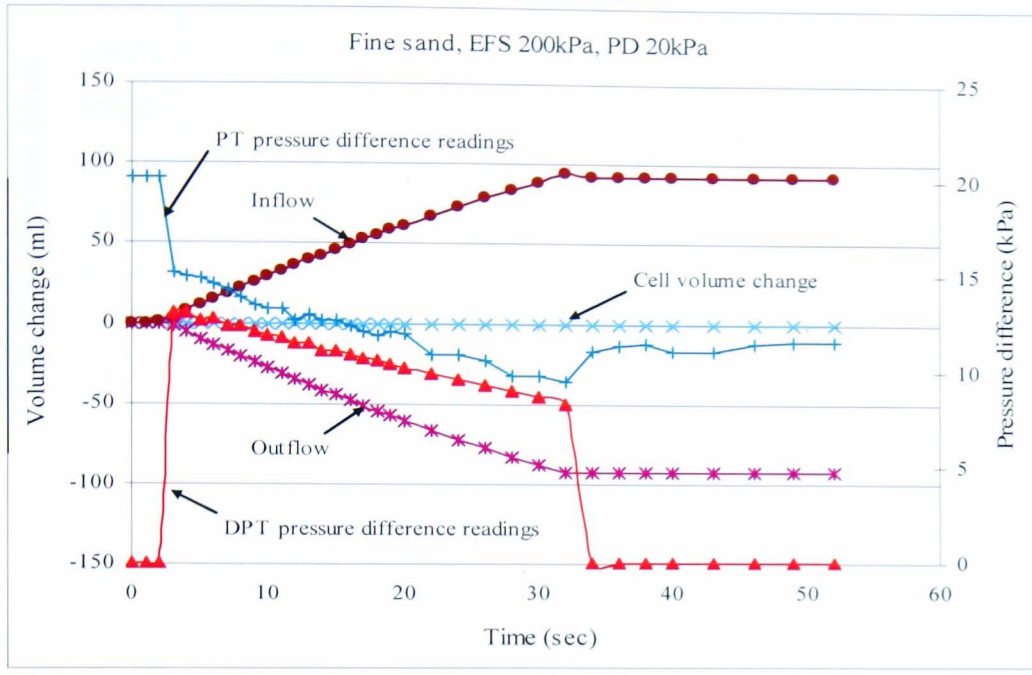

Figure 5.20 Results of falling head test on fine sand specimen at effective stress 200 kPa and initial pressure difference 20kPa.

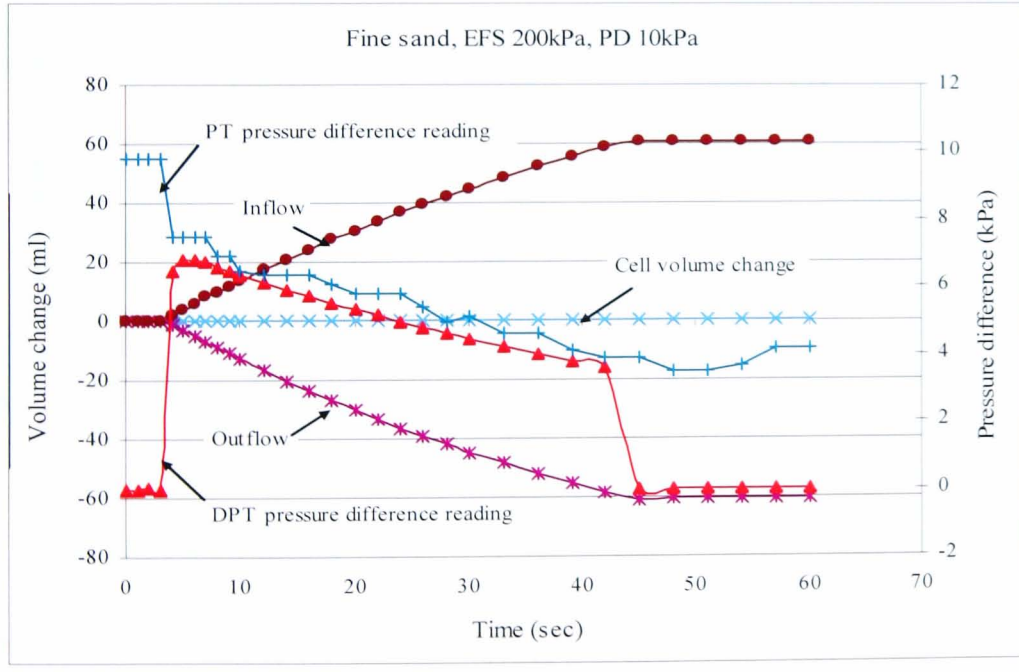

Figure 5. 21 Results of falling head test on fine sand specimen at effective stress 200 kPa and initial pressure difference 10kPa.

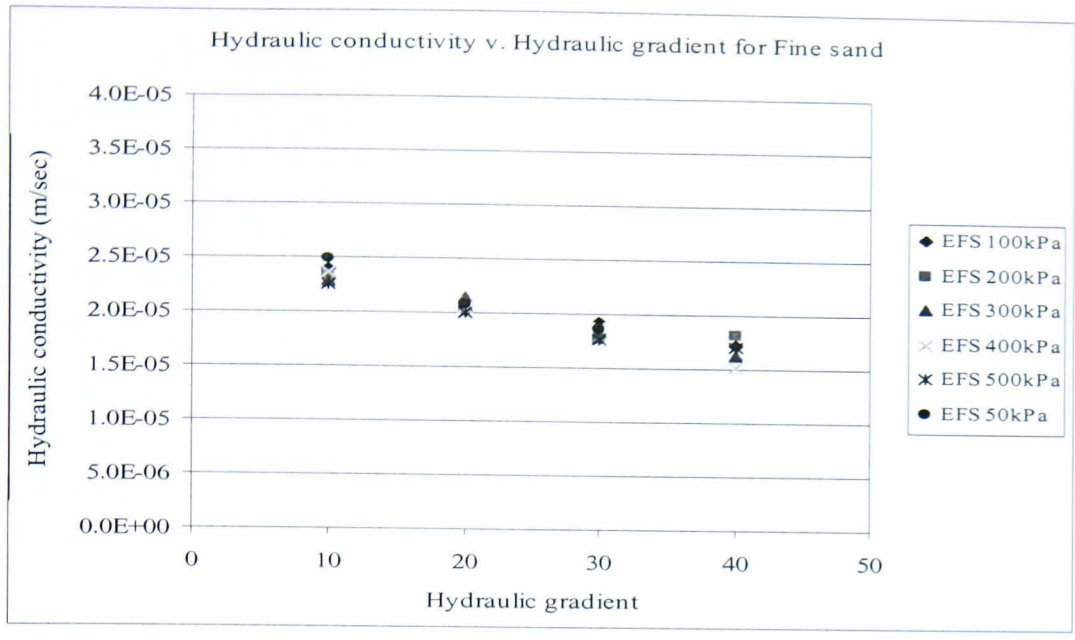

Figure 5.22 Hydraulic conductivity versus hydraulic gradient for fine sand.

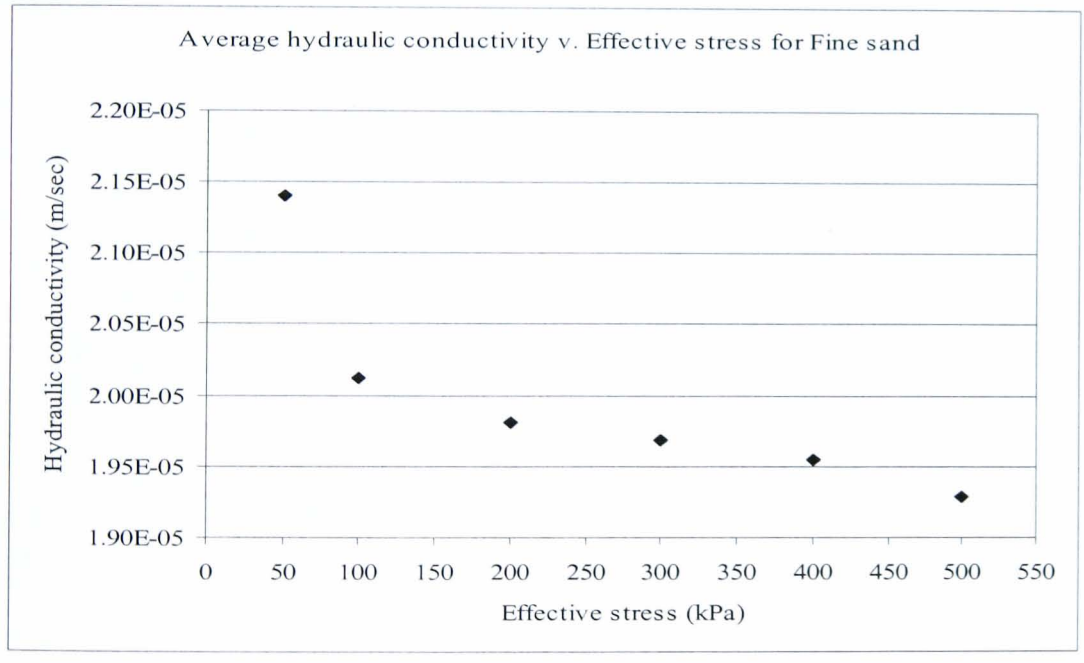

Figure 5.23 Average hydraulic conductivity versus effective stress for fine sand.

This was also the case for the medium and coarse sand specimens, where there was not much effect on the hydraulic conductivity with increasing the effective stress (Figure 5.24); at least in the range of the effective stresses used in this study. Further investigation of the effect of effective stress on the void ratio of sandy soils was carried out using the odometer test procedure outlined in the British standard.

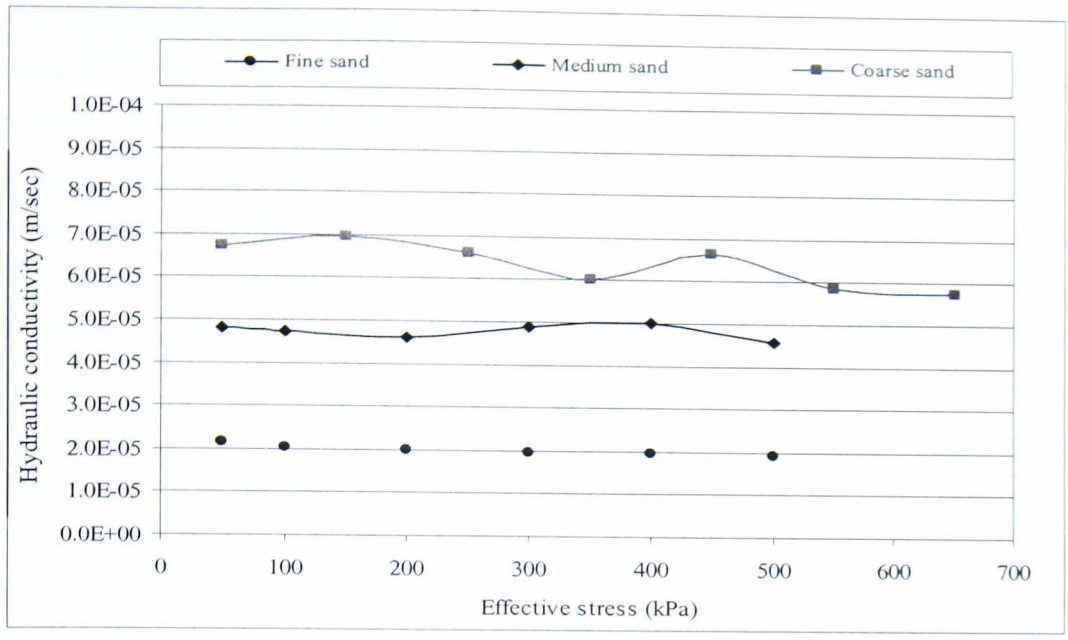

Figure 5.24 Hydraulic conductivity versus effective stress for sand specimens.

The results (Figure 5.25) show a very small change in the void ratio as the effective stress was increased up to 800 kPa.

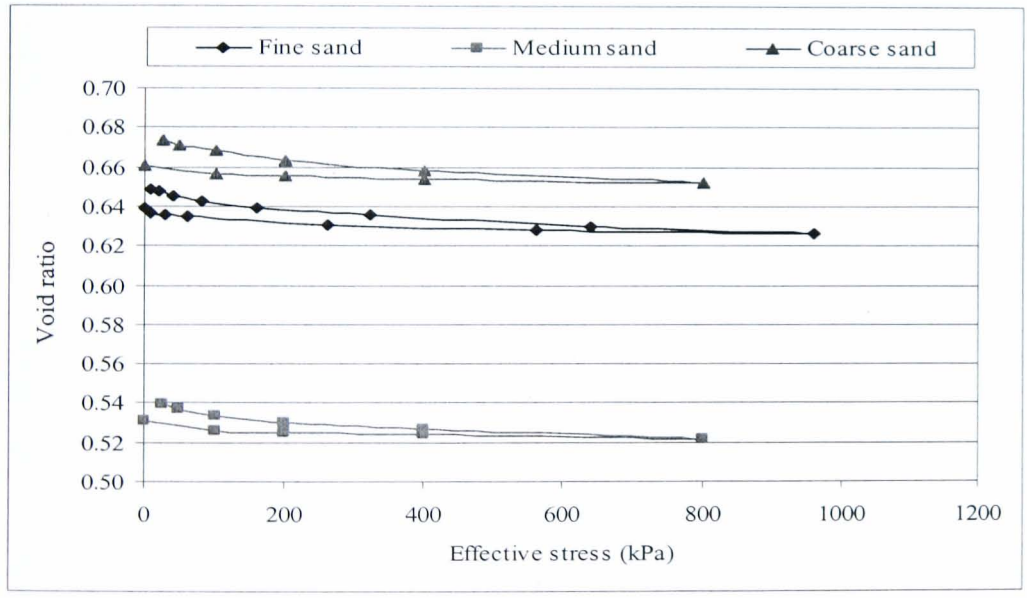

Figure 5.25 Void ratio versus effective stress for coarse specimens from oedometer tests.

The flexible wall permeameter using the falling head technique system produced a low pressure difference across the medium and coarse specimens due to an insufficient amount of inflow. This was because this system was originally designed to test fine soils such as clays and silts. After modifying the system to work as a falling head system as

well as a constant flow system, the internal outflow tube was changed to a tube with a bigger diameter and therefore greater capacity, so that coarser soils could be tested. After that the medium and coarse soils were tested in the system. A conventional rigid wall permeameter was used to determine the hydraulic conductivities of the coarse soils, including fine sand, medium sand and coarse sand (Table 5.7). These tests results were used to verify the test results of the flexible wall permeameter using the falling head technique. Figure 5.26 show a comparison of the results obtained by the falling head flexible wall and the constant head rigid wall permeameters. It can be seen that the results of the flexible wall permeameter using the falling head technique for medium and coarse sands were very low compared to those of the rigid wall permeameter using the constant head technique. This indicated that the use of the modified flexible wall permeameter should be limited to test only fine soils including fine sands, because it was expected that coarser material would have a greater hydraulic conductivity.

Table 5.7 Constant head test results of hydraulic conductivities

Specimen No.	EFS	l (mm)	D (mm)	A (cm^2)	V (cm^3)	W (g)	wc	e	n	bulk density	dry density	S (%)	Ave. k (CH)
Fine SAND	N/A	204	74	43.0	877.4	1672.1	0.31	0.83	0.45	1.91	1.45	100	3.9E-05
Medium SAND	N/A	204	74	43.0	877.4	1964.4	0.18	0.48	0.32	2.24	1.79	100	6.6E-04
Coarse SAND	N/A	204	74	43.0	877.4	1890.6	0.21	0.56	0.36	2.15	1.7	100	2.1E-03

CH = Constant head test

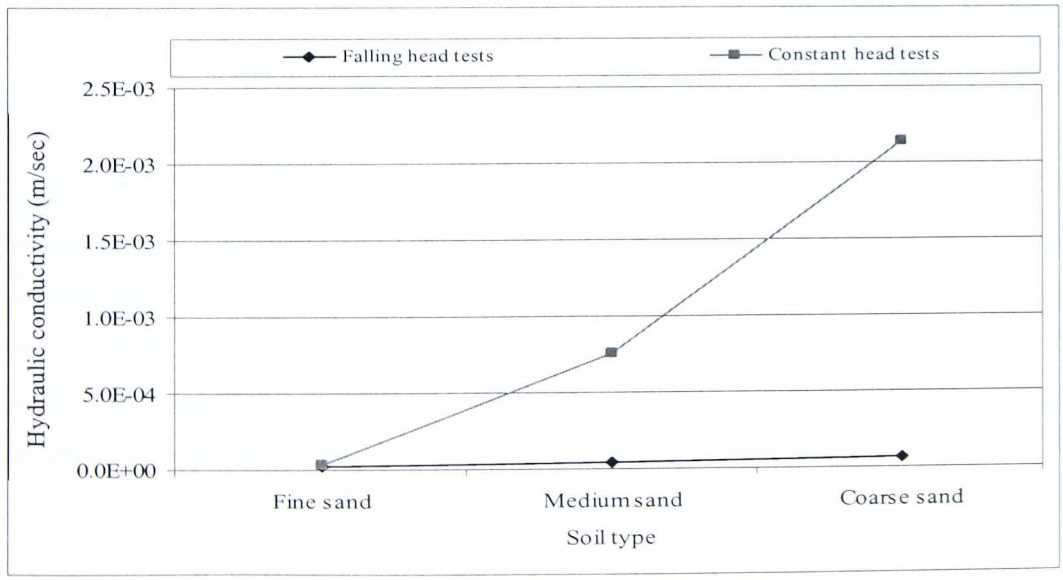

Figure 5.26 Comparison of the results of the flexible wall permeameter using falling head technique with the results of the rigid wall permeameter using constant head technique.

5.5 *Effect of Void ratio, density and effective stress on hydraulic conductivity determination*

It can be seen in Figure 5.27 that the hydraulic conductivity increases with increasing void ratio. Figure 5.27 also shows that particle size has a marked effect on the hydraulic conductivities on silty clay specimens, since the measured hydraulic conductivities of these specimens increased rapidly with a slight increase in void ratio. In contrast, the hydraulic conductivities of supreme clay increased only slightly with a change in void ratio.

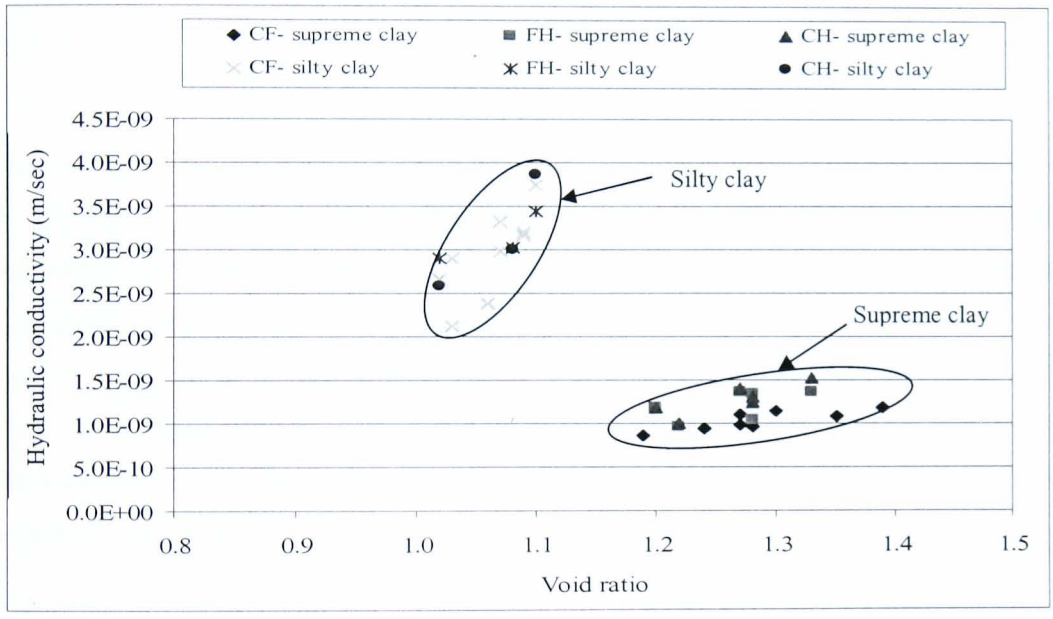

Figure 5.27 Hydraulic conductivity versus void ratio.

Figure 5.28 shows that hydraulic conductivity decreases as density increases, because increasing the density decreases the porosity of the specimen. A relation between the void ratio for the clayey specimens and fine sand versus the logarithm of effective stress was plotted in Figure 5.29. This decrease is higher with the clayey specimens than with the fine sand specimen. This indicates that the change in void ratio and effective stress is less effective with sands when determining its hydraulic conductivity.

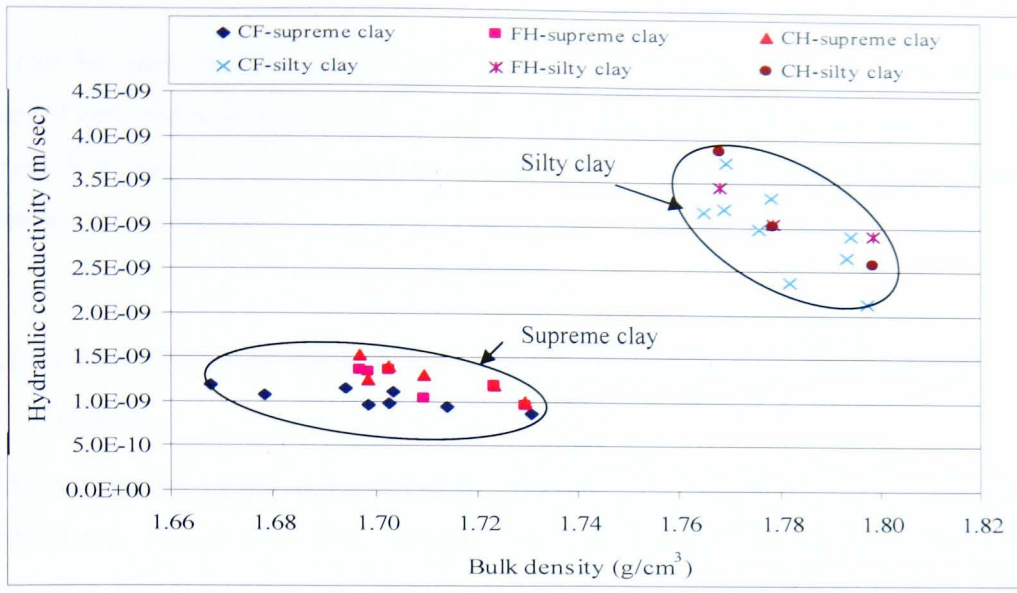

Figure 5.28 Hydraulic conductivity versus bulk density.

The void ratios for the three silty clay specimens were similar (Figure 5.29), however for the supreme clay it was not. This reflects the effect of the method of preparation on the specimen's void ratio. During the sample preparation the maximum axial stress for consolidating the supreme clay specimen (No.15) was applied all at once, where as for the other specimens it was applied in three increments. Appling the maximum axial stress all at once causes the rapid consolidation of the sample portion near to the drainages, therefore reducing the amount of water that could be expelled. This causes an increase in void ratio.

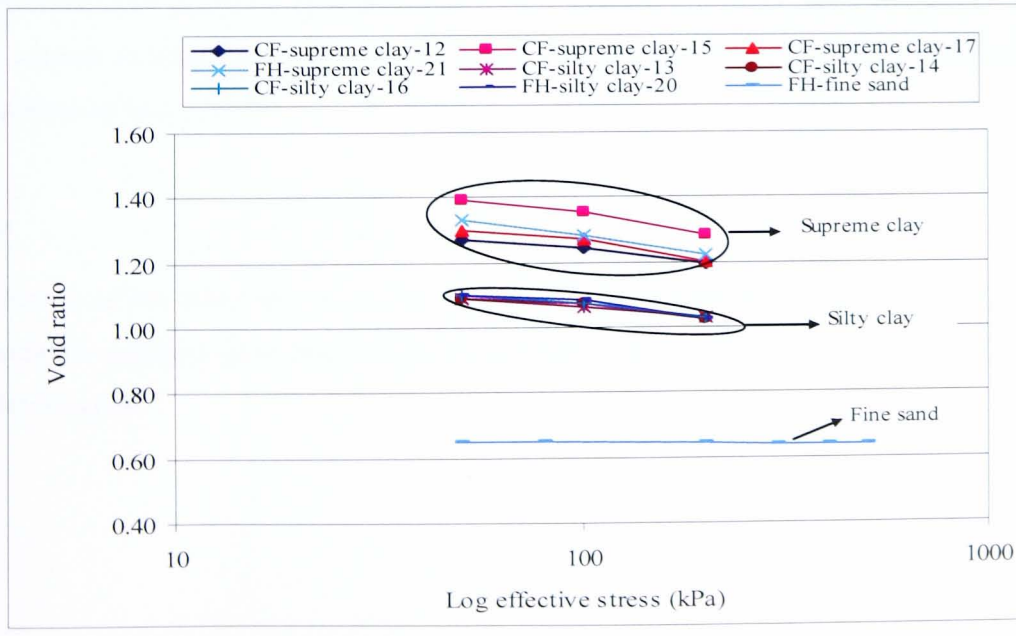

Figure 5.29 Void ratio versus log effective stress.

It can be seen that the three factors, void ratio, density and effective stress are interrelated, and a change in one of them affects the others. So an increase in effective stress decreases void ratio, and hence increases the density consequently the hydraulic conductivity decreases.

5.6 Comparison of the flexible wall constant flow and falling head results

An experimental comparison between the constant flow and falling head techniques was carried out. The constant flow apparatus was modified to also work as a falling head apparatus. The comparison between the two techniques was performed on two different types of clayey soils i.e. supreme clay and silty clay. The procedure for the preparation of specimens, saturation and consolidation was exactly the same for both clays.

In the constant flow rate test (Figure 5.30), the flow pump was used to produce a constant inflow rate, creating an increase in pore pressure at the bottom of the specimen and a corresponding swelling due to a decrease in effective stress. The amount of swelling of the specimen depended on the amount of the water that was infused at its base per unit time, so that the higher the inflow rate the higher the amount of swelling. This swelling began at the start of the permeation stage and continued until the steady state condition was reached, which took at least two hours because the pore pressure increased only gradually up to the steady state. The rate of inflow and the outflow were, as normal, averaged and used to compute the hydraulic conductivity using the following equation of Darcy's law:

$$k_h = \frac{q}{A \cdot i} \qquad 5.1$$

where q is the flow rate, A is the cross sectional area of the specimen and i is the hydraulic gradient generated across the specimen when the steady state condition has been reached.

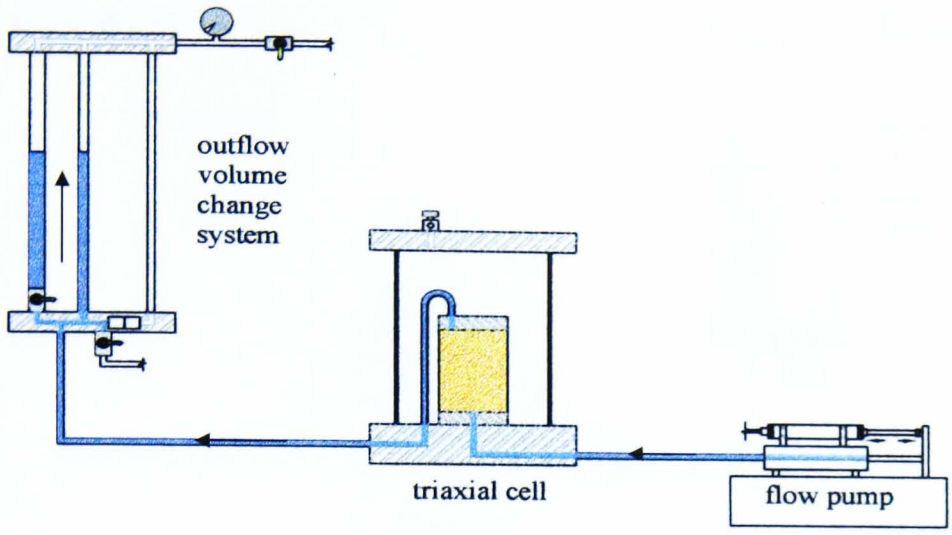

Figure 5.30 Schematic diagram of the constant flow technique.

In the falling head test (Figure 5.31), a pressure difference between the top and the bottom of the specimen was set to generate flow from the bottom to the top. The inflow and the outflow rates were measured by two Newcastle volume change gauges. A swelling at the bottom of the specimen due to the decrease in effective stress took place as soon as permeation started, finishing within about 20 to 30 minutes (unlike in the constant flow test). This made the test duration shorter than that of the constant flow test, at a maximum of one hour. Hydraulic conductivity was calculated using the following equation:

$$k_h = \frac{a \cdot L}{2 \cdot A \cdot \Delta t} \ln\left(\frac{\Delta p_1}{\Delta p_2}\right) \qquad 5.2$$

where a is the cross sectional area of the inflow tube of the Newcastle volume gauge, L is the length of the specimen, A is the cross sectional area of the specimen, Δp_1 and Δp_2 are the initial pressure difference and the pressure difference at the end of the test respectively, both were measured by the deferential pressure transducer (DPT) and Δt is the time elapsed.

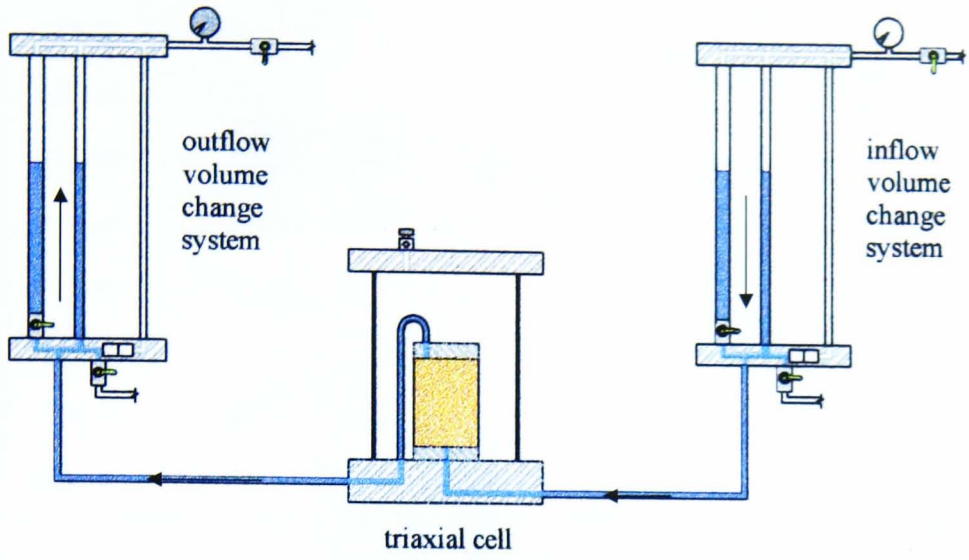

Figure 5.31 Schematic diagram of the falling head technique.

The hydraulic conductivity values for the silty and supreme clays obtained by both constant and falling head techniques and presented in the tables of results are compared in Figure 5.32. It can be seen that the hydraulic conductivity values for both types of specimens at different values of effective stress (50, 100 and 200 kPa) agree well, except for some of the values obtained by the falling head technique using low pressure differences when the air pressure regulator for the inflow system was not sensitive enough to operate at such low pressure difference. The values were higher than those obtained by the constant flow technique due to the irregular air supply, which caused small fluctuations in the pressure difference across the specimen, especially when using low pressure difference at low effective stresses, such as 50 kPa. This variation was not seen in the hydraulic conductivity values obtained using higher pressure differences across the specimens at high effective stress. Therefore, it is important to regularly check and maintain the air pressure regulators when using these testing systems especially with the falling head technique.

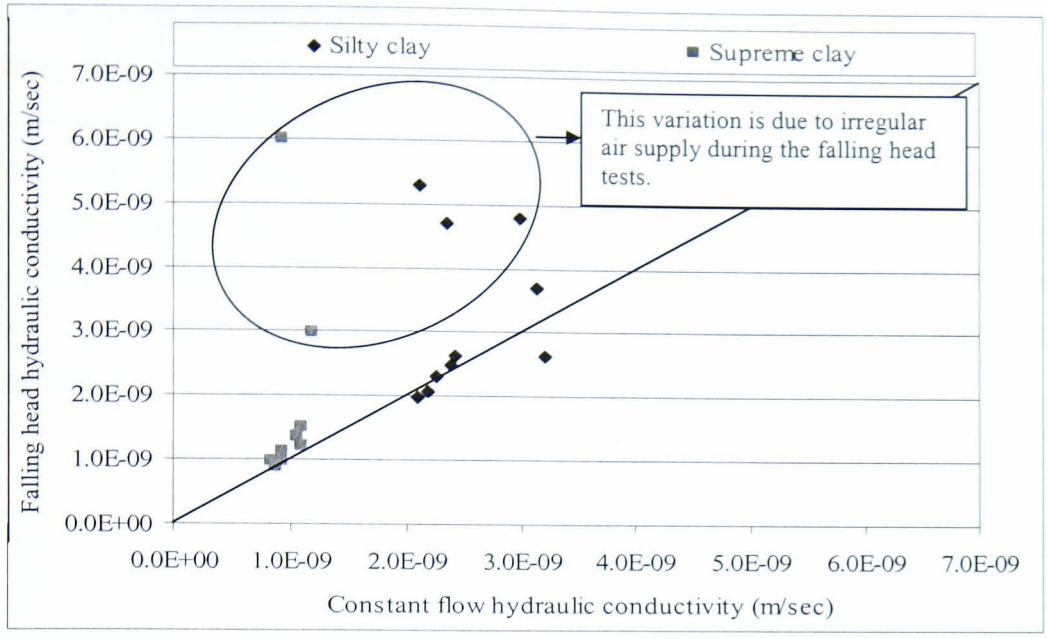

Figure 5.32 Comparison between the constant flow and falling head tests results.

5.7 *Comparison of the flexible wall constant flow and constant head results*

Since there was little reduction in the pressure difference across the clayey specimens during a test using the falling head technique, it was also possible to compute the hydraulic conductivities for this type of soil by using the constant head formula. These values were compared with the hydraulic conductivity values obtained from the constant flow techniques in order to validate the new modification of the apparatus. Although the hydraulic conductivity of each specimen was calculated using the same equation of Darcy's law that was used with the constant flow technique, as follows:

$$k_h = \frac{q}{A \cdot i} \qquad 5.3$$

Figure 5.33 shows that the constant head results were greater than constant flow results, especially for the silty clay specimen. This could be due to the assumption that the falling head test can be interpreted as a constant head test. The main advantage of the constant head test is that the test duration is shorter than for the constant flow test, because the volume changes during the test are complete within 20 to 30 minutes in which the test could be ended in an hour time. While in the constant flow test the time required to reach the steady state condition is more than two hours.

Also, by comparing Figure 5.32 and Figure 5.33, it can be seen that the air pressure supply fluctuations had less effect on the hydraulic conductivity results calculated based on the constant head formula depended on the inflow and outflow rates, which were not influenced by the small fluctuations in air pressure supply (Figure 5.6). However the hydraulic conductivities obtained with the constant head technique for the silty clay specimens were higher than those obtained with the constant flow technique, because there was a higher drop in pressure difference across the specimen than that of the supreme clay.

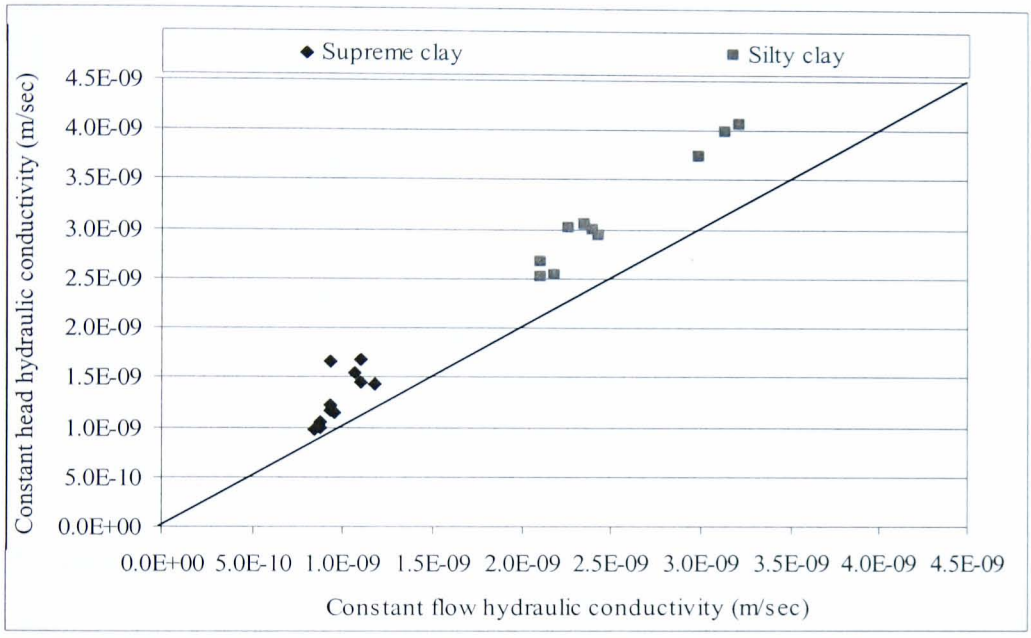

Figure 5.33 Comparison between the constant flow and the constant head tests results.

5.8 *Comparison of the flexible wall falling head and constant head results*

Figure 5.34 shows a comparison of the hydraulic conductivity results obtained by the flexible wall permeameter using the falling head formula (equation 5.2) with those obtained using the constant head formula (equation 5.3) for the same test results. During these tests it was assumed that there was not much change in the pressure difference across the clay specimens. Therefore it was possible to interpret the test as constant head tests using equation 5.3. The results were compared as shown in Figure 5.34, and it can be seen that for supreme clay specimens both equations 5.2 and 5.3 gave very good agreement. However, for the silty clay specimens the results of the constant head formula were greater than those of the falling head formula, which indicates that this

assumption can be used only with soil that has very low hydraulic conductivity. The coarser the soil the greater will be the drop in the pressure difference across the specimen, and hence this test should be interpreted only as a falling head test.

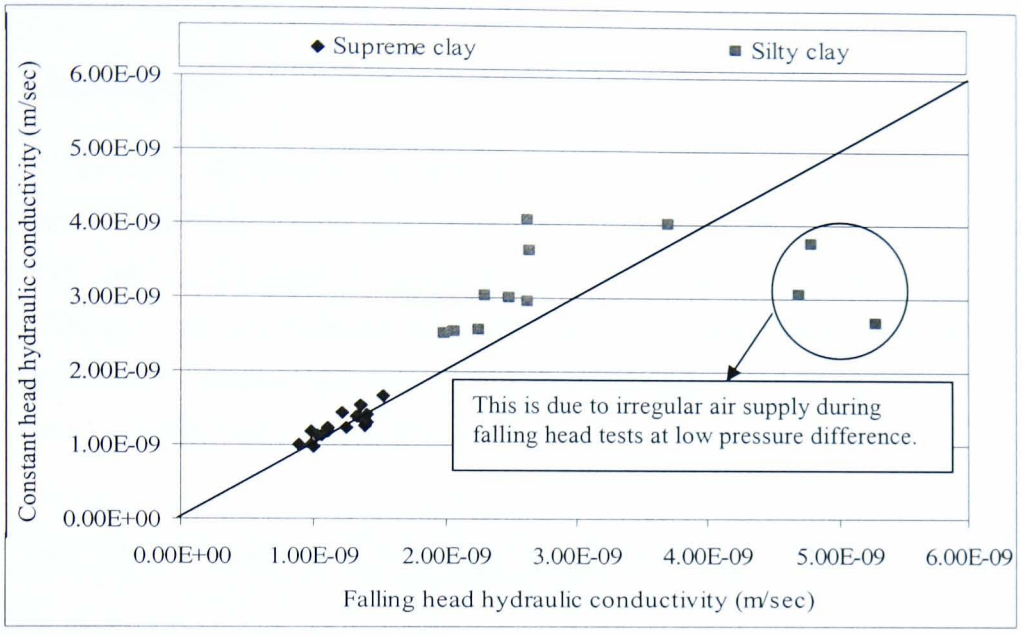

Figure 5.34 Comparison between test results using the falling head and constant head formulas.

5.9 Summary

In this chapter the results of hydraulic conductivity obtained by the flexible wall permeameter using both the constant flow and falling head techniques are presented and discussed. The flexible wall permeameter used for this research operated satisfactorily under both the constant flow and the falling head techniques, and both of which produced good quality data. The influence of the magnitude of hydraulic gradient on the hydraulic conductivity of reconstituted clays is investigated by generating the hydraulic gradient outside the practical range of engineering interest. When the hydraulic gradient across the specimen changes, it causes the state of stress to change as well; consequently the volume of the compressible specimen changes too. Therefore any change in hydraulic conductivity will occur when both the applied stress and the hydraulic gradient are altered.

Also discussed in this chapter is the effect the testing system had in the determination of hydraulic conductivity. Furthermore the results of the different techniques used are then compared and any variations are too discussed.

Chapter 6

Thermal Conductivity Results and Discussions

6.1 Introduction

Four of the soils tested were reconstituted soils which included silty clay, fine sand, medium sand and coarse sand. Natural soils were also tested and these included sandy silty clay, silty sand, medium to coarse sand and sandy gravel. The grading curves for these different soils are illustrated using the particle size distribution curves shown in Figure 6.1. Their characteristics and physical properties are presented in Tables 6.1 and 6.2. These were then used in the analysis of the test results.

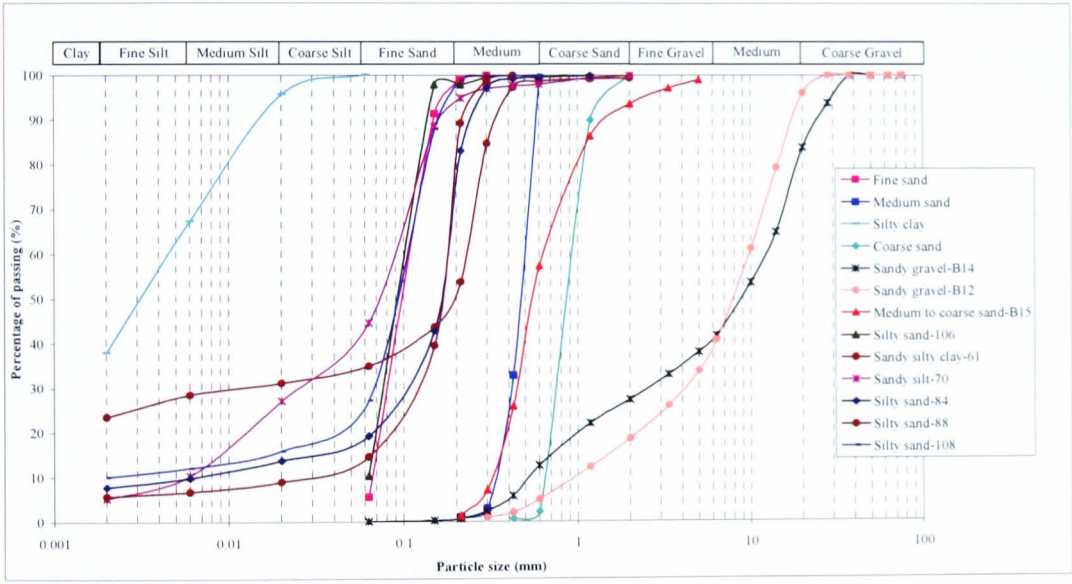

Figure 6.1 Particle size distribution curves for the studied soils.

Each of the reconstituted soils was tested under both dry and saturated conditions at different base temperatures, these being 30°C, 40°C and 50°C respectively. The natural soils were taken from disturbed (bulk samples) and undisturbed (U100 samples) samples. These soils were tested at their in-situ water content.

Table 6.1 Characteristics and physical properties of reconstituted soils.

Soil Type	l mm	D mm	A cm^2	V cm^3	*n*	e	w_c %	A	S %	Bulk Density Mg/m^3	Dry Density Mg/m^3
Dry Silty CLAY	100	98	75.4	754.3	0.47	0.9	0	0.47	0.0	1.39	1.39
Saturated Silty CLAY	100	102	81.7	817.1	0.55	1.22	46.2	0.00	99.6	1.73	1.2
Dry Fine SAND	100	100	78.5	785.4	0.40	0.66	0	0.40	0.0	1.6	1.6
Saturated Fine SAND	100	100	78.5	785.4	0.39	0.64	24.6	0.00	100	2.01	1.6
Dry Medium SAND	90	105	86.6	779.3	0.36	0.56	0	0.36	0.0	1.7	1.7
Sat. Medium SAND	98	102	81.7	800.8	0.33	0.5	20.2	0.00	100	2.08	1.7
Dry Coarse SAND	95	100	78.5	746.1	0.32	0.47	0	0.32	0.0	1.8	1.8
Saturated Coarse SAND	100	100	78.5	785.4	0.33	0.5	20.2	0.00	100	2.08	1.7

Table 6.2 Characteristics and physical properties of natural soils.

Soil Type	l mm	D mm	A cm^2	V cm^3	*n*	e	w_c %	A	S %	Bulk Density Mg/m^3	Dry Density Mg/m^3
Sandy Silty CLAY BH 9T 61	100	103	83.3	833.2	0.33	0.49	19.5	0.00	100	2.1	1.8
Sandy SILT BH 9T 70	101	103	83.3	841.6	0.43	0.75	26.5	0.02	92.9	1.89	1.5
Silty SAND BH C13 84	93	103	83.3	770.7	0.40	0.66	21.3	0.05	84.9	1.92	1.6
Silty SAND BH C13 88	96	107	89.9	863.2	0.41	0.69	22.9	0.04	87.3	1.91	1.6
Silty SAND BH C13 106	102	105	86.6	883.2	0.45	0.81	26.6	0.05	86.4	1.84	1.5
Silty SAND BH C13 108	94	108	91.6	861.1	0.44	0.79	27.2	0.03	90.6	1.87	1.5
M. to Coarse SAND BH 11T B15	91	100	78.5	714.7	0.38	0.62	12.3	0.18	52.6	1.84	1.6
M. to Coarse SAND BH 11T B10	100	100	78.5	785.4	0.31	0.45	4.8	0.22	28.3	1.91	1.8
Sandy GRAVEL BH 11T B12	93	100	78.5	730.4	0.36	0.56	2.6	0.31	12.3	1.75	1.7
Sandy GRAVEL BH 11T B14	102	100	78.5	801.1	0.31	0.44	2	0.27	12.0	1.88	1.8
GROUT (1-1)	99	103	83.3	824.9	0.83	4.75	166	0.05	94.4	1.25	0.47
GROUT (2-1)	100	103	83.3	833.2	0.84	5.09	167	0.10	88.6	1.18	0.44
GROUT (1-2)	101	103	83.3	841.6	0.85	5.52	199	0.02	97.3	1.24	0.41
GROUT (2-2)	103	102	81.7	841.6	0.84	5.3	187	0.04	95.4	1.2	0.4

l= Specimen's height, D= specimen's diameter, A= specimen's cross sectional area, V= specimen's total volume, n= porosity, e= void ratio, wc= water content, A= air content and S= degree of saturation.

6.2 *Thermal conductivity of Reconstituted Soils*

Twenty four experiments were carried out, and the results obtained are presented according to their soil type i.e. fine sand, medium sand, coarse sand and silty clay. The specimens were prepared separately and then placed in the thermal cell, they were then tested under different base temperatures according to the test procedure in Chapter four. The typical temperature versus time profiles for fine sand under both dry and saturated conditions are shown in Figure 6.2 and Figure 6.3 respectively.

The temperatures at three points 3.3cm, 6.6cm and at the top surface above the base of the specimen (Figure 6.4) started to increase in order of distance from the base to their steady state maximum values. These values depended upon the physical properties of the specimen and its composition. As soon as the steady state condition was obtained for all four points, the power was then switched off. The specimen was then left to cool down to room temperature, under the process of free convection via the top surface of the specimens.

During the cooling process, as shown in Figure 6.2 for the dry specimen, the base temperature decreased until equilibrium was reached between it and the temperature at 3.3cm away from the base, as this happened the temperature then continued to drop until equilibrium was also reached, where the temperature at the previous point indicated was then equal to the temperature at 6.6cm. The temperatures then continued to decrease further until equilibrium was reached where the temperature at 6.6cm was equal to that of the top surface of the specimen. It then decreased until the whole temperature of the specimen was in equilibrium with that of the room temperature. However for the saturated specimen, the temperature equilibrium occurred much more rapidly after the power was switched off (Figure 6.3), as this happened the temperature continued to decrease further until the whole temperature of the specimen was in equilibrium with that of the room temperature.

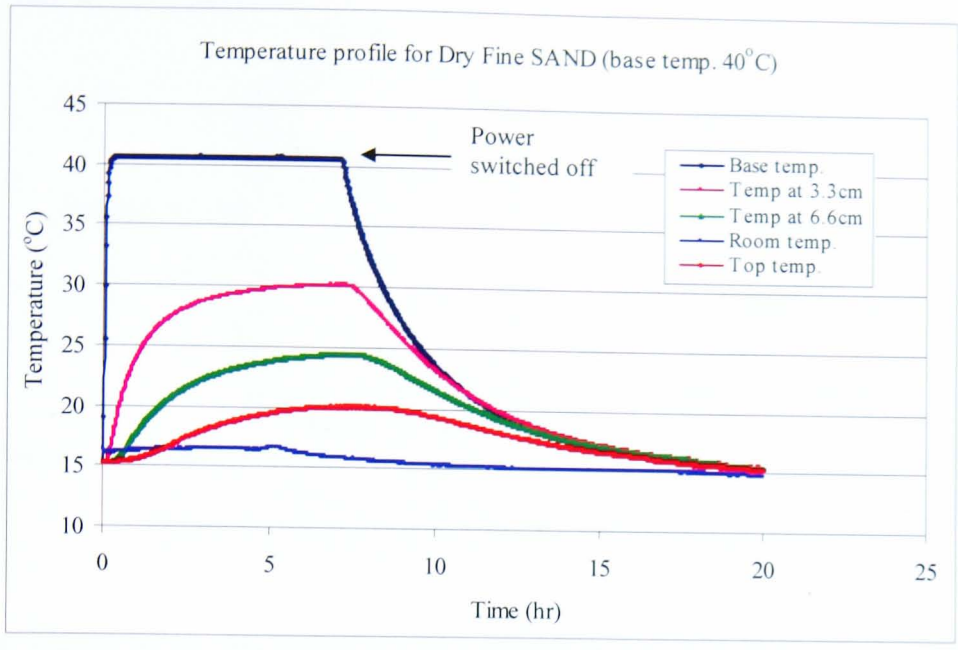

Figure 6.2 Typical temperatures v. time profile for dry soils.

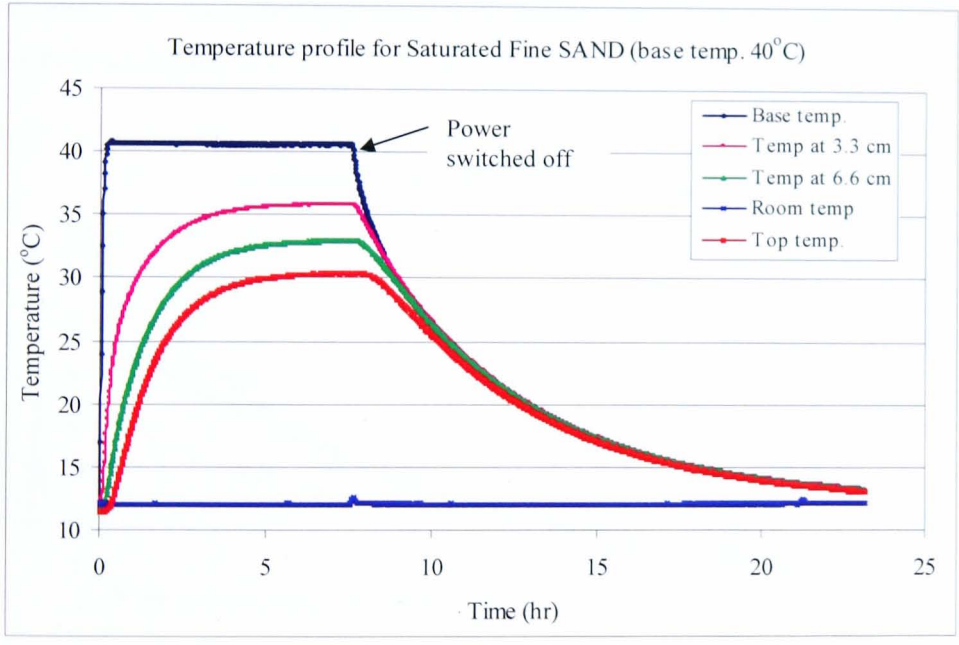

Figure 6.3 Typical temperatures v. time profile for saturated soils.

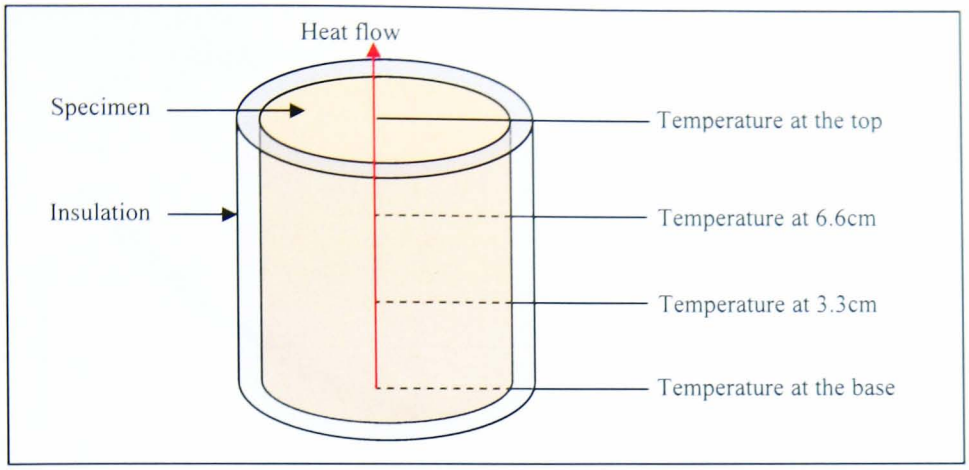

Figure 6.4 Diagram shows the thermocouples positions.

These cooling curves obtained during the cooling processes were then used to determine the convection heat transfer coefficients (h) using equation 4.8. This was carried out using the best fit method where the value of the convection heat transfer coefficient was altered until a best fit of the theoretical curve and the experimental results were obtained (Figure 6.5 and Figure 6.6).

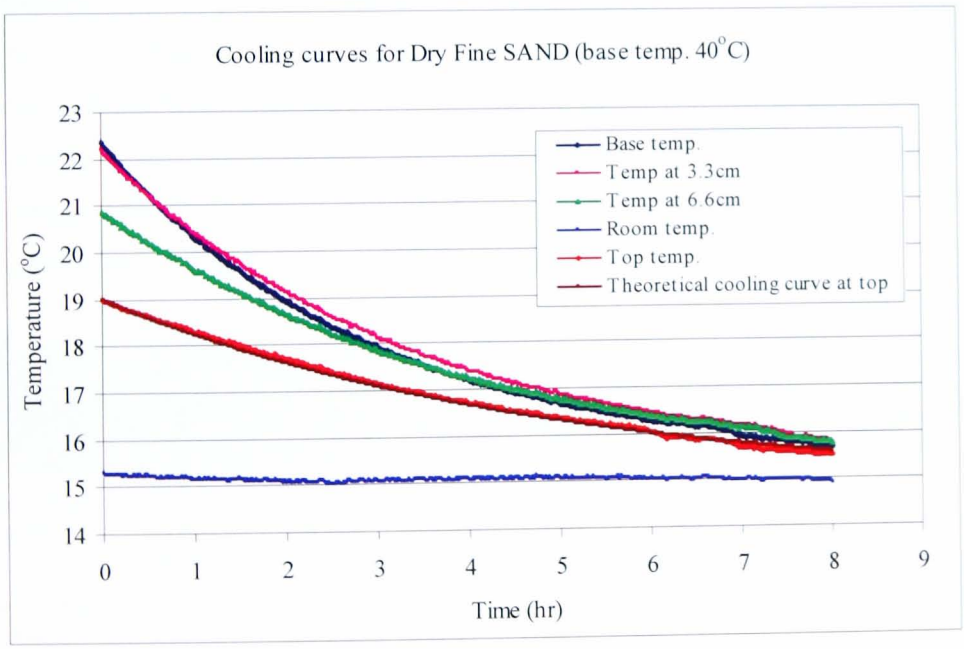

Figure 6.5 Typical cooling curves for Dry Soils.

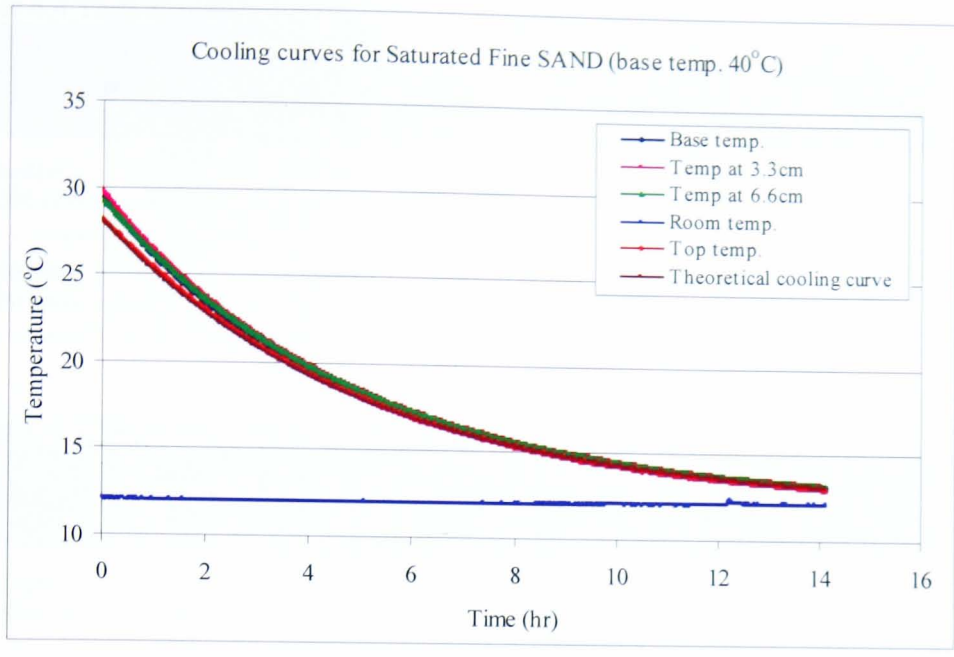

Figure 6.6 Typical cooling curves for Saturated Soils.

In order to determine the thermal conductivity of the specimen, temperature at three points within the specimen were measured for each test; these were the room temperature (T_∞), base temperature (T_{base}), and the top surface temperature (T_{top}) of the specimen at the steady state condition. However the convection heat transfer coefficient (h) was inferred from the cooling curves. They were then used to calculate the thermal conductivity of the soil (k_t) using equation 4.5 under the various base temperatures, and the average was then taken. A summary of these results for the reconstituted soils are presented in the following Tables 6.3, 6.4, 6.5 and 6.6.

Table 6.3 Tests Results of Dry and Saturated Fine SAND

Soil Type	T_∞ (°C)	T_1 (°C)	T_2 (°C)	h (W/m².°C)	k (W/m.°C)	k_{ave} (W/m.°C)
Fine SAND (dry)	14.0	30.7	17.3	5.8	0.14	0.15
	14.6	40.6	20.0	7.0	0.18	
	14.7	50.4	19.9	7.0	0.12	
Fine SAND (sat.)	15.3	30.8	25.5	13.8	2.62	2.75
	12.1	40.6	30.1	16.5	2.83	
	12.1	50.5	36.4	16.3	2.80	

Table 6.4 Tests Results of Dry and Saturated Medium SAND

Soil Type	T_∞ (°C)	T_1 (°C)	T_2 (°C)	h (W/m².°C)	k (W/m.°C)	k_{ave} (W/m.°C)
Medium SAND (dry)	15.0	30.8	19.4	8.0	0.28	0.27
	16.7	40.7	22.2	10.0	0.27	
	16.0	50.5	24.7	8.5	0.26	
Medium SAND (sat.)	17.5	31.0	27.5	13.0	3.58	3.36
	17.0	40.9	34.1	13.3	3.26	
	17.0	50.7	40.7	14.0	3.24	

Table 6.5 Tests Results for Dry and Saturated Coarse SAND

Soil Type	T_∞ (°C)	T_1 (°C)	T_2 (°C)	h (W/m².°C)	k (W/m.°C)	k_{ave} (W/m.°C)
Coarse SAND (dry)	14.8	30.8	18.6	8.5	0.25	0.26
	14.3	40.6	21.0	8.5	0.27	
	14.3	50.5	22.3	9.0	0.24	
Coarse SAND (sat.)	17.0	30.9	27.3	14.0	4.00	3.72
	16.0	40.7	34.0	14.0	3.73	
	15.6	50.5	39.6	15.5	3.43	

Table 6.6 Tests Results for the Dry and Saturated Silty CLAY.

Soil Type	T_∞ (°C)	T_1 (°C)	T_2 (°C)	h (W/m².°C)	k (W/m.°C)	k_{ave} (W/m.°C)
Silty CLAY (dry)	16.5	30.7	20.2	8.0	0.28	0.25
	16.5	40.5	22.9	7.0	0.25	
	16.4	50.3	23.7	8.0	0.22	
Silty CLAY (sat)	18.5	30.9	25.2	12.5	1.47	1.52
	16.5	40.6	30.1	12.5	1.62	
	17.0	50.5	34.8	13.0	1.48	

After inspecting all the figures and tables, it is apparent that at the same constant base temperature, the top surface temperature of the specimen in the dry condition is less than the top surface temperature in the saturation condition (Figure 6.7). This indicates that the saturated soils can store more heat than that under dry soil conditions, due to the water having a higher heat capacity than that of air.

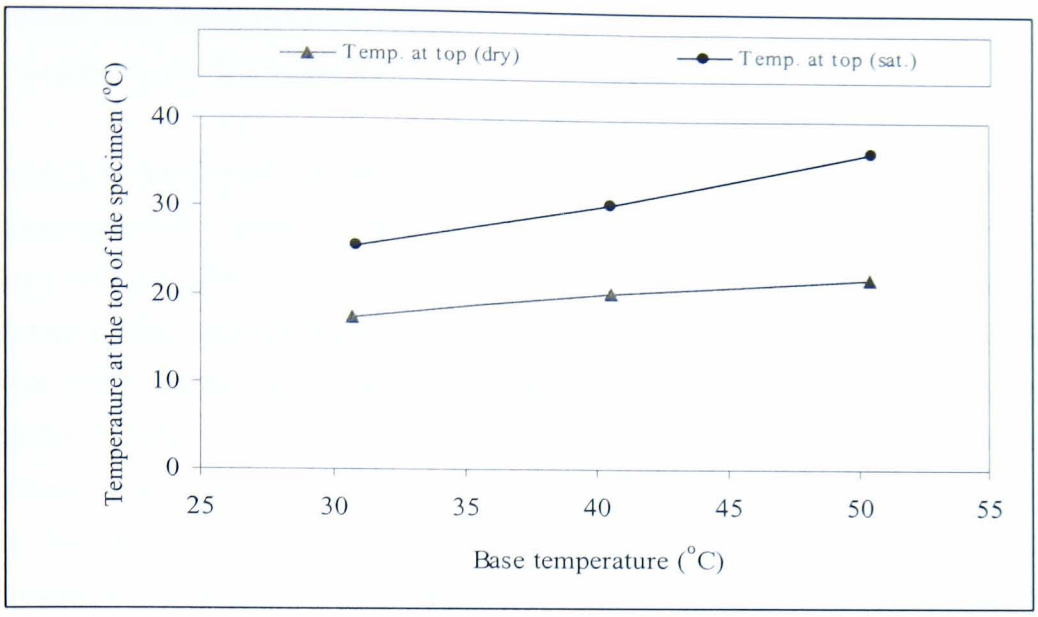

Figure 6.7 Top surface temperature for dry and saturated fine sand at different base temperatures.

It can also be seen from the tables of results that the convection heat transfer coefficient for different tests increases with decreasing room temperature. For example in Table 6.3, from the test of the saturated fine sand with a base temperature of 30°C, the convection heat transfer coefficient was 13.8W/m^2.°C at room temperature of 15.3°C. While in other tests at a base temperature of 40°C and 50°C with a room temperature of 12.1°C the coefficient was about 16W/m^2.°C. Hence it can be assumed that the convection heat transfer coefficient increases as the difference between the temperature of the convection surface and the surrounding temperature increases.

The convection heat transfer coefficients for dry soils were taken from the best fit curve using the cooling curve that represents the top surface of the specimen; this top surface temperature is then read from the thermocouple installed in the aluminium cap on the top of the specimen. It can be seen that at this point the temperature was lower than the other points. This was due to that the contact between the aluminium cap and the top surface of the specimen was limited to the point contact of the soil particles, also air filling the pores in which it acted as an insulator between the soil particles. In addition, the convection heat transfer coefficients for dry soils were less than those under saturated conditions. As a result this indicates the higher the convection heat transfer coefficients the higher the thermal conductivity of the specimen will be, and this means moist soils

conducts heat much faster than dry soils, which in effect results in the moist soils cooling down at a faster rate than dry soils.

Figure 6.8 shows a plot of the thermal conductivity results of the dry and saturated reconstituted soils versus their $D_{10\%}$ particle size. The thermal conductivities of the dry coarse soils ranged from 0.15W/m.°C for fine sand to 0.27 W/m.°C for medium sand. In the case of fine sand the thermal conductivity was less than that of medium and coarse sands, and it was due to the fact that the bigger the size of the particles, the smaller the number of particles present in a unit volume, which resulted in less thermal resistance between them during a heat transfer path. However, for saturated soils it was observed that the sandy soils had a higher thermal conductivity than clayey soils, and this increased dramatically with increase in size of particles and type (e.g. quartz or kaolin). The thermal conductivity for sandy soils ranged from 2.75W/m.°C for fine sand to 3.72W/m.°C for coarse sand. On the other hand for the fine soil (e.g. silty clay) the thermal conductivities under dry and saturated conditions were 0.25W/m.°C and 1.52W/m.°C respectively.

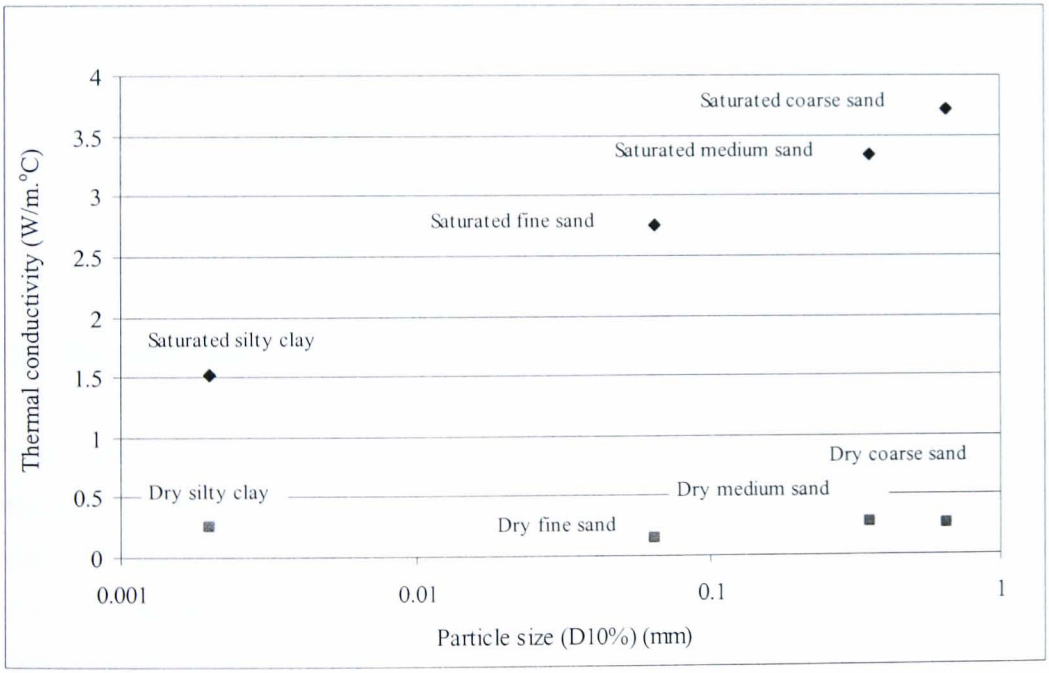

Figure 6.8 Thermal conductivity versus $D_{10\%}$ particle size of reconstituted soils.

The difference between the thermal conductivities of the soils was small in the dry condition, but higher in the saturation condition. The reason why dry soils have a lower thermal conductivity could be explained by the fact that for a dry specimen the pore

spaces between the solid particles are filled with air which has a high thermal resistance. Therefore, heat moves mainly from one particle to another through contact points between the particles. When water is present there is less thermal resistance. The water collects between the particles and acts like a bridge at these contact points making the thermal contact much larger than that of a single point (Figure 6.9). It can be concluded from this observation that the presence of water in the soil results in a better thermal conduction since water's thermal conductivity is twenty five times much greater than that of air. Therefore it can be concluded that the dominate factor in thermal conductivity is the degree of saturation.

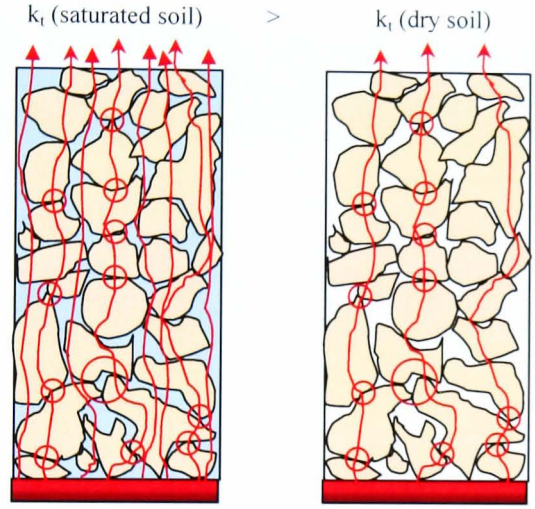

k_t (soil particle) > k_t (water) > k_t (air)

Figure 6.9 Dry and Saturated phase diagram

6.3 Thermal conductivity of Natural Soils and Grouts

Thirty eight thermal conductivity tests were conducted on fourteen samples that were obtained from Soil Mechanics Ltd. These samples comprised of six U100 samples and eight bulk samples which were taken at a site for proposed energy piles. Four samples of the U100 were grouts and these were obtained at various depths. The remaining two U100 samples, one of them was sandy silty clay and the other was sandy silt, these were obtained from a borehole at depths of 20.7m and 23.7m respectively. The eight bulk samples consisted of four silty sand, two medium-coarse sand and two sandy gravel. One specimen of each sample was prepared by the method described in previous chapter and placed in the thermal cell device. A small portion of each sample was taken in order to determine its actual water content by the oven drying method. Its physical properties

were determined; also a microscopic examination was used to determine the specimen's constituents (shape, type). Table 6.2 shows these properties that were used to analyse each test. The actual coarse and fine components of each specimen were then obtained, after determining its thermal conductivity, by the particle size distribution tests. Figure 6.1 shows the resulted particle size distribution curves of those specimens.

The resulting plots of temperature versus time profiles were similar in trend to those obtained from the reconstituted soils (Figure 6.2 and Figure 6.3. Summaries of the results are presented according to their soil type in Tables 6.7, 6.8, 6.9, 6.10 and 6.11.

Table 6.7 Tests Results for the fine soils.

Soil Type	Room temp. (°C)	T_1 (°C)	T_2 (°C)	h (W/m².°C)	k (W/m.°C)	k_{ave} (W/m.°C)
Sandy SILT BH 9T No.70	16.7	30.6	24.3	14.7	1.77	1.61
	17.0	40.5	29.4	13.5	1.52	
	17.0	50.4	34.6	13.8	1.55	
DRY	15.0	40.8	22.5	6.5	0.27	0.27
Sandy Silty CLAY BH 9T No.61	14.5	30.5	24.9	11.5	2.13	2.21
	14.6	40.4	30.7	13.3	2.22	
	15.0	50.3	36.8	14.0	2.27	
(w_c = 9%)	16.0	41.26	27.1	16	1.24	1.24

Table 6.7 shows the summary of the thermal conductivity results of two fine soil specimens (No.70 and No.61), these specimens were undisturbed and obtained from U100 samples, their particle size distribution curves and physical properties are shown in Figure 6.1 and Table 6.2 respectively. Specimen No.70 has lower thermal conductivity than specimen N°.61 due to various inter-related reasons. The first reason is that because its bulk density (1.89Mg/m^3) was lower than the bulk density for specimen N°.61 (2.1Mg/m^3), its porosity (43%) was higher than that for specimen No.61 (33%) this means more thermal resistance between the particles which decreases the effective thermal conductivity of the soil. The second reason was that specimen No.70 contained more fine soils (46.4%) than specimen No.61 (34.7%) and some rock fragments because the particle thermal conductivities of those materials (2.5W/m.°C) are less than that for quartz (8W/m.°C). Its coarse portion is very fine sand and for specimen N°.61 is medium sand. This increases the thermal resistance between the particles which consequently decreases the effective thermal conductivity of the soil. Figure 6.10 show that the fine particles also collect around the coarser particles in which they interfere with the

packing of the coarse particles, consequently the thermal resistance between the particles increases and the thermal conductivity decreases.

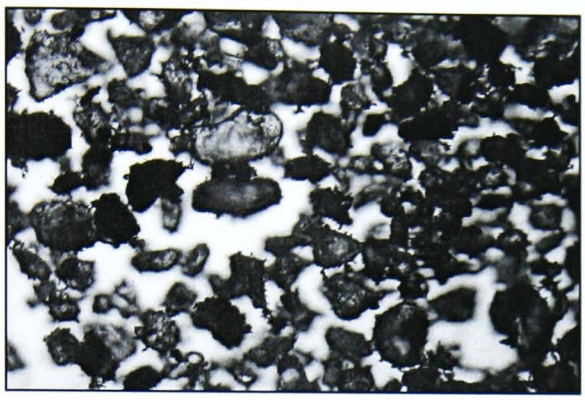

Figure 6.10 Fine particles surrounding coarse particles specimen No.70.

Both specimens No.70 and No. 61 were left to dry at room temperature and were retested again. The results showed that specimen No.70 was dry therefore its thermal conductivity was much lower than specimen No.61 which its water content was 9%. This was the same results for the dry reconstituted soils.

Table 6.8 shows the summary of the thermal conductivity results of the specimens' No.84, 88,106 and 108. These specimens were obtained from bulk samples, and their particle size distribution curves and physical properties are shown in Figure 6.1 and Table 6.2 respectively. The specimens engineering descriptions are silty sand. It is observed that the thermal conductivity for specimen numbers 84, 88 and 106 increased with increasing bulk density, and decreased with increasing porosity (Figure 6.11). However for specimen N°.108, despite its bulk density is higher than specimen N°.106, its thermal conductivity was lower than that of specimen N°.106. This indicates that the thermal conductivity varies with soil texture where this specimen has a higher percentage of fine soils (27%) than the other specimen (10%). Three of these specimens were left to dry in room temperature for a few months, the thermal conductivity tests were carried out again only under base temperature of 40°C, the results showed that specimens No.88 and No.84 had a higher thermal conductivity than specimen No.106. In this case, it can be due to that the two specimens had higher dry densities therefore the porosity and the voids were less between their coarse particles. This decreases the resistance between the solid particles, hence improves their effective thermal conductivities.

Table 6.8 Tests Results for the Silty SAND.

Soil Type	Room temp. (°C)	T_1 (°C)	T_2 (°C)	h (W/m².°C)	k (W/m.°C)	k_{ave} (W/m.°C)
Silty SAND BH C13 84	17.0	31.3	27.1	11.75	2.70	2.66
	17.4	41.3	33.8	12.5	2.64	
	17.6	51.3	40.5	13.0	2.64	
Silty SAND BH C13 88	17.0	31.4	27.5	11.8	2.92	2.73
	16.7	41.3	33.8	12.8	2.70	
	16.7	51.3	40.0	13.5	2.58	
Silty SAND BH C13 106	18.0	31.4	27.0	12.0	2.48	2.29
	17.7	41.3	32.6	13.0	2.28	
	17.5	51.2	38.2	13.0	2.10	
Silty SAND BH C13 108	16.4	31.0	25.8	12.25	2.07	2.08
	16.8	40.9	31.9	13.0	2.06	
	16.9	50.7	38.0	13.5	2.10	
Dry C13 84	15.5	40.76	27.68	8	0.71	0.71
Dry C13 88	14.5	40.72	26.38	9	0.69	0.69
Dry C13 106	14.7	41.35	23.83	7	0.37	0.37

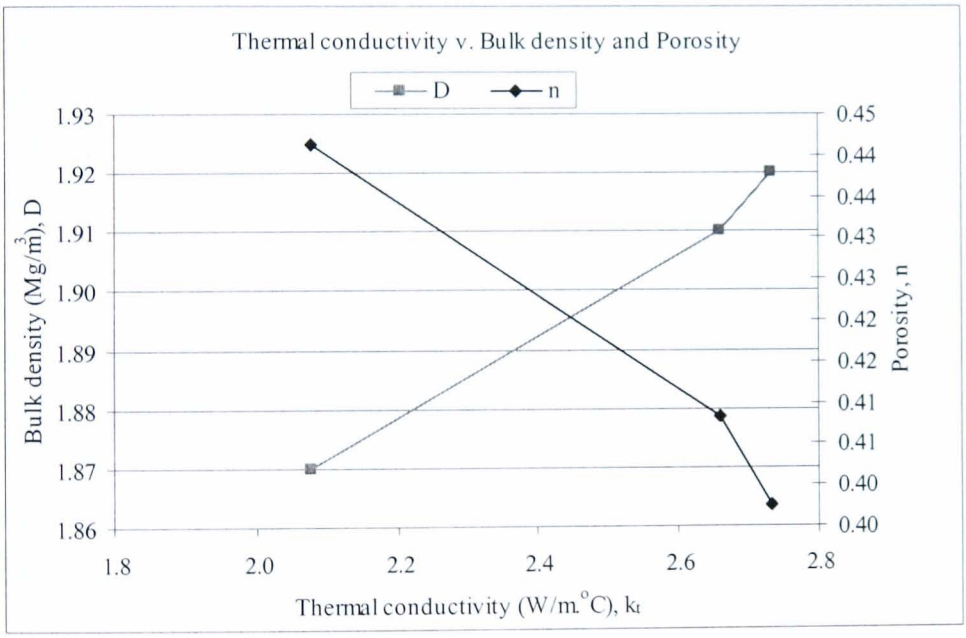

Figure 6.11 Thermal conductivity v. Bulk Density and Porosity

Table 6.9 presents the thermal conductivity results for two specimens (B10 and B15). These specimens consist of medium to coarse sand and their particle size distribution curve is shown in Figure 6.1. Their physical properties are listed in Table 6.2. The results show that for the same soil texture, despite specimen B10 having a higher bulk density (1.91Mg/m^3) than that of specimen B15 (1.84Mg/m^3), its thermal conductivity was lower than that for specimen B15, because its water content (4.8%) was lower than that of specimen B15 (12.3%). This highlighted the fact that for partially saturated soils,

their water contents affect the determination of their thermal conductivities, in which the thermal conductivity increased when the water content of the same soil increased. The specimens' saturation degrees were 28.27% for B10 and 52.57% for B15; this indicates that the thermal resistances between the particles were higher in the first specimen than the second one.

Table 6.9 Tests Results for the medium to coarse SAND.

Soil Type	Room temp. (°C)	T_1 (°C)	T_2 (°C)	h (W/m².°C)	k (W/m.°C)	k_{ave} (W/m.°C)
Medium to coarse SAND BH 11T B10	16.6	31.0	25.5	10.0	1.63	1.64
	16.7	40.8	31.1	11.3	1.65	
	16.5	50.7	36.7	11.5	1.65	
Medium to coarse SAND BH 11T B15	17.4	31.3	27.1	11.3	2.38	2.34
	17.2	41.3	33.6	12.0	2.34	
	17.1	51.2	40.0	12.5	2.32	

Also the thermal conductivity of the specimen's B15 was close to the values of the saturated specimens. Therefore it can be concluded that at a 50% degree of saturation or more the thermal conductivity of partially saturated specimen will be close to the saturated ones.

Table 6.10 presents the thermal conductivity results for two sandy medium to coarse gravel specimens (B12 and B14). The results showed that despite both specimens being at about the same water content (12%). The thermal conductivity of specimen B12 was less than that for B14, while their bulk densities were 1.75Mg/m^3 and 1.88Mg/m^3 respectively. This concluded that at the same water content, increasing the soil density increased its thermal conductivity (Figure 6.12).

Table 6.10 Tests Results for the Sandy medium to coarse GRAVEL.

Soil Type	Room temp. (°C)	T_1 (°C)	T_2 (°C)	h (W/m².°C)	k (W/m.°C)	k_{ave} (W/m.°C)
Sandy GRAVEL BH 11T B12	17.7	31.3	24.6	8.3	0.78	0.72
	17.7	41.3	28.5	8.5	0.67	
	17.8	51.3	32.6	9.5	0.70	
Sandy GRAVEL BH 11T B14	17.2	31.6	24.6	10.0	1.09	1.00
	17.0	40.9	28.5	10.3	0.97	
	17.2	50.7	32.6	10.8	0.93	

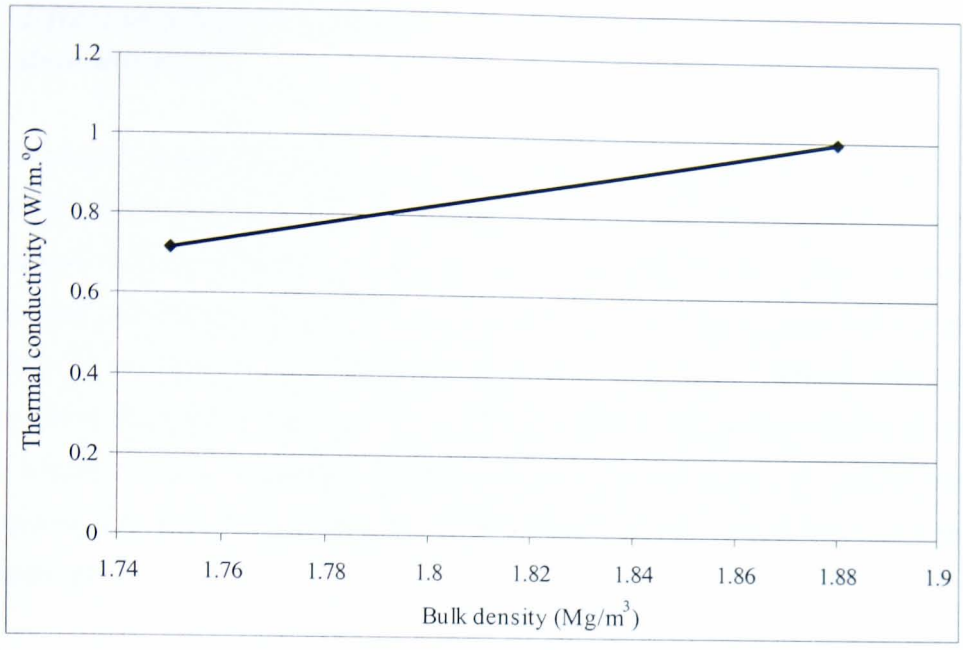

Figure 6.12 Thermal conductivity v. bulk density for sandy GRAVEL.

The last four U100 samples contained white grout of probably PFA and cement materials, their water contents were very high (166% to 199%) and this reflects the fact that this material could hold a high amount of water. The thermal conductivities of these results are presented in Table 6.11. The thermal conductivities of these materials at its in situ condition were close to the thermal conductivity of water (0.6 W/m.°C), because 80% of the specimen volume was water (Table 6.2). Water was the dominant medium for the heat conduction.

Table 6.11 Tests Results for the GROUT.

Soil Type	Room temp. (°C)	T_1 (°C)	T_2 (°C)	h (W/m².°C)	k (W/m.°C)	k_{ave} (W/m.°C)
BH11T GROUT1-1	14.7	30.7	21.7	8.5	0.65	0.63
	14.6	40.5	24.2	10.0	0.58	
	13.9	50.3	26.5	12.8	0.67	
GROUT1-2	18.3	50.8	29.0	12.5	0.61	0.61
BH24 GROUT2-1	14.8	30.6	20.8	11.0	0.67	0.71
	14.7	40.4	23.5	13.3	0.69	
	14.6	50.3	27.4	13.3	0.76	
GROUT2-2	18.7	51.3	31.0	12.3	0.77	0.77

6.4 *Effect of physical properties on the thermal conductivity determination*

Relationships between the thermal conductivities and some physical properties of the various soils used in this research are plotted in Figures 6.13, 6.15, 6.16, 6.17, and 6.18. It is shown that the thermal conductivity for reconstituted soils varies with the bulk density and simultaneously with porosity (Figure 6.13). It can be seen that the thermal conductivity increases with increasing bulk density, since at the same time the porosity of the soil is decreasing (Figure 6.13), resulting in an increase in the number of solid to solid contacts which increases the heat transfer paths between the grains, and this establishes that the porosity and the bulk density directly affect the soil's thermal conductivity.

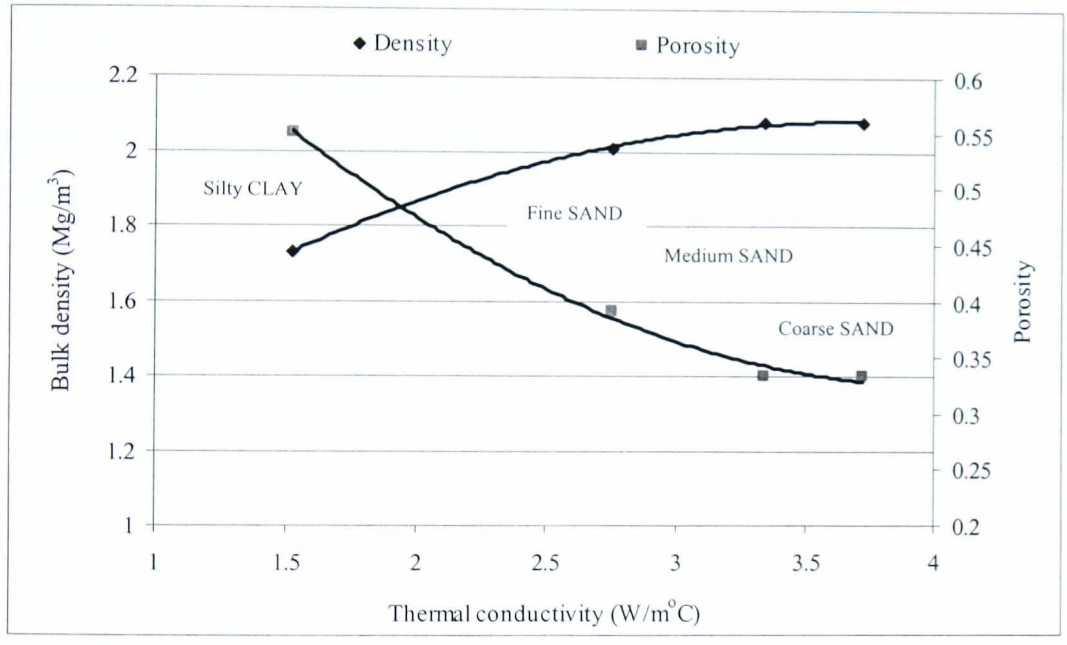

Figure 6.13 Thermal conductivity v. Bulk density and Porosity for saturated reconstituted soils.

The presence of the fine particles in uniform graded soils as the case in the silty sand specimens (No. 84, 88, 106 and 108) could affect the packing of particles in two ways; the fine particles would tend to fill the pores between the coarse particles, thus providing more solid matter per unit volume causing an increase in the thermal conductivity (Figure 6.14a), however some of these fines might interfere in the packing of the coarse particles by pushing them apart creating a reduction in the volume occupied by the coarse particles (Figure 6.14b), whereas the volume occupied by the finer particles

increases only a small percentage. This will result in an increase in the porosity of the soil, hence decrease in the thermal conductivity.

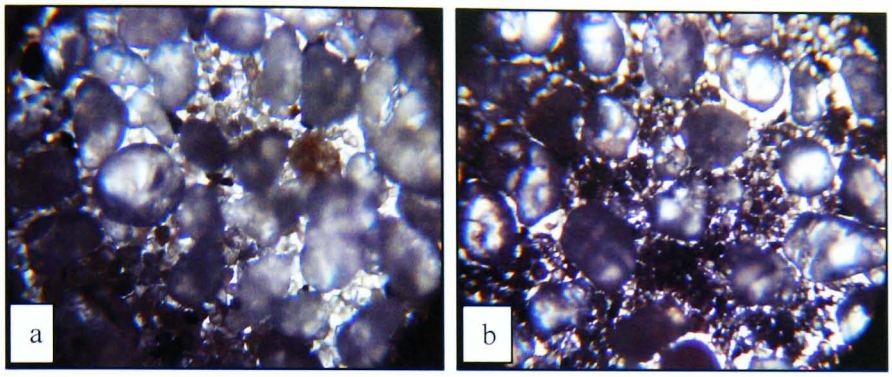

Figure 6.14 Mixture of medium particles with fine particles of soils.

Figure 6.15 shows the thermal conductivity of all specimens increases with increasing water content, and if water content is very high then a decrease in thermal conductivity is expected, because water will then become the dominant medium for transferring heat therefore the effective thermal conductivity will tend to reduce to a value close or equal to the thermal conductivity of water which is about 0.6 W/m.°C.

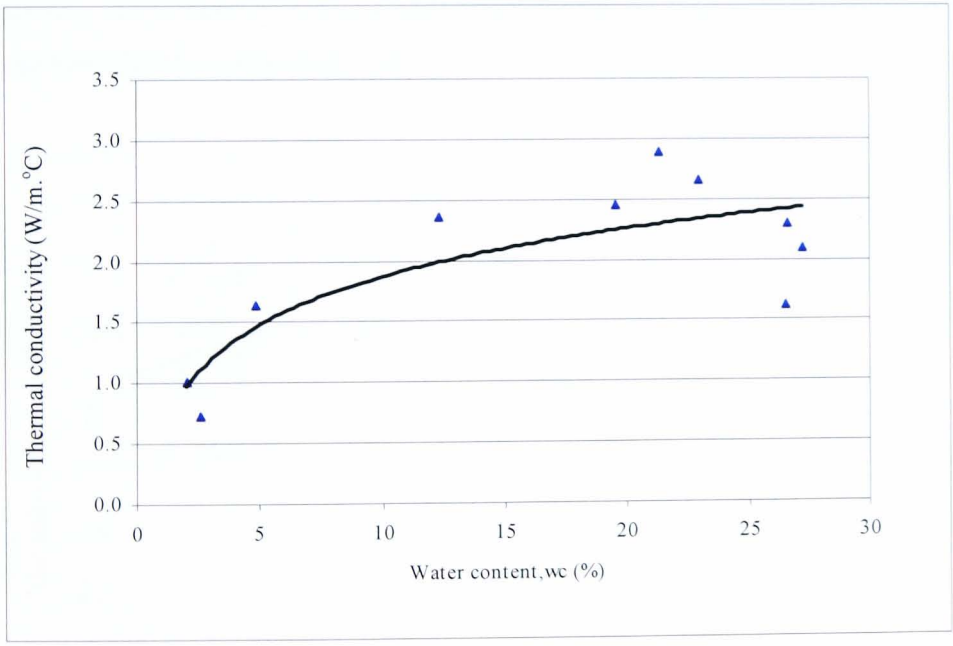

Figure 6.15 Thermal conductivity v. water content for natural soils.

Plotting the thermal conductivity of natural sandy soils versus their water content separately of other soils, a similar profile to that in Figure 6.15 is obtained (Figure 6.16). This concludes that apart from the particle size and mineralogy, water amount plays the major part in determining soil's thermal conductivity.

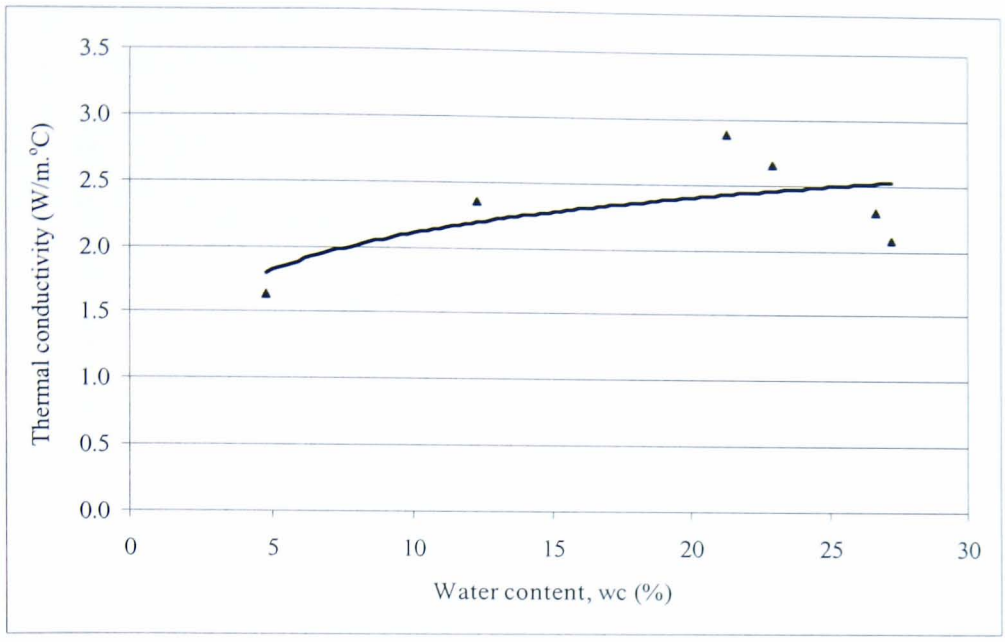

Figure 6.16 Thermal conductivity v. Water content for natural sands.

When the water content decreases the air content increases simultaneously. A plot of the thermal conductivity of natural soils versus air content (Figure 6.17) shows that as the air content increases the thermal conductivity decreases. In Figure 6.18, the thermal conductivity of the natural soils increases with increasing degree of saturation while at the same time the air content decreases.

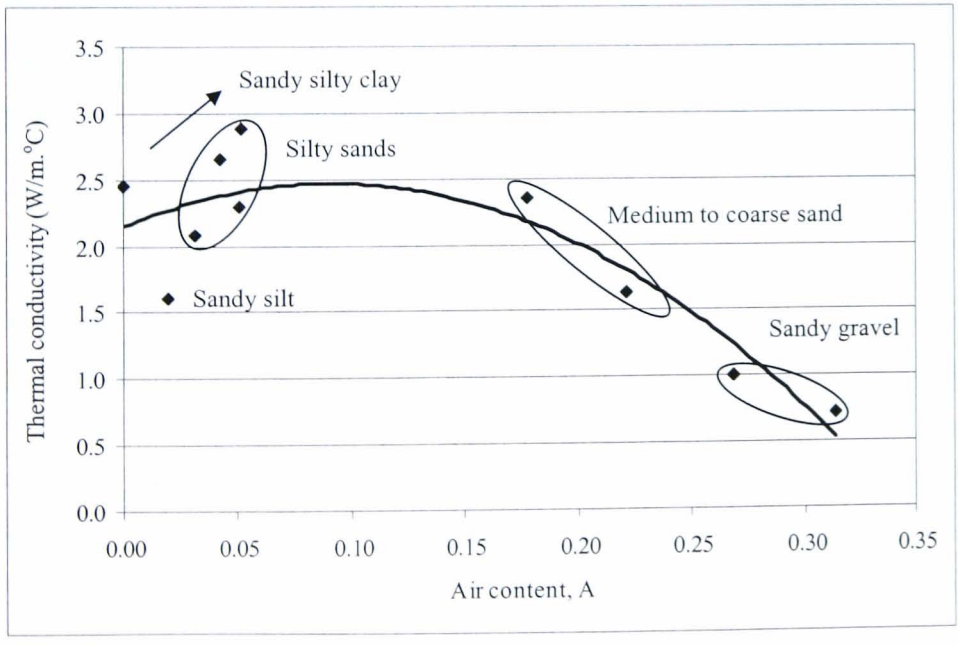

Figure 6.17 Thermal conductivity v. Air content for Natural soils.

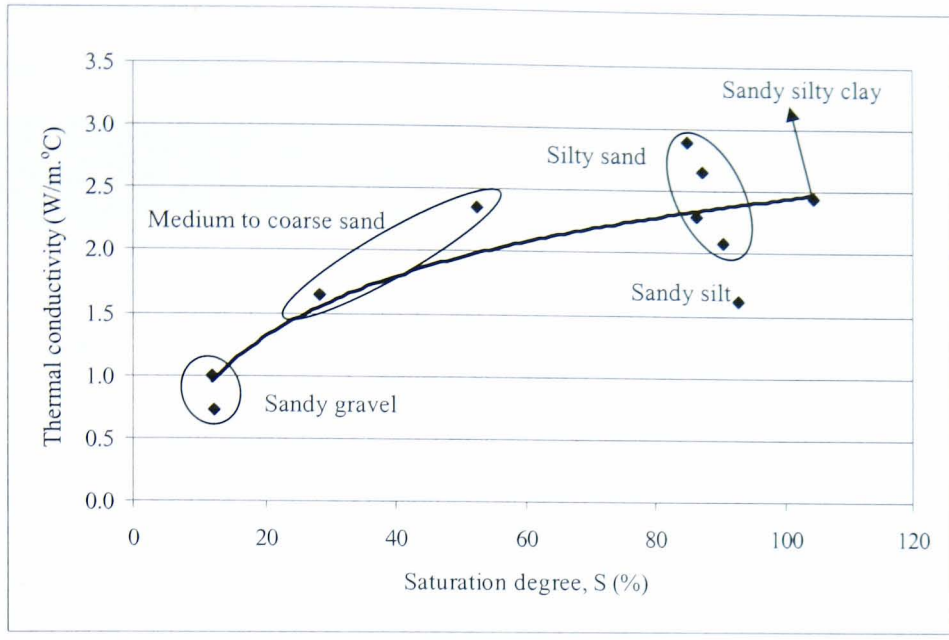

Figure 6.18 Thermal conductivity v. Saturation degree for Natural soils.

Based on the previous discussion, it is evident that the thermal conductivity of a soil is a function of its various inter-related physical properties, in which the water content plays the major role for heat transfer in the soil.

6.5 Comparison to data from the literature

To evaluate the results obtained from the present set of experiments, the thermal conductivities of the soils were compared with experimental data (Table 6.12) obtained by Penner et al. (1975), Cary (1978), Incropera and DeWitt (1996), Abu-Hamdeh (2000), Abu-Hamdeh et al. (2001), Nusir et al. (2003) and Hukseflux consulting company web site (2004).

In comparing these results it is evident that the range of the effective thermal conductivities obtained by the new thermal conductivity device in the present research is within the range of the reported values. In addition, all the effective thermal conductivities are comparable with those found in the literature. In particular, the effective thermal conductivities of the reconstituted dry and saturated sands agree well with the findings of Hukseflux consulting company. The thermal conductivities of dry and moist clays are in agreement with the data found in the literature.

Table 6.12 Some reported values of thermal conductivity in soils.

Soil Type	Thermal conductivity (W/m.°C)	Measurement method	Reference
Sand perfectly dry	0.15 - 0.25	The TNS01 Thermal needle Set	Hukseflux (2005)
Sand moist	0.25 - 2		
Sand saturated	2 - 4		
Clay dry to moist	0.15 - 1.8		
Clay saturated	0.6 - 2.5		
Soil with organic matter	0.15 - 2		
Saturated soil	0.6 - 4		
Range of all reported values for soil	0.15 - 4		
Sand	0.95 - 2.11	Single and dual probe methods	Nusir et al. (2003)
Loam	0.49 - 0.76		
Sandy Silt	0.7 - 2.9	Transient heat-flow method using a line heat source.	Penner et al. (1975)
Sandy silty Clay	1.3 - 2.75		
Silty Clay	0.5 - 2.0		
Silt Loam	2.26 - 3.25	Transient thermal conductivity probe	Cary (1978)
Loam Sand	2.32 - 3.81		
Silty Clay	1.9 - 2.89		
Clay Loam	0.33 - 0.72	Transient thermal conductivity probe	Abu-Hamdeh (2000)
Loam	0.4 - 0.75		
Sand	0.58 - 1.94	The hot wire method	Abu-Hamdeh et al. (2001)
Sandy Loam	0.19 - 1.12		
Clay Loam	0.36 - 0.69		
Clay	1.3	Not mentioned in the textbook	Incropera and DeWitt (1996)
Sand (dry)	0.27-0.33		
Clay (dry)	0.4	Not mentioned on their website	Enercret (2004)
Clay (moist-wet)	1.6		
Sand (moist)	1.0		
Sand (moist-saturated)	1.8-2.4		
Fine sand, water flow 1.16E-6 m/sec	4.0		
Medium sand, water flow 1.16E-5 m/sec	15.0		

As can be seen the tabulated values for soils give a (sometimes very wide) range of thermal conductivity values for each soil type, therefore it is possible to greatly under or overestimate the thermal properties of the soil, leading to a greatly over designed (and therefore uneconomic solution) system that would be unable to transfer enough energy to/from the ground to meet the heat exchange requirements of a building. Moreover, the flow of water can significantly increase the thermal conductivity of fine sand or coarser, as can be seen from the data obtained from the Enercret Company (2004). This variation in the thermal conductivity of a soil is caused by the change of the inter relation between the physical properties of the soils.

6.6 Comparison to results of thermal conduction models

The heat conduction models that have been presented in Chapter 2 were used to predict values of thermal conductivities for the soils used in this research. These models are the parallel and series models, geometric mean model, Maxwell's model, Kersten's model, Johanson's model, De Vries's model, Woodside & Messmer's model, Krupiczka's model, Numerical simulation model and Zehner & Schlunder's model. The parallel and series models predict the maximum and the minimum thermal conductivities of the soil respectively.

Estimates of the thermal conductivities of soils using these models were made based on the assumptions of the percentages of constituent minerals (with known conductivity) (Table 6.13). Consequently these methods may lead to misleading results if these assumptions were made based only on the particle size distribution and the exact mineralogical composition of the soil was not found. However, if the exact mineralogical composition is found this is an effective way of estimating soil's thermal conductivity.

Table 6.13 Used thermal conductivities of soil constituents

Material	Thermal conductivity (W/m.°C)
Air	0.0257
Water	0.6
Clays	2.0
Quartz	8.0
70% Quartz	6.0
Less than 60% Quartz	4.0

Mineralogical examination for the entire soils used in this research was made on the quantitative basis under a microscope (Figure 6.19, Figure 6.20 and Figure 6.21). Figure 6.19a, b and c shows that the reconstituted sandy soils consist of 100% quartz; however, the artificial silty clay particles (d) were kaolinite.

The thermal conductivities of the solid particles were based on the microscopic examination. It was taken as 8.0W/m.°C for fine, medium and coarse sands and for soils that contained a small percentage of fines (reconstituted sandy soils, silty sand specimens) because their particle consists of about 100% quartz. It was taken as 6.0W/m.°C for the sandy silty clay specimen No.61 and 4.0W/m.°C for the sandy silt specimen No.70 because it contains some rock fractions. For reconstituted silty clay it was taken as 2.0W/m.°C (Table 6.13). All calculated values are shown in Appendix D.

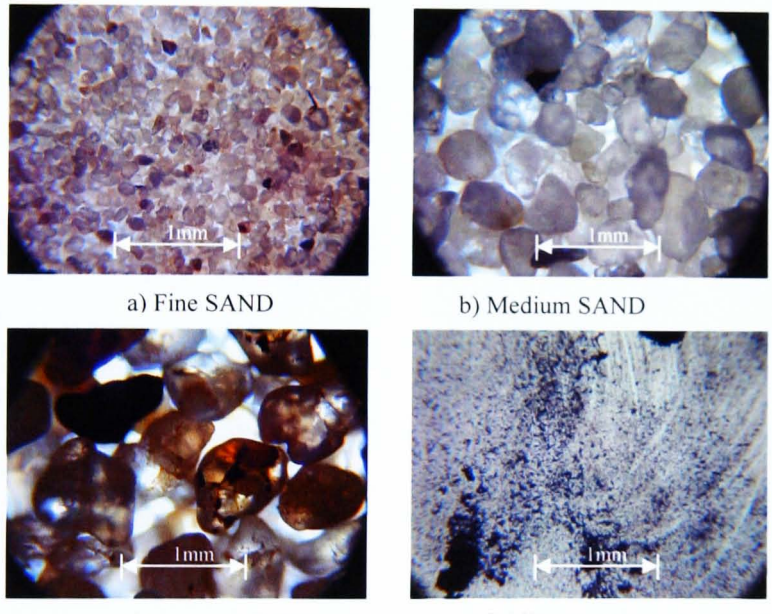

a) Fine SAND b) Medium SAND

c) Coarse SAND d) Silty CLAY

Figure 6.19 Particles of the reconstituted soils under the microscope.

A comparison of the measured thermal conductivities versus the predicted thermal conductivities by the previous models for the dry reconstituted soils, saturated reconstituted soils and natural soils is shown in Figure 6.23 and Figure 6.24 respectively. It is shown that all the results were located within the range of the parallel (maximum) and series (minimum) models. Most of the models are in a very good agreement with the experimental results. However for natural soils at a very low degree of saturation this was not the case. It is due to the fact that most of these models (parallel and series models, geometric mean, Maxwell, Woodside & Messmer, Krupiczka, Numerical

simulation, Krupiczka and Zehner & Schlunder's models) consider the materials as a two-phase material which is not the case in partially saturated soils. Where the soil consists of three phases (solids, water and air) (Figure 6.22), for example, as the case in sandy gravel specimens (saturation degree about 12%) (B12 and B14), these models take into account only the effect of the porosity of a material formed of elements of solids located in continuous immobile fluid that is either air or liquid. Their predicted thermal conductivities were higher comparing with the measured values.

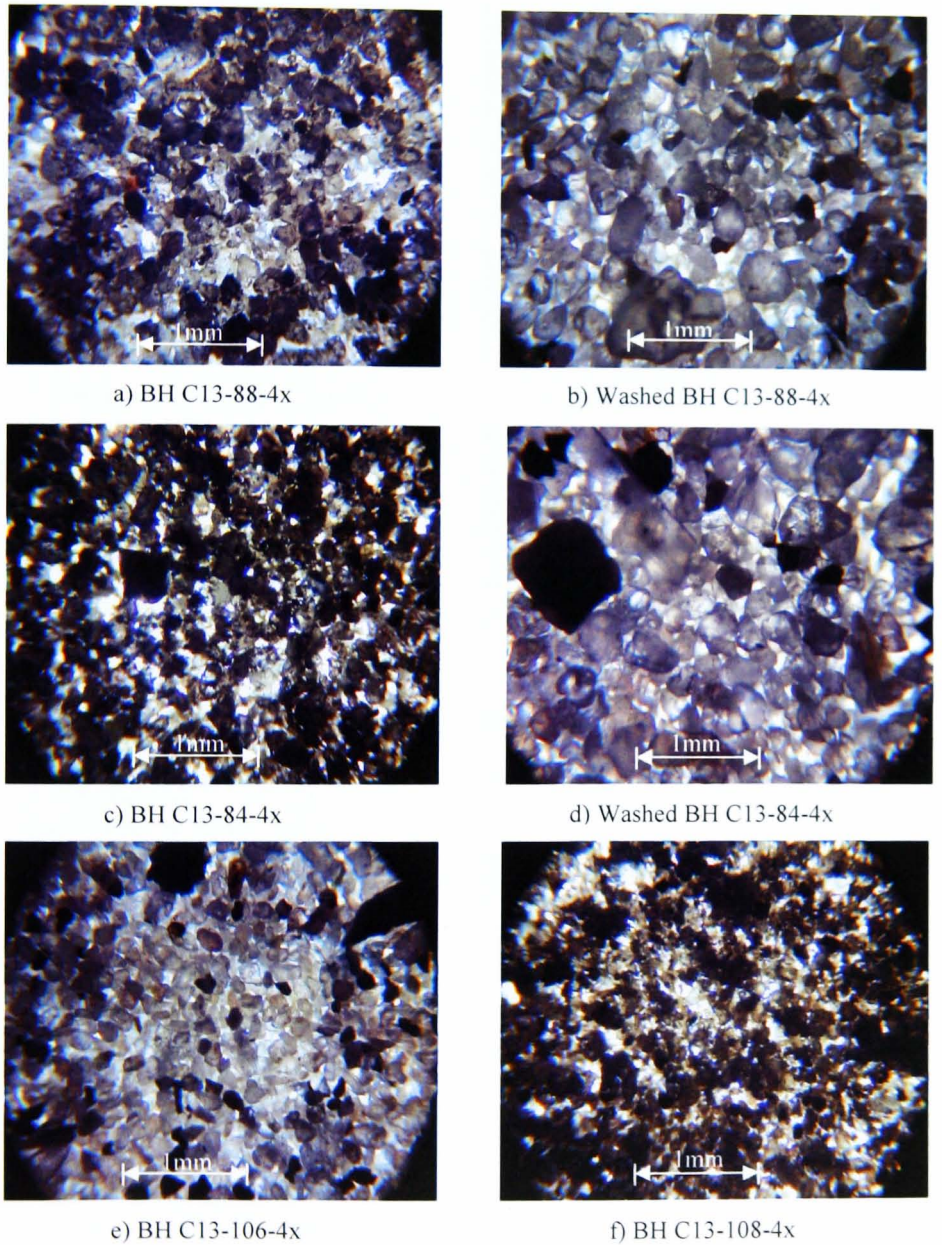

a) BH C13-88-4x

b) Washed BH C13-88-4x

c) BH C13-84-4x

d) Washed BH C13-84-4x

e) BH C13-106-4x

f) BH C13-108-4x

Figure 6.20 Particle of the natural sandy silt specimens under the microscope.

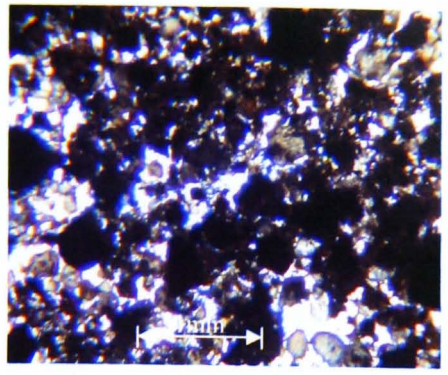

a) Sandy silty CLAY (61)

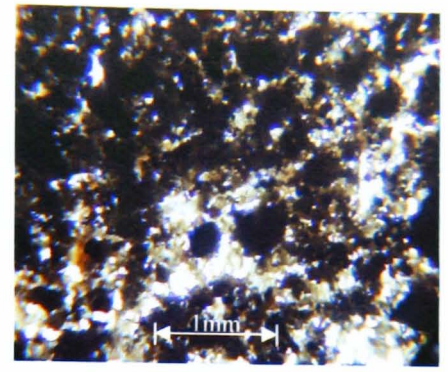

b) Sandy SILT (70)

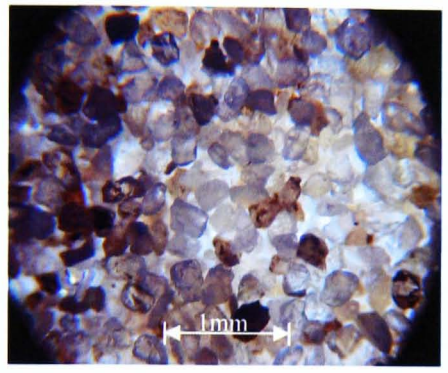

c) Washed sandy silty CLAY (61)

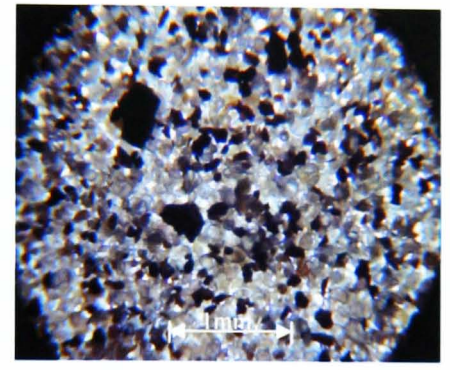

d) Washed sandy SILT (70)

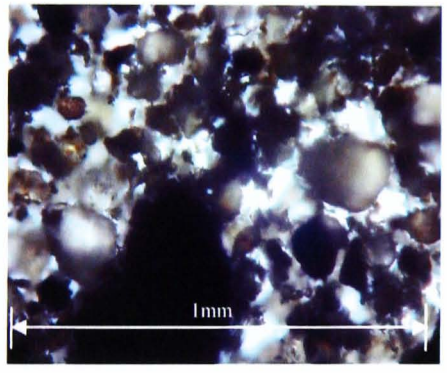

e) Sandy silty CLAY-20x

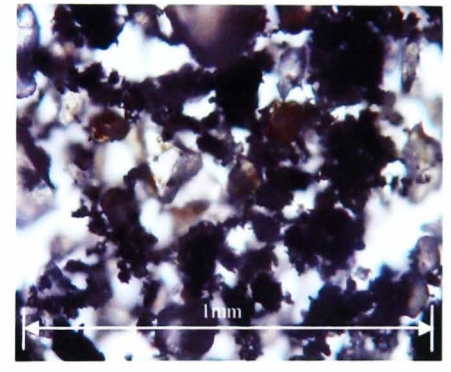

f) Sandy SILT-20x

g) Portion of Sandy silty CLAY

h) Portion of Sandy SILT

Figure 6.21 Particle of the natural sandy silty CLAY and sandy SILT specimens under the microscope.

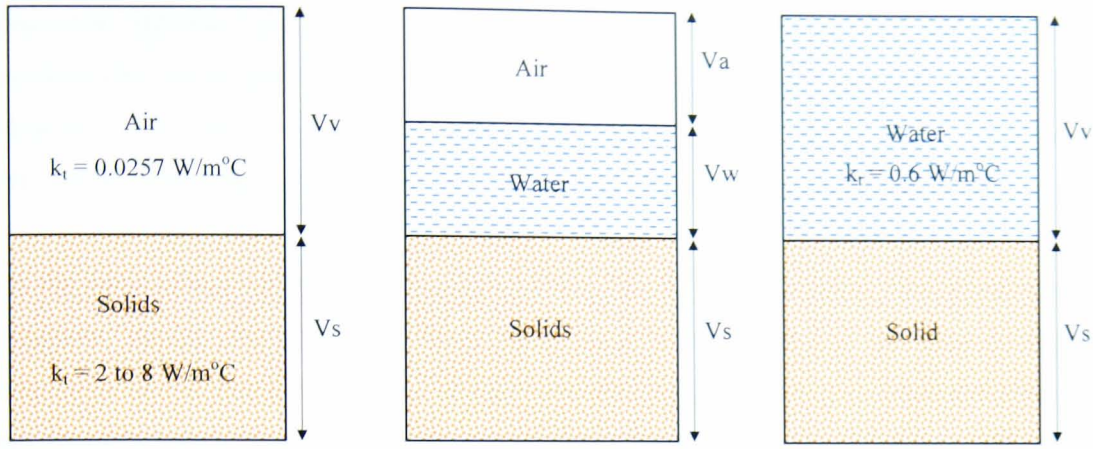

Figure 6.22 Phase diagrams of soil.

However, the models which take into account the water content, degree of saturation and three phase materials such as Kersten (equation 6.1 and 6.2), Johansen (equation 6.3) and De Vries models (equations 6.4) produced the best agreement between the predicted thermal conductivities and the measured ones. It can also be seen (Figure 6.24) that their values agreed well with those measured.

The thermal conductivity based on the Kersten empirical equations for unfrozen silt-clay soils containing 50% or more silt and clay (equation 6.1), while for unfrozen sandy soils (equation 6.2), the equations using metric units as following:

$$k_t = 0.1442 \cdot (0.9 \log w_c - 0.2) \cdot 10^{0.6243\gamma_d} \qquad \text{For } w \geq 7\% \qquad 6.1$$

$$k_t = 0.1442 \cdot (0.7 \log w_c - 0.4) \cdot 10^{0.6243\gamma_d} \qquad \text{For } w \geq 1\% \qquad 6.2$$

$$k_t = (k_{t\,sat} - k_{t\,dry}) \cdot K_e + k_{t\,dry} \qquad 6.3$$

$$k_t = \frac{x_w \cdot k_w + F_a x_a \cdot k_a + F_s \cdot x_s \cdot k_s}{x_w + F_a \cdot x_a + F_s \cdot x_s} \qquad 6.4$$

Figure 6.24 shows that in spite of the degree of saturation for the medium to coarse sand specimen (B15) was only 52.6%, the predicted and measured thermal conductivities were in a good agreement, they were also close to the thermal conductivities of saturated soils. This indicated that at a certain degree of saturation the soil could be treated as a two-phase material.

For the dry reconstituted soils, a part of the parallel, numerical simulation and the geometric models which predicted very high thermal conductivities, the thermal conductivity values predicted by the other models were reasonably good (Figure 6.23). Most of the conduction models produced a good agreement with the measured values for the saturated reconstituted soils except (as expected) the parallel and the series models.

On the basis of the experimental results of this research the best model was found to be Johansen' model, Because it predicted the thermal conductivities of all types of soils very close to the measured ones in both dry and saturated conditions. A relation between the thermal conductivity of a soil and the degree of saturation (Figure 6.25) was produced by Johansen's model using the thermal conductivities of dry and saturated reconstituted soils. The experimental thermal results for the natural soils were then superimposed on the figure. It can be seen (Figure 6.25) that the natural soils results were between the fine sand and silty clay lines. This is because most of the soils as seen in Figure 6.1 range between those two categories. Otherwise their solid constitutes were mix of quartz having high thermal conductivity (8 $W/m^{o}C$) and rock fragments having lower thermal conductivity (2.5 $W/m^{o}C$) such as the natural medium to coarse sand and sandy gravel specimens.

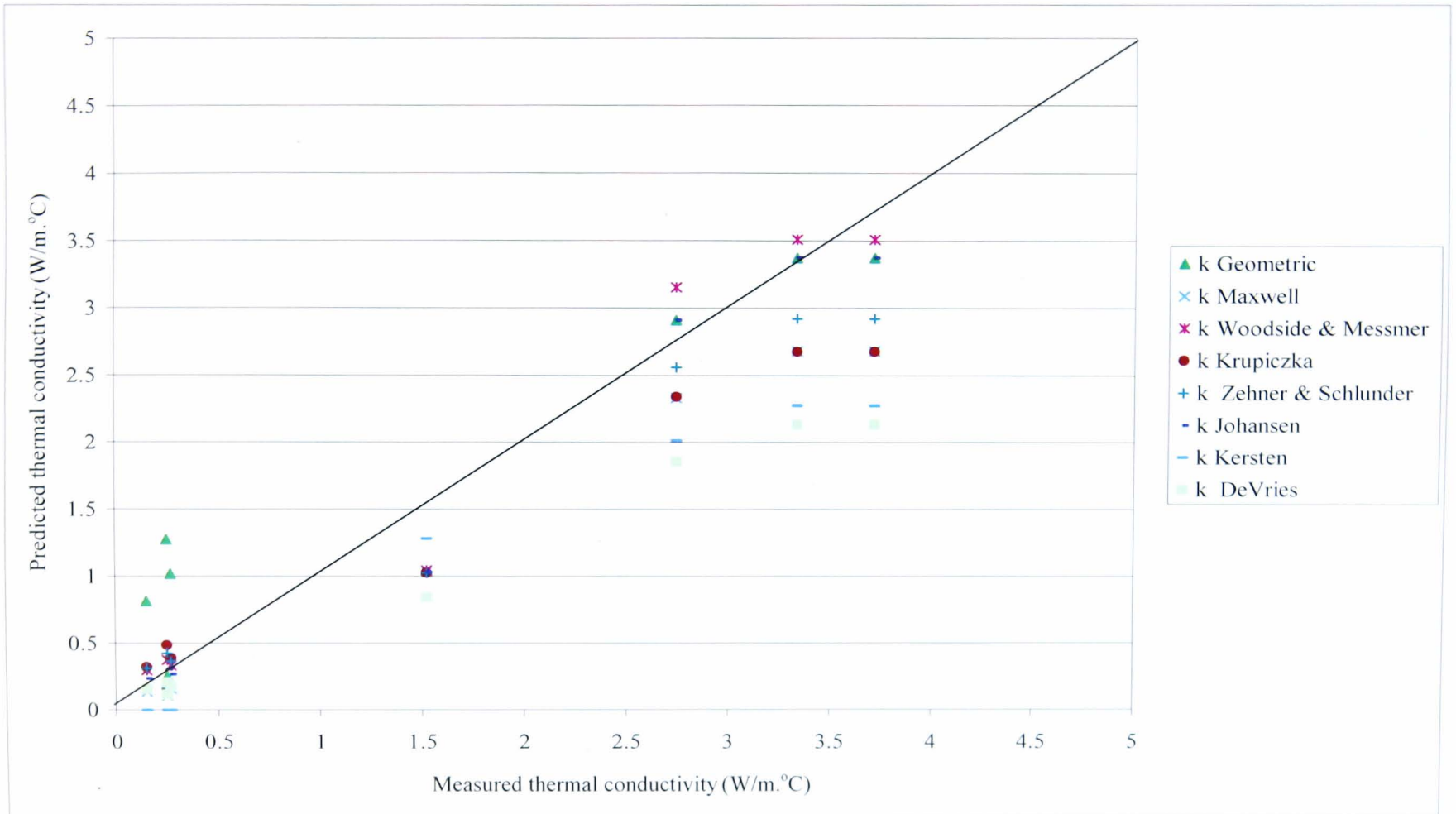

Figure 6.23 Measured and Predicted thermal conductivity of reconstituted soils.

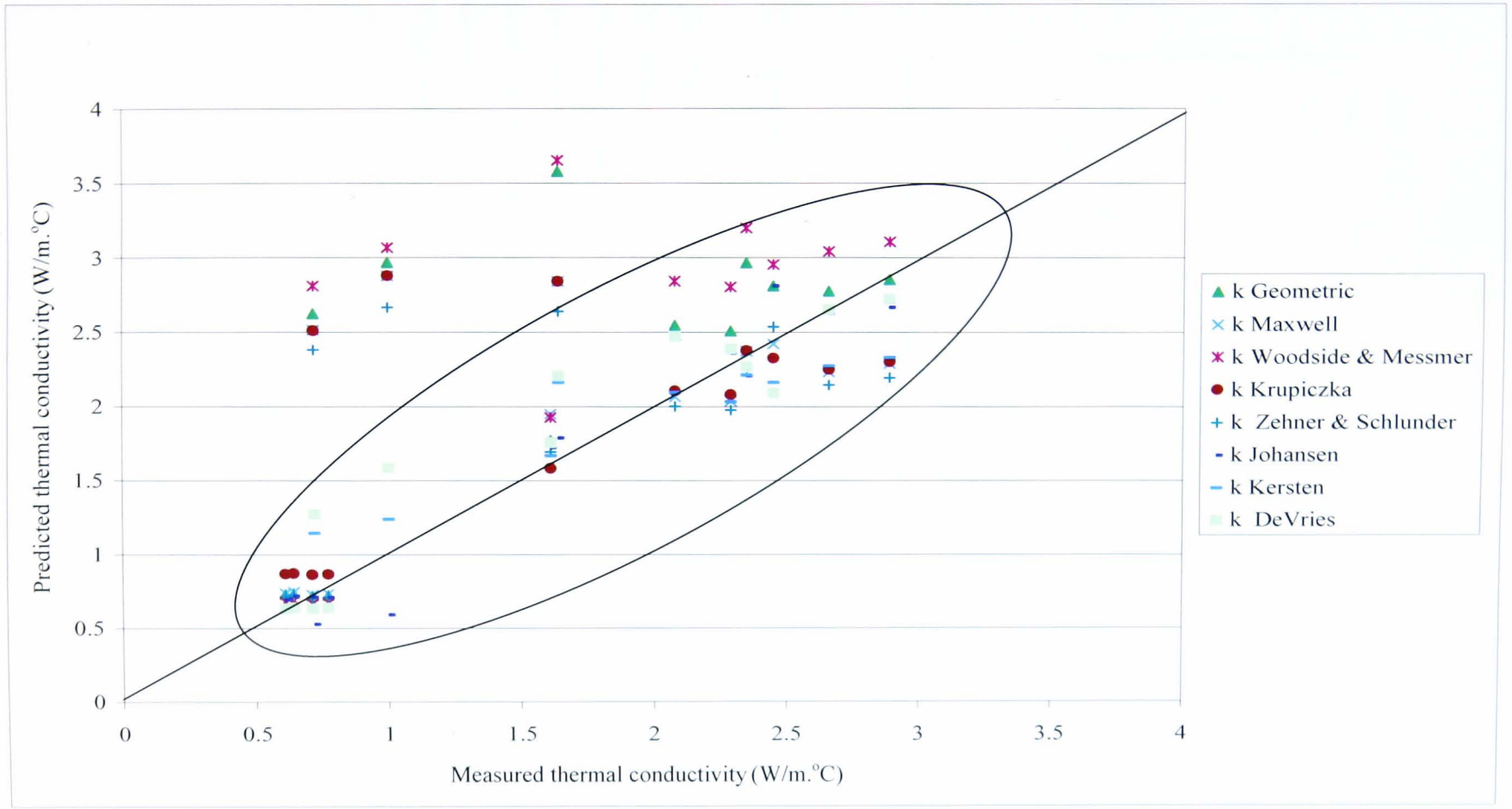

Figure 6.24 Measured and Predicted thermal conductivity of natural soils.

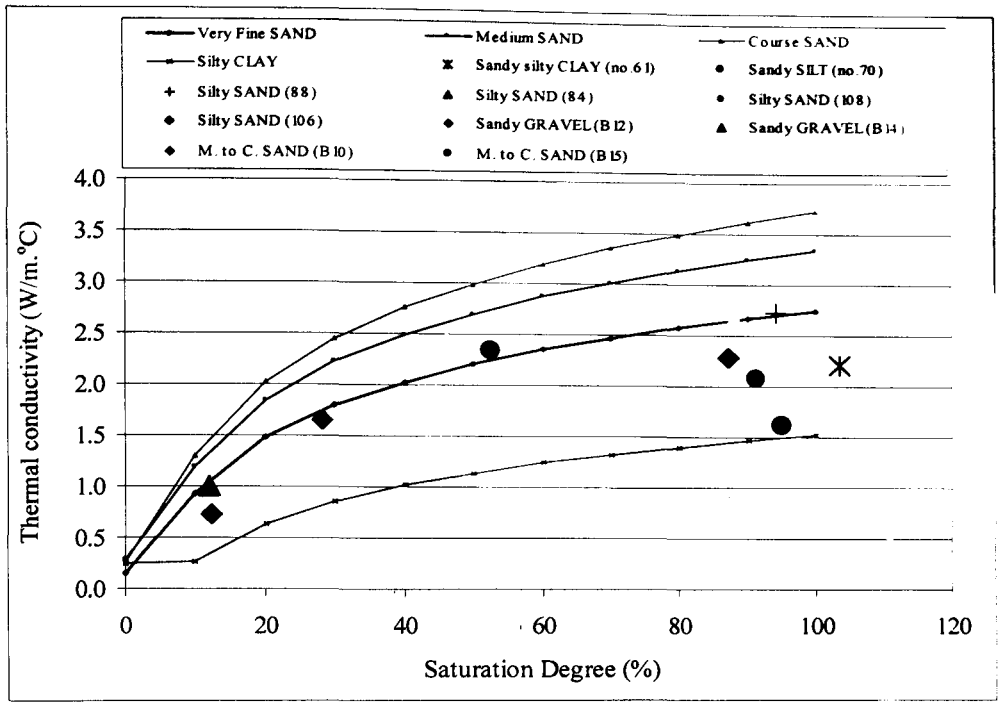

Figure 6.25 Thermal conductivity v. Degree of saturation by Johansen's model.

6.7 Summary

The results of the new thermal conductivity cell device are discussed and presented in this chapter. The main discussion revolves around the effect the different physical properties of the soil have on its thermal conductivity. These properties include the specimen's density or porosity, water content, air content and degree of saturation. The results are then compared with published data and those of the thermal conduction models in which it can be concluded the new method of determining the thermal conductivity of soils proved to be effective.

Chapter 7
Conclusions and Recommendations

7.1 Introduction

The research has investigated the effect of the physical properties of soils on the determination of hydraulic and thermal conductivities of soils and the use of different methods to determine hydraulic conductivity; and the flexible wall permeameter using constant flow technique was the most advanced test employed at the University of Newcastle upon Tyne. As part of the study, this system was also developed in order to operate as a falling head system. Also a new device and testing method of determining the thermal conductivity of soils has been developed.

It can be concluded that the soil's hydraulic and thermal conductivities are strongly dependent on the complexity in the variation of soil's physical properties, for example increasing density, decreases porosity, hence decreasing the hydraulic conductivity but increasing the thermal conductivity.

7.2 Conclusions on Hydraulic conductivity

Prior to this research the flexible wall permeameter could only be used to determine the hydraulic conductivity of clayey soils, and this was only applicable with the constant flow technique. However, in this study, modifications were carried out to the flexible wall permeameter equipment so that the falling head and the constant head techniques could both be used in determining the hydraulic conductivity of fine soils, including fine sand, using the same equipment.

One of the purposes of this investigation was to evaluate and then compare the results of the new modification carried out to the flexible wall permeameter for the various applied techniques as mentioned earlier. The results found using this equipment proved to be accurate and also represented a more rapid means to determine the hydraulic conductivity of fine soils in a matter of 30 to 60 minutes. Also the volume change during the testing of fine soils was complete within the first 20 minutes of the test period which

allows the termination of the test within one hour or even less. Using the constant flow technique the specimen's volume change continues until a steady state condition is reached after two hours, which makes the test duration longer than with the falling head test.

The termination of the constant flow test was unpredictable, and in most tests it took more than two hours to reach the steady state condition.

The most significant component in the flexible wall permeameter is the Newcastle volume change gauge. This device was designed by earlier researcher to achieve better performance than more commercial devices. It has proved to be accurate and rapid, producing a high resolution, and it can also easily distinguish between the various specific test stages (i.e. saturation, consolidation and permeation). The advantage of the modified equipment using the falling head technique is that the desired hydraulic gradient can be chosen and controlled by the air pressures in the inflow and outflow Newcastle volume gauges. In contrast using the constant flow pump technique the induced hydraulic gradient could not be precisely predicted.

The hydraulic conductivity calculated at the bottom of the specimen based on the inflow rate was higher than that at the top based on the outflow rate. This was due to the increase in the volume of the specimen at its bottom, which consequently increased the inflow rate.

A low hydraulic gradient should be used, such as 15 or lower, when determining the hydraulic conductivity of fine soils.

However, the pressure regulators used in this apparatus significantly affected the results for hydraulic conductivity when it came to the measurement of the hydraulic gradient at very low flow rates; this was due to that these regulators were not sensitive enough to maintain a constant pressure difference across the whole specimen, consequently resulting in changes in the specimen's volume. Therefore the pressure regulators should be checked and maintained regularly to achieve better performance and accuracy.

The phenomenon of seepage induced consolidation can not be eliminated in fine soils; however it can be detected and quantified by using the flexible wall permeameter with

an accurate volume change device such as the Newcastle volume change gauge. This phenomenon was most noticeable in the first test after the end of the consolidation stage when a low inflow rate was used.

There was a small increase in the pore water pressure at the top of the specimen for both constant flow and falling head techniques, due to increases in the water levels in the outflow volume change gauges. However this was negligible, because it caused only small volume changes compared to the large increase at the bottom of the specimen.

The physical properties of supreme and silty clays in terms of their effect on hydraulic conductivity were compared. A small change by the same amount in the void ratio can affect the hydraulic conductivity of the respected soils differently, where the void ratio has affected the silty clay (40% clay) hydraulic conductivity more than that of the supreme clay (90% clay).

As regards to the bulk density of the two clayey soils, the silty clay has a higher decrease in the values of hydraulic conductivity when its bulk density increases compared to that of the supreme clay.

The assumption that the falling head test can be interpreted as a constant head test is only valid for fine soils which have very low hydraulic conductivity, where as in coarse soils the pressure difference drops more rapidly than fine soils making the assumption of constant pressure not valid in such soils.

Hydraulic conductivity decreases as void ratio decreases for the same type of soil. However different types of soil having the same void ratio could have higher or lower hydraulic conductivity depending on other factors that could play a major rule in determining it.

The particle sizes of clayey soils have an effect on their hydraulic conductivities. The hydraulic conductivity of silty clay soils increases rapidly with a slight increase in the void ratio. In contrast, for supreme clay soils the hydraulic conductivity increases only slightly with larger increases in void ratio. This indicates that hydraulic conductivity is not only a function of void ratio but also of particle size and shape.

7.3 *Conclusions on Thermal conductivity*

Part of this study was to design the necessary equipment for determining the thermal conductivity of the various soils under consideration. Procedures were then developed in order to be able to use this equipment and also to interpret the results obtained from this device.

The equipment used to determine the thermal conductivity of the different types of soils carried out in this study proved to be simple and accurate when comparing the results with those carried out using other methods-in particular laboratory tests and conduction models. The results of this thesis proved that the thermal conductivity cell device was effective, straightforward and simple test method in determining the thermal conductivity of soils.

When comparing the physical properties of the laboratory soils and the natural soils in terms of the effect these have on the thermal conductivity, it was found that dry soils are generally have much lower thermal conductivities compared to saturated soils, and this has been proven to be the case in many previous researches.

Soil composition affects its thermal conductivity. As regards to the clayey soils, it was found that they have lower thermal conductivities under saturation than sandy soils in the same state. This was due to soil composition, because the particles of the clayey soil are consists of kaolinite which has much lower thermal conductivity than the quartz that the sandy soil consists of. However the artificial clay (kaolin) had lower thermal conductivity than those natural clays, because it consists of kaolinite with a thermal conductivity (2 W/m.°C) which is lower than the quartz (8W/m.°C) that the natural clays consist of.

The degree of saturation is an important factor affecting soil behaviour and its thermal conductivity. At a certain degree of saturation, the thermal conductivity of soils can vary within a wide range. The phase composition of soil water may depend strongly on the degree of saturation.

An increase in water content improves the contact between the solid particles by forming thermal bridges, and provides continuous path for heat transfer. However when water content exceeds a certain amount water, it is expected to become the dominant medium

for heat transfer therefore the effective thermal conductivity will tend to be closer to that of water.

The thermal conductivities of dry sandy soils consists of 100% quartz were 0.15, 0.27 and 0.26 W/m.°C for fine sand, medium sand and coarse sand respectively. For the same soils in the saturated condition, their thermal conductivities were 2.75, 3.36 and 3.72 W/m.°C.

The thermal conductivity of the artificial clay soils in the dry condition was 0.25 W/m.°C, while in the saturated condition was 1.52 W/m.°C, however for natural clayey soil its thermal conductivity was higher (2.21 W/m.°C) because it consists of quartz particles.

Several thermal conduction models have been used to predict the thermal conductivity of the soils used in this study. The use of these models should be carried out with a full understanding of the fact that soil is a three phase material. Most of the thermal conduction models deal with soil as only two phases. This assumption is only correct at two soil conditions either completely dry or fully saturated. After the comparison of the predicted thermal conductivity results with the experimental results, it can be concluded that the parallel and series models can only predict the values of soil's maximum and minimum thermal conductivity respectively. Therefore they can not be used to predict the actual thermal conductivity of a soil.

Most of the thermal conduction models have reasonably predicted the thermal conductivity of dry soils, except for the parallel, series, geometric and numerical simulation models.

The geometric mean model is better for predicting the thermal conductivity of saturated and nearly saturated soil; however for dry soil it over-predicts thermal conductivity. De Vries and Kersten's models under-predicted the thermal conductivity of the saturated poorly graded fine, medium and coarse sands with 100% quartz content.

The use of different thermal units in measuring thermal conductivity made comparison of the results difficult, especially when figures were used instead of tables. Johansen's

method generally gives the best results for all soils used in this study under different saturation conditions.

In this research, the range of thermal conductivities for different types of soils was between 0.25 and 3.75W/m.°C. This range agrees with the range found in the literature by many researchers who have used different methods of determination (from 0.15 to 4.0W/m.°C).

The problem of heat transfer in soils is very complicated, to understand it the soil must be subdivided into its constituent elements and facets. A study of each of these should show its relative importance and contribution to the soil's behaviour.

The transmission of heat within soil is dependent on the physical properties of the soil particles, their degree of compaction, and the moisture content of the soil. Because of the porosity and the variable amounts of air and water contained in the soil, the analysis of heat flow through soil is much more complicated than for a homogeneous solid, for which thermal conductivity and heat capacity are stable, well-defined parameters. Soil is a composite of mineral particles, organic matter, and pores which may contain either water or air. All of these differ widely in their thermal characteristics. For example, the heat conductivity of mineral particles is typically twelve times that of water, twenty four times that of organic matter, and about two hundreds times that of air. Hence the thermal conductivities of soil samples can vary considerably depending on the relative amounts of these components. Even for a soil of uniform mineral and porosity, thermal conductivity shows a marked dependence on water content because of the large differences between water and air. For a given soil profile, conductivity would tend to increase with depth due to increased soil density and decreased air content.

7.4 Contribution to soil mechanics

Two new methods to determine both the hydraulic and thermal conductivities of soils have been developed and designed respectively. The modified falling head technique, using the flexible wall permeameter equipped with different types of electronic transducers and the Newcastle volume change gauge, allows for a rapid determination of hydraulic conductivity of very fine soils as well as fine sands. The accurate measurement

of the volume changes of the specimen during the test could lead to a beater understanding of the soil behaviour under different conditions.

The new thermal conductivity device adds to the practice a new simple method for determining the thermal conductivity of soils. the new method was designed to be simple, robust operate in commercial laboratories using standard samples.

Nowadays there is a great interest among geotechnical engineers to make use of the ground temperature. Geotechnical engineers are trying to design an efficient way of extracting and storing heat from or into the ground to be used for building heating and cooling. Energy piles have been used in such systems (Figure 1.1) in which hydraulic and thermal conductivities of soils play a major part in the design.

Hydraulic and thermal conductivities can be used to model the transfer of heat by either finite element or finite differences packages. This is important in the design of ground energy systems, dissipation heat from the buried pipes and electric cables, and insulation of cold storage facilities.

7.5 Recommendations for further study

Hydraulic conductivity of soils beneath buildings plays a major role in using the ground either as a heat source or a heat sink. Even if the soil's hydraulic conductivity is very small, it is postulated that at the small scale of the area under a building makes the effect of hydraulic flow vital in such a project over seasonal periods.

The flow of heat in soils should be investigated when there is a flow of water. A model can be built in the laboratory and an experimental study could be carried out to determine the effect of hydraulic flow on the heat transfer in soils.

Development of the thermal conductivity cell device can be made by adding a pressure transducer to monitor the change in pore water pressure due to change in temperature of the soil.

The migration of water during the thermal conductivity test can be monitored by making use of the Newcastle volume change gauge. This gauge can be connected to the top cap

of the thermal cell device, so that any movement of water can be measured in quantity against time. Hence a relationship between the temperature and water movement could be developed.

The effect of the pore fluid on the determination of a soil's thermal conductivity could be investigated using different types of fluids.

References

Abu-Hamdeh, N.H., Khadair, A.I. and Reeder, R.C. (2001) A comparison of two methods used to evaluate thermal conductivity for some soils. *International Journal of Heat and Mass Transfer*, **44**, 5, 1073-1078.

Abu-Hamdeh, N.H. (2000) Effect of tillage treatments on soil thermal conductivity for some Jordanian clay loam and loam soils. *Soil & Tillage Research*, **56**, 145-151.

Achari, G. and Joshi, R. C. (1994) Discussion on a re-examination of the permeability index of clay by Sivakumar Babu *et al.* (1993). *Canadian Geotechnical Journal*, **31**, 1, 140-141.

ARUP company. Available at: http://www.arup.com/geotechnics/feature.cfm?pageid=662. (Accessed on May 3, 2004).

Aiban, S. A. and Znidarcic, D. (1989) Evaluation of the flow pump and constant head techniques for permeability measurements. *Geotechnique*, **39**, 4, 655-666.

American Society for Testing Materials (1997) Standard test method for measuring of hydraulic conductivity of saturated porous materials using a flexible wall permeameter. (D5084-90 (re-approved 1997)). *Annual Book of ASTM Standards* 04.08, 62-69.

American Society for Testing Materials (1997) Standard test method for Permeability of Granular Soils (Constant Head). (D2434-68). *Annual Book of ASTM Standards* 04.08, 285-289.

American Society for Testing Materials, (1997) Standard test method for determination of thermal conductivity of soil and soft rock by thermal needle probe procedure. (D5334-92). *Annual Book of ASTM Standards* 04.08, 233-237.

American Society for Testing Materials (1997) Standard test method for steady-state heat flux measurements and thermal transmission properties by means of Guarded-Hot-Plate apparatus. (C177-97). Annual *Book of ASTM Standards* 04.06, 20-41.

American Society for Testing Materials (1999) Standard test method for thermal conductivity of refractories by Hot Wire (Platinum resistance thermometer technique). (C1113-99). *Annual Book of ASTM Standards* 15.01, 211-216.

Araruna, J. T., Harwood, A. H. and Clarke, B. G. (1995) A practical, economical and precise volume change measurement device. *Geotechnique*, **45**, 3, 541-544.

Araruna, J. T. (1995) Measurement of Permeability of Soils using a Flow Pump: development and evaluation of equipment and test procedure. *PhD. Thesis, University of Newcastle upon Tyne.*

Austin, W., C. Yavuzturk, J.D. Spitler. (2000) Development Of An In-Situ System For Measuring Ground Thermal Properties. *American Society of Heating, Refrigerating and Air-Conditioning Engineers*, **106**, 1, 365-379.

Bachmann, J., Horton, R., Ren, T. and Van Der Ploeg (2001) Comparison of the thermal properties of four wettable and four water-repellent soils. Available at: http://soil.scijournals.org/cgi/content/full/65/6/1675#BIB8. (Accessed on April 6, 2004).

Bayer, L. D., Gardner, W. H. and Gardner W. R. (1972) Soil Physics, 4th Edition. New York: John Wiley & Sons, Inc.

Bowles, J. E. (1984). Physical and Geotechnical Properties of Soils, 2nd Edition. McGraw-Hill. USA.

British Standard 1377 (1990), Methods of Test for Civil Engineering purposes. *British Standards Institution*, London.

Bristow, Keith L., Kluitenberg, Gerard J. and Horton, Robert. (1994) Measurement of soil thermal properties with a dual-probe heat-pulse technique. *Soil Science Society of America Journal*, **58**, 1288-1294.

Carpenter, G. W. and Stephenson, R. W. (1986) Permeability testing in the Triaxial cell. *Geotechnical Testing Journal*, **9**, 1, 3-9.

Campbell, G. S., Callissendrorff, C. and Williams, J. H. (1991) Probe for measuring soil specific heat using a heat pulse method. *Soil Science Society of America Journal*, **55**, 291-293.

Cary, J.W. (1978) Soil heat transducers and water vapour flow. *Soil Science Society of America Journal*, **43**, 835-839.

Chaney, R. C., Ramanjaneya G., Hencey G., Kanchanastit P. and Fang H. (1983) Suggested test method for determination of thermal conductivity of soil by thermal-needle procedure. *American Society of Testing and Materials*, 220-225.

Chen, Chien-cheng. (1997) An Investigation into the relationship between effective stress and permeability of clays. PhD Thesis, University of Newcastle upon Tyne.

Cosenza, P., Guerin, R., and Tabbagh, A. (2003). Relationship between the thermal conductivity and water content of soils using numerical modelling. *European Journal of soil science*, **54**, 581-587.

Daniel, D. E., Trautwein, S. J., Boynton, S. S. and Foreman, D. E. (1984) Permeability testing with flexible-wall permeameters. *Geotechnical Testing Journal*, **7**, 3, 113-122.

Daniel, D. E., Anderson, D. C., and Boynton, S. S. (1985) Fixed-wall versus Flexible-wall Permeameters, Hydraulic Barriers in Soil and Rock, ASTM STP 874, A. I. Johnson, R. K. Frobel., N. J. Cavalli, and C. B. Pettersson, Eds., *American Society of Testing and Materials*, Philadelphia. 107-126.

Daniel, D. E. (1994). Laboratory Hydraulic Conductivity Tests for Saturated Soils. Hydraulic Conductivity and Waste Contaminant Transport in Soil. ASTM STP 1142, David E. Daniel, Stephen J. Trautwein, Eds., *American Society of Testing and Materials*, Philadelphia. 30-78.

Das, B. M. (1998). Principles of Geotechnical Engineering (4th Edition). PWS. USA, 712.

Das, B. M. (1997) Advanced Soil Mechanics (2nd Edition). Taylor & Francis. USA.

ECN Company. Available at: http://www.ecn.nl/_files/dego/products/projects/energypiles.pdf. (Accessed on April 12, 2003).

Enercret company website. Available at: http://www.enercret.com. (Accessed on April 26, 2004 from:

Farouki, O. T., (1986) Thermal properties of soils, *Series on Rock and Soil Mechanics*, **11**, 136.

Gelder, M. F. (1998). A Thermistor Based Method for Measurement of Thermal Conductivity and Thermal Diffusivity of Moist Food Materials at High Temperatures. *PhD. Thesis, Virginia Polytechnic Institute and State University.*

Harwood, A. H., Clarke, B. G. and Araruna, J. T. (1996) Discussion on stress- state-permeability relations for over consolidated clays by Nagaraj *et al.* (1994). *Geotechnique*, **46**, 2, 363-364.

Head, K. H. (1994) Manual of Soil Laboratory Testing, Pentech Press Limited, London, **2**.

Head, K. H. (1986) Manual of Soil Laboratory Testing, Pentech Press Limited, London, **3**.

Holman, J.P., (1997) Heat Transfer. McGraw-Hill Companies, Inc, Eight Edition, USA, 696.

Hukseflux Company. Available at: http://www.hukseflux.com/thermal%20conductivity/thermal.htm. (Accessed on May 3, 2005).

Hutcheon, N. B. and Paxton, J. A. (1952) Moisture migration in a closed guarded hot plate. *Heating, Piping and Air conditioning*, 113-122.

Incropera, F.P., and Dewitt, D.P., (1996) Fundamentals of Heat and Mass Transfer, John Wiley & Sons America.

Kezdi, A., (1974) Handbook of Soil Mechanics, Volume 1, Elsevier Scientific Publishing Company, Hungary.

Koene, F. and Geelen, C. (2000) Energy piles as an efficient way to store heat. Energy Research Centre of the Netherlands (ECN). Available at http://www.ecn.nl/_files/dego/products/projects/energypiles. (Accessed on March 2, 2004)

Lambe, T. W., and Whitman, R. V. (1979). Soil Mechanics (SI version), John Wiley & Sons, New York.

Leroueil, S., Bouclin, G., Tavenas, F., Bergeron, L. and Rochelle, P. L. (1990) Permeability anisotropy of natural clays as a function of strain. Canadian. *Geotechnical Journal,* **27**, 568-579.

Leroueil, S. Lerat, P., Hight, D. W. and Powell, J. J. M. (1992) Hydraulic Conductivity of recent silty clay at Bothkennar. *Geotechnique,* **42**, 2, 275-288.

Mesri, G., Feng, T. W., Ali, S. and Hayat, T. M. (1994) Permeability characteristics of soft clays. XIII ICSMFE, New Delhi, India, 187-192.

Mitchell, J. K. (1993) Fundamentals of Soil Behaviour, John Wiley & Sons, New York, 437.

Mitchell, J. K. and Kao, T. C. (1978) Measurement of soil thermal resistivity. American Society of Civil Engineering Proceedings. *Journal of Geotechnical Engineering Division,* 1307-1320.

Mohsenin, N.N. 1980. Thermal properties of foods and agricultural materials. Gordon and Breach Science Publishers, NY.

Nagaraj, T. S., Pandian, N. S. and Narasimha Raju, P. S. R. (1993) Stress state permeability relations for fine-grained soils. *Geotechnique,* **43**, 2, 333-336.

Nagaraj, T. S., Pandian, N. S. and Narasimha Raju, P. S. R. (1994) Stress state permeability relations for overconsolidated soils. *Geotechnique,* **44**, 2, 349-352.

Nusier, O. K., and Abu-Hamdeh N. H. (2003) Laboratory techniques to evaluate thermal conductivity for some soils. *Heat and Mass Transfer,* **39**, 119-123.

Olsen, H. W., and Daniel, D. E. (1981) Measurement of hydraulic conductivity of fine-grained soils. Permeability and Ground Water Contaminant Transport, ASTM STP 746, T. F. Zimmie and C. O. Riggs, Eds.,18-64.

Olsen, H. W., Nichols, R. W. and Rice, T. L. (1985) Low gradient permeability measurements in a triaxial system, *Geotechnique*, **35**, 2, 145-157.

Pane, V., Croce, P., Zindarcic, D., Ko, H. Y., Olsen, H. W. and Schiffman, R. L. (1983) Effects of consolidation on permeability measurements of soft clays. *Geotechnique* **33**. 1, 67-72.

Penner, E. (1962) Thermal conductivity of saturated Leda clay. *Geotechnique*, **12**, 2, 168-175.

Penner, E., Johnston, G. H. and Goodrich L. E. (1975) Thermal conductivity laboratory studies of some Mackenzie Highway soils. *Canadian Geotechnical Journal*, **12**, 3, 271-288.

PICO Technology limited. Available at: http://www.picotech.com/thermocouple.html. (Accessed on May, 3 2004).

PICO Technology Limited. Available at: http://www.picotech.com/applications/thermocouple.html. (Accessed on May, 3 2004).

Redmond, P. L. and Shackelford, C. D. (1994) Design and evaluation of a flow pump system for column testing. *Geotechnical Testing Journal*, GTJODJ **17**, 3, 269-281.

Rhoades, J.D., Manteghi, N.A., Shouse, P.J., and Alves, W.J. (1989) Soil electrical conductivity and soil salinity: New formulations and calibrations. *Soil Science Society of America Journal Soil*, **53**, 433-439.

Sepaskhah, A. R., and Boersma, L. (1979) Thermal conductivity of soils as a function of temperature and water content. *Soil Science Society of America Journal Soil*, **43**, 439-444.

Shackelford, C. D. and Glade, M. J. (1994) Constant flow and constant-gradient permeability tests on sand-bentonite-fly- ash mixtures: Hydraulic Conductivity and Waste Contaminant Transport in Soil. ASTM STP 1142, David E. Daniel and Stephen J. T., Eds., *American Society of Testing and Materials*, Philadelphia, 521-545.

Sivakumar Babu, G. L., Pandian, N. S. and Nagaraj, T. S. (1993) A Re-examination of the permeability index of clays. *Canadian Geotechnical Journal* **30**, 1, 187-197.

Silva, A. J., Hetherman, J. R., and Calnan, D. I. (1981) Low-gradient permeability testing of fine-grained marine sediments: Permeability and Ground Water Contaminant Transport, ASTM STP 746, T. F. Zimmie and C. O. Riggs, Eds., *American Society of Testing and Materials*, 121-136.

Smith, W. O. (1942) Thermal conductivity of dry soil. *Soil Science*, **53**, 435-459.

Smith, W. O. and Byers, M. G. (1938) The thermal conductivity of dry soils of certain of the great soil groups. *Soil Science Society of America Proceedings*, **3**, 13-19.

Stepkowska, E. T., Thorborg, B. and Wichman, B. (1995) Stress state-permeability relationships for dredged sludge and their dependence on microstructure, *Geotechnique*, **45**, 2, 307-316.

Suckling, T. P., and Smith, P. E. H. (2002) Environmentally Friendly Geothermal Piles at Keble College, Oxford, UK, *International Conference on Piling and Deep Foundations*: Nice, France. 445-452

Tarnawski, V.R. and Leong, W.H. (2002) Thermal conductivity of soils at very low moisture content and moderate temperatures. *Transport in Porous Media*, **41**, 137-147.

Tavenas, F., Leblond, P., Jean, P. and Leroueil, S. (1983a) The permeability of natural soft clays. Part I: Methods of laboratory measurement. *Canadian Geotechnical Journal,* **20**, 629-644.

Tavenas, F., Jean, P., Leblond, P. and Leroueil, S. (1983b) The permeability of natural soft clays. Part II: Permeability characteristics. *Canadian Geotechnical Journal,* **20**, 645-660.

Tavman, I. H. (1996) Effective thermal conductivity of granular porous materials. Int. Comm. *Heat Mass Transfer,* **23**, 2, 169-176.

Taylor, D. W. (1948) Fundamentals of Soil Mechanics. John Wiley & Sons, NewYork, 700.

Van Rooyen, M. and Winterkorn, H.F. (1959) Structural and textural influences on thermal conductivity of soils. *High way Research Board Proceedings*, **39**, 576-621.

Woodside, W. and De Bruyn, C. M. A. (1959) Heat transfer in moist clay. *Soil Science*, **87**, 166-173.

Yang, N. and Barbour, S. L. (1992) The impact of soil structure and confining stress on the hydraulic conductivity of clays in brine environments. *Canadian Geotechnical Journal*, **29**, 5, 730-739.

Zimmie, T.F. (1981) Geotechnical testing considerations in the determinations of laboratory permeability for hazards waste disposal siting. Hazardous solid waste testing: First conference, ASTM STP 760, R.A. Conway and B.C. Malloy, Eds., *American Society for Testing and Materials*, Philadelphia, 293-304.

Appendix A

A.1 Newcastle Volume Change Gauge Calibration

A Newcastle volume change gauge was calibrated according to BS 1377 (1990) which recommends the calibration of volume changes indicators to be carried out by weighing the amount of distilled water that the vessel contains or delivers. This method was easy to perform and accurate.

Figure A.1 shows the arrangement for the method of calibration. Each volume change gauge was calibrated twice to obtain the transducer constant that is required to convert the output of the transducer reading into engineering units; one for course setting, the second one for fine setting. In the course setting, both tubes (large and small) were used during the calibration. But only the small tube was used in the fine setting calibration. The results of this calibration are shown in Figure A.2.

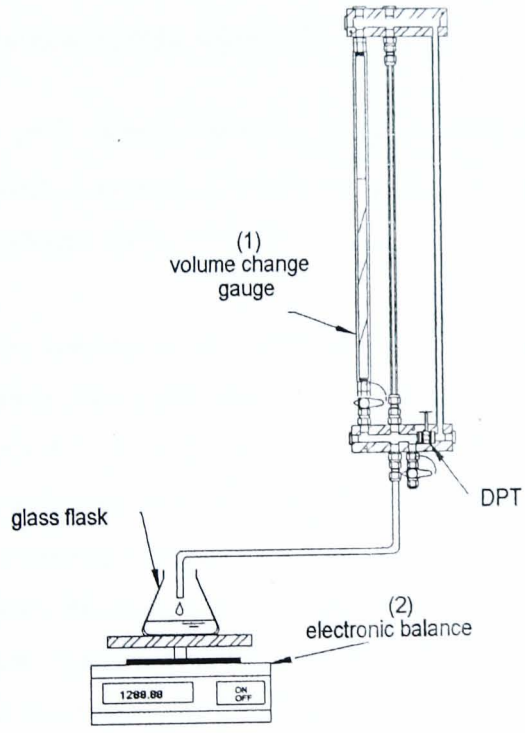

Figure A.1 Arrangement of volume change gauge calibration.
(After Chen, 1997)

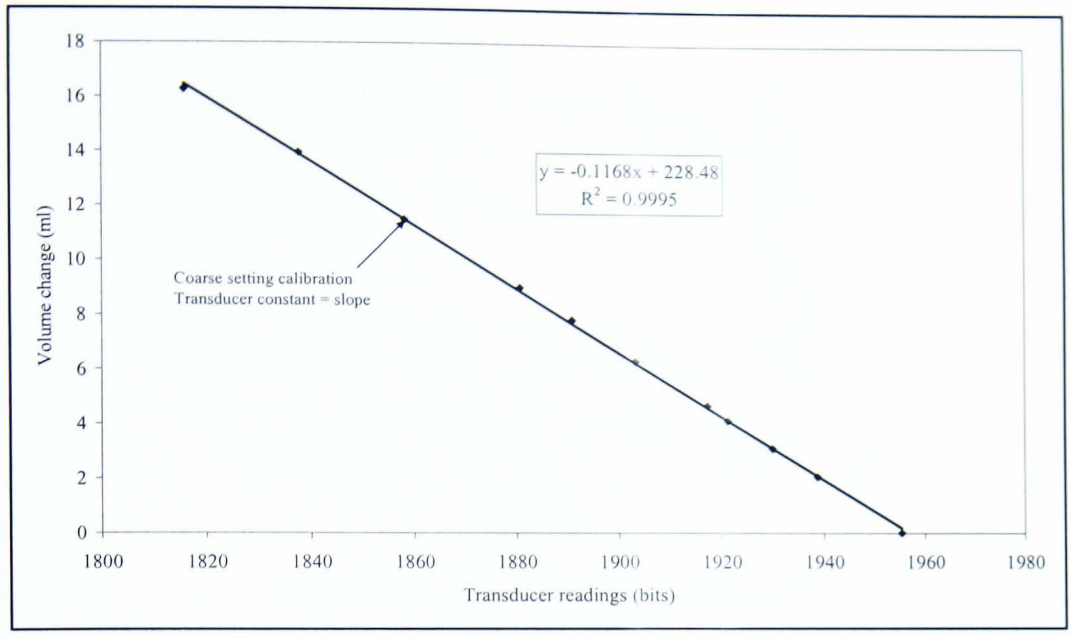

Figure A.2 Typical calibration results for the volume change gauge.

A.2 Pressure Transducer Calibration (PT)

Pressure transducers (PT) (**Error! Reference source not found.**a) were used to measure pore water (back pressures) and cell pressures during the three stages of a test (i.e. saturation, consolidation and permeation).

Cell and top and bottom back pressure transducers were calibrated against a Budenberg dead-weight gauge tester. The calibration procedure was in accordance with BS1377 Part1: 1990 Clause 4.4.4.7. A calibrated Budenberg dead weight tester providing a suitable reference pressure was used. Accurate dead weights resting on a precision made piston fitting into a matching vertical cylinder generate a pressure in the fluid of the system.Figure A.3 shows the arrangement for calibration of PT. The pressure transducer (1 in Figure A.3) was mounted vertically in the dead-weight tester, and then the pressure was raised in increments by the weight (2 in Figure A.3) on the dead-weight tester. Thus the pressure in the transducer was calculated from the known applied weights.

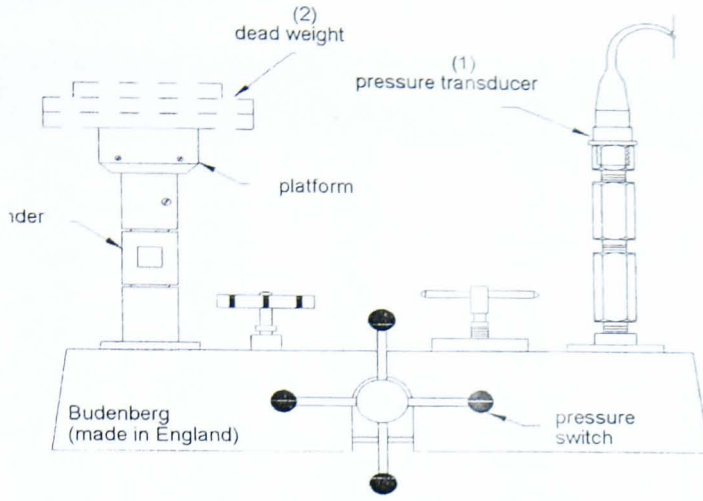

Figure A.3 Arrangement of calibration of PT
(After Chen, 1997)

A computer program was used to read the output of the transducer reading, and then a spreadsheet was used to plot the relationship between the transducer reading (bits) and the pressure (kPa). Thus from the slope of the calibration line, a transducer constant was obtained to convert the output of the transducer reading into engineering units. Figure A.4 and Table A.1 show typical calibration plot and data for pressure transducers.

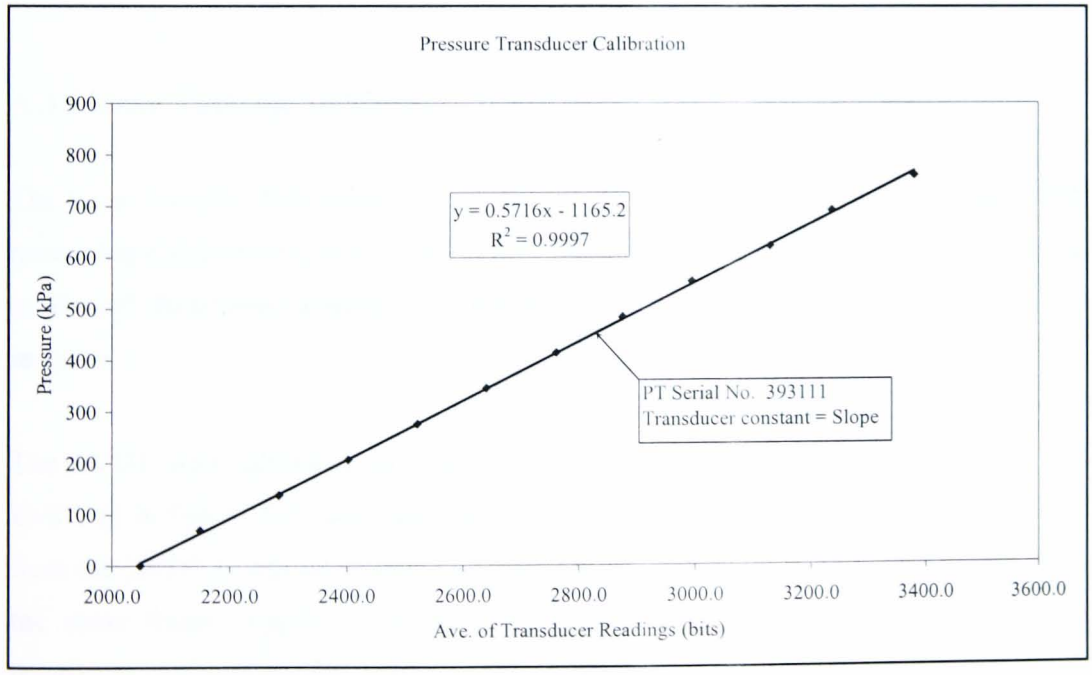

Figure A.4 Typical calibration plot of Pressure Transducer.

Table A.1 Typical calibration data for a Pressure Transducer.

Pressure (KPa)	Transducer readings (bits)			Ave. Transducer readings (bits)	Spread bits	Repeatability (%)
	test (1)	test (2)	test (3)			
0	2048	2048	2048	2048.0	0	0.0
69	2116	2167	2167	2150.0	51	2.4
137.9	2284	2284.3	2284.5	2284.3	0.5	0.0
206.9	2403	2402.2	2402.5	2402.6	0.8	0.0
275.8	2522	2520	2521	2521.0	2	0.1
344.8	2640	2640	2640	2640.0	0	0.0
413.7	2759.3	2764	2758.5	2760.6	5.5	0.2
482.7	2878.8	2876.67	2869	2874.8	9.8	0.3
551.6	2992.8	2996	2995	2994.6	3.2	0.1
620.6	3139.3	3121	3128	3129.4	18.3	0.6
689.5	3238.5	3235	3235.3	3236.3	3.5	0.1
758.5	3406.8	3380	3353	3379.9	53.8	1.6

The last column in Table A.1, repeatability, is determined as a percentage deviation from the mean value of three or more transducer readings as follows:

Repeatability (%) (R_r) $$R_r = \frac{R_s}{R_a} \cdot 100\% \qquad 3.1$$

Where

R_S = average of transducer readings

R_a = spread of each set of readings (difference between highest and lowest)

A.3 Linear Variable Differential Transducer Calibration (LVDT)

The linear variable differential transformer (LVDT) is a common type of transducer for measuring displacement in soil laboratories. A commercially available LVDT (as shown in **Error! Reference source not found.**b) with stroke of 50mm was used in this research.

The LVDT was calibrated as shown in **Error! Reference source not found.**. The LVDT (1 in Figure A.5) was mounted horizontally in a frame (2). The change in output from the LVDT is related to true displacement measured by micrometer (3) attached to the same frame. Typical calibration results are presented below where the actual transducer readings against displacement are shown in Table A.2 and Figure A.6 shows typical calibration plot of LVDT.

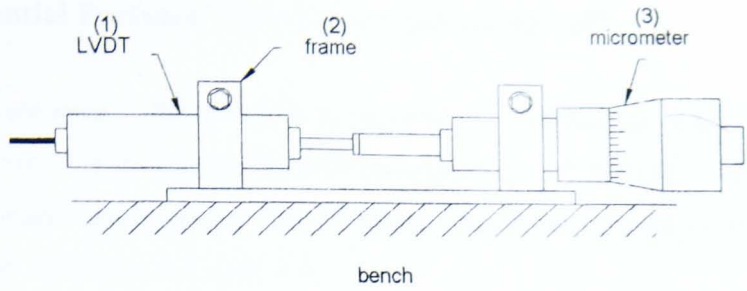

Figure A.5 Arrangement for calibration of LVDT.

Table A.2 Calibration data of LVDT.

Displacement	Transducer readings (bits)			Repeatability	
mm	Test 1	Test 2	Ave.	Spread bits	%
0	2048.1	2048.3	2048.2	0.2	0.01
1	2084.8	2084.8	2084.8	0.0	0.00
2	2122.8	2122.8	2122.8	0.0	0.00
3	2159.8	2159.8	2159.8	0.0	0.00
4	2196.8	2196	2196.4	0.8	0.04
5	2233.8	2233.8	2233.8	0.0	0.00
6	2271.8	2271.8	2271.8	0.0	0.00
7	2308	2307.8	2307.9	0.2	0.01
8	2345.6	2344.8	2345.2	0.8	0.03
9	2382.8	2382.8	2382.8	0.0	0.00
10	2419.8	2419.8	2419.8	0.0	0.00
11	2457.8	2457.8	2457.8	0.0	0.00
12	2495.8	2495.8	2495.8	0.0	0.00
13	2532.8	2532.8	2532.8	0.0	0.00
14	2569.8	2569.8	2569.8	0.0	0.00
15	2607.8	2607.8	2607.8	0.0	0.00
16	2644.8	2644.8	2644.8	0.0	0.00
17	2681.3	2680.8	2681.05	0.5	0.02
18	2718.8	2718.8	2718.8	0.0	0.00

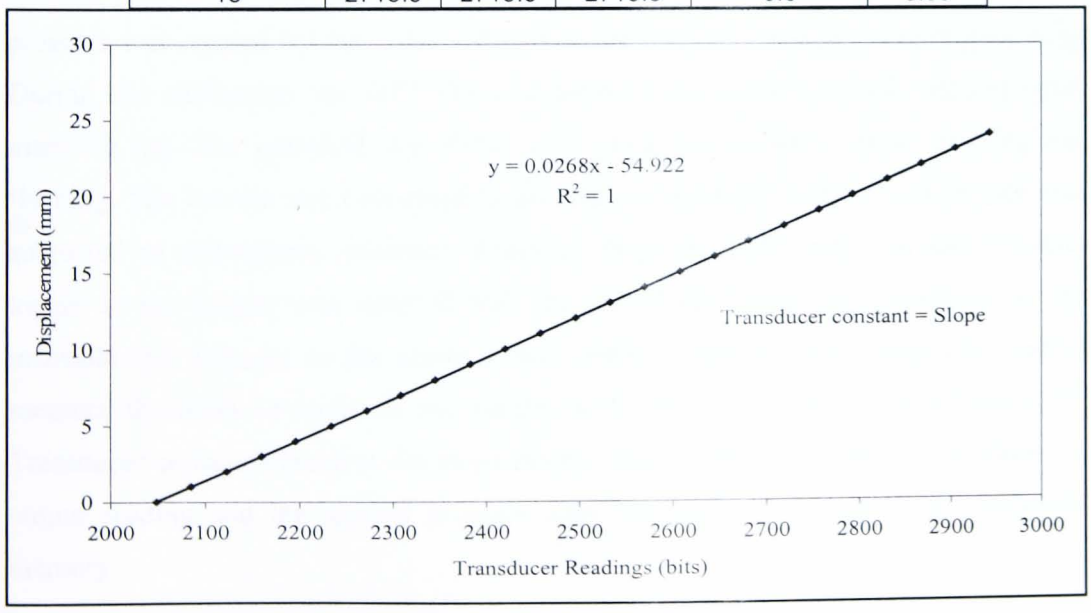

Figure A.6 Typical calibration plot of LVDT

A.4 Differential Pressure Transducer Calibration (DPT)

The DPTs were used in this research to measure both volume changes and the pressure difference across the specimen. The differential pressure transducer used in the pressure difference measurement system was calibrated against a graduated burette filled with de-aired water as shown in Figure A.7.

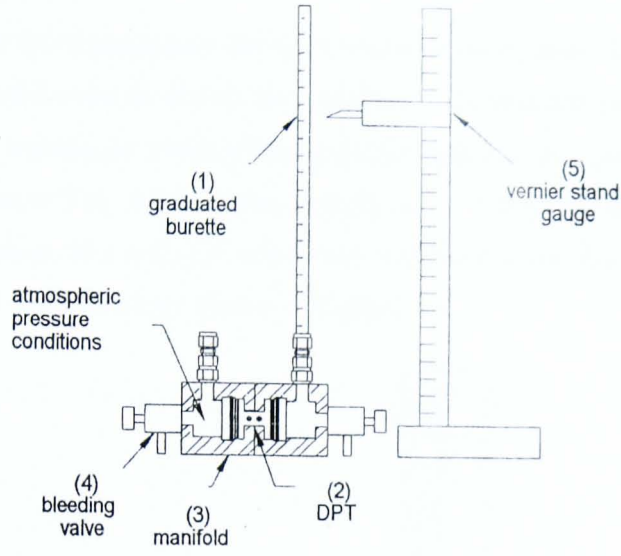

Figure A.7 Arrangement for calibration of the pressure difference measuring system (After Chen, 1997)

DPTs were calibrated by measuring the change in output as the pressure was increased on one side of the transducer relative to the atmospheric pressure. The increase in pressure was created by the water pressure at the base of a burette (1 in Figure A.7). During the calibration the DPT (2) was mounted in a custom built stainless steel manifold (3). The manifold was fitted with bleed valves (4) to allow deairing and flushing. The burette was connected to one side of the DPT while the other side was subjected to atmospheric pressure. Readings from the DPT were recorded by data logger as the burette was emptied with the aid of the bleed valve mounted on the manifold and adjacent to the sensor's face, while a vernier stand gauge (5) used to measure the level of water in the burette with reference to the level of the DPT. Transducer constants equal to the slope of the linear relationship between the electrical output reading and the applied pressure were obtained and stored in the computer memory.

A.1 Newcastle Volume Change Gauge Calibration

A Newcastle volume change gauge was calibrated according to BS 1377 (1990) which recommends the calibration of volume changes indicators to be carried out by weighing the amount of distilled water that the vessel contains or delivers. This method was easy to perform and accurate.

Figure A.1 shows the arrangement for the method of calibration. Each volume change gauge was calibrated twice to obtain the transducer constant that is required to convert the output of the transducer reading into engineering units; one for course setting, the second one for fine setting. In the course setting, both tubes (large and small) were used during the calibration. But only the small tube was used in the fine setting calibration. The results of this calibration are shown in Figure A.2.

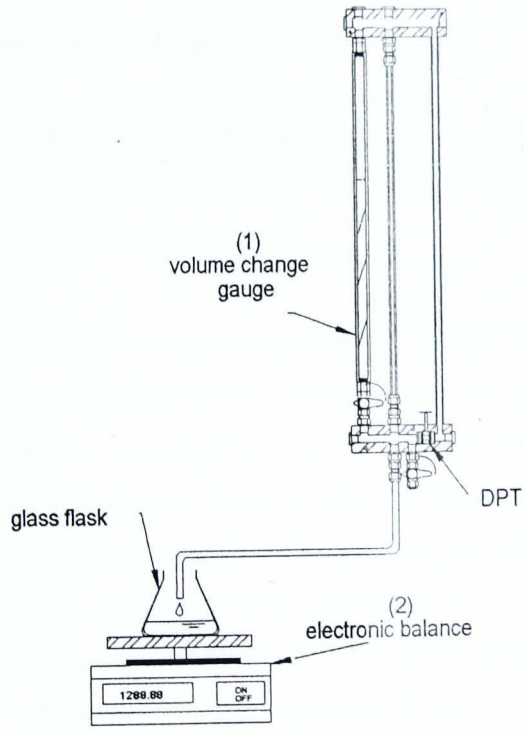

Figure A.1 Arrangement of volume change gauge calibration.
(After Chen, 1997)

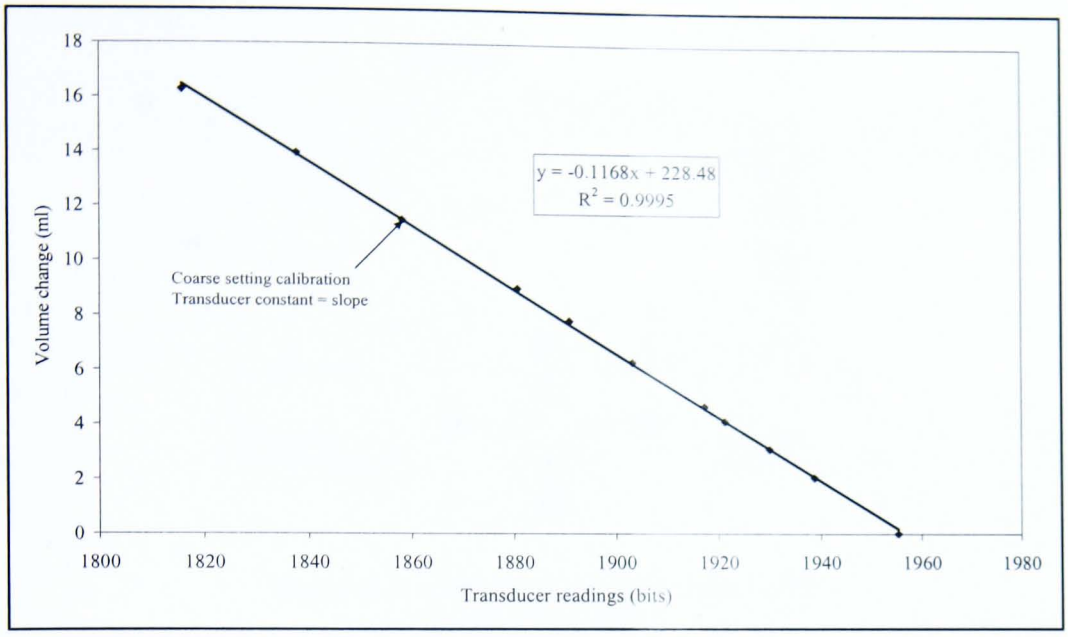

Figure A.2 Typical calibration results for the volume change gauge.

A.2 Pressure Transducer Calibration (PT)

Pressure transducers (PT) (**Error! Reference source not found.**a) were used to measure pore water (back pressures) and cell pressures during the three stages of a test (i.e. saturation, consolidation and permeation).

Cell and top and bottom back pressure transducers were calibrated against a Budenberg dead-weight gauge tester. The calibration procedure was in accordance with BS1377 Part1: 1990 Clause 4.4.4.7. A calibrated Budenberg dead weight tester providing a suitable reference pressure was used. Accurate dead weights resting on a precision made piston fitting into a matching vertical cylinder generate a pressure in the fluid of the system.Figure A.3 shows the arrangement for calibration of PT. The pressure transducer (1 in Figure A.3) was mounted vertically in the dead-weight tester, and then the pressure was raised in increments by the weight (2 in Figure A.3) on the dead-weight tester. Thus the pressure in the transducer was calculated from the known applied weights.

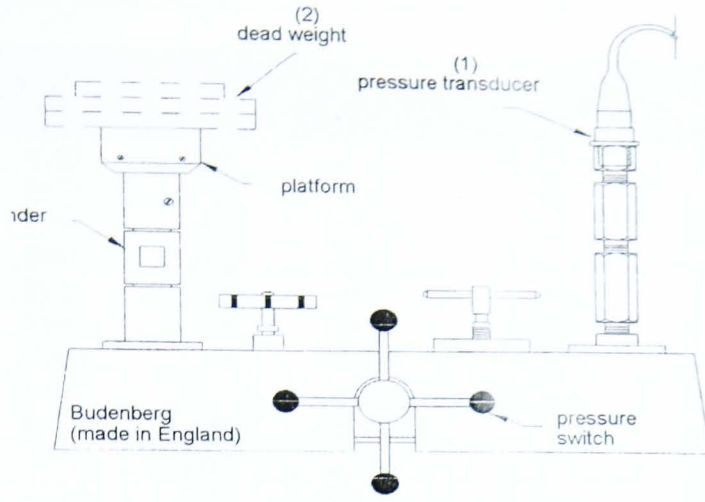

Figure A.3 Arrangement of calibration of PT
(After Chen, 1997)

A computer program was used to read the output of the transducer reading, and then a spreadsheet was used to plot the relationship between the transducer reading (bits) and the pressure (kPa). Thus from the slope of the calibration line, a transducer constant was obtained to convert the output of the transducer reading into engineering units. Figure A.4 and Table A.1 show typical calibration plot and data for pressure transducers.

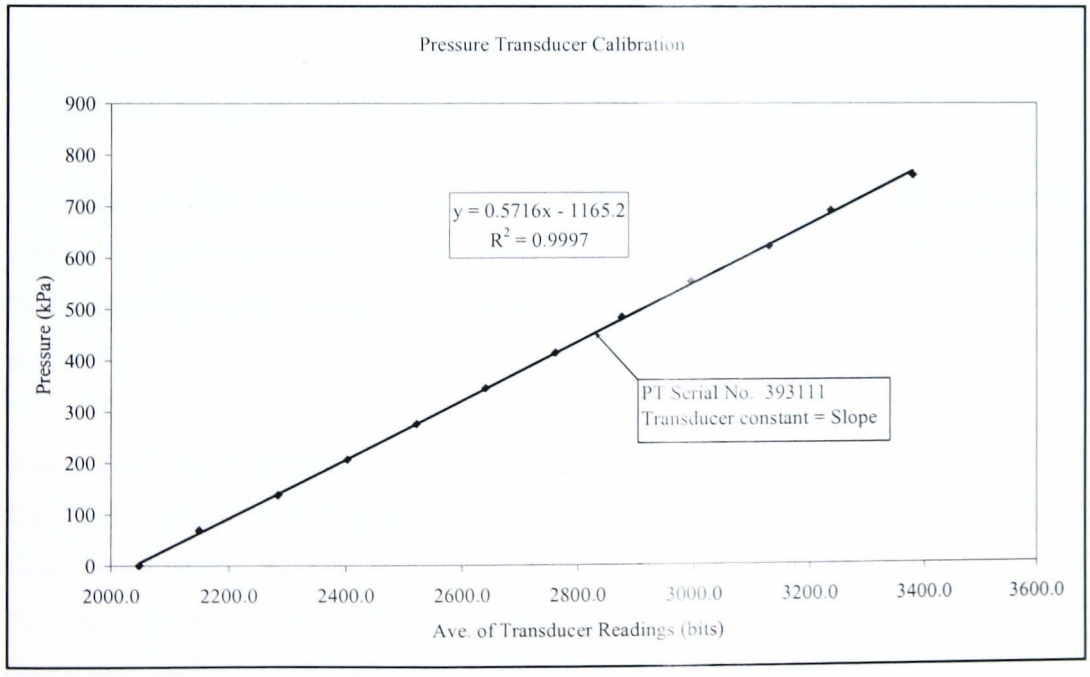

Figure A.4 Typical calibration plot of Pressure Transducer.

Table A.1 Typical calibration data for a Pressure Transducer.

Pressure (KPa)	Transducer readings (bits)			Ave. Transducer readings (bits)	Spread bits	Repeatability (%)
	test (1)	test (2)	test (3)			
0	2048	2048	2048	2048.0	0	0.0
69	2116	2167	2167	2150.0	51	2.4
137.9	2284	2284.3	2284.5	2284.3	0.5	0.0
206.9	2403	2402.2	2402.5	2402.6	0.8	0.0
275.8	2522	2520	2521	2521.0	2	0.1
344.8	2640	2640	2640	2640.0	0	0.0
413.7	2759.3	2764	2758.5	2760.6	5.5	0.2
482.7	2878.8	2876.67	2869	2874.8	9.8	0.3
551.6	2992.8	2996	2995	2994.6	3.2	0.1
620.6	3139.3	3121	3128	3129.4	18.3	0.6
689.5	3238.5	3235	3235.3	3236.3	3.5	0.1
758.5	3406.8	3380	3353	3379.9	53.8	1.6

The last column in Table A.1, repeatability, is determined as a percentage deviation from the mean value of three or more transducer readings as follows:

Repeatability (%) (R_r) $$R_r = \frac{R_s}{R_a} \cdot 100\% \qquad 3.1$$

Where

R_S = average of transducer readings

R_a = spread of each set of readings (difference between highest and lowest)

A.3 Linear Variable Differential Transducer Calibration (LVDT)

The linear variable differential transformer (LVDT) is a common type of transducer for measuring displacement in soil laboratories. A commercially available LVDT (as shown in **Error! Reference source not found.**b) with stroke of 50mm was used in this research.

The LVDT was calibrated as shown in **Error! Reference source not found.**. The LVDT (1 in Figure A.5) was mounted horizontally in a frame (2). The change in output from the LVDT is related to true displacement measured by micrometer (3) attached to the same frame. Typical calibration results are presented below where the actual transducer readings against displacement are shown in Table A.2 and Figure A.6 shows typical calibration plot of LVDT.

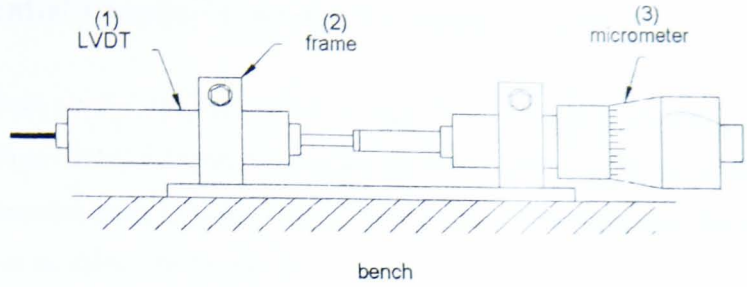

Figure A.5 Arrangement for calibration of LVDT.

Table A.2 Calibration data of LVDT.

Displacement	Transducer readings (bits)			Repeatability	
mm	Test 1	Test 2	Ave.	Spread bits	%
0	2048.1	2048.3	2048.2	0.2	0.01
1	2084.8	2084.8	2084.8	0.0	0.00
2	2122.8	2122.8	2122.8	0.0	0.00
3	2159.8	2159.8	2159.8	0.0	0.00
4	2196.8	2196	2196.4	0.8	0.04
5	2233.8	2233.8	2233.8	0.0	0.00
6	2271.8	2271.8	2271.8	0.0	0.00
7	2308	2307.8	2307.9	0.2	0.01
8	2345.6	2344.8	2345.2	0.8	0.03
9	2382.8	2382.8	2382.8	0.0	0.00
10	2419.8	2419.8	2419.8	0.0	0.00
11	2457.8	2457.8	2457.8	0.0	0.00
12	2495.8	2495.8	2495.8	0.0	0.00
13	2532.8	2532.8	2532.8	0.0	0.00
14	2569.8	2569.8	2569.8	0.0	0.00
15	2607.8	2607.8	2607.8	0.0	0.00
16	2644.8	2644.8	2644.8	0.0	0.00
17	2681.3	2680.8	2681.05	0.5	0.02
18	2718.8	2718.8	2718.8	0.0	0.00

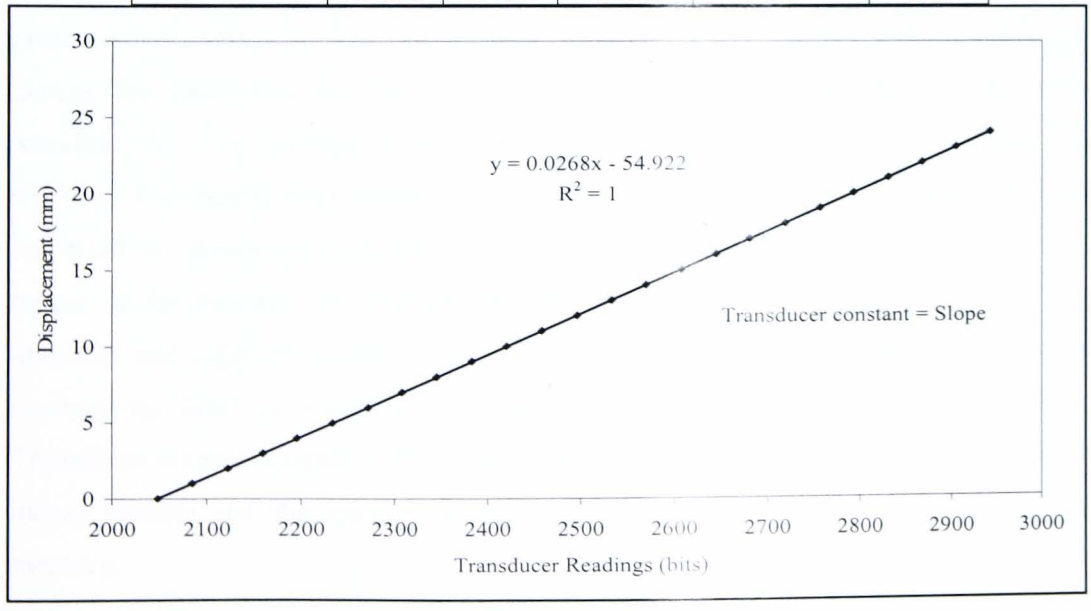

Figure A.6 Typical calibration plot of LVDT

A.4 Differential Pressure Transducer Calibration (DPT)

The DPTs were used in this research to measure both volume changes and the pressure difference across the specimen. The differential pressure transducer used in the pressure difference measurement system was calibrated against a graduated burette filled with de-aired water as shown in Figure A.7.

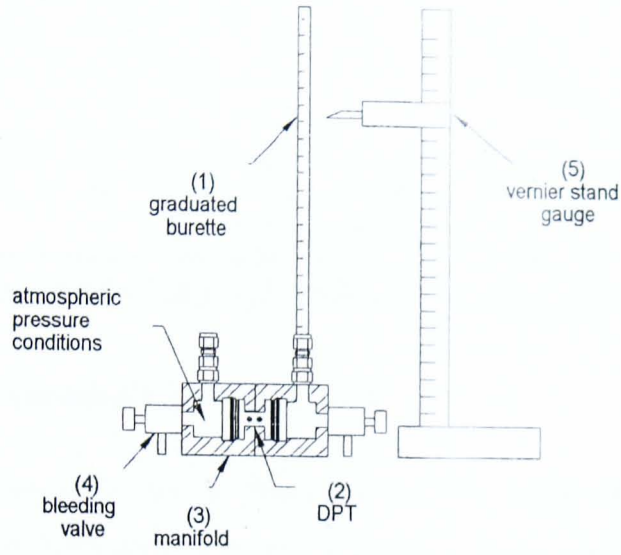

Figure A.7 Arrangement for calibration of the pressure difference measuring system (After Chen, 1997)

DPTs were calibrated by measuring the change in output as the pressure was increased on one side of the transducer relative to the atmospheric pressure. The increase in pressure was created by the water pressure at the base of a burette (1 in Figure A.7). During the calibration the DPT (2) was mounted in a custom built stainless steel manifold (3). The manifold was fitted with bleed valves (4) to allow deairing and flushing. The burette was connected to one side of the DPT while the other side was subjected to atmospheric pressure. Readings from the DPT were recorded by data logger as the burette was emptied with the aid of the bleed valve mounted on the manifold and adjacent to the sensor's face, while a vernier stand gauge (5) used to measure the level of water in the burette with reference to the level of the DPT. Transducer constants equal to the slope of the linear relationship between the electrical output reading and the applied pressure were obtained and stored in the computer memory.

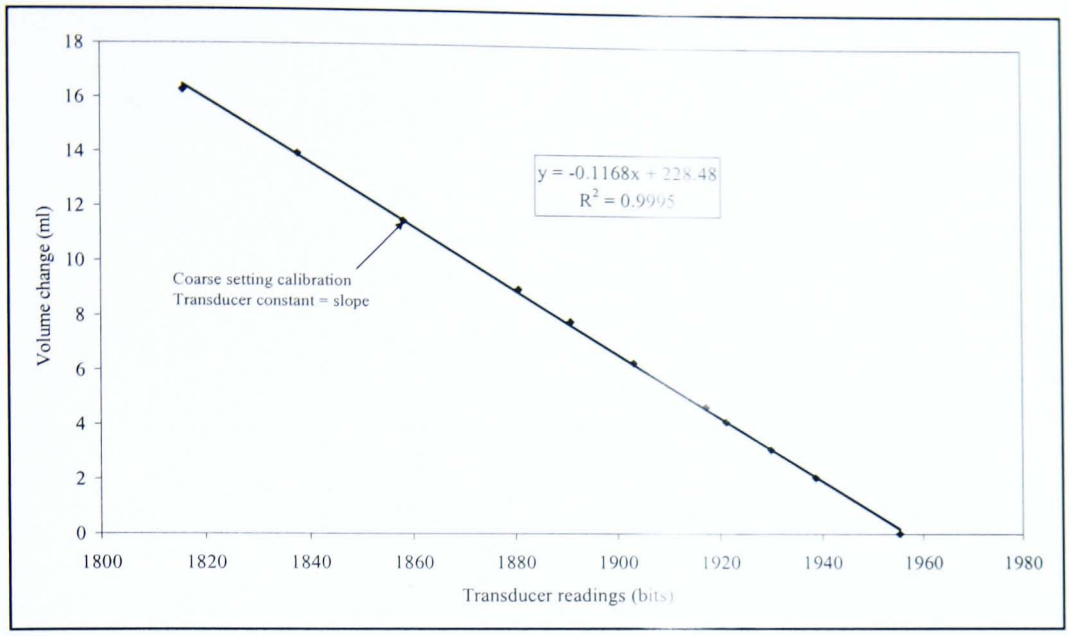

Figure A.2 Typical calibration results for the volume change gauge.

A.2 Pressure Transducer Calibration (PT)

Pressure transducers (PT) (**Error! Reference source not found.**a) were used to measure pore water (back pressures) and cell pressures during the three stages of a test (i.e. saturation, consolidation and permeation).

Cell and top and bottom back pressure transducers were calibrated against a Budenberg dead-weight gauge tester. The calibration procedure was in accordance with BS1377 Part1: 1990 Clause 4.4.4.7. A calibrated Budenberg dead weight tester providing a suitable reference pressure was used. Accurate dead weights resting on a precision made piston fitting into a matching vertical cylinder generate a pressure in the fluid of the system.Figure A.3 shows the arrangement for calibration of PT. The pressure transducer (1 in Figure A.3) was mounted vertically in the dead-weight tester, and then the pressure was raised in increments by the weight (2 in Figure A.3) on the dead-weight tester. Thus the pressure in the transducer was calculated from the known applied weights.

Appendix B

Table B.1 Hydraulic conductivity results for specimens No.12 and No.15 of supreme clay.

Specimen No.	EFS	l (mm)	D (mm)	A (cm^2)	V (cm^3)	W (g)	wc	e	n	Bulk density	Dry density	S (%)	HG	k (CF)	Ave. k (CF)	HG	k (FH)	Ave. k (FH)	k (CH)	Ave. k (CH)
Supreme CLAY Spec. 12	Intial	100.5	102.5	82.5	829.3	1411.6	0.48	1.26	0.56	1.7	1.16	98.1								
	50	100.6	102.2	82.0	824.5			1.27	0.56				2.7	1.07E-09						
													4.7	1.18E-09						
													9.2	1.10E-09						
													17.1	1.10E-09						
													34.2	1.06E-09						
	50														1.10E-09					
	100	100.3	101.7	81.2	813.1			1.24	0.55				2.8	9.85E-10						
													5.8	9.50E-10						
													11.2	9.29E-10						
													21.1	9.31E-10						
													29.1	9.24E-10						
	100														9.44E-10					
	200	100.0	100.8	79.8	795.4			1.19	0.54				3.7	8.87E-10						
													6.5	8.72E-10						
													12.6	8.75E-10						
	200												25.5	8.36E-10	8.68E-10					
Supreme CLAY Spec. 15	Intial	100.5	102.3	82.2	826.1	1389	0.52	1.38	0.58	1.7	1.11	99.7								
	50	100.7	102.4	82.3	827.5			1.39	0.58				2.4	1.22E-09						
													4.4	1.18E-09						
													8.4	1.11E-09						
													15.7	1.16E-09						
													27.4	1.24E-09						
	50														1.18E-09					
	100	100.3	101.8	81.3	814.27			1.35	0.57				2.7	1.17E-09						
													4.9	1.03E-09						
													9.6	1.08E-09						
													18.2	1.03E-09						
													34.5	1.07E-09						
	100														1.08E-09					
	200	99.9	100.5	79.4	790.7			1.28	0.56				3.7	9.85E-10						
													5.7	8.89E-10						
													11.6	9.26E-10		10.9	1.50E-09		1.30E-09	
													22.2	9.53E-10		27.7	1.18E-09		1.17E-09	
	200												40.0	1.02E-09	9.55E-10			1.34E-09		1.24E-09

(k_h) = Hydraulic conductivity, (CF) = Constant flow technique, (FH) = Falling head technique, (CH) = Constant head technique.

Table B.2 Hydraulic conductivity results for specimens No.17 and No.21 of supreme clay.

Specimen No.	EFS	l (mm)	D (mm)	A (cm^2)	V (cm^3)	W (g)	wc	e	n	Bulk density	Dry density	S (%)	HG	k (CF)	Ave. k (CF)	HG	k (FH)	Ave. k (FH)	k (CH)	Ave. k (CH)
Supreme CLAY Spec. 17	Intial	100	102.5	82.5	825.2	1408.7	0.49	1.29	0.56	1.7	1.15	99.5								
	50	100.2	102.6	82.7	826.9			1.30	0.57				2.5	1.17E-09						
													4.5	1.10E-09						
													8.6	1.13E-09						
													15.8	1.17E-09						
													29.0	1.16E-09						
	50														1.15E-09					
	100	99.8	102.1	81.9	816.6			1.27	0.56				2.7	1.01E-09						
	100												5.2	9.59E-10	9.85E-10					
																10.5	1.40E-09		1.42E-09	
																21.4	1.32E-09		1.37E-09	
																29.7	1.34E-09		1.39E-09	
	100																	1.35E-09		1.40E-09
	200	99.5	100.9	79.9	793.4			1.20	0.55							5.9	1.39E-09		1.25E-09	
																10.5	1.25E-09		1.22E-09	
																21.1	1.06E-09		1.14E-09	
																31.2	1.02E-09		1.13E-09	
	200																	1.18E-09		1.19E-09
Supreme CLAY Spec. 21	Intial	100	103	83.3	833.2	1421.5	0.51	1.35	0.57	1.7	1.12	100.1								
	50	100.2	103.0	83.3	833.0			1.33	0.57							6.7	2.97E-09		1.43E-09	
																10.3	1.52E-09		1.67E-09	
																19.4	1.22E-09		1.44E-09	
																30.4	1.35E-09		1.55E-09	
	50																	1.765E-09		1.52E-09
	100	99.8	102.2	82.0	817.8			1.28	0.56							5.2	-		1.14E-09	
																10.9	6.00E-09		1.65E-09	
																19.6	9.78E-10		1.17E-09	
																29.4	1.11E-09		1.22E-09	
	100																	1.04E-09		1.30E-09
	200	99.4	101.1	80.3	795.6			1.22	0.55							5.3	-		1.05E-09	
																10.1	9.83E-10		9.88E-10	
																19.3	8.86E-10		1.00E-09	
																29.5	9.88E-10		9.69E-10	
	200																	9.52E-10		1.00E-09

(k_h) = Hydraulic conductivity, (CF) = Constant flow technique, (FH) = Falling head technique, (CH) = Constant head technique.

Table B.3 Hydraulic conductivity results for specimens No.13 and No.14 of silty clay.

Specimen No.	EFS	l (mm)	D (mm)	A (cm^2)	V (cm^3)	W (g)	wc	e	n	Bulk density	Dry density	S (%)	HG	k (CF)	Ave. k (CF)
Silty CLAY Spec. 13	Intial	100	101.8	81.4	813.9	1440.7	0.41	1.11	0.53	1.8	1.25	99.9			
	50	100	101.7	81.2	812.2			1.09	0.52				1.0	3.15E-09	
													1.6	3.54E-09	
													3.5	3.13E-09	
													7.1	2.99E-09	
													12.6	3.21E-09	
													27.6	3.13E-09	
	50														3.19E-09
	100	99.8	101.2	80.4	801.81			1.06	0.51				1.2	2.46E-09	
													2.5	2.35E-09	
													4.8	2.35E-09	
													9.0	2.43E-09	
													12.7	2.39E-09	
													25.0	2.26E-09	
	100														2.37E-09
	200	99.5	100.4	79.2	786.8			1.03	0.51				1.5	2.19E-09	
													2.9	2.05E-09	
													5.5	2.11E-09	
													10.5	2.18E-09	
	200												20.7	2.10E-09	2.13E-09
Silty CLAY Spec. 14	Intial	100.5	102	81.7	821.2	1459.4	0.41	1.10	0.52	1.8	1.25	99.2			
	50	100.5	102.2	82.0	824.1			1.09	0.52				1.3	3.27E-09	
													1.8	3.33E-09	
													3.4	3.16E-09	
													6.9	3.12E-09	
													13.3	3.07E-09	
													24.4	3.02E-09	
	50														3.16E-09
	100	100.3	101.7	81.2	814.05			1.07	0.52				2.0	3.06E-09	
													3.8	2.97E-09	
													7.4	2.96E-09	
													14.4	2.96E-09	
													27.6	2.92E-09	
	100														2.97E-09
	200	100.1	100.8	79.8	797.2			1.02	0.50				1.2	2.86E-09	
													2.3	2.60E-09	
													4.4	2.70E-09	
													8.7	2.56E-09	
													17.0	2.60E-09	
	200												32.7	2.59E-09	2.65E-09

(k_h) = Hydraulic conductivity, (CF) = Constant flow technique.

Table B.4 Hydraulic conductivity results for specimen's No. 16 and No. 20 of silty clay.

Specimen No.	EFS	l (mm)	D (mm)	A (cm^2)	V (cm^3)	W (g)	wc	e	n	Bulk density	Dry density	S (%)	HG	k (CF)	Ave. k (CF)	HG	k (FH)	Ave. k (FH)	k (CH)	Ave. k (CH)
Silty CLAY Spec. 16	Intial	100.4	102.5	82.5	828.5	1470.3	0.42	1.11	0.53	1.8	1.25	99.9								
	50	100.5	102.4	82.4	827.5			1.10	0.52				0.8	4.01E-09						
													1.5	3.82E-09						
													3.0	3.72E-09						
													5.8	3.69E-09						
													11.4	3.62E-09						
													21.5	3.55E-09						
	50														3.74E-09					
	100	100.3	102.0	81.7	818			1.07	0.52				0.9	3.47E-09						
													1.8	3.16E-09						
													3.3	3.37E-09						
													6.5	3.32E-09						
													12.5	3.39E-09						
													25.0	3.23E-09						
	100														3.32E-09					
	200	100	101.2	80.4	801.9			1.03	0.51				1.0	3.05E-09						
	200												2.1	2.75E-09	2.90E-09					
Silty CLAY Spec. 20	Intial	100	103	83.3	833.2	1481	0.42	1.12	0.53	1.8	1.24	100.5								
	50	100.1	103.1	83.4	834.2			1.10	0.52							5.1	4.78E-09		3.74E-09	
																11.3	2.62E-09		4.06E-09	
																19.3	2.65E-09		3.64E-09	
																29.5	3.7E-09		3.99E-09	
																		3.4375E-09		3.86E-09
	100	99.9	102.5	82.5	822.89			1.08	0.52							5.2	4.7E-09		3.06E-09	
																9.5	2.62E-09		2.94E-09	
																18.8	2.49E-09		3.00E-09	
																27.9	2.3E-09		3.02E-09	
																		3.0275E-09		3.01E-09
	200	99.5	101.4	80.8	802.7			1.02	0.50							4.9	5.28E-09		2.66E-09	
																10.1	2.06E-09		2.54E-09	
																19.1	1.99E-09		2.52E-09	
																28.8	2.25E-09		2.57E-09	
																		2.895E-09		2.57E-09

(k_h) = Hydraulic conductivity, (CF) = Constant flow technique, (FH) = Falling head technique, (CH) = Constant head technique.

Table B.5 Hydraulic conductivity results for specimen's No. 18 of fine sand.

Specimen No.	EFS	l (mm)	D (mm)	A (cm^2)	V (cm^3)	W (g)	wc	e	n	Bulk density	Dry density	S (%)	HG	k (FH)	Ave. k (FH)
Fine SAND	Intial	100	100	78.54	785.4	1548.9	0.22	0.647	0.393	1.97	1.61	99.2			
	50	100	99.9	78.44	784.4			0.647	0.393				10	2.48E-05	
													20	2.07E-05	
													30	1.86E-05	
	50														2.14E-05
	100	99.92	99.9	78.40	783.4			0.645	0.392				10	2.39E-05	
													20	2.01E-05	
													30	1.93E-05	
													40	1.72E-05	
	100														2.01E-05
	200	99.87	99.8	78.27	781.7			0.642	0.391				10	2.33E-05	
													20	2.03E-05	
													30	1.76E-05	
													40	1.80E-05	
	200														1.98E-05
	300	99.8	99.8	78.21	780.5			0.639	0.390				10	2.28E-05	
													20	2.14E-05	
													30	1.83E-05	
													40	1.62E-05	
	300														1.97E-05
	400	99.75	99.7	78.12	779.2			0.636	0.389				10	2.36E-05	
													20	2.05E-05	
													30	1.88E-05	
													40	1.52E-05	
	400														1.95E-05
	500	99.69	99.7	78.10	778.6			0.635	0.388				10	2.25E-05	
													20	2.00E-05	
													30	1.76E-05	
													40	1.71E-05	
	500														1.93E-05

Appendix C

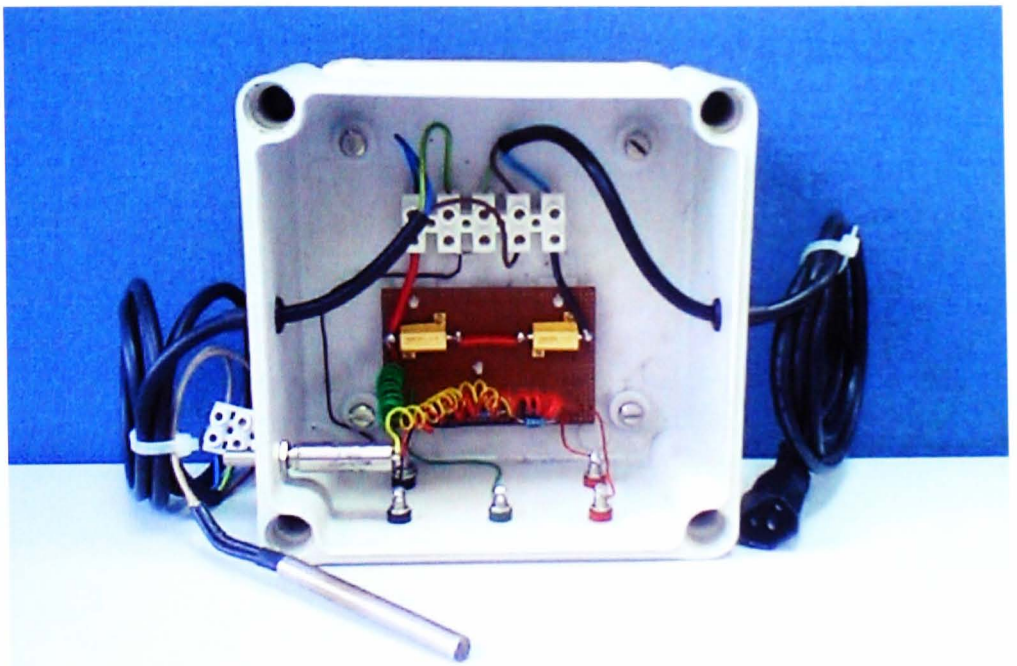

C-1 Photograph of the meter electronic box

Appendix D

Table D-1 Comparison between the measured and predicted thermal conductivities of reconstituted Soils.

No.	Soil Type	ka	kw	ks	k Measured	Conduction Models							
						k Series (Min.)	k Parallel (Max)	k Geometric	k Maxwell	k Woodside & Messmer	k Krupiczka	k Zehner & Schlunder	k Johansen
1	Dry Fine SAND	0.0257	0.6	8	0.15	0.06	4.83	0.82	0.14	0.30	0.32	0.31	0.24
2	Dry Medium SAND	0.0257	0.6	8	0.27	0.07	5.14	1.02	0.16	0.34	0.39	0.36	0.27
3	Dry Coarse SAND	0.0257	0.6	8	0.25	0.08	5.45	1.28	0.18	0.38	0.49	0.43	0.31
4	Dry Silty CLAY	0.0257	0.6	2	0.25	0.05	1.06	0.25	0.10	0.20	0.16	0.17	0.18
5	Sat. Fine SAND	0.0257	0.6	8	2.75	1.38	5.11	2.91	2.33	3.15	2.34	2.56	2.91
6	Sat. Medium SAND	0.0257	0.6	8	3.34	1.57	5.53	3.37	2.68	3.51	2.68	2.92	3.37
7	Sat. Coarse SAND	0.0257	0.6	8	3.72	1.57	5.53	3.37	2.68	3.51	2.68	2.92	3.37
8	Sat. Silty CLAY	0.0257	0.6	2	1.52	0.88	1.23	1.03	1.04	1.05	1.03	1.03	1.03

No.	Soil Type	ka	kw	ks	Conduction Models				Factor	
					k Kersten	k Campbell	k DeVries	k Numerical Simulation	F	B
1	Dry Fine SAND	0.0257	0.6	8	N/A	0.29	0.16	2.73	0.008	1.983
2	Dry Medium SAND	0.0257	0.6	8	N/A	0.32	0.18	2.98	0.008	2.381
3	Dry Coarse SAND	0.0257	0.6	8	N/A	0.35	0.21	3.24	0.008	2.892
4	Dry Silty CLAY	0.0257	0.6	2	N/A	0.22	0.12	0.74	0.031	1.405
5	Sat. Fine SAND	0.0257	0.6	8	2.01	1.24	1.86	3.20	0.131	2.052
6	Sat. Medium SAND	0.0257	0.6	8	2.28	1.18	2.14	3.52	0.131	2.700
7	Sat. Coarse SAND	0.0257	0.6	8	2.28	1.18	2.14	3.52	0.131	2.700
8	Sat. Silty CLAY	0.0257	0.6	2	1.28	1.25	0.84	1.14	0.258	1.002

F= DeVries model's factor, B= Zehner & Schlunder model's factor

Table D-2 Comparison between the measured and predicted thermal conductivities of natural Soils.

No.	Sample No.	Soil Type	k_a	k_w	k_s	k Measured	Conduction Models				
							k Series (Min.)	k Parallel (Max)	k Geometric	k Maxwell	k Woodside & Messmer
1	BH9T no.61	Sandy Silty CLAY	0.0257	0.6	6	2.45	1.52	4.22	2.81	2.42	2.96
2	BH9T no.70	Sandy SILT	0.0257	0.6	4	1.61	1.17	2.54	1.77	1.95	1.93
3	BH C13 88	Silty SAND	0.0257	0.6	8	2.89	1.36	5.06	2.86	2.29	3.11
4	BH C13 84	Silty SAND	0.0257	0.6	6	2.66	1.28	3.80	2.78	2.23	3.04
5	BH C13 108	Silty SAND	0.0257	0.6	6	2.08	1.21	3.62	2.55	2.07	2.84
6	BH C13 106	Silty SAND	0.0257	0.6	6	2.29	1.19	3.58	2.51	2.04	2.81
7	BH 11T B15	Coarse SAND	0.0257	0.6	6	2.35	1.35	3.93	2.97	2.38	3.20
8	BH 11T B10	Coarse SAND	0.0257	0.6	6	1.64	1.58	4.32	3.58	2.84	3.65
9	BH 11T B12	Sandy GRAVEL	0.0257	0.6	6	0.72	1.42	4.06	2.63	2.52	2.81
10	BH 11T B14	Sandy GRAVEL	0.0257	0.6	6	1.00	1.60	4.35	2.97	2.88	3.07
11	BH11T Grout1	GROUT (1-1)	0.0257	0.6	6	0.64	0.71	1.54	0.74	0.75	0.69
12	BH11T Grout2	GROUT (1-2)	0.0257	0.6	6	0.61	0.70	1.49	0.73	0.74	0.68
13	BH24 Grout1	GROUT (2-1)	0.0257	0.6	6	0.71	0.70	1.43	0.72	0.73	0.67
14	BH24 Grout2	GROUT (2-2)	0.0257	0.6	6	0.77	0.70	1.46	0.73	0.73	0.67

Table D-3 Continue of table D-2

No.	Sample No.	Soil Type	Conduction Models							Factor		
			k Krupiczka	k Zehner & Schlunder	k Johansen	k Kersten	k Campbell	k DeVries	k Numerical Simulation	Fs	Fa	B
1	BH9T no.61	Sandy Silty CLAY	2.33	2.54	2.81	2.17	1.25	2.09	3.57	0.131		2.761
2	BH9T no.70	Sandy SILT	1.58	1.70	1.72	1.67	1.20	1.76	2.12	0.131		1.721
3	BH C13 88	Silty SAND	2.30	2.20	2.67	2.33	1.11	2.72	3.11	0.295	1.509	1.983
4	BH C13 84	Silty SAND	2.25	2.15	2.63	2.28	1.12	2.65	3.05	0.295	1.509	1.888
5	BH C13 108	Silty SAND	2.11	2.00	2.45	2.09	1.16	2.47	2.87	0.295	1.507	1.624
6	BH C13 106	Silty SAND	2.08	1.98	2.36	2.03	1.12	2.39	2.81	0.295	1.513	1.580
7	BH 11T B15	Coarse SAND	2.38	2.27	2.21	2.21	0.75	2.27	3.04	0.295	1.709	2.126
8	BH 11T B10	Coarse SAND	2.84	2.64	1.79	2.16	0.58	2.21	3.40	0.295	2.140	3.035
9	BH 11T B12	Sandy GRAVEL	2.51	2.38	0.53	1.15	0.41	1.28	3.03	0.295	3.128	2.381
10	BH 11T B14	Sandy GRAVEL	2.88	2.67	0.59	1.24	0.46	1.59	3.38	0.295	3.048	3.112
11	BH11T Grout1	GROUT (1-1)	0.87	0.73	0.72	0.64	1.21	0.64	0.70	0.131		0.221
12	BH11T Grout2	GROUT (1-2)	0.87	0.72	0.70	0.61	1.22	0.63	0.73	0.131		0.205
13	BH24 Grout1	GROUT (2-1)	0.87	0.71	0.71	0.61	1.23	0.63	0.67	0.131		0.187
14	BH24 Grout2	GROUT (2-2)	0.87	0.71	0.71	0.62	1.14	0.64	0.62	0.131		0.196

Fs & Fa = DeVries model's factors, B= Zehner & Schlunder model's factor